

STUDIES ON POTENTIAL USAGE OF FLY ASH IN STEEL FIBER REINFORCED CONCRETE FOR RIGID PAVEMENTS

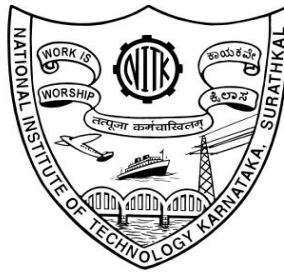
Thesis

Submitted in partial fulfillment of the requirements for the degree of

DOCTOR OF PHILOSOPHY

by

CHANDRASHEKHAR.A



**DEPARTMENT OF CIVIL ENGINEERING
NATIONAL INSTITUTE OF TECHNOLOGY KARNATAKA
SURATHKAL, MANGALORE -575 025
July 2013**

STUDIES ON POTENTIAL USAGE OF FLY ASH IN STEEL FIBER REINFORCED CONCRETE FOR RIGID PAVEMENTS

Thesis

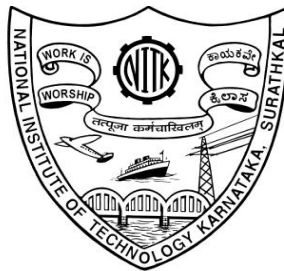
Submitted in partial fulfillment of the requirements for the degree of

DOCTOR OF PHILOSOPHY

by

CHANDRASHEKHAR.A

[Reg No: 060414CV06F01]



**DEPARTMENT OF CIVIL ENGINEERING
NATIONAL INSTITUTE OF TECHNOLOGY KARNATAKA
SURATHKAL, MANGALORE -575 025
July 2013**

DECLARATION

I hereby declare that the research Thesis entitled “**Studies on Potential Usage of Fly Ash in Steel Fiber Reinforced Concrete for Rigid Pavements**” which is being submitted to the **National Institute of Technology Karnataka, Surathkal** in partial fulfillment of the requirements for the award of the degree of **Doctor of Philosophy in Civil Engineering**, is a bonafide report of the research work carried out by me. The material contained in this research Thesis has not been submitted to any University or Institution for the award of any degree.

(Chandrashekhar.A)
060414CV06F01
Department of Civil Engineering.

Place: NITK, Surathkal
Date: 27-07-2013

CERTIFICATE

This is to certify that the Research Thesis entitled “**Studies on Potential Usage of Fly Ash in Steel Fiber Reinforced Concrete for Rigid Pavements**” submitted by **Chandrashekhar.A.** (Register Number: 060414CV06F01) as the record of research work carried out by him, is accepted as the Research Thesis submission in partial fulfillment of the requirements for the award of the degree of **Doctor of Philosophy.**

Dr. A.U Ravi Shankar
Research Guide
Department of Civil Engineering.
National Institute of Technology Karnataka, Surathkal

Chairman (DRPC)
Department of Civil Engineering.
National Institute of Technology Karnataka, Surathkal

DEDICATED

TO

MY PARENTS,

FAMILY MEMBERS

AND

FRIENDS

ACKNOWLEDGEMENT

I would like to express my sincere gratitude to my research supervisor and Head of Department, Prof. A.U Ravi Shankar for his motivation and invaluable guidance throughout my research work. I am grateful to him for his keen interest in the preparation of this thesis. It has been my pleasure to work with him.

I profusely thank My guru Dr. K.S.Babunarayana for his valuable guidance, suggestions and encouragement throughout the research work. I also thank him for his efforts to bring the thesis in the required form. I will be failing in my duty if I do not remember the invaluable suggestions, guidance, and support given by Dr. R.K.Yaji, former professor, Department of Civil Engineering, NITK, Surathkal. I sincerely and wholeheartedly acknowledge the love and affection showed by Dr. R.K.Yaji at every stage of my research and to bring the thesis in the required format.

I acknowledge my sincere thanks to thank Prof. D V R Murthy, Dept of Chemical Engineering and Dr.Sitaram Nayak Dept of Civil Engineering for being the members of Research Progress Assessment Committee and giving valuable suggestions and the encouragement provided at various stages of this work.

I wish to thank Director NITK Surathkal, Prof. R. Shivashankar, Prof. M. C. Narasimhan, Prof. Katta Venkataramana, former Heads of the Civil Engineering Department, Prof. S.G.Mayya Chairman Civil Engineering sciences, Prof. Lokesh, Professor, Civil Engineering for their support and encouragement throughout my stay at the NITK campus.

My thanks are due to Dr. Subhash Yaragal, Dr.Swaminathan, Dr. Varghese George, Dr. Shrihari and Dr. Jayalexmi B.R., Dr. Muralidhar. N for the help and support extended to me.

My greatest thanks are due to Dr. Kurunji Venkatramana Gowda, Founder President, Academy of Liberal Education Sullia, and the management for providing a great opportunity to me to do my research work at NITK, Surathkal.

I would like to thank Dr. N. A. Jnanesh, Principal, K V G College of Engineering Sullia, Dr. S G Gopalakrishna former principal, K V G College of Engineering Sullia, all Heads of Department for their encouraging words and appreciation towards me.

I would like to thank all the professors at NITK Surathkal, for passing their knowledge on to me. I take this opportunity to thank Mr. Pruthviraj, Asst. Professor, Department of Applied Mechanics for the help extended during slab test.

I appreciate the co-operation and help rendered by the staff of laboratories and the office of the Civil Engineering Department. My special thanks to Mr. Dinesh Achar, Mr. Shashikanth, Mr. Ramanath Achar, Mr. Sadanada Kadri and Mr. Viswanath for their help in completing my experimental work.

Financial assistance from the DIST, TEQIP grant and from Department of Civil Engineering, NITK Surathkal to my research work is highly acknowledged.

I am especially grateful to my colleagues in the Research Group whose contributions and encouragements have taken me this far. The informal support and encouragement of many friends has been indispensable. I also acknowledge the good company and help received by of postgraduate students Mr. Abhishek Patil, Mr. Girish, Mr. Akshay and Mr. Abhilash.

I am grateful to my pretty sister Ms Susmitha, for her constant support and help during the preparation of report. I also grateful to Ms Sridevi and Ms Ashwini for their support. Invaluable cooperation and support extended to me from my parents, family members, my wife Mrs. Savitha and children - Vineeth and Anvitha, I lovingly acknowledge their help and cooperation during this research work. They have always been a source of inspiration for me.

Finally I am grateful to everybody who helped and encouraged me during this research work.

NITK

CHANDRASHEKHAR.A

Date: 27-07-2013

ABSTRACT

The ever-growing needs of transportation systems have always necessitated continuous research to make pavements functional, stable, safe, serviceable and durable. With demands exponentially increasing and available resources decreasing, search for materials, construction techniques and performance appraisal is more than ever. Any material when rejected as worthless after its utility period was over is termed as waste material. The tendency of throwing such material not only led to resource crunch and also their collection, conveyance, processing and disposal posed severe problems. Serious attempts began to seek no waste, low waste and waste utilization. Recovery, recycle and reuse of wastes, product, plant and process modifications are being tried. Highway construction industry also has embraced these methods where in waste is being utilized as ingredients in paving material. Industrial wastes like coal ash, blast furnace slag, bottom ash, rubber tires have significant potential to replace conventional materials for various applications in highway construction. Steel fiber reinforced concrete has been investigated and successfully employed in various applications in Civil Engineering projects.

The present work is an experimental and analytical investigation to study the usage potential of **steel fiber reinforced fly ash** concrete(SFRC) with special emphasis to serviceability and durability. Issues like material characterization, cause effect relationship between fatigue failure and load stress level, and temperature gradients effects have been addressed. Concrete grades M₄₀ and M₃₀ have been considered for the investigation as these are widely used. The mixes have been designed as per relevant Codes of Practice. Cubes for compression tests, prisms for modulus of rupture and flexural fatigue tests have been cast, cured and tested. To study the effect of temperature profile on performance and to know the load deformation characteristics of the proposed material, 900 mm x 900mm x 150mm slabs have been used.

The use of fly ash in plain concrete as cement replacement tends to reduce all the strengths at the age of 28 days. Along with steel fibers ($V_f = 1\%$), fly ash concrete (with 40% cement replacement) overcomes this deficiency and the enhancement of

strength of 10% was observed. The steel fiber fly ash concretes have shown better fatigue performance comparative to the reference concrete. A new fatigue equation for projection of design fatigue life has been proposed. The thermal absorption characteristics were found to be unchanged by addition of fly ash to the conventional concrete. Investigations on influence of nonlinear temperature profiles on performance have shown that the resulting temperature stress is 10-30% higher than that obtained using the conventional linear temperature gradient assumption and its incorporation in pavement design has been highlighted.

Key Words: SFRC, Fly ash, Concrete pavement, Fatigue, Temperature stresses, EverFE, Weibull distribution

CONTENTS

ABSTRACT	i
CONTENTS	iii
LIST OF FIGURES	viii
LIST OF TABLES	xiv
NOMENCLATURE	xvi
1.0 INTRODUCTION	1-12
1.1 BACKGROUND	1
1.2 RIGID PAVEMENTS	3
1.2.1 Rigid Pavements- in Indian Context	4
1.2.2 Spectrum of Concrete in Rigid Pavement	5
1.2.3 Fiber Reinforced Concrete	5
1.3 FLY ASH	6
1.4 NEED FOR PRESENT INVESTIGATION	8
1.5 RESEARCH OBJECTIVES	10
1.6 SCOPE OF WORK	10
1.7 ORGANIZATION OF THESIS	11
2.0 REVIEW OF LITERATURE	13-39
2.1 GENERAL	13
2.2 CONCRETE PROPERTIES	13
2.3 SUPPORT IDEALIZATION FOR CONCRETE PAVEMENT	15
2.4 FLY ASH IN CONCRETE AND CONCRETE PAVEMENTS	16
2.5 STEEL FIBER REINFORCED CONCRETE (SFRC)	20
2.6 FLEXURAL FATIGUE CHARACTERISTICS OF PAVEMENT	24
2.7 THERMAL/CURLING STRESSES IN CONCRETE PAVEMENTS	28
2.8 FINITE ELEMENT ANALYSIS OF PAVEMENT	31
2.9 HEAT TRANSFER MECHANISM IN PAVEMENTS	32
2.10 ANALYSIS OF NON-LINEAR TEMPERATURE DISTRIBUTION	33
2.11 DIFFERENT APPROACHES FOR ANALYSING NONLINEAR TEMPERATURE GRADIENT	36

2.11.1 NOLA Concept	37
2.11.2 Temperature Moment (TM) Concept	37
2.11.3 Ever FE Software	38
2.12 SUMMARY	39
3.0 EXPERIMENTAL WORK AND RESULTS	40-85
3.1 INTRODUCTION	40
3.2 PRELIMINARY INVESTIGATION OF MATERIALS	40
3.2.1 Cement	40
3.2.2 Aggregates	41
3.2.3 Water	42
3.2.4 Superplasticizer	42
3.2.5 Fly ash	43
3.2.6 Steel Fibers	44
3.3 CONCRETE MIX DESIGN	44
3.4 SPECIMEN DETAILS	47
3.5 MIXING, PLACING AND COMPACTING CONCRETE MIX	48
3.6 CURING OF SPECIMENS	49
3.7 TESTS	50
3.7.1 Tests on Fresh Concrete	50
3.7.2 Tests on Hardened Concrete	50
3.8 RESULTS	55
3.9 DISCUSSIONS	62
3.9.1 Effect of addition of fly ash and/or steel fibers to the concrete on slump values	62
3.9.2 Comparison of static strength characteristics of various mixes	64
3.9.3 Effect of Fly ash on strength properties of plain concrete	67
3.9.4 Effect of incorporation of steel fibers on strength properties of plain concrete	69
3.9.5 Effect of Fly ash on strength properties of SFRC	71
3.9.6 Effect of insertion of steel fibers into fly ash-cement concrete on strength	75

3.9.7 Relationship between Compressive strength and Flexural strength	78
3.9.8 Relationship between Compressive strength and Modulus of elasticity	81
3.10 SUMMARY	85
4.0 FATIGUE STUDIES AND ANALYSIS	86-123
4.1 GENERAL	86
4.1.1 S-N Curve	86
4.2 FATIGUE MODELS	89
4.3 PROBABILISTIC ANALYSIS OF FATIGUE DATA	90
4.3.1 Graphical Method	91
4.3.2 Method of Moments	92
4.3.3 Least squares Method (LSM)	93
4.3.4 Maximum Likelihood Estimator (MLE) Method	93
4.3.5 Availability Workbench(AWB)- Weibull Module	94
4.4 DESIGN FATIGUE LIFE	95
4.5 ACCELERATED FATIGUE TESTING EQUIPMENT	95
4.6 METHODOLOGY	97
4.7 FATIGUE TEST RESULTS	98
4.8 ANALYSIS OF THE FATIGUE DATA	104
4.8.1 Method of Selection of Weibull Parameters	109
4.9 GOODNESS OF FIT TEST FOR THE FATIGUE DATA	111
4.10 SURVIVAL PROBABILITY AND S-N- P_f RELATION	115
4.11 DISCUSSIONS	118
4.11.1 Effect of addition of steel fibers on fatigue life of the concrete	120
4.11.2 Effect of addition of fly ash on fatigue life of the steel fiber concrete	122
4.12 SUMMARY	123
5 TEMPERATURE STUDIES ON CONCRETE SLAB	124-151
5.1 GENERAL	124
5.2 TEMPERATURE DATA ACQUISITION SYSTEM	124
5.2.1 Resistance Temperature Recorder(RTD)	125
5.3 PREPARATION OF SPECIMENS	127

5.4 TEMPERATURE DATA	128
5.5 TEMPERATURE DIFFERENTIAL	132
5.6 TEMPERATURE PROFILES	134
5.6.1 Temperature Distribution equations	136
5.7 DEVELOPMENT OF EQUATION FOR NON-LINEAR TEMPERATURE PROFILE	139
5.8 COMPARISON OF ANALYTICAL RESULTS	142
5.9 DISCUSSIONS	150
5.10 SUMMARY	151
6 LOAD STUDY ON SFRC SLABS	152-167
6.1 GENERAL	152
6.2 EXPERIMENTAL SET UP	152
6.3 RESULTS	159
6.4 STRESS ANALYSIS	164
6.5 SUMMARY	167
7 PAVEMENT DESIGN	168-173
7.1 GENERAL	168
7.2 DESIGN STRESSES AND PARAMETRS	168
7.3 FATIGUE MODELS USED	170
7.4 DESIGN THICKNESS	171
7.5 TEMPERATURE STRESSES	172
7.6 DISCUSSIONS	172
7.7 SUMMARY	173
8 CONCLUSIONS	174-176
8.1 SCOPE FOR FURTHER STUDY	176
REFERENCES	177-189
APPENDIX I	190-194
Comparison of Weibull Parameters obtained by various methods	190
APPENDIX II	195-206
II-1 Recorded Average Temperature Data during April –May 2010	195
II-2 Temperature profile across the thickness of slab	199

II-3 Comparison of third degree polynomial and quadratic equation of temperature distribution across the thickness using regression	203
APPENDIX III	207-212
Comparison of Experimental and Analytical(ANSYS) results	
APPENDIX IV	213-220
IV-1 Pavement Design Examples-Fatigue approach	213
IV-2 Pavement Design Examples-Combined load and temperature stress	218
LIST OF PUBLICATIONS	221
BIO DATA	222

LIST OF FIGURES

Figure	Description	Page No
1.1	Increase in Vehicle population in India	2
1.2	Geographical location of major thermal power plants in India	7
2.1	Transfer of wheel load to sub layer of pavement structure	13
2.2	S-N curve for SFRC (Source: IRC SP: 46)	27
2.3	Upward and downward curling of concrete pavement	30
2.4	Heat transfer in concrete pavements	33
2.5	Three components of Non linear Temperature distribution	34
2.6	Temperature moment calculation	38
3.1	Steel Fibers	44
3.2	Addition of steel fibers to the concrete and mixing of concrete in a mixer	49
3.3	Curing of concrete specimens in a water tank	50
3.4	Compression Testing	52
3.5	Splitting Tension Test	52
3.6	Flexural test by Third Point Loading	54
3.7	Determination of Modulus of Elasticity	54
3.8	Variation of compressive strength of different mixes with age	58
3.9	Flexural strength of various mixes after 28 and 90 days curing	59
3.10	Comparison of split tensile strength of various mixes	60
3.11	Stress –strain relationship under compressive load to determine Modulus of elasticity of reference mix(R)	61
3.12	Effect of addition of fly ash to the concrete on slump value	62
3.13	Effect of addition of steel fibers to the concrete on slump value	62
3.14	Effect of addition of fly ash to the steel fiber reinforced concrete(Steel fiber 0.5%) on slump value	63
3.15	Effect of addition of fly ash to the steel fiber reinforced concrete(Steel fiber 1.0%) on slump value	63
3.16	Comparison of compressive strengths (28days) of various mixes with reference concrete	64

3.17	Comparison of Flexural strengths(28 days) of various mixes with reference concrete	66
3.18	Comparison of Split Tensile strengths(28 days) of various mixes with reference concrete	66
3.19	Effect of addition of fly ash in plain concrete on compressive strength (28 days)	68
3.20	Effect of addition of fly ash in plain concrete on flexural strength (28 days)	68
3.21	Effect of addition of fly ash in plain concrete on split tensile strength (28 days)	68
3.22	Effect of addition of fly ash to concrete on modulus of elasticity	69
3.23	Effect of steel fibers in plain concrete on compressive strength (28 days)	70
3.24	Effect of steel fibers in plain concrete on flexural strength (28 days)	70
3.25	Effect of use of steel fibers in plain concrete on split tensile strength (28 days)	70
3.26	Effect of steel fibers in concrete on modulus of elasticity	71
3.27	Effect of fly ash in steel fiber (0.5%) concrete on 28 days compressive strength	72
3.28	Effect of fly ash in steel fiber (0.5%) concrete on flexural strength (28 days)	72
3.29	Effect of fly ash in steel fiber (0.5%) concrete on 28 days split tensile strength	72
3.30	Effect of fly ash in steel fiber (0.5%) reinforced concrete on Modulus of elasticity	73
3.31	Effect of fly ash in steel fiber (1.0%) concrete on compressive strength (28 days)	73
3.32	Effect of fly ash in steel fiber (1.0%) concrete on flexural strength (28 days)	73
3.33	Effect of fly ash in steel fiber (1.0%) concrete on 28 days split tensile strength	74
3.34	Effect of fly ash in steel fiber (1.0%) reinforced concrete on Modulus of elasticity	74
3.35	Compressive strengths of SFRC ($V_f=1\%$) with different percentage of Fly ash (M_{40} mix)	75
3.36	Compressive strengths of SFRC ($V_f=1\%$) with different percentage of Fly ash (M_{30} mix)	75
3.37	Effect of steel fibers in fly ash (20%) concrete on compressive strength (28 days)	76
3.38	Effect of steel fibers in fly ash (20%) concrete on flexural strength (28 days)	76
3.39	Effect of steel fibers in fly ash (20%) concrete on Split tensile strength (28 days)	76

3.40	Effect of steel fibers in fly ash (20%) concrete on Modulus of Elasticity	77
3.41	Effect of steel fibers in fly ash (40%) concrete on compressive strength (28 days)	77
3.42	Effect of steel fibers in fly ash (40%) concrete on flexural strength (28 days)	77
3.43	Effect of steel fibers in fly ash (40%) concrete on Split tensile strength (28 days)	78
3.44	Effect of steel fibers in fly ash (40%) concrete on Modulus of Elasticity	78
3.45	Plot of Observed flexural strength v/s predicted flexural strength	81
3.46	Plot of observed modulus of elasticity v/s predicted modulus of elasticity	84
4.1	Typical Wohler diagram	87
4.2	Weibull distribution - probability density function plot	94
4.3	Accelerated Fatigue (repeated load) test set up	96
4.4	Failure mechanism of beam under flexural fatigue test	97
4.5	Crack propagation during flexural fatigue test	97
4.6	Fractured surface of Steel Fiber Reinforced Fly ash concrete beam	98
4.7	Failed specimens (FS3)	98
4.8	S-N Curves for REF, FS2 and FS4 mixes (M_{30} & M_{40})	102
4.9	S-N curve considering all the fatigue data	103
4.10	General S-N curve for Design of Rigid pavements	104
4.11a	Graphical Method to evaluate Weibull parameters (M_{30} concrete- REF and FS4)	105
4.11b	Graphical method to evaluate Weibull parameters (M_{30} concrete -FS4 and M_{40} Concrete REF)	106
4.11c	Graphical method to evaluate Weibull parameters (M_{30} concrete and M_{40} concrete All data)	107
4.11d	Graphical method to evaluate Weibull parameters (M_{30} and M_{40} together)	108
4.12	S-N- P_f Curve for combined data at various failure probabilities	117
4.13	Hazard function of Weibull distribution v/s number of cycles for stress level=0.85	119
4.14	Shape parameters at various stress level	119

4.15	S-N curve of M ₃₀ and M ₄₀ concrete with and without steel fibers	121
4.16	S-N curves of fly ash concrete (20%) with steel fibers	121
4.17	S-N curves of fly ash concrete(40%) with steel fibers	121
4.18	S-N curves of steel fiber concrete(0.5%) with and without fly ash	122
4.19	S-N curves of steel fiber concrete (1.0%) with and without fly ash	122
5.1	Block diagram of Temperature data acquisition unit	125
5.2	Temperature Data Acquisition unit	126
5.3	RTD sensor	126
5.4	Location of drilled holes and RTD sensors	127
5.5	Test slabs with temperature sensors	127
5.6a	Hourly variation of temperature across the thickness-150mm (REF concrete)	128
5.6b	Hourly variation of temperature across the thickness-150mm (FA20 concrete)	129
5.6c	Hourly variation of temperature across the thickness-150mm (FA40 concrete)	129
5.7a	Hourly variation of temperature across the thickness-200mm (REF concrete)	129
5.7b	Hourly variation of temperature across the thickness-200mm (FA20 concrete)	130
5.7c	Hourly variation of temperature across the thickness-200mm (FA40 concrete)	130
5.8a	Hourly variation of temperature across the thickness-250mm (REF concrete)	130
5.8b	Hourly variation of temperature across the thickness-250mm (FA20 concrete)	131
5.8c	Hourly variation of temperature across the thickness-250mm (FA40 concrete)	131
5.9a	Hourly variation of temperature across the thickness-300mm (REF concrete)	131
5.9b	Hourly variation of temperature across the thickness-300mm (FA20 concrete)	132
5.9c	Hourly variation of temperature across the thickness-300mm (FA40 concrete)	132
5.10a	Temperature Differential between the surfaces across the thickness-150mm	133

5.10b	Temperature Differential between the surfaces across the thickness-200mm	133
5.10c	Temperature Differential between the surfaces across the thickness-250mm	134
5.10d	Temperature Differential between the surfaces across the thickness-300mm	134
5.11	Temperature profiles across 150mm thick slab specimens (REF, FA20, FA40)	135
5.12a	Temperature profile across thickness (150mm&200mm) at 02.00hours	137
5.12b	Temperature profile across thickness (250mm&300mm) at 02.00 hours	138
5.13	Comparison of stress due to linear and non linear temperature distribution across the thickness of slab(150mm)	146
5.14	Comparison of Stresses at top and bottom using nonlinear temperature distribution (3 rd degree polynomial) and EverFE software	147
5.15	Comparison of stresses at different timings for 300mm thick slab	149
6.1	Testing arrangement for stiffness of steel box	153
6.2	Plot of load Vs deflection of a box spring	153
6.3	Spring box model (ANSYS) a) meshing and loading b) Deflection contours	154
6.4	Arrangement of box springs	155
6.5	Data Acquisition Unit	155
6.6	Position of strain gauges and load	156
6.7	Placing of slab over steel box springs	157
6.8	Loading arrangement a) centre loading b) edge loading	157
6.9	Recording of data	158
6.10a	Strain at different instants of time (REF gauge 1) -Central loading	159
6.10b	Strain at different instants of time (FS4 gauge 2) -Central loading	159
6.10c	Strain at different instants of time (FS4 gauge 4) -Central loading	160

6.11	Load v/s strain relation in Fly ash SFRC (FS4) under central and edge loading	161
6.12	ANSYS strain contour under central loading(E= 30000, $\mu=0.15$)	162
6.13	Comparison of strain gauge data with ANSYS results	163
6.14	Comparison of experimental and ANSYS results	164
6.15	Loading position of dual wheel load assembly	165
6.16	Edge load stress v/s thickness of slab obtained using ANSYS	166
6.17	Comparison of stress in slab due to edge load	167

LIST OF TABLES

Table	Description	Page No
1.1	Indian Road Network	2
1.2	Existing/Proposed Projects of NHAI utilizing Fly Ash	8
3.1	Properties of Ordinary Portland Cement used in this study	40
3.2	Properties of Coarse and Fine aggregates	41
3.3	Particle Size Distribution of Coarse aggregate	41
3.4	Particle Size Distribution of Fine aggregate	42
3.5	Properties of Conplast SP430	42
3.6	Chemical Properties of Fly ash (Class F)	43
3.7	Physical Properties of Fly ash (Class F)	43
3.8	Details of Concrete Mix Proportions	45
3.9a	Different Ingredients/m ³ of M ₃₀ Concrete Mix	46
3.9b	Different Ingredients/m ³ of M ₄₀ Concrete Mix	47
3.10	Specimen Details for Various Tests (Each in M ₄₀ and M ₃₀ Mix)	48
3.11	Slump Values for Different Mixes	51
3.12	Compressive strength results of various mixes (M ₃₀ and M ₄₀)	55
3.13	Flexural strength results of various mixes (M ₃₀ and M ₄₀)	56
3.14	Split tensile strength results of various mixes (M ₃₀ and M ₄₀)	56
3.15	Test results of static Modulus of Elasticity	61
3.16	Relationship between compressive strength and flexural strength for M ₄₀ concrete	79
3.17	Relationship between compressive strength and flexural strength for M ₃₀ concrete	79
3.18	Chi-square test for prediction model of flexural strength	80
3.19	Relationship between compressive strength and modulus of elasticity for M ₄₀ concrete	82
3.20	Relationship between compressive strength and modulus of elasticity for M ₃₀ concrete	82
3.21	Chi-square test for prediction model of Modulus of elasticity	83
4.1	Fatigue life data(number of cycles to failure) in ascending order for M ₃₀ concrete	99
4.2	Fatigue life data(number of cycles to failure) in ascending order for M ₄₀ concrete	100
4.3	Regression Equations (S-N curves)	101

4.4	Comparison of different fatigue models	103
4.5	Weibull parameters selected for various mixes based on MSE	110
4.6	Kolmogorov–Smirnov test for Reference concrete (M_{30})	111
4.7	Kolmogorov–Smirnov test for FS2 concrete (M_{30})	112
4.8	Kolmogorov–Smirnov test for FS4 concrete (M_{30})	113
4.9	Kolmogorov–Smirnov test for Reference concrete (M_{40})	113
4.10	Kolmogorov–Smirnov test for FS2 Concrete (M_{40})	114
4.11	Kolmogorov–Smirnov test for FS4 concrete (M_{40})	115
4.12	Calculated fatigue lives (N_D) corresponding to different failure probabilities ($P_f = 95\%, 50\%, 5\%$) for M_{30} concrete	116
4.13	Calculated fatigue lives (N_D) corresponding to different failure probabilities ($P_f = 95\%, 50\%, 5\%$) for M_{40} concrete	117
4.14	Calculated(Design) fatigue lives (N_D) corresponding to different failure probabilities for any concrete	117
4.15	Comparison of stress ratios corresponding to different fatigue lives (for different failure probabilities)	120
5.1	Hourly variation of ambient temperature on 21-05-2010	128
5.2	Third degree polynomial equation of temperature distribution across the thickness(150mm) using regression	139
5.3a	Calculation of stress using nonlinear and linear temperature gradient assumptions for 150mm thick slab	142
5.3b	Calculation of stress using nonlinear and linear temperature gradient assumptions for 200mm thick slab	143
5.3c	Calculation of stress using nonlinear and linear temperature gradient assumptions for 250mm thick slab	144
5.3d	Calculation of stress using nonlinear and linear temperature gradient assumptions for 300mm thick slab	145
5.4	Comparison of stress due to nonlinear component by various approaches	148
6.1	Predicted Modulus of Elasticity of Various Concretes of grade M_{40}	163
6.2	Edge load stresses in fly ash SFRC(FS4)	166
7.1	Predicted Flexural strength and Modulus of Elasticity	169
7.2	The axle load spectrum for high volume road (IRC 58-2002)	170
7.3	The axle load spectrum for low volume roads	170
7.4	Calculated thickness of pavement for reference and steel fiber fly ash concrete	171
7.5	Temperature Differential for coastal areas(IRC 58-2002)	172
7.6	Calculated thickness based on combined wheel load and temperature	172

NOMENCLATURE

ACI	American Concrete Institute
ASTM	American Society for Testing and Materials
AWB	Availability Workbench software
BIS	Bureau of Indian standards
BPK	Billion passenger kilometre
BTK	Billion Tonne kilometre
CA	Coarse Aggregate
CANMET	Canada Centre for Mineral and Energy Technology
E_c	Elastic modulus of concrete
F	Fine Aggregate
FA	Fly ash
f_{ck}	Characteristic strength of concrete
f_r	Flexural strength (Modulus of rupture) of concrete
Gb	Foundation shear modulus
GGBFS	Ground Granulated Blast Furnace Slag
HVFA	High Volume Fly Ash
IRC	Indian Roads Concrete
IS	Indian standards
K	Spring stiffness
k	Modulus of subgrade reaction
K-S table	Kolmogorov–Smirnov table
MORTH	Ministry of Road Transport and Highways
MSE	Minimum Mean squared error
NOLA	Nonlinear area
OPC	Ordinary Portland Cement
PCA	Portland Cement Association
R^2	Coefficient of Determination
RTPC	Raichur Thermal Power Corporation
SFRC	Steel Fiber Reinforced Concrete
SR	Stress ratio or stress level
α	Shape parameter of Weibull distribution
μ	Scale parameter(Charecteristic life) of Weibull distribution
σ	Stress

CHAPTER 1

INTRODUCTION

1.1 BACK GROUND

Transportation is vital for economical, industrial, social, and cultural development of any country. The inadequate transportation facilities retard the process of socio-economic development of the country. Road network is the only mode of transportation which gives maximum service to all and is the only mode which offers the maximum flexibility to travellers in selecting route, direction, time, and speed of travel (MORTH, 2012a). Road network alone serves the remote areas. The well-being of citizen, economical growth and status of a country is judged by how well organized and efficient the road network is. A wide variety and range of roads is in use all-round the globe. The terrain, topography, population, culture, the functional and structural requirements are the factors that decide the type.

India has become one of the fastest growing nations of the world. Today, India has one of the largest highway and road networks. The total length of roads in the country exceeds 4.10 million kilometers. This network consists of 71,772 km of National highways, 1,54,522 km of State highways, and an informal network running to an astounding 38,83,298 km. As per estimates, the road network carries nearly 65% of total freight and 85% of total passenger traffic (MORTH 2012a). Freight transport by road has risen from 6 BTK (Billion Tonne km) in 1951 to 762 BTK in 2000 and passenger traffic has risen from 23 BPK (Billion-Passenger km) to 2046 BPK during the same period. Freight and passenger traffic is expected to increase to 1835 BTK and 11421 BPK respectively, by the year 2015-16 (MORTH 2012b). The annual growth of traffic is 8 to 10%. Motor vehicle population has grown from 0.3 million in 1951 to 115 million during 2009-10 (Fig 1.1). During the same period, the road network has expanded from 0.4 million km to 3.3 million km, i.e. only an 8-fold increase in road length (MORTH 2012c).

There has also been a tremendous pressure on road surface due to rapid growth of road vehicles and considerable increase in freight traffic with higher load carrying capacity. This has led to earlier failures of road surfaces (Sharma et.al 1995). Roads in India are poorly maintained and the damaged surfaces are not repaired properly. It is important to note that the naturally available road materials are being depleted day by day and there is an urgent need for such material(s) which serves as an alternate to depleting natural road materials and should also enhance engineering property of pavement surface.

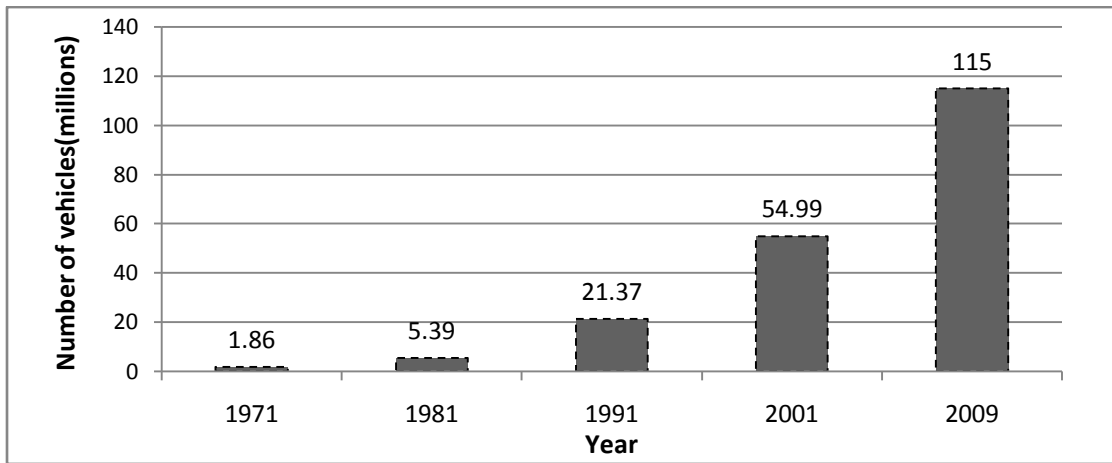


Fig 1.1 Increase in Vehicle population in India

(Source: Annual report 2011-12, Ministry of Road Transport and Highways, GOI, New Delhi)

India, having one of the largest road networks, consists of National highways, Expressways, State highways, major district roads, other district roads and village roads. The length distribution of each type of road is given in Table 1.1.

Table1.1: Indian Road Network

(Source: Annual report 2011-12, Ministry of Road Transport and Highways, GOI, New Delhi)

Type of Roads	Length
National Highways/Expressway	71,772 km
State Highways	1,54,522 km
Major District Roads	2,66,058 km
Other District Roads & Rural Roads	36, 17, 240 km

Indian Road Congress has formulated the Vision 2021 for the road development in the first two decades of the 21st century for the country as a whole and proposed that all our National highways should have a minimum of two lane carriageway with hard shoulders and half of the total National highways network should have four/six lanes. Further, it is recommended to expand the present National highway system to 80000 km by the end of the year 2021 and the entire length of State highways should be of minimum two lane standards. Out of this, some segments should be with additional hard shoulders and 10,000 km to be having four lanes.

1.2 RIGID PAVEMENTS

Concrete perhaps is the most versatile construction material in use all over the world. The versatility is attributed to its mouldability. Concrete pavements are well known rigid pavements. Concrete roads, on techno-economic considerations, are far superior to bituminous roads and will prove to be sustainable in future road construction. Many experts are of the opinion that, concrete roads would have to be given serious consideration, for arteries of national road network, which carry a high volume of traffic with increase in axle loads (Chakravarthy and Kadiyali 1989, Bhattacharya 2005). Concrete roads are more attractive in case of Expressways, Bypasses and urban roads. Concrete roads are also preferable for coastal areas bound by hills having high rainfall, more curves and for high and low traffic rural roads (Bhattacharya 2005).

Concrete roads have number of advantages over bituminous roads. Concrete roads do not deflect under heavy loads like flexible pavements. Hence, vehicles require less energy (fuel requirement) while travelling on concrete road. As per the trials carried out by Central Road Research Institute (CRRI), trucks consume 15-20% less fuel on concrete roads (CMA 2007). Heavy trucks get up to 20% better mileage on concrete surfaces. The concrete roads require very little maintenance (CPAM 2012). Increased speeds of vehicles on concrete road reduce congestion and traffic jams. The concrete roads are neither damaged by rain nor distorted by excessive heat. The construction of modern highways require huge amount of natural resources such as stones and natural sand. The design life of bituminous roads may be 10 years with proper maintenance which create huge burden on natural resources (CMA 2007). Concrete roads will have

longer maintenance-free life which reduces the impact on nature (Chakravarthy and Kadiyali 1989). Concrete pavements reflect 33 to 50% more light than asphalt surface (CAC 2012). It offers a better visibility on rainy nights (CPAM 2012). Concrete provides better and durable skid resistance. Hence, they provide safety for the drivers. It is generally less slippery in wet weather than bituminous pavement (CPAM 2012). Concrete pavements promote utilization of industrial by-products like fly ash and slag (Naik 2008).

Over the years, concrete pavement design has become a more important part for promotion of concrete roads. A high initial investment has to be motivated and the benefits of a pavement with less maintenance over a design life (generally designed for 30 to 40 years), have to be proved before construction. Efforts are on to avoid premature performance failure of concrete roads at a larger degree and to consider the other pavement alternatives as rehabilitation techniques are expensive. The design methodology has to take into account the change of environmental conditions as well as traffic growth. The optimal utilization of materials in the pavement structure demands for long-term fatigue resistance at the lowest cost and eco-friendly material.

1.2.1 Rigid Pavements- in Indian Context

Till the mid 90's barring a meager 1%, all the Indian roads were flexible pavements. Since mid 90's, rigid pavements have caught the attention of Indian Road Engineers as an attractive alternative. The first major concrete highway was built in 1960 (Agra-Mathura road). The second one was 60 km, two lane stretch of concrete road between Delhi and Mathura constructed during 1990. Then in the late 90's – a six lane 95 km Mumbai –Pune Expressway boosted the construction of concrete roads. As a part of improvement of country's infrastructure facilities, the Government of India has constituted prestigious National Highway Development Project (NHDP), which was initially involved in converting the existing two lane National highways into four lanes. The project involved 5846 km of Golden Quadrilateral connecting four metros and 7300 km of North-South–East-West corridor. NHDP has decided to construct concrete road over 1100 km of Golden Quadrilateral. (www.Indiainfra.com/article/25845/issue149)

In India, the cement production scenario is encouraging the adoption of concrete pavement instead of bituminous pavement as the raw materials for cement, like limestone is available in plenty. The bitumen obtained from the imported crude oil is likely to reduce in the near future and will hamper the maintenance of bituminous roads. Road traffic in India is increasing exponentially and also due to lack of multi-axle vehicles, axle loads are going up. Trucks in India carry loads much higher than the legal limits and are responsible for poor road conditions. This has resulted in severe damage to the road system, which has led to further maintenance problem (Sharma et.al 1995). As per recommendations of IRC on rural roads, concrete pavements offer an alternative to flexible pavements where the soil strength is poor, the aggregates are costly, and drainage conditions are poor as in the portions of the roads passing through villages and waterlogged areas (IRC: SP:62-2004).

1.2.2 Spectrum of Concrete in Rigid Pavement

A giant stride made by concrete technology has resulted in a spectrum of concrete that constitute Plain Cement Concrete (PC), High Density Concrete (HDC), High Performance Concrete (HPC), Fiber reinforced concrete (FRC), Light weight concrete (LWC), Self compacting Concrete (SSC) and so on, opening vistas for a wide and varied range of possible application.

1.2.3 Fiber Reinforced Concrete

Normal or conventional concrete containing discontinuous discrete fibers is known as Fiber Reinforced Concrete (FRC). Fibers of various shapes, sizes, and materials can be used in FRC. Ordinary concrete contains numerous micro cracks and rapid propagation of micro crack under flexural tensile stress which is responsible for low strength of the material. Concrete is a brittle material which will not carry loads under pure bending when cracked and fails suddenly when deflection corresponding to ultimate flexure strength is exceeded. By incorporating fibers, FRC continues to sustain considerable loads even at deflection in excess of failure deflection of plain cement concrete. The most significant influence of the incorporation of steel fibers in concrete (SFRC) is to delay and control the tensile cracking of the composite material. This positively influences the mechanical properties of concrete. Laboratory studies

on SFRC specimen suggests that dispersion of steel fibers in concrete improves mechanical characteristics of composite, resistance to dynamic loading, fatigue resistance and post cracking strength (Johnston and Zemp 1991, Lee and Barr 2004). Thus, the SFRC is much tougher and more resistant to impact. Magnitude of improvement in toughness is influenced by fiber concentration, fiber aspect ratio (length to diameter ratio) and shape (surface texture) (Mehta 1997). Fiber reinforcement improves structural durability, reduces the number of joints, and enhances the fatigue resistance of concrete structures (Zhang and Stang 1998).

1.3 FLY ASH

Fly ashes are finely divided residue resulting from the combustion of powdered coal. They are generally finer than cement and consist mainly of glassy-spherical particles as well as residues of hematite and magnetite, char and some crystalline phases formed during cooling. Use of large-scale coal firing for power generation began in US in early 1930's. Davis, R. E. at University of California presented the first comprehensive study on fly ash (FHWA, 2012). The current annual production of coal ash worldwide is estimated around 600 million tonnes, out of which 500 million tonnes being fly ash and the disposal of such a large amount of fly ash has become a serious environmental problem (Ahmaruzzaaman 2010).

In India, thermal power plants produce $2/3^{\text{rd}}$ of the electricity demand of the country. Coal is a dominant fuel for thermal stations in India, where 565 mines are operated by Coal India and other subsidiaries. Nearly 130 thermal power stations are operative (Fig 1.2) and utilize nearly 400 million tonnes of coal annually with an increasing rate of 2.25% per annum (Planning Commission Report, 2011a). In the process of generation of electricity using combustion of coal, 110 million tonne of fly ash is produced every year, which may exceed 170 million tonne by year 2020 AD (Dayal et. al 1999). This huge quantity of fly ash requires large valuable agricultural land for storage (presently around 113 million m^2) and poses severe environmental degradation and other serious problems in the form of land uses, health hazards etc. in the near future. Both in disposal, as well as in the utilization, utmost care has to be taken, to safeguard the interest of human life, wildlife and environment. Presently,

majority of the coal ash generated is being handled in wet form and disposed off in ash ponds, which are harmful for the environment and moreover ash remains unutilized for gainful applications. It has now become essential to find out ways and means for safe disposal and large-scale utilization of fly ash.



Fig 1.2 Geographical location of major thermal power plants in India
(Source: www.mapsindia.com)

In India, even after large number of research investigations on fly ash, only about 25% of total fly ash generated in the country was utilized mainly for manufacturing cement, bricks and construction of roads and embankments during the year 2003-04 (Ahmaruzzaaman 2010). The present utilization of fly ash is touching the mark of 40%, yet, the unutilized fraction is also growing considerably (Pattanaik and Sabat 2010). Therefore thermal power stations are under great pressure to find useful applications of fly ash. Table 1.2 shows some of the projects where fly ash is being used in NHAI's (National Highway Authority of India) road projects mainly for roads embankments.

Utilization of fly ash for useful purpose provides both economic and ecological benefits. In addition, use of fly ash in concrete improves its workability, reduces

segregation, bleeding, heat evolution, and permeability, inhibits alkali-aggregate reaction, and sulphate resistance. Due to its excellent pozzolanic properties, fly ash can be utilized as partial replacement of cement in preparation of concrete. (Tripathy and Mukherjee 1997)

Table1.2 Existing/Proposed projects of NHA utilizing Fly Ash
[\[http://www.crridom.gov.in\]](http://www.crridom.gov.in)

Sl. No	Name of the project	Total quantity of Fly Ash proposed to be used (m ³)
1	kms 8.200 to 29.30 of NH-1 in Delhi	1.00 lakh
2	HALDIA Port Connectivity Project -4 laning of NH-41 from kms 0 to 52.7	11.80 lakhs
3	kms 470 to 483.33 & kms 0 to 38 of NH-2 in Uttar Pradesh.	3.35 lakhs
4	4/6 - laning of NH-6 in the state of WB from kms 17.60 to 72.00	32.35 lakhs
5	4/6-laning of NH-6 in the state of WB from kms 72 to 132.45	3.21 lakhs
6	DURGAPUR Expressway	9.00 lakhs
7	ALLAHABAD bypass on NH-2	67.32 lakhs

1.4 NEED FOR PRESENT INVESTIGATION

The vehicular population is increasing every year. Between 1951 and 2002, the vehicle population grew at a compound annual growth rate (CAGR) of close to 11 per cent. The CAGR rate of commercial vehicles during the same period was recorded as 7%. However, in the last decade this rate was about 8% (Planning Commission Report, 2011b). The number of vehicles with exceeding legal axle load (10.2T for single axle with four tyres and 19T for tandem axle with eight tyres) has also increased as the load carrying capacity of newer vehicles increased tremendously. However, the construction and maintenance methodology being older, the road conditions are poor which results in a heavy loss of revenue in the form of raw materials, fuel consumption, delay in transportation of materials etc. Well-designed cement concrete roads will overcome this deficiency. The only drawback of cement concrete road is higher initial cost.

The challenge for the civil engineering community in the near future will be to realize projects in harmony with the concept of sustainable development, and this involves

the use of high performance materials and products manufactured at reasonable cost with the lowest possible environmental impact. Even though concrete is the most widely used construction material worldwide, it is not an environmentally friendly material. The production of Portland cement, an essential constituent of concrete, releases large amounts of CO₂ into the atmosphere, i.e. about one ton of CO₂ for every ton of Portland cement produced. As CO₂ is a major contributor to the greenhouse effect and the global warming of the planet, the developed countries are considering very severe regulations and limitations on CO₂ emissions (Radhakrishna et al. 2009). The manufacture of Portland cement is the most energy intensive process. For each metric ton of Portland cement, about 5.5 million British thermal units (BTU) of energy is needed (Naik 2008).

In this scenario, the use of supplementary cementing materials (SCMs), such as fly ash, slag and silica fume, as a replacement for Portland cement in concrete presents one viable solution with multiple benefits such as reduction in greenhouse gas emission, energy consumption, cost effectiveness etc. for the sustainable development of the concrete industry. The most commonly available SCM worldwide is fly ash, a by-product from the combustion of pulverized coal in thermal power stations, considered as a “waste” product. However, research and development has shown that fly ash actually represents a highly valuable concrete material. One of the most important fields of application for fly ash is PCC pavement, where a large quantity of concrete is used and economy is an important factor for selecting concrete as pavement material.

Improved engineering properties of SFRC have implications for pavement design criterion, as SFRC has improved fatigue performance and flexural strength (Zhang and Stang 1998). Apart from the technical aspects, the economy is the main aim that design strives for. The SFRC is found to have a significant impact on economy of the pavements due to the possibility of providing less thickness, longer joint spacing, less maintenance cost and longer useful life compared to the plain cement concrete pavements.

1.5 RESEARCH OBJECTIVES

Available literature suggests that investigation on usage potential of FRC and Fly ash based concrete needs to be more thoroughly considered as data available, conclusions drawn from analytical and experimental studies on these aspects are inadequate for exploitation of these concretes in commercial terms especially in India.

Hence, the present work envisages investigating potential use of fly ash based concrete by the way of

- 1) Characterization of materials, design of mixes, determination of properties of wet and set concrete: workability, strength tests like Cube Compressive strength, Split Tensile strength, Modulus of Rupture, Modulus of Elasticity and Fatigue tests.
- 2) Parametric studies on steel fibers for inclusion in concrete (PQC)
- 3) Establishing fatigue behavior using S-N curve and probabilistic analysis of fatigue data.
- 4) Studying of the temperature effects on fly ash concrete and to establish the temperature distribution pattern across the slab.
- 5) Studying the behavior of steel fiber fly ash concrete slabs under centre and edge loading.
- 6) Interpretation of results and development of mathematical models for analysis and design.

1.6 SCOPE OF WORK

As pavement concrete mix design based on flexural strength requirement for pavement quality concrete, two grades of concrete mixes M_{30} and M_{40} were considered in this study for catering both low volume and high volume roads. Two varieties of steel fibers (short and long) mixed in equal proportion were used in preparation of SFRC in two volume fractions 0.5% and 1%. Addition of fly ash was limited to 20% and 40% of cement in replacement. Preliminary strength characteristics such as compressive strength, split tensile strength, flexural strength, and modulus of elasticity of different concretes have been estimated using tests as per relevant Indian Standards.

Repeated load tests were carried out on different concrete beam specimens using repeated load testing equipment. Fatigue life data were analyzed by plotting S-N

curves and establishing fatigue equations. Probabilistic approach was adopted to fit the fatigue data with two parameter Weibull distribution and to establish fatigue life of different materials. Further, goodness-of-fit test was carried out to show the validity of distribution model for the statistical description of fatigue life of plain and steel fiber concrete with fly ash.

Four different thicknesses of slabs 150 mm, 200 mm, 250 mm and 300 mm concrete with and without fly ash slabs were used to establish temperature distribution across the thickness. Stress due to linear and nonlinear temperature distribution was calculated and compared. Steel fiber reinforced slab specimen of 150mm thick, with and without fly ash, supported on elastic foundation modeled using steel springs were tested for strain under concentrated (patch) load at centre and edge. Using experiment result, critical stress in real time pavement slabs of different thickness was analysed using ANSYS software. The results are presented in this thesis.

1.7 ORGANIZATION OF THESIS

This thesis is organized into eight chapters followed by the list of references and Appendixes.

CHAPTER 1

The background on road network and the need for use of concrete roads in India; brief note on fly ash generation and the necessity of its utilisation; history of steel fiber reinforced concrete; necessity, objectives and scope of the research are presented in this chapter.

CHAPTER 2

In this Chapter, the most significant properties of concrete which affects the performance of concrete pavement are discussed. A comprehensive literature review has been carried out to collect adequate information about materials like fly ash and steel fiber concrete in concrete pavements. Information gathered about the research works carried out so far on flexural fatigue studies, thermal and finite element analysis are also presented.

CHAPTER 3

The details of various materials used during laboratory investigation of basic properties of concrete ingredients and the design mix for M₃₀ and M₄₀ concrete are presented in this chapter. Further, the laboratory tests and outcomes of concrete properties such as compressive strength, tensile strength, flexural strength, and modulus of elasticity which are significantly affecting the performance of concrete pavements are presented. This also includes the discussions about the effect of fly ash and steel fiber inclusion on these properties.

CHAPTER 4

This chapter deals with the equipment used, flexural fatigue test details, results of steel fiber reinforced fly ash concrete and discussions of the fatigue strength studies carried out on beam specimens at various stress levels. A probabilistic analysis is carried out on the test data to describe suitable life prediction models.

CHAPTER 5

This Chapter presents the temperature study carried out on the fly ash-cement concrete pavements. It includes the equipment and methods used to capture temperature across various concrete slabs, temperature profiles and establishing the equation for temperature profile. The comparative study of various approaches has been presented to calculate stress due to nonlinear temperature profiles.

CHAPTER 6

Experimental study of elastic deformation behaviour of the steel fiber reinforced fly ash concrete slab specimens have been carried out under central and edge loading. The results are compared using a software, ANSYS, and are presented in this Chapter.

CHAPTER 7

The pavement analysis and design for thickness of slab using proposed fatigue equation are presented in this Chapter. The thickness thus obtained is compared with IRC fatigue model. Total stress in pavement due to load and curling is also discussed.

CHAPTER 8

Observations and conclusions drawn based on the investigation; recommendations and scope for the future study are presented in this Chapter.

CHAPTER 2

REVIEW OF LITERATURE

2.1 GENERAL

A comprehensive review of literature was performed on concrete properties and utilisation of fly ash in concrete pavements. This chapter gives an overview of the background literature on the performance and durability properties of fly ash and steel fiber reinforced concretes. A review of research findings on fatigue analysis and various approaches in thermal analysis has been discussed in this section.

2.2 CONCRETE PROPERTIES

Concrete is a versatile construction material and has been used in many Civil Engineering applications, such as pavements, retaining wall etc. As the performance and deterioration of concrete pavement are related to the concrete properties, such as strength, modulus of elasticity, coefficient of thermal expansion, shrinkage and fatigue life, it is very essential to know the properties of concrete.

Concrete strength: Rigid pavement has a high degree of rigidity and resulting beam action enables rigid pavement to distribute loads over large areas of the subgrade (Fig 2.1). As a result of beam action, tensile stresses will be induced at the bottom or on the top layers. If the tensile stress induced is greater or equal to the flexural strength of concrete, cracks may form on the surface and then propagate into the depth of the slab.

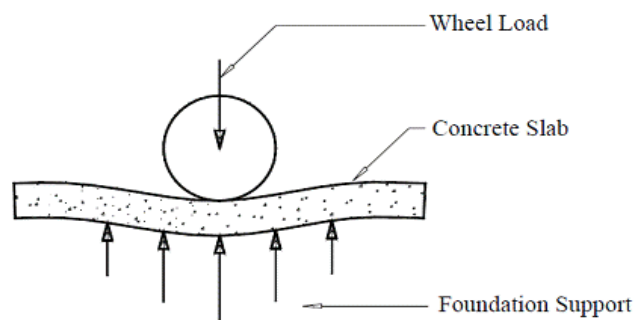


Fig 2.1 Transfer of wheel load to sub layer of pavement structure

Hence, flexural strength or modulus of rupture becomes an important property of concrete while designing the concrete pavements. However, the general practice is to design the mix based on cube compressive strength and the corresponding flexural strength is obtained from a well-established relationship between the characteristic compressive strength and the flexural strength.

A number of formulae has been provided by different agencies to estimate the concrete flexural strength.

According to the code IS 456: 2000 $fr = 0.7\sqrt{fck}$ ----(2.1)

According to the ACI 363(1992) $fr = 0.94\sqrt{fc}$ ----(2.2)

Flexural strength plays an important role in design of concrete pavements, a small change in predicting the strength can substantially change the critical failure mode and the thickness of the slab. A minimum flexural strength at 28days has been restricted to 4.5MPa for normal concrete pavements and 3.8MPa for rural roads (IRC 44, 2008).

Modulus of Elasticity: It is an important property to indicate the stiffness under static load. This mechanical property of concrete is highly dependent on the properties and proportions of binders and aggregates. Modulus of elasticity of concrete is frequently expressed in terms of compressive strength. Many empirical equations for predicting modulus of elasticity were proposed by many investigators (Neville 1995).

For normal density concrete:

According to the code IS 456: 2000 $Ec = 5000\sqrt{fck}$ ----(2.3)

According to the ACI 318-89(1992) $Ec = 4730\sqrt{fc}$ ----(2.4)

Thermal properties of Concrete: Thermal conductivity and diffusivity are important parameters while developing temperature gradients, and warping of concrete. Coefficient of thermal expansion is essential in case of pavement design in assessing the temperature induced stresses. The linear coefficient of thermal expansion of cement paste varies between 11×10^{-6} to $20 \times 10^{-6}/^{\circ}\text{C}$ and is higher than aggregate. Hence, the coefficient of thermal expansion of concrete is a function of content and type of aggregate and curing methods (Neville 1995).

Fatigue life: Fatigue is a type of failure of a structural element subjected to cyclic or repeated load each smaller than its static strength. Mechanical properties of hardened concrete, its composition and loading condition can affect the concrete fatigue life. Ratio of fatigue strength to static strength is independent of w/c ratio, cement content, type of aggregate, age at loading at a given number of cycles; fatigue failure occurs at the same fraction of ultimate strength. Hence, it is independent of magnitude of strength, age and material properties (Neville 1995).

2.3 SUPPORT IDEALIZATION FOR CONCRETE PAVEMENT

The structural behaviour of concrete pavement is affected by number of factors such as concrete properties; thickness and dimensions of pavement; joint spacing; load transfer devices; support condition; base/subbase type; thickness of slab; environmental condition; magnitude position and configuration of wheel load. Generally, concrete pavements are of finite length and width resting over base material (Dry Lean Cement Concrete). The subgrade idealization is one of the important stages in analyzing the concrete pavements. Westergaard's solutions for structural responses of a rigid slab resting on Winkler foundation have been widely used in the analysis and design of concrete pavement. Variety of subgrade idealization has been developed and employed in finite element method of analysis of rigid pavement. Dense liquid foundation (Winkler foundation) is most employed idealization where modulus of subgrade reaction (k) is the only parameter assumed to be constant during soil deflection under load (Khazanovich 2003). Spring model is another simple idealization in which the nodes at the bottom layer of the mesh are assigned discrete vertical spring stiffness (K) equivalent to a distributed spring foundation (Brill and Parsons 2001). Pasternak foundation allows the transverse connection in the supporting subgrade or subbase layer of a slab to be considered in addition to the modulus of subgrade reaction. The application of the improved model requires the determination of two foundation parameters, namely the modulus of subgrade reaction (k) and the foundation shear modulus, (G_b). Winkler foundation is a special case of the more general Pasternak foundation, where shear modulus is equal to zero (Fwa et al. 1996).

2.4 FLY ASH IN CONCRETE AND CONCRETE PAVEMENTS

Minimizing the environmental impact, energy and CO₂ intensity of concrete used for construction is increasingly becoming important as resources decline and the impact of green house emissions becomes more evident. Thus, it is logical to use life cycle and sustainable engineering approaches to concrete mix design. This requires several elements: maximizing concrete durability, conservation of materials, and use of waste and supplementary cementing materials. Waste and supplementary cementing materials, such as fly ash, blast furnace slag, silica fume, rice husk, and Metakaolin can be used as partial replacements for Portland cement. These materials can improve durability, reduce the risk of thermal cracking in mass concrete and are less energy and CO₂ intensive than OPC (Berndt 2009).

Fly ash is very fine, light gray and dust like ash which results from burning of powdered coal, found in suspension form in the air. Generally three types of fly ash are available. When powdered coal is burnt in the furnace of a power station, it produces a fine ash called fly ash, which is carried along with flue gases. Fly ash particles of silt size (0.074-0.005mm) are collected in electrostatic precipitators. About 80% of the ash produced is fly ash. The remaining ash sinters down to the bottom of the furnace. This coarse fraction is referred to as bottom ash. When both fly ash and bottom ash are mixed in water and pumped to ash ponds, it is called as pond ash.

Fly ash consists of inorganic matter present in the coal that has been fused during coal combustion. The major constituents of fly ash are oxide of silica, aluminum, iron, calcium, and magnesium. Fly ash consists of fine glassy spherical particles along with some crystalline matter and varying amount of unburnt carbon. Although fly ash does not generally have much cementitious property of its own, it reacts with alumina-silicates which have cementitious property. This is referred to as pazzolanic activity and it is attributed to SiO₂ and Al₂O₃ present in amorphous form. Bottom ash and pond ash are less pazzolanic in nature compared to fly ash.

Being fine particulate waste material, fly ash can be effectively used to replace part of cement in production of concrete. The fly ash collected in dry form contains reactive

silica which is a pozzolanic material whereas pond ash disposed in wet slurry form loses reactive particles. The reactivity of fly ash increases with fineness ($<45\mu$) and large particles contain crystalline inert materials due to slow cooling rate. (Mullick 2005a). The availability of good quality fly ash from modern coal fired thermal power plants has facilitated its use in Portland cement concrete both as extra ingredient as well as partial replacement for Portland cement. Use of fly ash in concrete not only economizes the mix, but also enhances the properties of green and hardened concrete (Binodkumar et al. 2007). Fly ash as a supplementary cementitious material has been studied extensively and observed that fly ash refines the micro structure of Portland cement matrix and thereby enhancing the durability. The reactivity of fly ash- lime mixture increases by optimization of fine particle range due to enlargement of surface area and enrichment of chemically active constituents (Malek et al. 2005). In 1980s CANMET developed high volume fly ash (HVFA) concrete, in which 55% to 60% of OPC was replaced by low calcium fly ash. This type of concrete has demonstrated excellent mechanical properties and durability characteristics (Bouzoubaa et al.1998; Desai 2004). Since then, many researchers have been trying to establish various factors that contribute towards utilization of industrial waste materials such as fly ash, ground granulated blast furnace slag (GGBFS) etc in Portland cement concrete.

The pore filling effect and pozzolanic properties of fly ash improve the properties of fresh and hardened concrete. Fly ash increases workability and requires shorter vibration time. At a given workability, addition of fly ash reduces the water demand of the concrete by 10 to 20% (Jiang and Malhotra 2000). Fly ash addition increases the fluidity of cement fly ash paste due to its particle size distribution and roundness, results in good pumpability and compactability (Yijin et.al 2003).

Heat of hydration of concrete can be reduced by the addition of fly ash thereby reducing thermal cracks. Use of pozzolanic materials, like fly ash and silica fume reduce plastic shrinkage. Distress due to drying shrinkage of fly ash concrete is less than 10% compared to conventional concrete (Ozyildiim et al. 1994). Differential shrinkage which can occur in concrete slab used for road construction can also cause warping or curling and tensile stresses. Reduction in shrinkage values of 30% has been reported for fly ash concrete when compared with OPC concrete (Atis 2003).

Volume change due to shrinkage is of considerable importance because in practice this movement is partly or fully restrained in concrete slabs laid on granular sub base which provides high friction and can cause high tensile stresses.

The fly ash has been reported to improve the mechanical properties, freeze–thaw resistance, sulphate resistance, alkali–silica reaction, and abrasion resistance, when it is used as a cement replacement material in concrete (Gencel et al. 2011). In addition, shrinkage and permeability of hardened concrete are decreased due to the filling of micro-pores by fly ash thereby reducing shrinkage cracks (Topcu and Canbaz 2007). Use of fly ash with small quantity of silica fume in concrete enhances the permeability property and also enhances the compressive strength (Obla et al. 2003).

Compressive and flexural strengths, drying shrinkage and abrasion resistance are the important properties of concrete which affect the design and performance of the concrete pavements. Many researchers (Naik et al. 2002; Binodkumar et al. 2007; Jerath and Hanson 2007) have studied the properties of fly ash admixed cement concrete and found fly ash concrete attained higher compressive and tensile strengths compared to OPC concrete . When fly ash was used as partial replacement for cement, compressive strength and flexural strength increased up to 10% at the age of 28 days. Fly ash concrete showed better abrasion resistance than OPC concrete (Naik et al. 1995). When dense graded aggregates are used in concrete, then the use of fly ash is beneficial as it requires less water content (Jerath and Hanson 2007).

Research findings revealed that fly ash is beneficial in the cases of corrosion of steel reinforcement, sulphate attack, alkali-silica reactivity which are major issues of durability. (Mullick 2005b). The durability of concrete mixtures against freeze and thaw and penetration of chloride ion can be increased by using fly ash content up to 45% in replacement of Portland cement without the loss of compressive or flexural strengths (Jerath and Hanson 2007). Some researchers, for instance, (Murthy and Ramesh, 2005) have contradicted this. Even though the permeability and chloride diffusion coefficient were increased to small degree by the use of fly ash, the concrete is still found to be durable (Bilodeau et al. 1994).

All the sources of fly ash may not improve the properties of concrete and it is necessary to test the compatibility with cement and other materials and the mix proportion before using it in construction sites. With the use of fly ash from certain sources, high strength concrete could be produced. It depends on the properties of fly ash, fly ash and cement content, compatibility with super-plasticizer used and the water/cementitious material ratio. At an early age, the use of fly ash in the concrete was found to be affecting the strength characteristics adversely. This reduction in early age strength could be retrieved to a large extent by adding fibers (Siddique 2004). Curing of fly ash concrete for a longer period shows a considerable improvement in strength. This increased strength may be due to formation of C-S-H gel by continued secondary and tertiary reaction between silica present in fly ash and hydroxide (lime) produced during primary hydration of Portland cement. Reactivity of fly ash increases with increase in temperature. This behaviour may be helpful in gaining more strength in the case of massive sections like pavements. The large temperature rise of concrete mass exerts temperature stresses and can lead to micro-cracks. When fly ash is used as part of cementitious material, quantum of heat liberated is low and staggers through pozzolanic reactions and thus reduces micro-cracking and improves soundness of concrete mass. The strength of concrete with fly ash as partial replacement for OPC up to 40% was found to be higher than OPC concrete at the age of 90 days (Atis 2003). Use of fly ash up to 50% reduces the initial cost of concrete road construction and it is suitable to use high volume fly ash concrete technology for concrete pavement (Srinivasan et al. 2004).

Different opinions were given by different researchers and codes about the quantity of fly ash that can be used in concrete. IRC 68-1976 provides the guidelines for design of Cement-Fly ash concrete wherein it suggests the usage of fly ash to replace cement(15-20%) and also the fine aggregate (about10%). According to Neville (1995), 25% to 30% of fly ash by mass of total cementitious material would be the optimum amount to achieve required performance. As per IS 456-2000 Plain and Reinforced cement concrete code of practice, fly ash (conforming to IS 3812 part 1) up to 35% can be used as part replacement of OPC in the concrete. Many such standard codes of practice recommend the same (AS3582.1-1998, ACI 318 Building

Code 2008). Coarser particles of fly ash act as micro-aggregates in filling the pores and improve the density of the concrete. This is beneficial with respect to strength and resistance to crack propagation and stiffness (Neville 1995). Use of coarser fly ash (pond ash) requires more water for maintaining constant workability (Mangaraj and Krishnamoorthy 1994). With the use of pond ash as sand replacement material (SRM), improved mechanical strength properties such as compressive, split tensile and flexural strengths and abrasion resistance can be achieved (Mangaraj and Krishnamoorthy 1994; Siddique 2003).

Research findings of the literature clearly indicated that fly ash addition enhances the mechanical strength properties of green and hardened concrete (Bouzoubaa et.al. 1998; Naik 2002; Desai 2004; Binodkumar et. al 2007). However, there are some contradictions that the addition of fly ash may affect adversely at an early age (Siddique 2004). The reactivity of fly ash depends on the type of fly ash, finer particle ranges, source and compatibility with other ingredients of concrete. There are different opinions about the quantity of fly ash that can be used effectively in concrete (Neville 1995, Atis 2003, IRC 68:1976, IS 456:2000), which lead to the need of research in this area as a part of large scale utilization of fly ash in India.

2.5 STEEL FIBER REINFORCED CONCRETE (SFRC)

Over the past 40 years, considerable research, development, and applications of SFRC are taking place in many parts of the world (ACI 544.1R-96, 1996). Addition of steel fibers to cement mortar or concrete leads to improvement in the following properties besides improving crack resistance and tensile strength of matrix (Nataraj et al 1999).

- a) Shear strength
- b) Spalling resistance
- c) Torsional strength
- d) Energy absorption
- e) Resistance to wear
- f) Durability
- g) Resistance to freeze and thawing
- h) Resistance to shock and dynamic loads
- i) Impact and fatigue strength

SFRC have been extensively used in industrial slabs, shotcrete for tunnels and pipelines and their use in pavements is negligible. SFRC provides additional strength in flexure, fatigue, impact, and spalling of base coarse of pavement. It is therefore, possible to reduce the thickness of the pavement and at the same time increase the

spacing of contraction joints. Due to the higher strength of SFRC, shrinkage cracks and warping cracks due to thermal stresses are also minimized. In recent years, the use of fibers for enhancing the mechanical properties of concrete has increased significantly (Bishoff 2003, Neocleous et al. 2006). The most of the researchers agree with the mechanical behaviour of SFRCs is the action of fibers on the process of cracking. The actual behaviour of fibers is either knitting together the cracks and delaying the crack propagation thereby improving the strength of the material or by transferring the forces across the micro-cracks created (like reinforcement in RCC) to impart ductility to the structure. Generally, first case requires short fibers and the second case need long fibers (>25mm) in small quantity. Commercially available steel fibers in the market are of size more than 25mm; and the ductility of the structure can be enhanced with these fibers.

The real contribution of the fiber is to increase the toughness of the concrete under any type of loading. Toughness is defined as some function of the area under the load vs. deflection curve. A concrete beam containing steel fibers suffers damage by gradual development of single or multiple cracks with increasing deflection, but retains some degree of structural integrity and post-crack resistance even under considerable deflection. A similar beam without steel fibers fails suddenly at a small deflection by separation into two pieces. Experimental investigations have indicated that the increase of the volume fraction of steel fibers contributed positively to the enhancement of the flexural toughness (Soulioti et al. 2011; Nataraj et al 1999). It is mainly due to the ability of fibers in arresting the cracks at micro and macro levels. Initially they arrest micro cracks and delay the crack initiation and then provide effective bridging at macro cracks.

The reinforcing fibers can be found in different shapes. Their cross sections include circular, rectangular, half-round, and irregular or varying shape. Fibers with non circular cross sections can be characterized by fiber intrinsic efficiency ratio to represent better fiber matrix reinforcing effectiveness. Steel fibers can be smooth, deformed, crimped, coiled and twisted with end hooks, paddles or other anchorages. They may be straight or bent, and come in various lengths (ACI 544.4R-88 1988). A number of studies have been carried out on relative effectiveness of different types of

steel fiber in concrete (Soroushian and Bayasi 1991; Bayasi and Soroushian 1992). The effect of fiber shapes and fiber volume fraction has been of great interest in recent years. A number of studies led to the development of new fiber geometries to optimize the fiber-concrete bond, reduce the rebound and offer high toughness in shotcrete. To enhance flexural behaviour of SFRC, it is essential to increase bond strength of concrete which depends on w/c ratio, fiber surface characteristic and aspect ratio. For normal weight concrete, fiber contents vary from as low as 30 kg /m³ to as high as 157 kg/ m³, although the high range limit is usually about 95 to 118 kg/ m³ (ACI 544.3R-93,1993). The most suitable volume fractions values for concrete mixes are between 0.5% and 2.5% by volume of concrete (Yazıcı et al. 2007). IRC: SP 46(1997) suggests fiber content of 0.75-1.25% by volume would be the optimum dosage for the steel fiber concrete pavements. It has given more emphasis on the research need and development of material for steel fiber reinforced concrete that could be used in pavement in future extensively.

Three bond components, such as mechanical, friction and interlock, could be optimized by adopting scientific approach for fiber cross section and geometry (Naaman 2003). Steel fibers made of deformed hot or cold drawn wire, after debonding, pulls out in their initial path with minor matrix internal degradation. The straightening of wires dissipate significant amount of plastic energy (Shannag et al. 1997). Corrugated wires are efficient in dissipating energy and thereby enhance the toughness of the concrete. The corrugated fibers impart ductility by getting large slip at peak load due to straightening of fibers along with increased load carrying capacity and enhanced pull out resistance. The maximum value of peak load depends on the mechanical anchorage and length of fiber (Chanvillard and Pierre-Claude 1996). Hooked fibers are effective in enhancing compressive and flexural strength compared to crimped fibers (Soroushian and Bayasi 1991). This may be due to occurrence of local damage in surrounding matrix during initial straightening of fibers when crimped one are used. Longer fibers are able to bridge the matrix cracks more effectively and consume more energy when pulled out. This leads to both higher strength and fracture toughness of the concrete. Bayasi and Kaiser (2001) had reported that the use of small diameter, closely spaced and randomly distributed steel

fibers are able to arrest cracks effectively. Study of literature on length of fiber had led to the opinion that different lengths of steel fibers in concrete slabs would dissipate higher energy at crack opening and may absorb energy at different stages of cracking.

Mechanical properties of SFRC depend on dispersion characteristics of the micro-reinforcement (Ferrara and Meda 2006). Uniformly dispersed fibers can impart higher strength and be effective in absorbing higher energy whereas poorly dispersed fibers may lead to poor performance both in fresh and hardened state. The cross section containing reduced amount of fibers may become critical and affect the structural behaviour. The average force transferred perpendicular to the crack depends on the number of fibers intersecting the crack (Stroeven 2009). Non alignment of fibers and stresses leads to reduced efficiency for stress transfer.

Fiber type, orientation and percentage of fibers and aspect ratio (l/d) significantly affect the workability of the mix. Fiber factor, the product of volume fraction, aspect ratio and steel- concrete interfacial friction, is an important parameter which governs the performance characteristics of SFRC materials. The improvements in mechanical properties in concrete due to the addition of steel fibers can be expressed as a function of fiber reinforcing index and concrete strength (Ghosh et al. 1989; Agarawala et al. 1996; Gao et al. 1997; Thomas and Ramaswamy 2007). Deflection hardening behaviour of steel fiber concrete in bending depends on fiber orientation and distribution (Kang and Kim 2012). Introduction of fibers into the concrete results in post-elastic property changes depending upon a number of factors, including matrix strength, fiber type, fiber modulus, fiber aspect ratio, fiber strength, fiber surface bonding characteristics, fiber content, fiber orientation, and aggregate size effects (Lok and Pei 1998). The effect of fiber volume fraction on bond strength and slip mechanism is insignificant when the volume fraction is less than 3%. The bond strength between fiber and concrete would be enhanced with the addition of fly ash or such materials (Naaman and Husamuddin 1991).

Many researchers through their experimental investigation indicated that there would be increase in compressive strength of concrete when steel fibers are used. The

enhancement in strength might be depending on several factors such as fiber volumes and aspect ratio (Williamson 1974; Yazıcı et al. 2007). This shows that fiber content and fiber aspect ratio are important parameters to enhance the mechanical strength properties. Preferred aspect ratios of steel fibers for the use in concrete pavements are 50-100 (IRC: SP 46-1997). Higher steel fiber content might increase the porosity thereby reducing the compressive strength (Russi 1994). Hence, it is essential to find out optimum dosage of steel fibers in concrete. For the given fiber content, steel fibers with lower aspect ratio yield better workability (Ramli and Dawood 2011). The influence of steel fibers on the flexural strength of concrete and mortar is much greater than in the case of the tensile or compressive properties of these materials. The use of steel fibers in concrete significantly increases the flexural strength of the material. Furthermore, an increase in fiber aspect ratio (i.e. fiber length/fiber diameter ratio) and fiber volume fraction, enhances the flexural strength of SFRC. SFRC imparts extra strength in flexural fatigue and impact, which are the properties needed for concrete pavement for highways (Bayasi and Kaiser 2001).

The addition of fibers with fly ash provides better concrete, as fly ash in the mixture may adjust the workability and strength –loss caused by fibers and improves strength gain (Topcu and Canbaz 2007). Atis and Karahan (2009) expressed contradictory opinion that there is no recovery in strength by fly ash when used along with steel fibers.

2.6 FLEXURAL FATIGUE CHARACTERISTICS OF PAVEMENT

Fatigue is one of the principal modes of failure to be considered in the design of structures subjected to repeated application of load such as pavements. The fatigue failure takes place under the influence of such repetitive or cyclic loads, whose peak values are considerably smaller than safe loads estimated on the basis of static load tests. The term fatigue applies to the progressive and permanent internal structural changes in material properties when subjected to repeated application of stress or loading. Usually, this change leads to cracking or failure. The failure may takes place in different forms:

- Fluctuation in applied stress results in mechanical fatigue.

- Cyclic loads in association with high temperature cause creep fatigue
- When temperature along with cyclic load fluctuates, this leads to thermo-mechanical fatigue.

In concrete, the fatigue is associated with progressive growth of internal micro-crack which results in a significant increase of irrecoverable strain. Fatigue loading can be classified as low cycle and high cycle loading. Low cycle loading involves the application of few load cycles at higher stress levels and high cycle loading is characterized by large number of load repetition at lower stress levels. Generally the concrete pavements for highway are subjected to more than 10^6 axle load repetitions and airport pavements subjected to 10^3 to 10^4 load repetitions during their design life and are classified under high cycle loading (Hsu 1981). Hence, fatigue strength of concrete is important parameter in designing concrete pavement for roads and airfields. Most common method of fatigue testing is by using flexural tests.

Wohler (1860) conducted systematic investigation of fatigue failure and the work led to characterization of fatigue behaviour in terms of stress amplitude-life (S-N) curve and the concept of fatigue endurance limit. The endurance in dynamic cyclic flexural loading is an important property of FRC, particularly in applications involving repeated loadings, such as pavements and industrial floor slabs. To establish flexural fatigue performance, testing can be conducted using reversing and non-reversing loading, with applied loads normally corresponding to 10 to 90 percent of the static flexural strength. Short beam specimens with small required deflection movements could be tested up to 20 cycles per second (cps) using hydraulic testing machines with adequate pump capacity and specimens with large deflections are need to be tested at reduced rates of 1 to 3 cycles per second to minimize inertia effects. Specimen testing at later ages might reduce the influence of aging when testing at the lower strain rates. Test results in the range of 60 to 90 percent of the static flexural strength for up to 10 million cycles have been reported for non-reversed loading to SFRC with 0.5 to 1.0% fiber content (ACI 544.2R-89).

Fatigue failure under fixed amplitude of cyclic stresses generally forms the basis for fundamental studies; service conditions in engineering applications invariably involve the exposure of structural components to variable amplitude spectrum loads, and low

or elevated temperatures (Murthy 2003). Most of the fatigue studies on concrete focus on constant amplitude loadings, but practically it occurs rarely and comprises stress levels of varying amplitude. In analyzing the influence of complex loading, the classical hypothesis of linear cumulative damage employing the S-N relation which can be obtained from constant amplitude fatigue loadings. The linear damage theory proposed by Palmgren and Miner is not directly applicable to the concrete subjected to stresses of varying amplitude where non-linear damage theory can be useful (Oh 1991a; 1991b). Fatigue life can be defined as the number of load cycles that can be repeated before failure. Fatigue behaviour and life prediction in concrete is extremely complicated due to influence of concrete composition (mix proportion) and environmental effects. Fatigue resistance of plain concrete structures can be considered based on type of loading

- Fatigue resistance of concrete in compression
- Fatigue resistance of concrete in tension
- Fatigue resistance of concrete in flexure

The concrete pavements generally are unreinforced and concrete has to resist tension in bending. This tension resistance in beam is termed as modulus of rupture (flexural strength). The concrete mix design for the pavements depends on this parameter. The development of reliable flexural fatigue life prediction model is one of the toughest challenges in research (Phull and Rao 2007). IRC:SP 46-1997 suggested S-N curve for flexural fatigue of fiber reinforced concrete based on experiments carried out at Central Road Research Institute (CRRI), as shown in Fig 2.2. Here, stress level is the ratio of applied stress to the static flexural strength of equivalent plain concrete without the fibers. But it is logical to define flexural fatigue behaviour of fiber reinforced concrete in terms of its static flexural strength rather than in terms of static strength of equivalent plain concrete (Johnston and Zemp 1991).

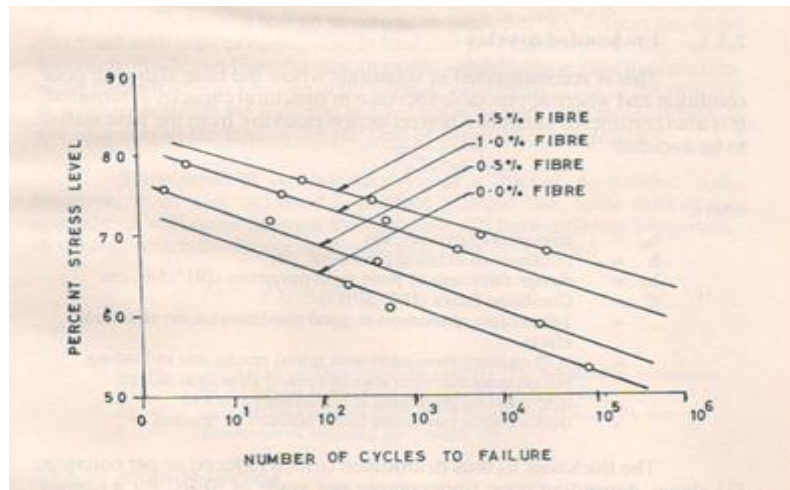


Fig 2.2 S-N curve for SFRC (Source: IRC SP: 46-1997)

Majority of the fatigue life prediction and design of FRC structures have been carried out empirically. Numerous factors such as different loading frequency, load sequencing, matrix composition, test configuration etc. affect the fatigue behaviour. The experimental data of various researchers indicated that, there would be significant spread of fatigue data and requires more attention during interpretation of trend line. The inclusion of fiber in to the concrete benefits the fatigue performance under flexural fatigue loading. In general, parameters such as loading conditions, load frequency, number of cycles, matrix composition, environmental condition and mechanical properties will influence the fatigue performance of concrete (Lee and Barr 2004).

A number of studies was conducted to evaluate fatigue performance of plain concrete (Hsu 1981; Shi et al. 1993) and steel fiber reinforced concrete (Johnston and Zemp 1991; Zhang and Stang 1998; Zhang et al. 1999; Singh and Kaushik 2003; Neito et al. 2006). The fiber material (steel or polypropylene) and type (hooked or plain) has no significant effect on fatigue performance, but increased fiber content improves the fatigue strength. The fatigue performance could be improved using steel fibers with optimum volume fraction of 1% when compared to plain concrete. Improvement in relative fatigue strength while adding 1% volume fraction of steel fiber was about 30% for 100000 load cycles (Zhang and Stang 1998). The fatigue life is dependent on micro-cracking, which in turn is dependent on micro-structure of concrete matrix,

water-cement ratio, size and proportion of aggregates and size, distribution and contents of fiber. It is also affected by bridging performance of fiber in fracture zone under fatigue loading. Hence, fatigue behaviour in flexure of fiber reinforced concrete can be predicted based on equilibrium of forces in critical cracked section (Zhang et al. 1999). Fiber contents of up to 1% volume improve performance, by raising the 100000 cycle endurance limit to 86% of ultimate stress. According to Johnston and Zemp (1991) fiber content is the primary governing parameter in enhancing the strength followed by aspect ratio and type. Increasing aspect ratio up to 75 is beneficial and beyond which it has little effect for the particular fiber type. Aspect ratio and fiber type may increase water demand thereby counteract the strength improvement. Fiber type has little impact on fatigue performance (Johnston and Zemp 1991).

The two-parameter Weibull distribution is an effective model to describe the equivalent fatigue life distribution of SFRC at a given stress level (Singh and Kaushik 2000; 2001; 2003). The variability in distribution of fatigue life was larger for higher fiber content, lower aspect ratio and lower stress levels (Mohammadi and Kaushik 2005). The scatter in mechanical properties of SFRC with higher fiber content, introduces large uncertainties in prediction of fatigue life. Damage mechanics model with irreversible strain increment would give reasonable fatigue life prediction (Alliche and Francois 1992). Use of stress ratio with the slab strength is more realistic than using beam strength values to define the fatigue life of concrete slabs, as in the case of pavements (Roesler et al. 2005). A small quantity of nano-particles such as nano TiO_2 enhances the fatigue performance compared to the plain concrete (Li et al. 2006). The presence of pores in concrete reduces the fatigue strength. The addition of fly ash to the concrete reduces the harmful pores with diameter larger than 200nm, thus enhancing the fatigue strength (Sun et al. 1997).

2.7 THERMAL/CURLING STRESSES IN CONCRETE PAVEMENTS

Temperature is one of the most important environmental factors affecting the design, functioning, and performance of both rigid and flexible pavements. This importance invites special interest and attention in research to develop temperature predictive

models and design methodology that accounts for temperature considerations. Temperature variations within the pavement structure contribute in many different ways to the distress and possible failure of that structure. Knowledge of temperature effects is essential for the determination of frequency and type of maintenance required throughout the service life of the pavement. The structural performance of pavements is highly dependent on the temperatures to which these pavements are exposed. Daily and seasonal variations of maximum, minimum, average, and gradient across the pavement depth must be considered in determining thermal stresses and design parameters of rigid and flexible pavements. The important factor is not the actual temperature at or near the surface, but the temperature gradients within the slab that can cause cracking of the slab of the rigid pavement (Ramadhan and Wahaab 1997).

In rigid pavements, temperature variations between the top and bottom of the Portland cement concrete layer result in temperature gradients across the depth which, in turn, results in differential expansions and tendency to curl. This curling tendency is restrained by the weight of the concrete slab and the support pressure from subgrade with the result that thermal stresses are induced in the slab material. These thermal stresses combined with the traffic load stresses may contribute to the pavement cracking, particularly during early age of concrete curing in the pavement structure. Depending on the position of the externally applied load and the time of the day, curling stresses can be sufficiently high causing failure of the slab (Yoder and Witczak 1975). Many studies on temperature distribution in flexible and rigid pavements were carried out, in different climatic areas of the world (Harik et al. 1994, Choubane and Tia 1992, Tang et al. 1993, Masad et al 1996). These studies were either of manifestations of temperature variations or attempts to incorporate temperature effects in pavement analysis and design.

The analysis of curling stresses in concrete pavement slabs was first carried out by Westergaard (1926). Under the assumption that temperature varied linearly through the thickness of a pavement slab, Westergaard (1926) derived solutions of curling stresses in slabs infinitely long in both X and Y direction supported on Winkler foundation. For a slab of finite dimensions, Bradbury (1938) derived an approximate

solution for estimating the maximum stress in the slab. Recently, there have been numerous efforts in improving the model of the interaction between slab and subgrade (Tang et al. 1993). Concrete expands and contracts with changes in temperature and moisture content. Temperature and moisture gradients through the vertical profile of a slab result in differential expansion and contraction between the top and the bottom of the slab. If the pavement slab is subjected to a negative temperature gradient through its thickness, with the temperature of bottom surface higher than the temperature of top surface, the slab tends to deform with its edges in an upward position resulting in a concave curvature (upward curl). The expansion of the top of the slab relative to the bottom, results in a convex curvature (downward curl) (Fig 2.3).



Fig 2.3 Upward and downward curling of concrete pavement

Curling of a concrete slab in the field is restrained by the slab's self-weight, shoulder and adjacent slabs through aggregate interlock, load transfer devices, and tie bars, and through non-uniform friction between the base layer and concrete slab (Poblete et al. 1987; Rao and Roesler 2005). The effect of transverse connection with the foundation could be modeled when Pasternak foundation is used instead of Winkler foundation in prediction of temperature stresses (Shi et al. 1993).

Major factors affecting curling stresses are i) temperature differential ii) self weight of slab and iii) support under the slab. As most of these factors are coupled, the analysis becomes more complex (Kuo 1998). The evaluation of curling stresses in concrete pavements requires the input of a temperature differential or even a temperature distribution between the top and bottom of slabs. However, the slab temperature fluctuates throughout a day with many weather factors, such as air temperature, sunshine, clouds, and rain. In addition, theoretical analysis of the induced stresses suggests the consideration of the total temperature distribution throughout the concrete slab depth rather than the temperature differential between the

extreme slab fibers. The present day analysis and design of rigid pavements for thermally induced stresses are based on the assumption of linear temperature distribution across the slab thickness (IRC 58:2000). But the studies revealed that the temperature distributions across the slab vary nonlinearly with slab thickness (Thompson et al. 1987, Choubane and Tia 1992). Different equations such as quadratic and higher degree polynomial equation were established to fit the field temperature data of pavement slab (Choubane and Tia 1995, Zhang et al. 2003). The studies carried out by Choubane and Tia (1992) have shown that the errors in the computed maximum curling stresses caused by the assumption of linear temperature distribution was as high as 30% or more. However, Masad et al. (1996) reported that the difference in tensile stresses between two distributions was approximately 3-13% of the modulus of rupture of concrete. During daytime condition, the maximum computed tensile stresses using linear temperature gradient in the concrete slab would be higher compared to that with the consideration of the effects of the nonlinear temperature distribution (Choubane and Tia 1995). Hence, Nonlinear temperature distribution across the pavement thickness might govern the critical stress analysis. Use of fly ash reduces the effective temperature difference between surface and interior of concrete and thus, thermal cracking due to temperature differential can be avoided. (Ozyildirim et al. 1994).

2.8 FINITE ELEMENT ANALYSIS OF PAVEMENT

Finite element packages are extensively used to solve complex engineering problems in several areas like structural, thermal, mechanical, electrical etc. In general, finite element packages are grouped into 2 categories. General purpose software such as ANSYS and ABAQUS have a powerful nonlinear dynamic analysis capability with specific modules for concrete pavement using thin plate theory. Other packages like ILLISLAB, JSLAB, WESLISLAB, WESLAYER, FEACONS, KENSLAB and HIPERPAV are specific software for analyzing the concrete pavements using thin plate theory. Programs like ISLAB2000, JSLAB, WESLIQID and FEACONS are able to consider linear and non linear differential temperature gradient along the depth of concrete slab. EverFE is 3-D finite element analysis software developed at Washington and Maine Universities to simulate the jointed concrete pavement under

axle and environmental effects (Davids 2003). Many researchers adopted three dimensional FE model to analyze the thermal effects on rigid-pavement (Choubane and Tia 1995; Kuo 1998; Mahboub et al. 2004; Kuo and Huang 2006). Experimental and analytical data reported by various researchers suggest that temperature fluctuations produce a significant amount of stresses and strains in concrete pavements (Armaghani et al. 1987; Faraggi et al. 1987; Hudson and Flanagan 1987; Barenberg and Zollinger 1990). Temperature gradient in a rigid pavement slab is also related to fatigue damage. A gradient of 1°F/inch in the slab increases the fatigue damage due to truck traffic by a factor of 10 compared to that of a zero temperature gradient condition (Masad et al. 1996; Ahmad et al. 1998).

Kuo and Huang (2006) used a three dimensional (3D) finite-element model 3DPAVE developed with ABAQUS, a multipurpose structural analysis package to simulate curling. Subroutines of the three-dimensional finite element analysis in the ABAQUS package were developed for nonlinear behaviour of a coarse-grained base and subgrade of the pavement. A three-dimensional (3D) finite element pavement model was developed by Mahboub et al. (2004) using the ANSYS program for predicting the stresses and strains in the concrete slabs. The temperature-induced pavement responses were more significant than traffic-induced responses (Mahboub et al. 2004). Choubane and Tia (1995) developed an analytical tool, a FEACONS IV, at the University of Florida to analyze the response of a concrete-pavement system subjected to a combination of applied loads and temperature changes to compute the bending stresses in the case of a linear temperature distribution across the concrete pavement depth.

2.9 HEAT TRANSFER MECHANISM IN PAVEMENTS

The rigid pavement temperature-depth relationship is complex. However, pavement temperature is directly related to air temperature and solar radiation but varies considerably with depth. Under field conditions the sun's rays (radiant energy) strike the exposed surface of the concrete pavement; part of the radiation is reflected, part is absorbed, and part is transmitted. Fig 2.4 explains the heat transfer in concrete pavements. As the absorbed thermal energy warms the roadway's surface, convective

heat transfer, along with the incident, emitted, and reflected radiation, raises the ambient air temperature. As the air circulates, it further warms or cools the surface of the slab through convection. The transmissivity of a body is the fraction of incident energy that travels straight through the slab. The availability of solar energy at a particular spot on the earth's surface depends on the latitude, season, time of day, and prevailing weather conditions (Adkins and Merkley 1990).

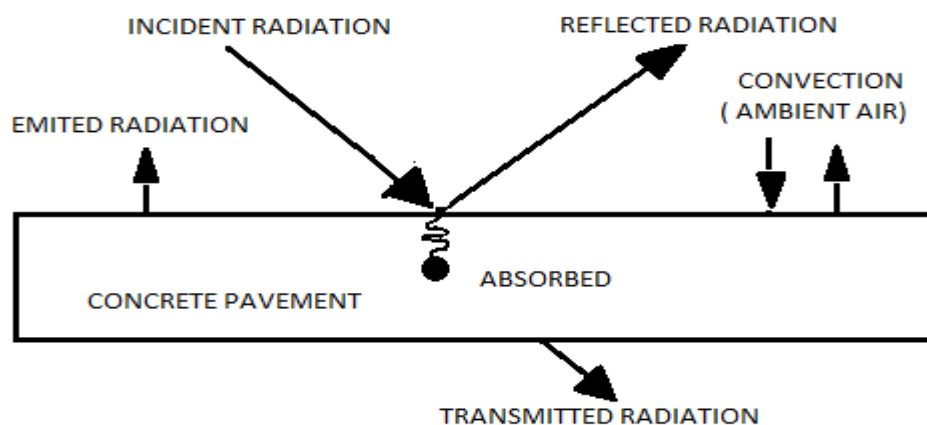


Fig 2.4 Heat transfer in concrete pavements

The relationship between average temperature differential (DIFF) and corresponding air temperature (AIR) was established by statistical model based on field temperature data and it could be fairly represented by linear regression equation (Adkins and Merkley 1990)

$$\text{Temp DIFF} = 0.248 * (\text{AIR}) + 1.577 \text{ with } R^2 = 0.81$$

The maximum temperature differential variation curve has a sinusoidal shape and there are two times of zero differentials, when the top and bottom temperatures are equal: one in the morning hour and another in the afternoon (Ramadhan and Wahaab 1997).

2.10 ANALYSIS OF NON-LINEAR TEMPERATURE DISTRIBUTION

Thomlinson (1940) proposed the importance of nonlinear temperature distribution across the thickness of a pavement slab. The total thermal stress can be split into three components (Fig 2.5). As per the classical theory of thick plates, the planes perpendicular to the plane of bending remain plane after bending, these three

components of stresses can only result in axial or bending stress in the plate. (1) The stress due to uniform temperature profile resulting in expansion or contraction of slab. Resistance to such movement of the slab is the friction offered by underneath layer of sub base/base or by adjacent slab can generate stress (Fig 2.5a). (2) The stress due to linear temperature gradient through the thickness causes bending of slab in the same manner of classical bending theory. Restraint to this bending is the self-weight of slab, external loads and the subgrade reaction (Fig 2.5b). (3) The final component is the stress due to nonlinearity of the temperature distribution (Fig 2.5c). This is an internal stress due to imaginary external forces that balances each other, so that net force in any section is zero. It contributes to the tensile or compressive force at top and bottom surface of the slab but it does not affect the deflection of slab (Ioannides and Khazanovich 1998). This component of stress termed as self-equilibrating (Hiller & Roesler 2010) or residual stress (Mohamed and Hansen 1996). Thus the actual temperature profile across the thickness can be expressed as the individual temperature components

$$T(z) = T_{axial} + T_L(z) + T_{NL}(z) \quad \text{--(2.5)}$$

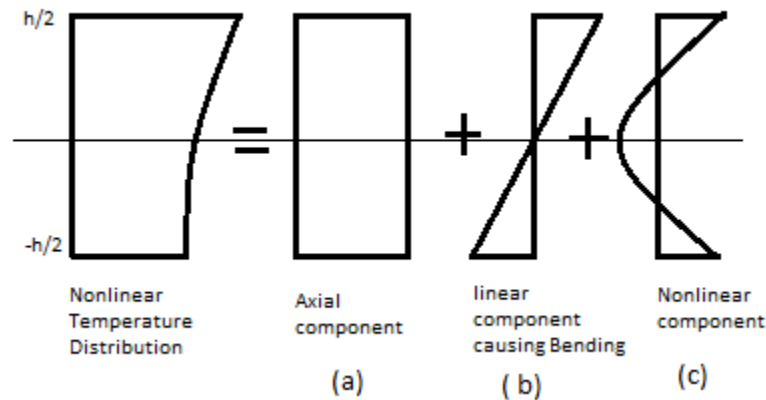


Fig 2.5 Three components of Non linear Temperature distribution

In conventional method, the axial movement of slab is unrestrained with the help of polythene sheet and expansion joints, keeping the axial stress minimal (IRC: 58-2000). The stress due to linear temperature distribution was well established by various researchers. Westergaard (1927) developed equation for infinite slab over

dense liquid foundation. The maximum stress in the concrete slab due to temperature differential Δt ,

$$\sigma = \frac{E\alpha\Delta t}{2(1-\mu)} \quad \text{-- (2.6)}$$

Where E – modulus of elasticity of the concrete,

α – Coefficient of thermal expansion of the concrete

Δt – Linear temperature difference between top and bottom surface of slab

μ – Poisson's ratio

Bradbury(1938) later modified the above equation for slab of finite dimensions in both direction with modification factor

$$\sigma = \frac{E\alpha\Delta t}{2(1-\mu^2)} (C_x + \mu C_y) \quad \text{--(2.7)}$$

where C -the Bradbury coefficient can be written as

$$C = 1 - \frac{2\cos\lambda\cosh\lambda(\tan\lambda + \tanh\lambda)}{\sin 2\lambda + \sinh 2\lambda}$$

$$\lambda = \frac{L}{l\sqrt{8}}$$

L = length or width of slab

l = radius of relative stiffness defined as $l = \sqrt[4]{\frac{Eh^3}{12(1-\mu^2)k}}$

h = thickness of slab

E = Modulus of elasticity of concrete

k = modulus of subgrade reaction

Adhering to the basic assumption that the cross section of a plane remains plane under the action of thermal loading, the stresses caused by the nonlinear part of the temperature distribution can be computed as those generated as if the slab were restrained from any form of deformation (Choubane and Tia 1995). Thus, the stress $\sigma_{\text{nonlinear}}$ caused by this nonlinear part can be obtained as follows:

$$\sigma_{\text{nonlinear}} = -E\alpha t_{\text{nonlinear}} \quad \text{----(2.8)}$$

where

E =elastic modulus of concrete;

α =coefficient of thermal expansion;

$t_{\text{nonlinear}}$ =nonlinear part of the temperature.

The final solutions obtained by superposition of the stresses caused by the three components of temperature distribution.

2.11 DIFFERENT APPROACHES FOR ANALYSING NONLINEAR TEMPERATURE GRADIENT

The temperature distribution within the slab is mostly non-linear. The total stress due to the critical thermal loading condition could be obtained by adding algebraically the stresses due to linear temperature and loading condition to the stresses due to non-linear component of temperature. For finite slab, maximum stress can be calculated by approximate formula, which uses plate theory on elastic plate resting on Winkler foundation. It serves as a general elastic solution and applies not only concrete but also to other materials (Tang et al. 1993).

The effect of non linear temperature profile can be determined by analyzing the residual stresses in concrete pavements subjected to non-linear gradients throughout the slab thickness. Most of the researchers (Choubane and Tia, 1995; Mohamed and Hansen 1996; Hiller & Roesler 2010) agreed that the analysis of non linear temperature distribution can be done in two parts: a) calculation of self equilibrated stresses within a cross-section due to internal restraints (i.e. by satisfying equilibrium conditions and continuity of the strain field within the cross-section) b) calculation of the stresses due to external restraints (i.e. self-weight and subgrade reaction). The maximum computed stresses in slab using conventional linear temperature distribution tend to be overestimated at day time and underestimated for night condition compared to non-linear temperature distribution (Choubane and Tia, 1995). Similar observations were made by Mohamed and Hansen (1996). Hence, the real temperature distribution along the slab depth was important in the analysis of the effect of temperature variation, but not the difference in temperature between the top and bottom surfaces of pavement slabs, which is the basic input in the analysis by linear temperature distribution assumption. The actual nonlinear temperature distribution, instead of the conventional linear temperature distribution assumption should be used for concrete pavement design and evaluation (Liu and Fwa 2003, Zhang et al. 2003). In the case of multilayered concrete pavement systems concept of equivalent

temperature distribution could be used (Ioannides and Khazanovich 1998). However, the approach is complex and require finite element method.

2.11.1 NOLA Concept

A simplified method termed NOLA, or nonlinear area, to incorporate the effect of temperature nonlinearity on rigid pavement responses was proposed by Hiller and Roesler (2010). A parameter named NOLA (Nonlinear area) was adopted to directly relate self equilibrating stress to the degree of nonlinearity in any given temperature profile. It is defined as the area between actual temperature profile $T(z)$ and assumed linear temperature profile (using top and bottom temperature).

Mathematically NOLA is expressed as
$$NOLA = \int_0^h (T(z) - \frac{\Delta T}{h} z) dz$$

$$\text{Solving} \quad NOLA = \frac{2(TM-TB)-(TT-TB)}{3} h \quad --(2.9)$$

where TT, TB, TM are the temperatures at top, bottom and mid depth of the slab

$$\text{And self equilibrating stress } \sigma(z) = \frac{-6NOLA E\alpha (z^2 - hz + \frac{h^2}{6})}{h^3(1-\mu)} \quad --(2.10)$$

$$\text{at top and bottom } \sigma = \frac{-NOLA E\alpha}{h(1-\mu)}$$

$$\text{at mid depth } \sigma = \frac{-NOLA E\alpha}{2h(1-\mu)}$$

2.11.2 Temperature Moment (TM) Concept

Though linear temperature gradients are both easy to determine and easy to visualize, they are not an accurate quantification of the actual temperature profile. A procedure for quantification of a pavement temperature profile called the temperature-moment for the analysis of pavement temperature profile data was proposed by Janssen and Snyder (2000). Here, temperature-moment is the summation of the individual moment of temperature area about the bottom surface. The entire temperature profile is divided into small areas and temperatures of such areas are defined as the difference between average temperature of that area and the average temperature of the profile (Fig 2.6).

$$\text{Mathematically,} \quad TM = \sum_{i=1}^n \text{Area}_i \times R_i$$

Where, R_i is the arm distance from bottom of the slab to the CG of the area considered

The TM has direct relationship with equivalent linear temperature ΔT_{eq} which gives the same moment as nonlinear temperature profile.

$$\Delta T_{eq} = \frac{-12TM}{h^2} \quad \text{and} \quad T_L(z) = \frac{\Delta T_{eq}}{h} z$$

Finally, $T_{NL}(z) = T(z) - T_{Axial} - T_L(z)$ and

$$\text{Self equilibrating stress } \sigma = \frac{-E\alpha T_{NL}(z)}{(1-\mu)}$$

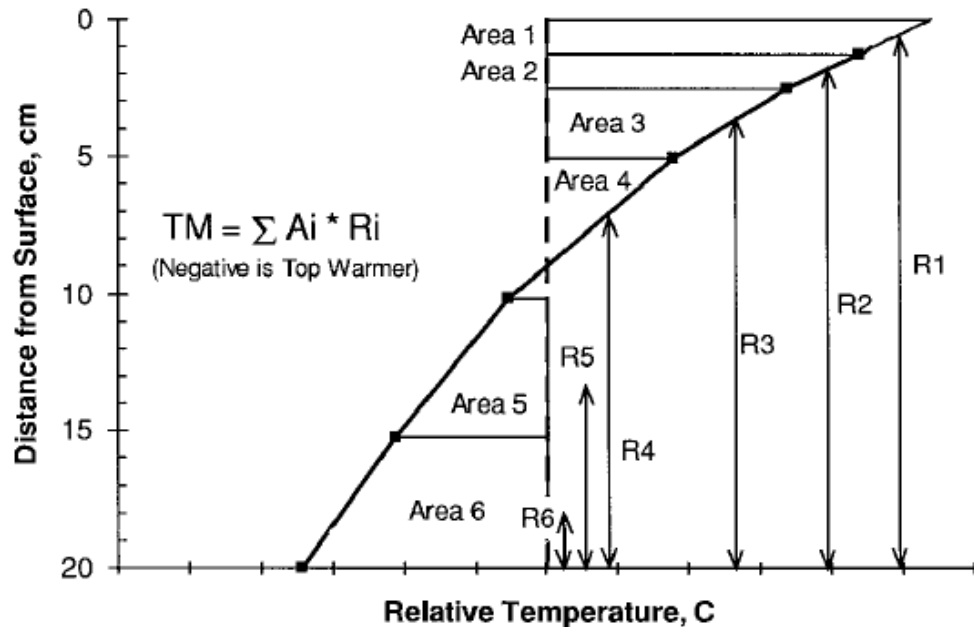


Fig 2.6 Temperature moment calculation (Janssen and Snyder 2000)

2.9.3 Ever FE Software

EverFE, is a special purpose code developed at the University of Washington. It is a 3-D finite element analysis tool for simulating jointed plain concrete pavement subjected to axle load and environmental effects. It is equipped with an efficient computational model to operate on personal computers. It can solve multiple slabs consisting up to nine slabs, with up to three base layers. EverFE is able to model wheel loading and temperature curling effects. There are five elements in EverFE finite element library. EverFE couples a highly interactive graphical user interface for

model development and result visualization written in object-oriented C++. EverFE is an effective finite element analysis tool which can handle linear and non-linear (upto 4 points) temperature distribution data.

2.12 SUMMARY

Concrete pavements are advantageous in the long run as the maintenance cost is negligible. In order to reduce the initial cost of construction, environmental impact of thermal plants and for sustainable development, utilization of fly ash, a waste product of thermal power plants in large quantity is essential in pavements. Use of fly ash reduce the water demand with graded aggregates and provide durability to the concrete. On the other hand steel fibers enhance the post cracking behaviour of concrete and enhance the flexural strength. The review of literature reveals the need for the development of sustainable material for the future Indian roads. Researchers have studied fly ash concrete and fiber reinforced concrete separately; however, reinforcing of hybrid fibers especially steel fibers with fly ash in concrete is the area that needs more investigation. A detailed laboratory investigation is required to characterize these materials and to address the important parameters like temperature variation, fatigue characteristics and wheel load distribution at different locations of pavement for different cross sections. These aspects have become objectives of this study.

CHAPTER 3

EXPERIMENTAL WORK AND RESULTS

3.1 INTRODUCTION

This chapter describes details of the experimental work conducted in the present investigation. Preliminary test results on constituent materials, concrete mix design, preparation of test specimens and test results of fresh and hardened concrete are discussed. Experimental set up for repetitive load test (Fatigue test), temperature and load-deformation study are discussed in later chapters.

3.2 PRELIMINARY INVESTIGATION OF MATERIALS

3.2.1 Cement

Cement is one of the important constituents of the concrete mix. For the present investigation Ordinary Portland Cement of 43 grade conforming to IS 8112:1989 was used. The properties of the cement used are given in Table 3.1.

Table 3.1 Properties of Ordinary Portland Cement used in this work

Sl.No	Test	Result (OPC)	Limits as per IS 8112-1989
1	Specific Gravity	3.14	-
2	Standard Consistency,%	30	
3	Fineness of cement (m^2/kg) (Blaine's air permeability)	300	>225
4	Setting time - Initial (minutes)	55	> 30
	- Final (minutes)	275	<600
5	Compressive Strength (MPa)		
	3 Days	28	23
	7 Days	35	33
	28 Days	48	43

3.2.2 Aggregates

Crushed stone aggregates (granite) of maximum size 31.5 mm (31.5mm to 4.75mm) was used as coarse aggregate and locally available river sand (<4.75 mm) was used as fine aggregate in this study. They were tested as per relevant Indian standard codes. The results are presented in Tables 3.2 to 3.4.

Table 3.2 Properties of Coarse and Fine aggregates

Sl. No	Test	Coarse aggregate	Fine aggregate	Method of Test, reference to
1	Specific Gravity	2.65	2.6	IS 2386 (P-III) -1963
2	Bulk Density a) Dry loose b) Dry compact	1480 kg/m ³ 1632 kg/m ³	1455 kg/m ³ 1729 kg/m ³	
3	Aggregate Crushing Value	24%		IS 2386 (PIV)-1963
4	Los Angeles Abrasion Test	27%		
5	Aggregate Impact value	16%		
6	Flakiness and Elongation index	28%		IS 2386 (P I) -1999

Table 3.3 Particle Size Distribution of Coarse aggregate

IS Sieve Designation (mm)	Percentage Passing	Remarks
40	100	Conforming to Graded aggregate Requirement as per IS: 383 – 1963
31.5	100	
25	84	
20	60	
12.5	25	
10	13	
4.75	1.30	

The fineness modulus of the fine aggregate was 2.74 (medium sand) and conforms to Zone II grading as per IS: 383 – 1963 requirement.

Table 3.4 Particle Size Distribution of Fine aggregate

Sieve Size(mm)	Percentage Passing	Grading requirement as per IS 383(1963) for Zone II	Remarks
10mm	100	100	Conforming to Zone II Grading requirement
4.75mm	99.45	90 – 100	
2.36mm	96.4	75 – 100	
1.18mm	75.65	55 – 90	
600μ	44.5	35 – 59	
300μ	9.35	8 – 30	
150μ	0.2	0 - 10	
Fineness Modulus : 2.74			

3.2.3 Water

Tap water available in the institute laboratory was used for casting and curing of all the specimens in the present investigation.

3.2.4 Superplasticizer

A commercially available sulfonated naphthalene formaldehyde (SNF) polymer based water-reducing admixture (“Conplast SP 430” supplied by FOSROC, Chemicals (India) Pvt. Ltd) was used as superplasticizer for present investigation. Properties of superplasticizer is given in Table 3.5

Table 3.5 Properties of Conplast SP 430

(source:FOSROC Chemicals(India) Ltd.)

Specific Gravity	1.20-1.25
Chloride Content	nil
Solid content	40%
Recommended dosage	5ml to 20ml/kg of binder
Operating Temperature	10 to 40°C
Color	Dark brown liquid

3.2.5 Fly ash

Fly ash procured from Raichur Thermal Power Plant (RTPS), Karnataka was used for the present investigation. RTPS generates about 1.5 million tons of fly ash annually. The chemical and physical properties of fly ash conforming the requirements of IS 3812 Part I & II (2003) are reported below in Tables 3.6 and 3.7

Table 3.6 Chemical Properties of Fly ash (Class F)

Source: RTPC, Raichur, Karnataka

Chemical Properties	Composition (%)	Requirement as per IS 3812(Part II) - 2003
SiO ₂	85.67	35% min
Al ₂ O ₃	5.62	SiO ₂ + Al ₂ O ₃ + Fe ₂ O ₃ combined 70% min
Fe ₂ O ₃	1.28	
CaO	5.33	
MgO	0.2	5% max
Na ₂ O	0.06	Total alkalies, 5% max
K ₂ O	0.07	
SO ₃	0.23	2.75% max
Loss of Ignition	1.54	12% max

Table 3.7 Physical Properties of Fly ash (Class F)

Characteristics	Results	Requirement as per IS 3812 (part I) - 2003	Method of Test, reference to
Lime reactivity (N/mm ²)	6.80	Min 4.5	IS1727-1967
Fineness (m ² /kg) (Blaine's air permeability)	350	320	IS 4031 (Part II) -1999
Specific Gravity	2.2		

3.2.6 Steel Fibers

In this study, two types of fibers, as shown in Fig 3.1 were used. One was the crimped round (CR) type with 30 mm length, 0.5 mm diameter and aspect ratio 60 and the other was crimped flat (CF) fibers with 50 mm length, 2.5 mm width, 0.5 mm thickness ($d_{eq}=1.25\text{mm}$) and aspect ratio 40. The properties of steel fibers (ASTM A820-11: source: Stewols India (P) Ltd., Nagpur, India) used are:

Tensile strength = 1000MPa,
Young's modulus = 2×10^5 MPa
Specific gravity = 7.86

The main idea of using two different lengths of fibers was to bridge both micro and macro cracks at different stages of crack propagation (Sorelli et. al 2006). These two types of steel fibers were mixed in equal quantities (50% each) to form hybrid mixture with total fiber content of 40 kg/m^3 (0.5% volume fraction) and 80 kg/m^3 (1% volume fraction). Steel fiber was procured from Stewols India (P) Ltd., Nagpur, India.



30mm long 0.5mm dia
crimped round (CR)

50mm long 2.5mm wide 0.5mm thick
crimped flat fiber (CF)

Fig 3.1 Steel Fibers

3.3 CONCRETE MIX DESIGN

Usual criterion for evaluating the strength of concrete in the construction industry is the compressive strength. However, in pavement constructions, such as highways and

airport runways, the flexural strength of concrete is considered to be more important, as concrete pavements fail due to bending stresses. Therefore, flexural strength is more often specified than compressive strength in the design of concrete mixes for pavement construction. Even though it is not reliable to predict flexural strength from compressive strength, some codes (IRC: SP: 62-2004) suggest using the mix design procedure by compressive strength values and obtain the flexural strength using well-established relation. A minimum M₄₀ grade of concrete (flexural strength of 4.5MPa) for normal concrete pavements and M₃₀ grade of concrete (flexural strength of 3.8MPa) for rural roads shall be used (IRC: 44-2008). Hence, in this study, mix proportions were designed for M₄₀ and M₃₀ grades of concrete based on the guidelines of IS: 10262-1978, SP 23-1982 and IRC: 44-2008. Ordinary Portland Cement (OPC) of 43 grade conforming to IS 8112-1989, crushed stone aggregates (31.5mm down) and river sand were used in the present investigation. The mix proportions for two grades of reference (control) concrete were arrived at based on the test results with number of trial mixes and are given in Table 3.8.

Table 3.8 Details of Concrete Mix Proportions

Sl.No	Mix Designation	Cement (kg/m ³)	Proportions C: F: CA	w/c ratio	Super plasticizer (% by wt of binder)	Compressive Strength (N/mm ²) (28days)	Slump (mm)
1	M ₃₀	375	1:1.65:3.10	0.48	-	45.0	45
2	M ₄₀	400	1:1.6:3.00	0.40	1.0	51.0	40

The mix design for SFRC is quite different from that of usual method adopted for ordinary concrete. Procedures for proportioning of SFRC mixtures, with emphasis on workability, are available (ACI 544.3R). However, many researchers used conventional mix design for SFRC (Ravishankar et al. 2006). Hence, in this study, steel fibers were added directly to the conventional mix proportions without considering any change in volume. To provide better workability of concrete, more paste is needed in the mixture. Therefore, superplasticizers are often used. The other factors which have a major effect on workability are aspect ratio (l/d) and volume

fraction of the fibers. In early applications, coarse aggregate larger than 19mm was not recommended for SFRC. However, larger aggregates upto 38 mm were successfully used (Rettberg 1986). The use of pozzolans such as fly ash and slag as partial replacement of cement, also improves the workability of SFRC (ACI 544.3R). The change in volume of concrete due to addition of fly ash was adjusted with the quantity of fine aggregate keeping coarse aggregate fraction constant. The quantities of various ingredients required per m³ of both M₃₀ and M₄₀ are tabulated in Table 3.9a and 3.9b.

Table 3.9a Different Ingredients/m³ of M₃₀ Concrete Mix

Sl. No	Type of Mix and Designation	C(kg)	Fly ash (kg)	FA (kg)	CA (kg)	W (kg)	Steel Fiber (kg)	
							Crimped round	Crimped Flat
1	Reference Concrete (R)	375	-	619	1163	180	-	-
2	Steel Fibre Reinforced Concrete 1 (HS1)	375	-	619	1163	180	20	20
3	Steel Fibre Reinforced Concrete 2 (HS 2)	375	-	619	1163	180	40	40
4	Fly Ash Steel Fiber Concrete 1 (FS1)	300	75	592	1163	180	20	20
5	Fly Ash Steel Fiber Concrete 2 (FS2)	225	150	501	1163	180	40	40
6	Fly Ash Steel Fiber Concrete 3 (FS3)	300	75	592	1163	180	20	20
7	Fly Ash Steel Fiber Concrete 4 (FS4)	225	150	501	1163	180	40	40
8	Fly Ash Concrete (FA20)	300	75	592	1163	180	-	-
9	Fly Ash Concrete (FA40)	225	150	501	1163	180	-	-

Table 3.9b Different Ingredients/m³ of M₄₀ Concrete Mix

Sl. No	Type of Mix and Designation	C(kg)	Fly ash (kg)	FA (kg)	CA (kg)	W (kg)	SP (kg)	Steel Fiber (kg)	
								Crimped round	Crimped Flat
1	Reference Concrete (R)	400	-	638	1200	160	4	-	-
2	Steel Fibre Reinforced Concrete 1 (HS1)	400	-	638	1200	160	4	20	20
3	Steel Fibre Reinforced Concrete 2 (HS 2)	400	-	638	1200	160	4	40	40
4	Fly Ash Steel Fiber Concrete 1 (FS1)	320	80	608	1200	160	4	20	20
5	Fly Ash Steel Fiber Concrete 2 (FS2)	240	160	580	1200	160	4	40	40
6	Fly Ash Steel Fiber Concrete 3 (FS3)	320	80	608	1200	160	4	20	20
7	Fly Ash Steel Fiber Concrete 4 (FS4)	240	160	580	1200	160	4	40	40
8	Fly Ash Concrete (FA20)	320	80	608	1200	160	4	-	-
9	Fly Ash Concrete (FA40)	240	160	580	1200	160	4	-	-

3.4 SPECIMEN DETAILS

In order to evaluate the strength characteristics and strength attaining behaviour of various mixes, specimens were tested at different ages viz. 7, 28, 56 and 90 days.

The details of the specimens used for various tests are given in Table 3.10

Table 3.10 Specimen Details for Various Tests (Each in M₄₀ and M₃₀ Mix)

No.	Types of test	Specimen type	Specimen dimension	No. of specimens
1	Cube Compression	Cubes	100*100*100	20
2	Third-point flexure	Beams	100*100*500	06
3	Split tensile strength	Cylinders	150(dia)*300(depth)	03
4	Modulus of elasticity	Cylinders	150(dia)*300(depth)	02
5	Fatigue strength	Beams	100*100*500	30

3.5 MIXING, PLACING AND COMPACTING CONCRETE MIX

The SFR Concrete is produced in a similar manner to that of conventional concrete. The only problem is to introduce a sufficient volume of uniformly dispersed fiber to achieve the desired improvements in mechanical behavior (Ferrara and Meda, 2006), while retaining sufficient workability in the fresh mix to permit proper mixing, placing, and finishing. One of the chief difficulties in obtaining a uniform fiber distribution is the tendency of steel fibers to ball or clump together. Most fiber balling occurs somewhere before fibers get into the mixture. This may be due to the following reasons (ACI 544.3R)

- i. The fibers may already be clumped together before they are added to the mix; normal mixing action will not break down these clumps.
- ii. Fibers may be added too fast in such way that they fall on each other and get stacked up.
- iii. Adding too high volume (more than 2% by volume or even 1% with high aspect ratio) of fibers.
- iv. Adding fibers to too harsh mixture (the mixture is not fluid enough or workable enough and fibers do not get mixed in faster).
- v. Introducing the fibers to the mixer before the other concrete ingredients will cause them to clump together.
- vi. Equipment with worn-out mixing blades

Mixing of concrete ingredients was carried out using a ribbon mixer of 125 kg capacity (Fig 3.2) as per IS 516-1959 specifications and sufficient care was taken to avoid balling of steel fibers.



Fig. 3.2 Addition of steel fibers to the concrete and mixing of concrete in a mixer

The prepared mix was then poured in to the cast iron moulds in layers and compaction was done simultaneously using a table vibrator for about 3 minutes. Then the specimens were allowed to cure in a humid and cool place with relative humidity 75-90% and at a temperature of $27 \pm 2^\circ\text{C}$ for about 24 hours. After 24 hours, the specimens were removed from moulds and allowed to cure in a curing tank.

3.6 CURING OF SPECIMENS

The curing was done by immersing concrete specimens in a tank containing water. The concrete specimens were cured for specified number of days (7, 28, 56 and 90 days) in the curing tank where water temperature was maintained at $27 \pm 2^\circ\text{C}$ until they were tested. Fig. 3.3 shows the curing of concrete specimens in a water tank.



Fig. 3.3 Curing of concrete specimens in a water tank

3.7 TESTS

3.7.1 Tests on Fresh Concrete

The tests on fresh concrete were conducted to know the level of ease in concrete mixing, compacting and moulding into required shapes etc. Workability is the term used to define these qualities of concrete. It is defined as the amount of useful internal work necessary to achieve full compaction. The size of aggregate, water/cement ratio and fiber content are important variables affecting the level of workability.

In the present investigation the level of workability was measured using slump cone test. A compaction factor of 0.8 was used for reference concrete during mix design which was obtained for a w/c ratio of 0.40 with 1% superplasticizer content for M₄₀ concrete, and with a w/c ratio of 0.48 for M₃₀ concrete. It was observed that the use of steel fibers in concrete marginally decreases the workability. Slump values of various mixes ranged from 45 to 80mm and are given in Table 3.11.

3.7.2 Tests on Hardened Concrete

The following tests were conducted on hardened concrete

1. Compression testing
2. Splitting tension testing
3. Flexural strength testing
4. Modulus of Elasticity

Compression Testing: Compressive strength test is the simplest and most common of all tests performed on concrete. The compression test is quite resourceful because most of the desirable characteristic properties of concrete are qualitatively related to

its compressive strength (Neville, 1995). The main purpose of the test is to know the strength and the strength attaining behavior at prolonged curing for all the mixes.

Table 3.11 Slump Values for Different Mixes

Type of Mix	Mean Slump in mm	
	M40 mix	M30 mix
Reference Concrete (R)	68	62
Fly Ash Concrete (FA20)	75	70
Fly Ash Concrete (FA40)	80	73
Steel Fibre Reinforced Concrete 1 (HS1)	52	55
Steel Fibre Reinforced Concrete 2 (HS 2)	45	50
Fly Ash Steel Fiber Concrete 1 (FS1)	54	56
Fly Ash Steel Fiber Concrete 2 (FS2)	48	52
Fly Ash Steel Fiber Concrete 3 (FS3)	60	58
Fly Ash Steel Fiber Concrete 4 (FS4)	62	65

The specimens were tested in a 2000kN capacity compression testing machine as per IS 516-1959 (Fig 3.4). The mean values of five specimens of each trial were taken as the final compressive strength. The cube specimens of both M₄₀ and M₃₀ mixes were tested for compressive strength after 7, 28, 56 and 90 days of curing period.

Splitting Tensile Test: Splitting tensile test is an indirect method of applying tension in the form of splitting. In this test, concrete cylinders of 150mm diameter, 300mm height are subjected to compressive loads along two axial lines which are diametrically opposite. The load is applied at a constant rate 1.2 to 2.4 N/mm²/ min (as per IS 5816:1999) until specimens fail (Fig 3.5). The compressive stress produces a transverse tensile stress which is almost uniform along the vertical diameter.

The split tensile strength (N/mm²) is computed as $f_{st} = 2P/\pi LD$ --(3.1)

Where P = failure load in N; D = diameter of specimen in mm and L = length of specimen in mm

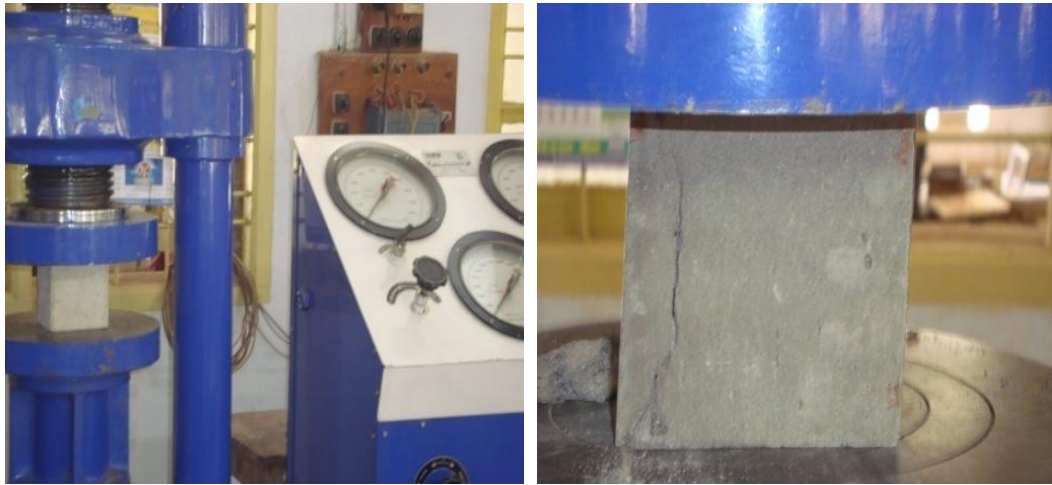


Fig. 3.4 Compression Testing



Fig 3.5 Splitting Tension Test

Flexural Strength Test by Third Point loading: Third point flexural loading test (Fig 3.6) was conducted on test prism of dimension 100mm x 100mm x 500mm over an effective span of 400mm under two symmetrical load point loads spaced at 1/3rd of the span. The rate of loading was kept at 0.8 to 1.2 MPa/min. The test was carried out as per IS 516:1959 (ASTM C 78-94, BS 1881 Part 118: 1983) guidelines. The theoretical maximum tensile stress reached at the bottommost fibre of test beam is known as flexural strength or modulus of rupture. If the fracture occurs within the central one-third portion of the beam, the modulus of rupture (f_r) in N/mm² is calculated on the basis of elastic theory of bending and is equal to

$$f_r = \frac{PL}{bd^2} \quad \text{--(3.2)}$$

Where P = Maximum load on the beam in N, L = Span in mm
b = Width of beam in mm, d = Depth of beam in mm

If fracture occurs outside the load points at a distance 'a' from nearest support, the

modulus of rupture is given by $f_r = \frac{3Pa}{bd^2}$ --(3.3)

Where 'a' = distance of fracture point from nearest support in mm

Modulus of Elasticity: The modulus of elasticity of material under compression or tension is given by the slope of stress- strain relationship of concrete under uni-axial loading. Test specimen consists of concrete cylinders 150mm in diameter and 300mm long. The linear deformation is measured with the help of LVDT or dial gauge over a gauge length of 200mm. The deformation is recorded at regular interval of loading up to 40% of its compressive strength. The strain results plotted graphically against stress. The slope of straight line indicates the modulus of elasticity. The mean value of results is reported as the Modulus of elasticity for the particular mix. Fig. 3.7 shows experimental setup of Modulus of elasticity test.



Fig 3.6 Flexural Test by Third Point Loading



Fig 3.7 Determination of Modulus of Elasticity

3.8 RESULTS

In this section, static test results are presented. Tables 3.12 to 3.14 give the various strength properties of M_{30} and M_{40} mix for all the designated mixes and are discussed in next section 3.9.

Table 3.12 Compressive strength results of various mixes (M_{30} and M_{40})

Sl. No	Type of Mix	Age in Days	M_{30} mix		M_{40} mix	
			Average Compressive Strength (MPa)	COV (%)	Average Compressive Strength (MPa)	COV (%)
1	Reference Concrete (R)	7	28	6.34	40	6.40
		28	45	4.07	50	8.90
		56	47	4.26	54	6.20
		90	49	9.77	56	9.00
2	Fly Ash Concrete (FA20)	7	26	9.65	37	4.81
		28	42	6.79	49	8.05
		56	45	8.41	54	4.78
		90	48	8.22	55	2.87
3	Fly Ash Concrete (FA40)	7	24	3.45	36	9.23
		28	40	9.54	48	5.58
		56	44	7.71	52	5.08
		90	47	9.14	53	2.55
4	Steel Fibre Reinforced Concrete 1 (HS1)	7	35	6.16	45	9.16
		28	50	4.12	54	5.40
		56	51	4.03	61	5.63
		90	53	8.24	64	5.51
5	Steel Fibre Reinforced Concrete 2 (HS 2)	7	40	5.73	46	5.95
		28	53	7.97	58	6.04
		56	55	8.82	62	3.86
		90	58	3.36	65	4.32
6	Fly Ash Steel Fiber Concrete 1 (FS1)	7	35	5.86	39	5.13
		28	46	7.69	54	4.54
		56	50	7.51	58	5.03
		90	52	5.53	60	6.12
7	Fly Ash Steel Fiber Concrete 2 (FS2)	7	37	6.71	41	8.75
		28	48	8.96	56	6.06
		56	50	4.00	58	6.79
		90	54	5.40	62	5.46
8	Fly Ash Steel Fiber Concrete 3 (FS3)	7	34	7.66	38	8.70
		28	44	7.40	52	6.60
		56	48	4.77	56	6.06
		90	51	6.96	59	7.09
9	Fly Ash Steel Fiber Concrete 4 (FS4)	7	34	9.40	41	8.09
		28	45	9.29	56	5.65
		56	49	5.16	58	5.85
		90	51	7.98	60	4.25

Table 3.13 Flexural strength results of various mixes (M₃₀ and M₄₀)

Sl. No	Type of Mix	Age in Days	Average Flexural Strength(MPa)	
			M ₃₀ mix	M ₄₀ mix
1	Reference Concrete (R)	28	4.80	5.10
		90	5.30	5.47
2	Fly Ash Concrete (FA20)	28	4.80	5.00
		90	5.40	5.67
3	Fly Ash Concrete (FA40)	28	4.80	4.65
		90	5.40	5.00
4	Steel Fibre Reinforced Concrete 1 (HS1)	28	5.20	5.60
		90	5.63	6.30
5	Steel Fibre Reinforced Concrete 2 (HS 2)	28	5.70	5.80
		90	6.00	6.60
6	Fly Ash Steel Fiber Concrete 1 (FS1)	28	5.20	5.60
		90	5.50	6.20
7	Fly Ash Steel Fiber Concrete 2 (FS2)	28	5.60	5.80
		90	5.82	6.40
8	Fly Ash Steel Fiber Concrete 3 (FS3)	28	5.20	5.60
		90	5.40	6.00
9	Fly Ash Steel Fiber Concrete 4 (FS4)	28	5.45	5.70
		90	5.60	6.20

Table 3.14 Split tensile strength results of various mixes (M₃₀ and M₄₀)

Sl. No	Type of Mix	Age in Days	Average Split Tensile Strength (MPa)	
			M ₃₀ mix	M ₄₀ mix
1	Reference Concrete (R)	28	2.62	3.63
2	Fly Ash Concrete (FA20)	28	2.51	3.35
3	Fly Ash Concrete (FA40)	28	2.45	3.30
4	Steel Fibre Reinforced Concrete 1 (HS1)	28	3.00	3.81
5	Steel Fibre Reinforced Concrete 2 (HS 2)	28	3.20	3.96
6	Fly Ash Steel Fiber Concrete 1 (FS1)	28	2.97	3.73
7	Fly Ash Steel Fiber Concrete 2 (FS2)	28	3.15	3.95
8	Fly Ash Steel Fiber Concrete 3 (FS3)	28	2.91	3.72
9	Fly Ash Steel Fiber Concrete 4 (FS4)	28	3.00	3.92

Compressive strength: Fig 3.8 depicts the variation of compressive strength with age, for all the nine mixes. It was observed that the compressive strength of all the concrete mixes gradually increased as curing period progressed from 7 days to 90 days. The 28 day compressive strength of all the mixes met the desired characteristic strengths of 30 MPa and 40 MPa for M₃₀ and M₄₀ grade concrete respectively. The coefficients of variation of compressive strength result were found less than 10%. Compressive strength in the produced concretes of M₃₀ grade ranged between 24 and 40 MPa on day 7, between 40 and 53 MPa on day 28, between 44 and 55 MPa on day 56, between 41 and 58 MPa on day 90. The same in the case of M₄₀ grade ranged between 36 and 46 MPa on day 7, between 48 and 58 MPa on day 28, between 52 and 62 MPa on day 56, between 53 and 65 MPa on day 90. Among these results, the highest compressive strength was obtained in the concretes in which 1% steel fibers were used (HS2). The addition of steel fibers and fly ash has slight influence in increasing the compressive strength of concrete as observed by several researchers. It was observed that the compressive strength of SFRC (HS1 and HS2) is more than that of the reference concrete (R) and SFRC with fly ash.

In SFRC, the addition of fly ash as partial replacement of cement (FS1, FS2, FS3 & FS4) slightly reduces the compressive strength but it was higher than that of the reference concrete for all the curing periods. The fly ash concretes without steel fibers (FA20 and FA40) showed the least strength. It is evident from Fig 3.8 that, the use of fly ash with steel fibers enhanced the compressive strength of concrete. When fly ash of 20% was used in SFR concrete (FS1 & FS2), the compressive strength gain in 56 and 90 days were in the range of 4-6% and 10-13% respectively when compared to its 28 days strength. Similarly for 40% fly ash in SFRC (FS3 & FS4), increase in strength compared to its 28 days strength was in the range of 7-8% and 13-17%. For reference concrete (R), increase in strength was 4-8% and 10-12% in 56 and 90 days respectively. FA20 concrete gained almost same compressive strength as that of reference concrete after 90 days of curing. The rate of strength gain in concrete with fly ash is significant between 28 and 90 days. This indicates that secondary C-S-H gels formed due to the pozzolanic reaction of fly ash with free lime at the later age.

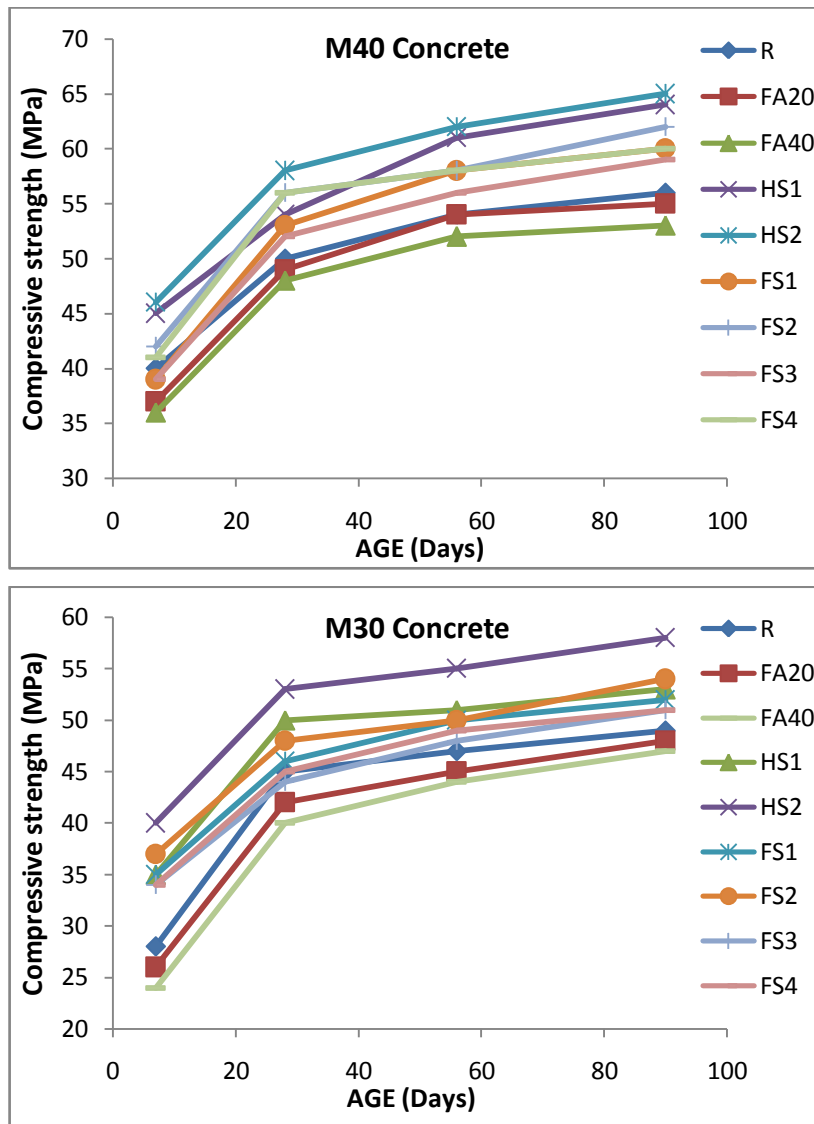


Fig 3.8 Variation of compressive strength of different mixes with age

Flexural Strength: Flexural strength testing of concrete beam was carried out based on 3rd point loading as per IS 516 (1978). The flexural strength of various mixes varied from 4.8 MPa to 5.45MPa at 28 days for M₃₀ concrete and 5.1 MPa to 5.8 MPa at 28 days for M₄₀ concrete. From Fig. 3.9 it is evident that fly ash- steel fiber reinforced concretes (FS1, FS2, FS3 & FS4) gain more flexural strength than reference concrete (R). The flexural strength is enhanced by 6-7% in reference concrete(R) , 6-10 % for FS2 and 11-14% for HS2 after 90 days of curing when compared with that of 28 days. The use of 1% steel fibers (HS2, FS2, FS4) and 0.5%

steel fibers (HS1, FS1, FS3) enhanced the flexural strength by about 13% and 9% respectively when compared to the reference concrete.

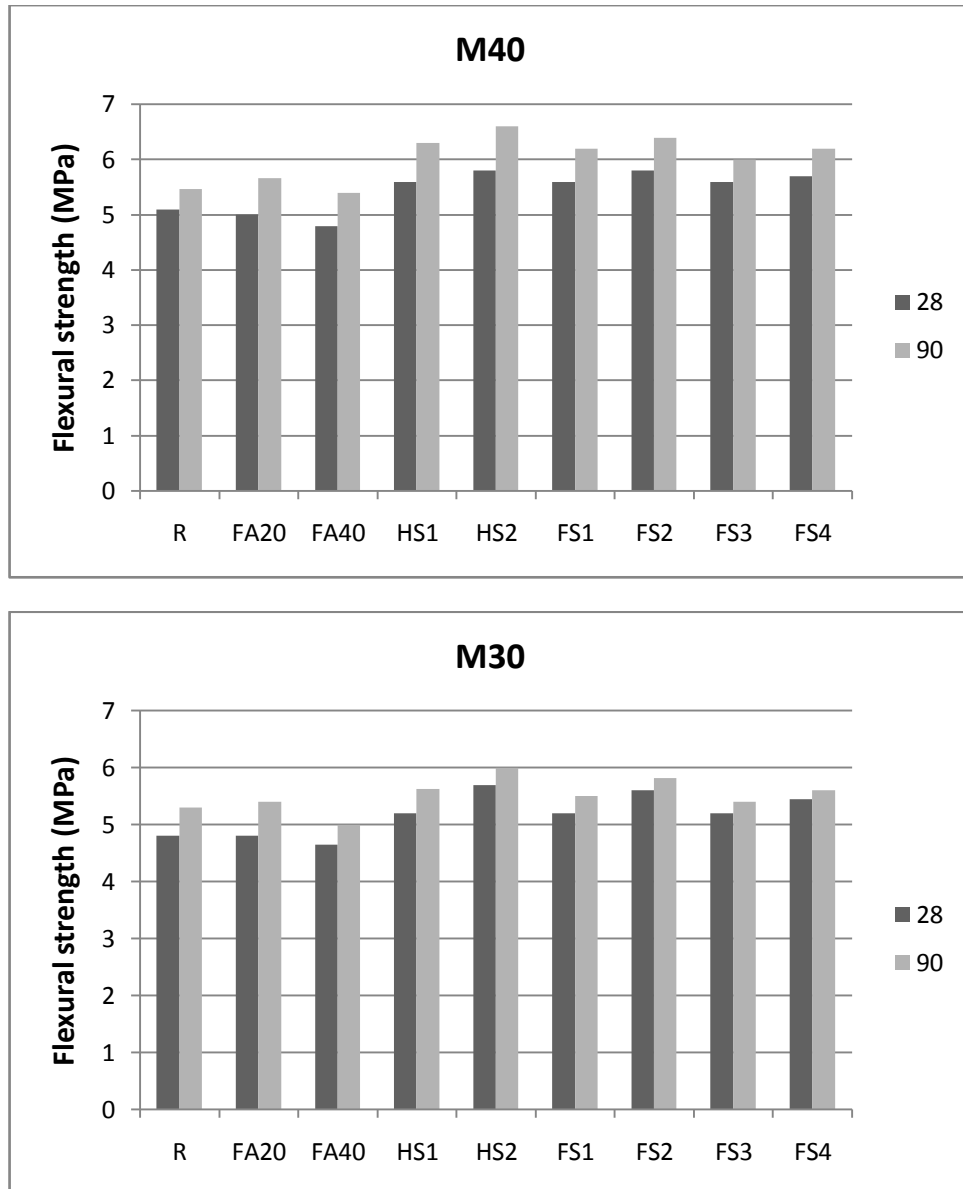


Fig 3.9 Flexural strength of various mixes after 28 and 90 days curing

Split Tensile Strength: The tensile strength is one of the basic and important properties of the concrete. In the case of pavements, the determination of tensile strength of concrete is necessary to determine the load at which the concrete members may crack. The direct method suffers from a number of difficulties related to application of axial tensile load, avoiding stress concentration at support point etc. As

the concrete is weak in tension even a small eccentricity of load will induce combined bending and axial force condition and the concrete fails at the apparent tensile stress other than the tensile strength. As there are many difficulties associated with the direct tension test, a number of indirect methods like split tensile and flexural tests have been developed to determine the tensile strength.

The comparison of split tensile strength at the age of 28 days for different mixes is shown in Fig 3.10. Except FA20 and FA40 all other mixes gained higher tensile strength than that of reference concrete(R). Concretes with 1% steel fibers (HS2, FS2 and FS4) gained maximum tensile strength after 28 days curing. Addition of fly ash tends to reduce the tensile strength of concrete whereas introducing steel fiber along with fly ash overcomes this deficiency.

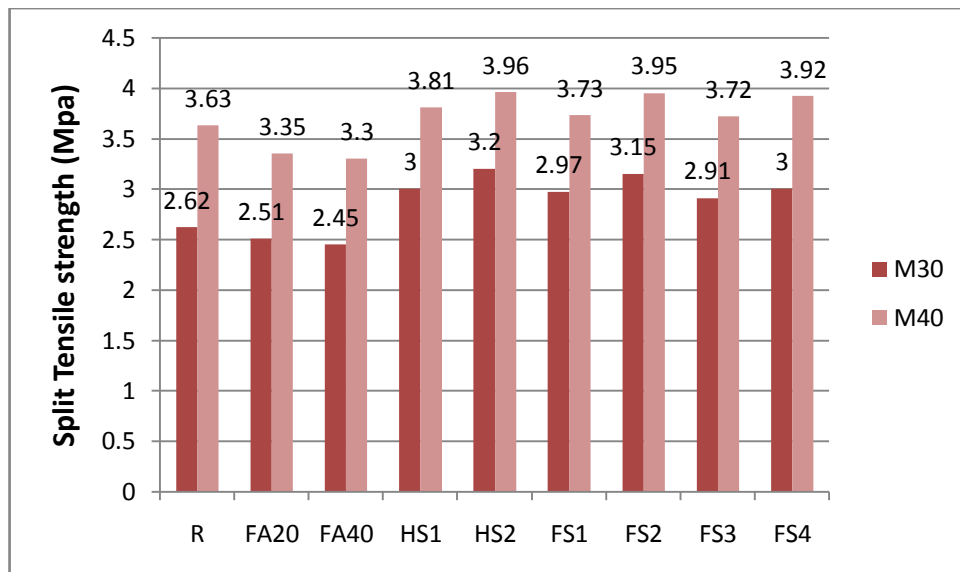


Fig 3.10 Comparison of split tensile strength of various mixes

Modulus of Elasticity: Modulus of elasticity of various concrete mixes was determined using stress- strain relation under compressive load. Fig 3.11 depicts the stress- strain relation of reference concrete (R) for both M₃₀ and M₄₀ grades of concrete under compressive load. The slope of the linear trend line was reported as modulus of elasticity. The values of modulus of elasticity for various mixes are given in Table 3.15.

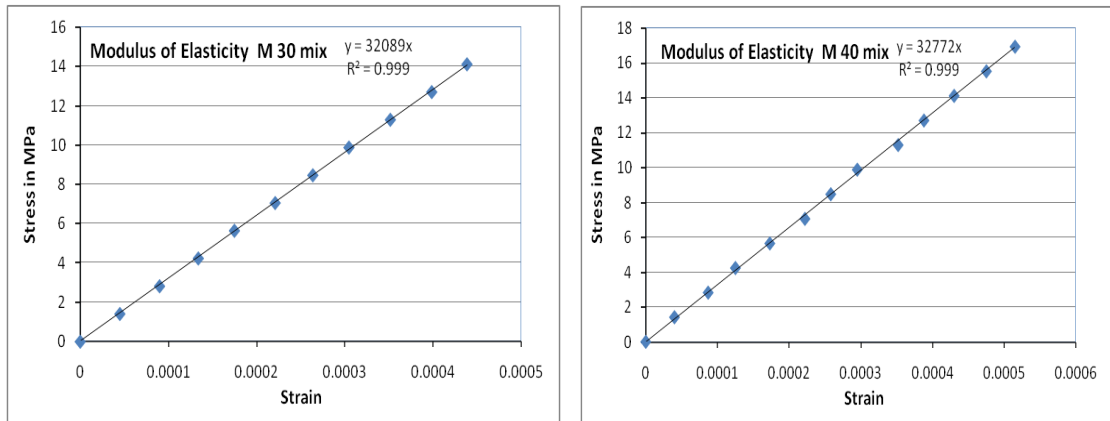


Fig 3.11 Stress –strain relationship under compressive load to determine modulus of elasticity of reference mix(R)

Table 3.15 Test results of static modulus of elasticity

Sl. No	Type of Mix	Age in Days	Modulus of Elasticity (MPa)	
			M ₃₀ mix	M ₄₀ mix
1	Reference Concrete (R)	28	32089	32772
2	Fly Ash Concrete (FA20)	28	31656	32943
3	Fly Ash Concrete (FA40)	28	30137	31742
4	Steel Fiber Reinforced Concrete (HS1)	28	37214	42647
5	Steel Fiber Reinforced Concrete (HS2)	28	40099	44131
6	Fly Ash & Steel Fiber Concrete (FS1)	28	37233	39079
7	Fly Ash & Steel Fiber Concrete (FS2)	28	39473	41883
8	Fly Ash & Steel Fiber Concrete (FS3)	28	35336	37478
9	Fly Ash & Steel Fiber Concrete (FS4)	28	36680	39450

3.9 DISCUSSIONS

3.9.1 Effect of addition of fly ash and/or steel fibers to the concrete on slump values

Figs 3.12 to 3.15 show the comparison of slump value when fly ash and/or steel fibers added to the concrete. It is clearly observed that the addition of fly ash enhanced the slump value from 62 to 73mm and 68 to 80mm in the case of M₃₀ and M₄₀ concrete respectively. Being spherical particles, when used in concrete, the fly ash improves workability as reported by many researchers. It indicates that there is a reduction in water demand for a given workability when the fly ash content was 40 per cent, where as the literature (Neville, 1995) mentioned that the beneficial influence of fly ash upon water demand does not extend beyond a fly ash content of 20 per cent. The slightly enhanced slump of fresh concrete containing higher fly ash replacement could have been caused by increased finer particles in the matrix.

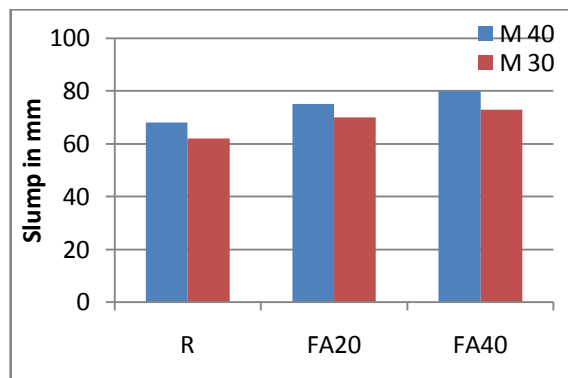


Fig 3.12 Effect of addition of fly ash to the concrete on slump value

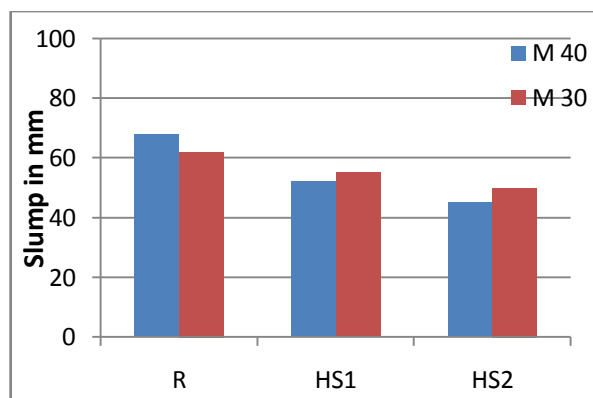


Fig 3.13 Effect of addition of steel fibers to the concrete on slump value

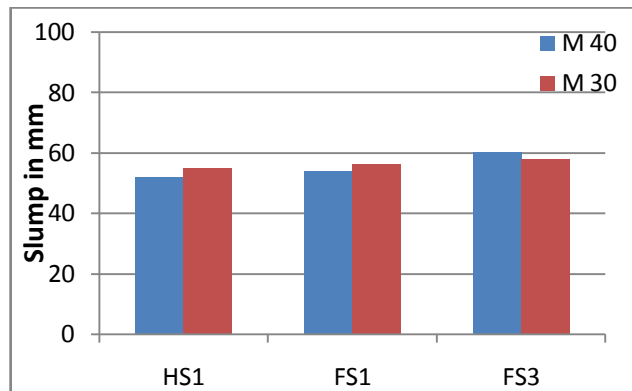


Fig 3.14 Effect of addition of fly ash to the steel fiber reinforced concrete (Steel fiber 0.5%) on slump value

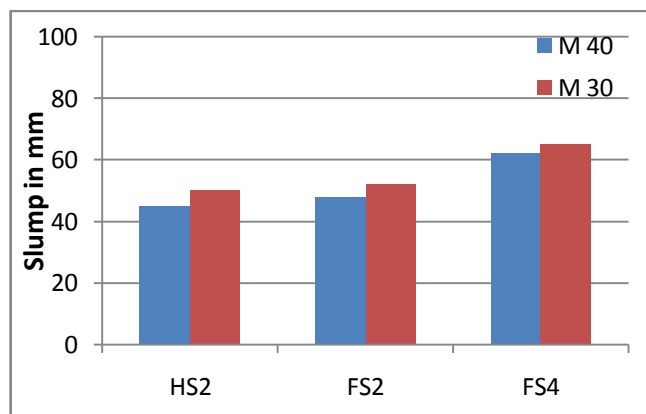


Fig 3.15 Effect of addition of fly ash to the steel fiber reinforced concrete (Steel fiber 1.0%) on slump value

Addition of steel fibers to the normal concrete mix decreased the slump value by about 20mm indicating the reduction in workability. The reduction is more (from 65 to 45mm) in the case of 1% percent steel fiber volume fraction (HS2) comparative to that of 0.5% (from 65 to 55). This clearly indicates that, addition of steel fiber needs extra water or superplasticizer to maintain the same level of workability. This may be due to the frictional resistance offered by steel fibers inside the matrix. When fly ash was used with steel fibers (FS3 and FS4) the slump value was almost same as that of reference concrete. This proves that, the addition of fly ash into the SFRC helps in gaining of reduced workability due to incorporation of steel fibers with the same amount of water.

3.9.2 Comparison of static strength characteristics of various mixes

Figs 3.16 to 3.18 show the comparison of various strength properties such as compressive, flexural and splitting tensile strengths for different mixes. From Fig 3.16, it is evident that for M₄₀ grade of concrete, the maximum increase in compressive strength due to the addition of 1% steel fibers (HS2) was found to be 15% when compared to conventional concrete (R). The addition of 20% and 40% fly ash in partial replacement to SFRC with 1% steel fibers (FS2 and FS4) the increase was found to be 12%. The increase in compressive strength for steel fibers of 0.5% (HS1) was less than 10% and addition of 40% fly ash in partial replacement to cement (FS3) was found to be less than 5%.

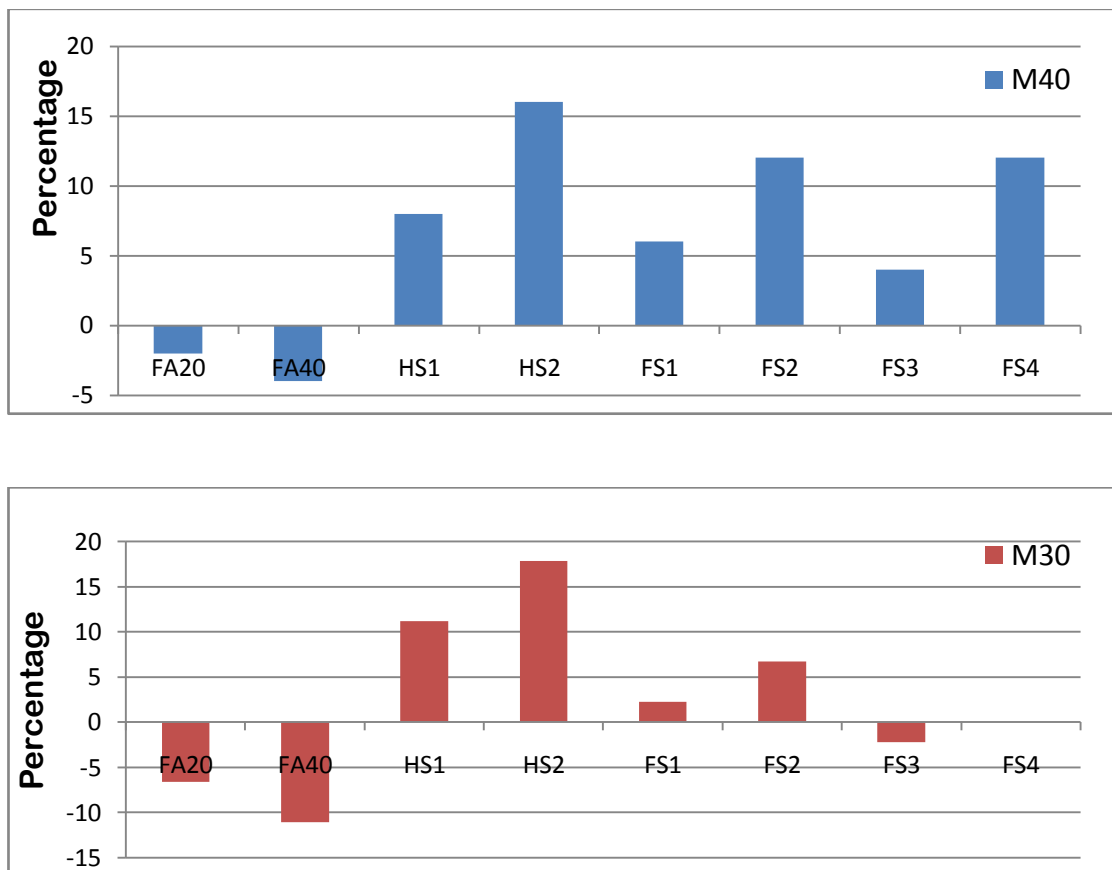


Fig 3.16 Comparison of compressive strengths (28 days) of various mixes with reference concrete

In case of M₃₀ grade concrete, with 20% fly ash and 1% steel fibers (FS2), the compressive strength increased by 6 % and with 40% fly ash (FS3 & FS4), the compressive strength is either same or slightly reduced when compared to the control concrete. The higher strength for M₄₀ concrete obtained through the use of superplasticizer is attributed to lower water-binder ratio and also the compatibility of the superplasticizer to the fly ash and the cement, whereas no superplasticizer was used for M₃₀ grade concrete.

From Fig 3.17, it is clear that the use of 1% volume fraction of steel fibers in concrete (HS2) enhances the flexural strength by 14% in the case of M₄₀ concrete and 18% for M₃₀ concrete when compared to the reference concrete(R). It also indicates that the increase in strength is more in the case of lower grade of concrete (M₃₀) compared to the higher grade (M₄₀). In contradiction to compressive strength, percentage increase of flexural strength is lower in case of higher grade of concrete. Similar trend has been observed in split tensile strength. This may be due to the resistance offered by the steel fibers during straightening and pulling at the failure plane. The use of fly ash of 40% has shown to have negligible reduction in strength in the case of 0.5% steel fibers (FS3) compared to HS1, where as it is 2-6% in the case of 1% of steel fibers (FS4) compared to HS2.

From Fig 3.18, it is evident that steel fibers enhance the tensile capacity of concrete. Inclusion of 1% steel fibers (HS2, FS2, and FS4) shows better strength than 0.5% steel fibers (HS1, FS1, FS3). The reduction in tensile strength is observed when fly ash is used. The reduction is in the order of 2 to 3% for FS1, FS2 and 5 to 6% for FS3, FS4 concretes when compared to HS1 and HS2. All the mixes with steel fibers gained higher tensile strength when compared to the reference mix and the addition of fly ash in concrete (FA20 and FA40) reduces the tensile strength by less than 6%.

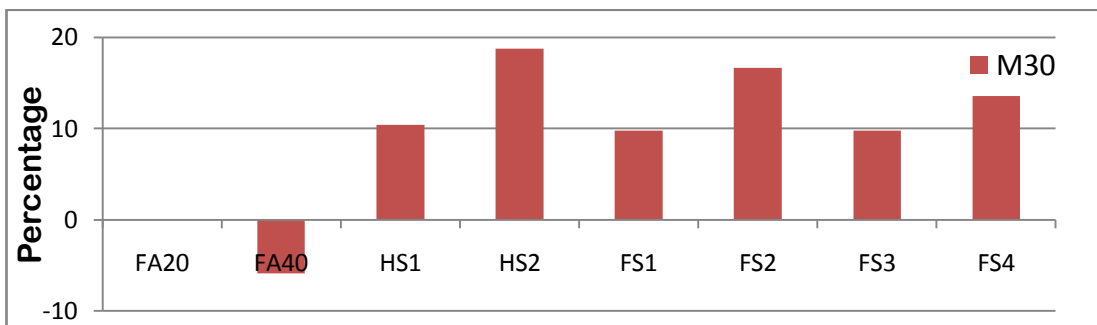
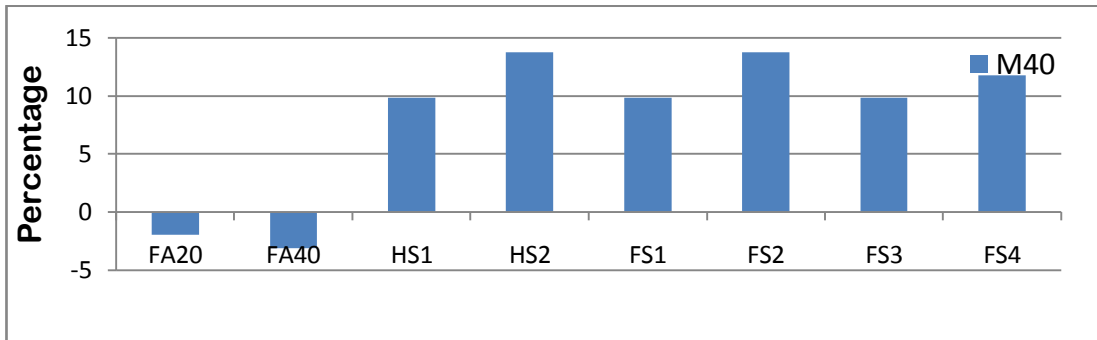


Fig 3.17 Comparison of flexural strengths (28 days) of various mixes with reference concrete

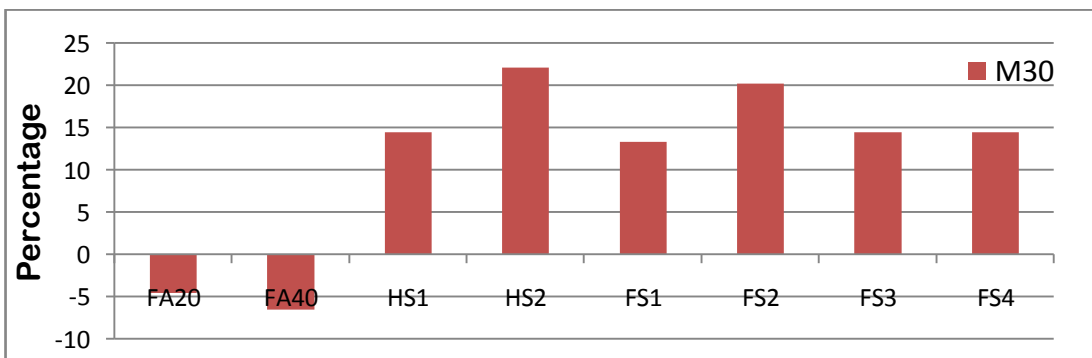
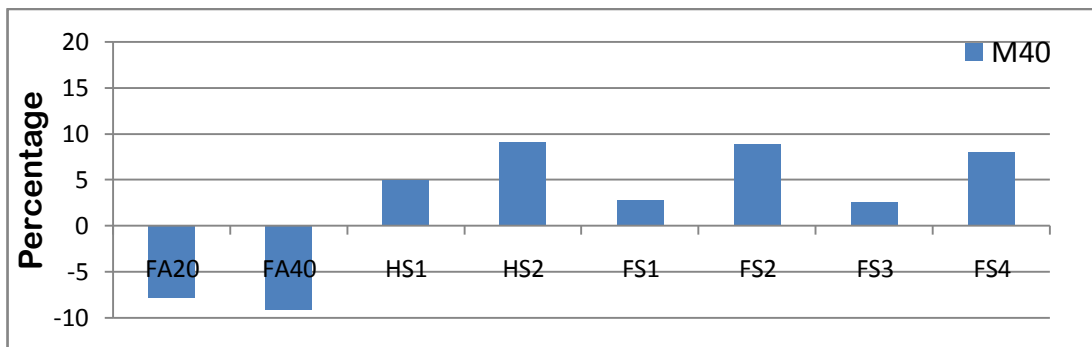


Fig 3.18 Comparison of split tensile strengths (28 days) of various mixes with reference concrete

3.9.3 Effect of fly ash on strength properties of plain concrete

Figs 3.19 to 3.22 demonstrate the effect of using fly ash as partial replacement of cement on strength characteristics such as compressive, flexure and splitting tensile strengths and modulus of elasticity at the age of 28 days. Both M₃₀ and M₄₀ grades of concrete have shown slight reduction in all the strength values when fly ash was used to replace cement partially as indicated by earlier studies (Mohammed et al 2009). However, this reduction is marginal. Compared to reference concrete, the reduction in 28 days compressive strength of 4% and 11% for M₄₀ and M₃₀ mixes respectively was observed when 40 % fly ash was used. FA20 mix has shown almost negligible reduction in strength as compared to reference mix. The reductions in compressive strengths observed in this research work are in very small percentage while in literature (Gebler and Klieger 1986) this value was as high as 25%. Improvement in strength of fly ash concrete might be due to the use of large sized aggregates (MAS 31.5mm) and the better packing of fly ash around coarse aggregate particles. A negligible reduction (up to 6%) was observed in flexural strength and splitting tensile strength for the same mix (FA40) as compared to the reference mix. This indicates that the use of fly ash do not adversely affect the tensile strength of concrete, which is an important parameter to be considered while designing pavements. The development of good strength in fly ash concrete might be the result of formation of additional C-S-H gel (pozzalanic action) and the filler effect of fine fly ash particles. At the same time, possible increase in porosity lowers the strength. Fly ash concrete (40%) had slightly lesser modulus of elasticity, compared to that of reference concrete, whereas fly ash concrete with 20% replacement had almost same value as the reference concrete.

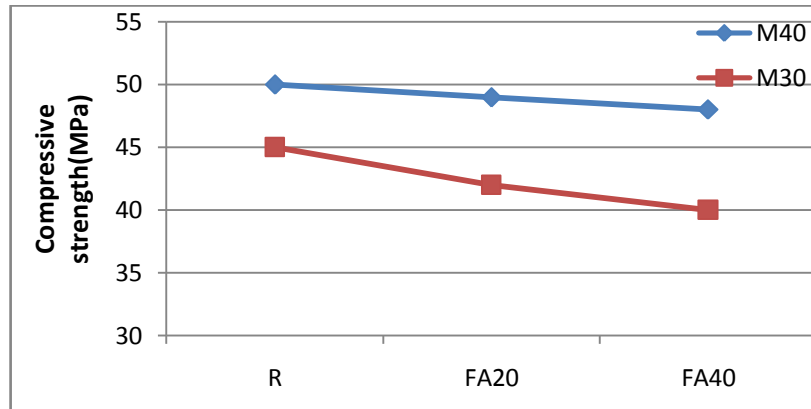


Fig 3.19 Effect of addition of fly ash in plain concrete on compressive strength (28 days)

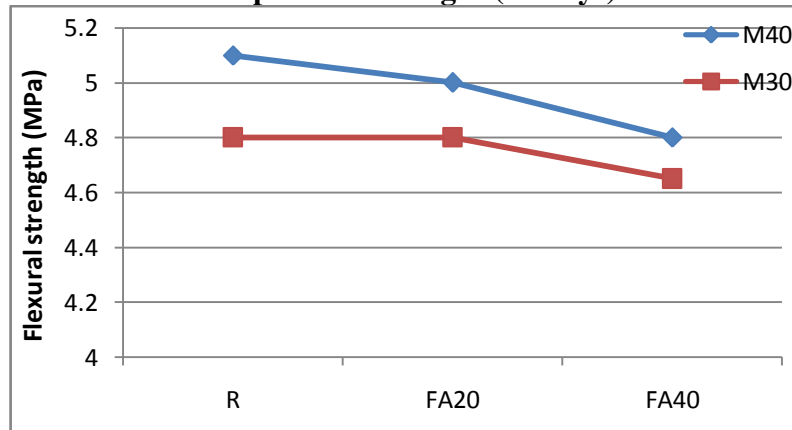


Fig 3.20 Effect of addition of fly ash in plain concrete on flexural strength (28 days)

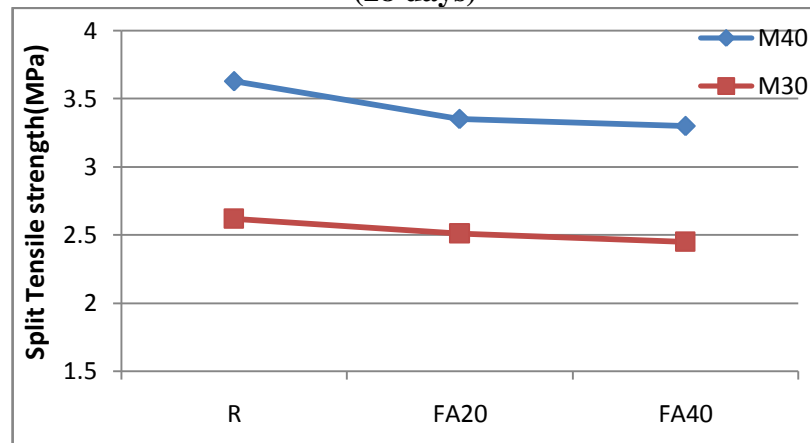


Fig 3.21 Effect of addition of fly ash in plain concrete on split tensile strength (28 days)

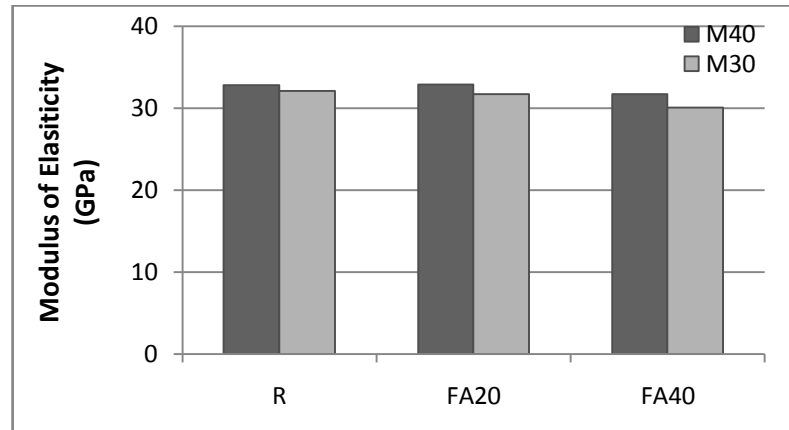


Fig 3.22 Effect of addition of fly ash to concrete on modulus of elasticity

3.9.4 Effect of incorporation of steel fibers on strength properties of plain concrete

Fig 3.23 to 3.26 show the effect of incorporation of steel fibers into plain concrete on strength characteristics such as compressive, flexure and splitting tensile strengths and modulus of elasticity at the age of 28 days. Both M₃₀ and M₄₀ grades of concrete have shown improvements in all the strength values. Compared to reference concrete(R), the increase in 28 days compressive strength of 8% and 11% for M₃₀ and M₄₀ mixes respectively with 0.5% steel fibers(HS1) and 16% and 18% for M₃₀ and M₄₀ mixes respectively with 1.0% steel fibers(HS2) was observed. This result contradicted the observation made by Rossi (1994). The use of mixed fibers (long and short) used in the mix might have provided better resistance against cracking of specimen under compressive load. The enhancement of flexural strength of 10 -13% and split tensile strength of 4 -10% was observed when 1% steel fibers were used in normal concrete. The enhancement of strength is attributed to the geometry and adhering property of steel fibers with strong matrix and the bridging action of mixed fibers across the micro cracks in the matrix. The modulus of elasticity of steel fiber reinforced concrete has higher value as compared to reference concrete.

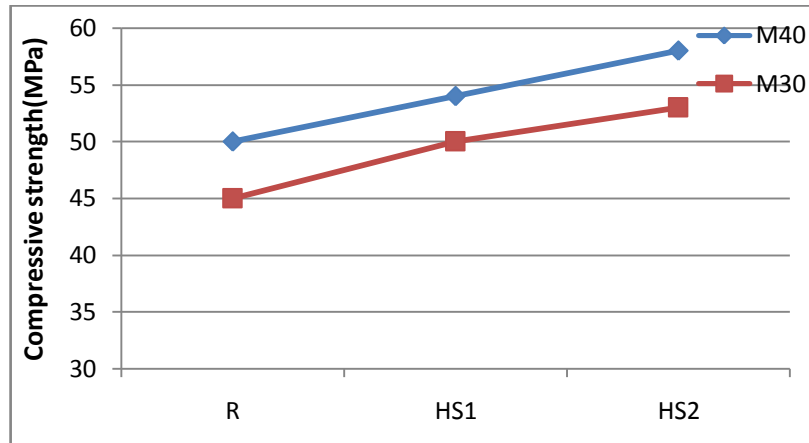


Fig 3.23 Effect of steel fibers in plain concrete on compressive strength (28 days)

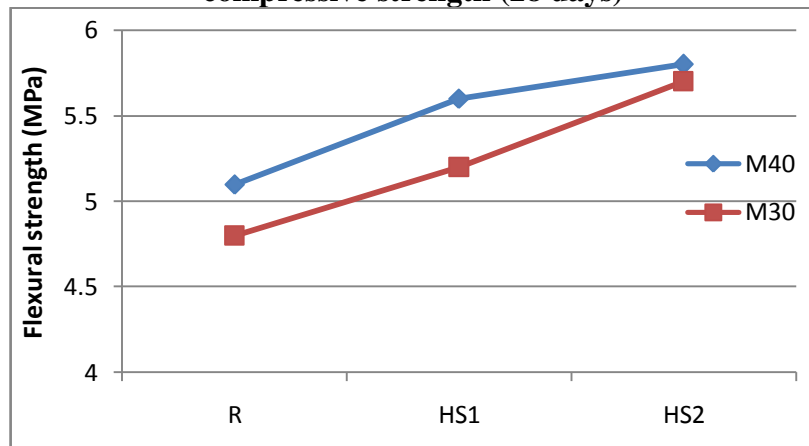


Fig 3.24 Effect of steel fibers in plain concrete on flexural strength (28 days)

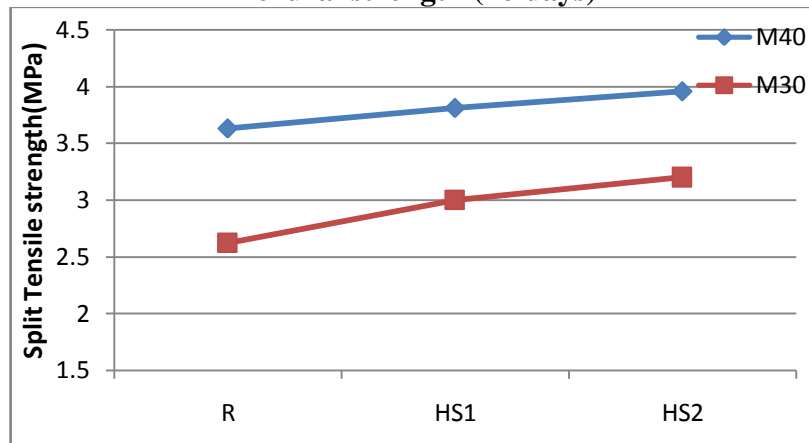


Fig 3.25 Effect of steel fibers in plain concrete on split tensile strength (28 days)

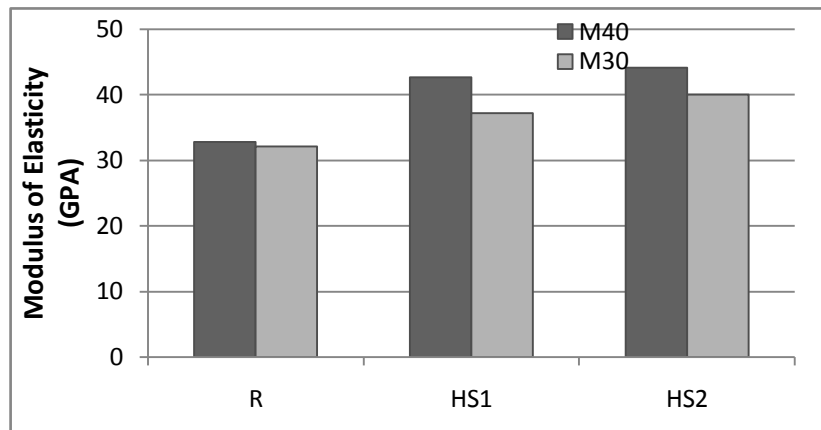


Fig 3.26 Effect of steel fibers in concrete on modulus of elasticity

3.9.5 Effect of fly ash on strength properties of SFRC

Fig 3.27 to 3.34 show the effect of fly ash utilization as partial replacement of cement (0%, 20% and 40%) in SFRC on strength characteristics such as compressive, flexure and splitting tensile strengths and modulus of elasticity at the age of 28 days. In the case of M_{40} concrete, the compressive strength of SFRC with 0.5% (HS1) or 1% steel fibers (HS2) found to be reduced by a marginal value of 3%, when 20% and 40% cement was replaced by fly ash (FS1, FS2, FS3 & FS4), whereas the reduction is about 9-15% in the case of M_{30} grade of concrete. This indicates that the bond between fly ash concrete and steel fibers played an important role during failure under compressive load. It also shows that fly ash concrete has better bond strength at higher grade (M_{40}) of concrete. The flexural and split tensile strengths of steel fiber reinforced fly ash concrete were almost equal or slightly lesser than that of steel fiber concrete. This reveals that the partial replacement of cement by fly ash do not affect the tensile behaviour of SFRC. The two lines (M_{30} and M_{40}) in Figs 3.28, 3.29, 3.32 & 3.33 found almost parallel to each other, indicating no change in bonding capacity due to the use of fly ash as partial replacement of cement. As flexural strength is one of the main requirements in design of concrete pavements, these results encourage the use of fly ash as partial replacement of cement. Further, desired strength and workability can be attained by adjusting water binder ratio and quantity of superplasticizer. The inclusion of fly ash (20% or 40%) reduces the modulus of elasticity of steel fiber concrete (0.5% & 1% steel fibers) up to 10%. In design of rigid

pavements, this marginal reduction of elastic modulus would affect a least. Also the obtained modulus of elasticity values when fly ash (40%) was used is sufficient for all structural applications.

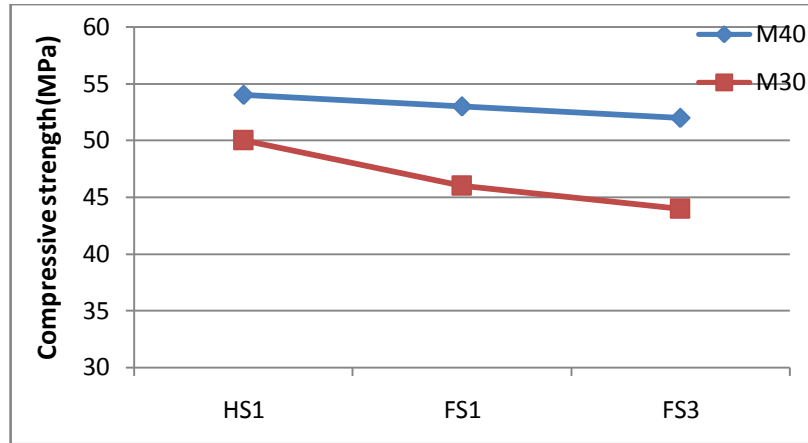


Fig 3.27 Effect of fly ash in steel fiber (0.5%) concrete on 28 days compressive strength

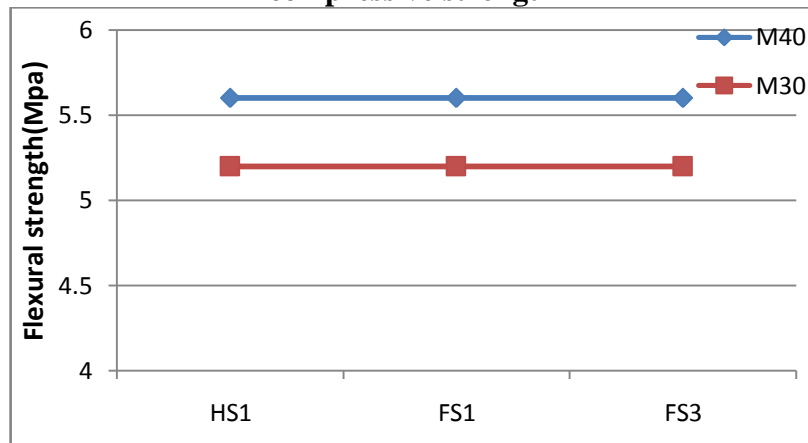


Fig 3.28 Effect of fly ash in steel fiber (0.5%) concrete on flexural strength (28 days)

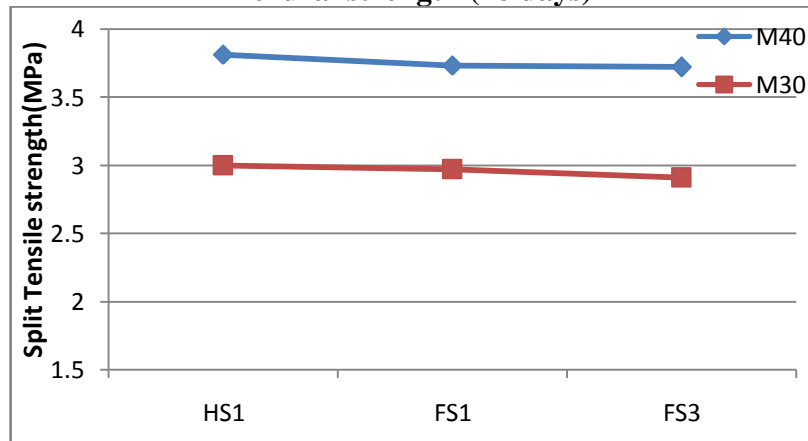


Fig 3.29 Effect of fly ash in steel fiber (0.5%) concrete on 28 days split tensile strength

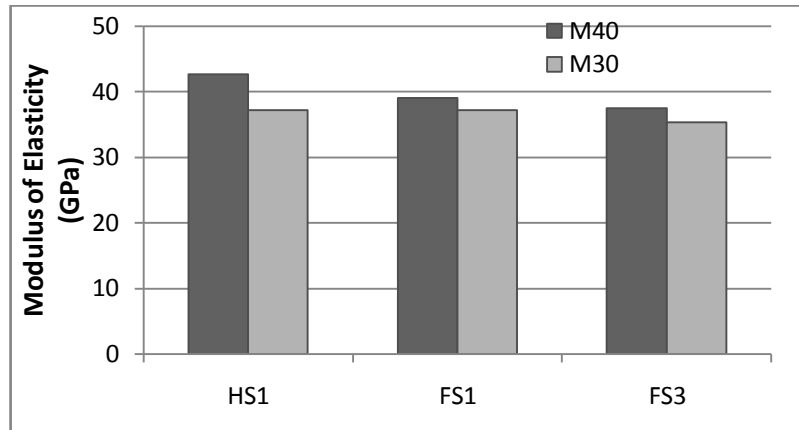


Fig 3.30 Effect of fly ash in steel fiber (0.5%) reinforced concrete on modulus of elasticity

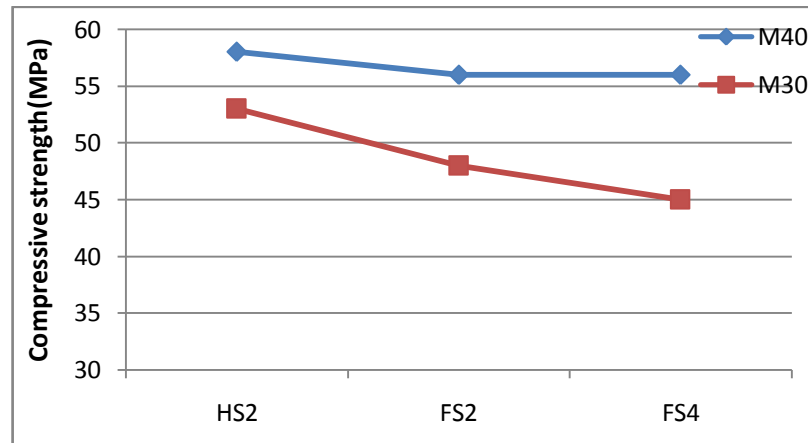


Fig 3.31 Effect of fly ash in steel fiber (1.0%) concrete on compressive strength (28 days)

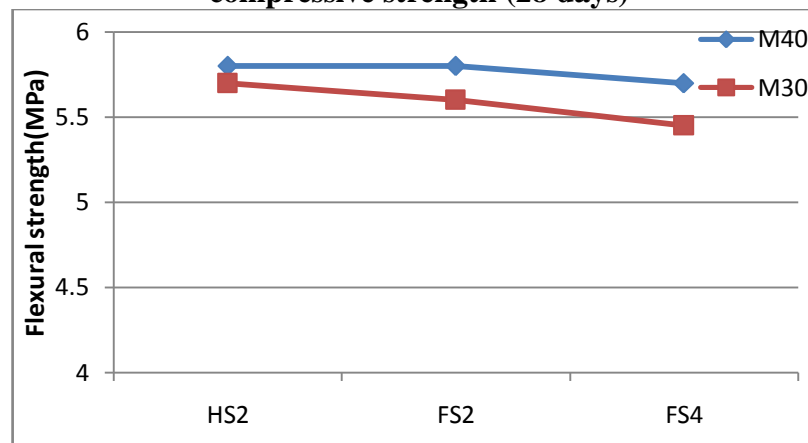


Fig 3.32 Effect of fly ash in steel fiber ((1.0%) concrete on flexural strength (28 days)

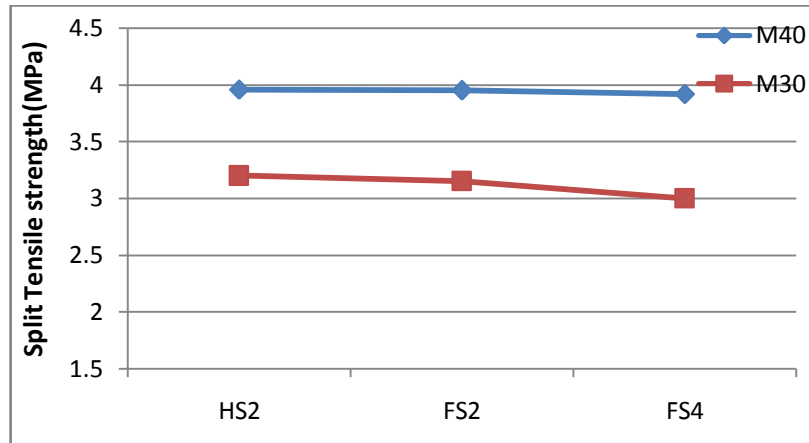


Fig 3.33 Effect of fly ash in steel fiber (1.0%) concrete on split tensile strength (28 days)

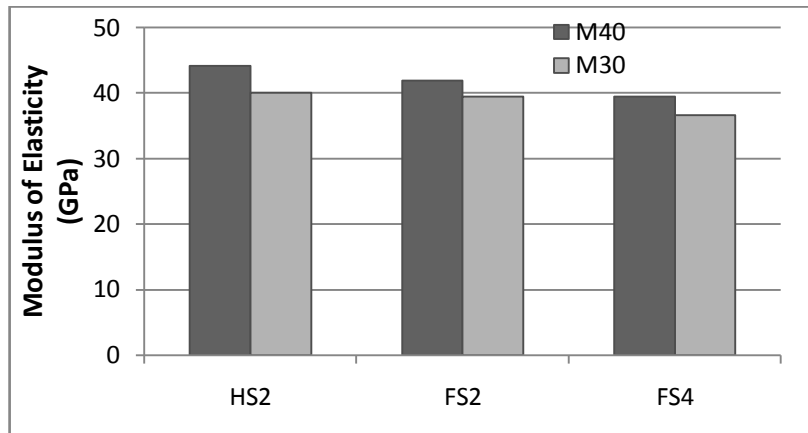


Fig 3.34 Effect of fly ash in steel fiber (1.0%) reinforced concrete on modulus of elasticity

Fig 3.35 and 3.36 demonstrate the strength gaining behaviour of steel fiber reinforced concrete with and without fly ash in longer curing periods. The addition of fly ash as partial replacement to cement in steel fiber reinforced concrete shows marginal reduction in compressive strength in all the curing days. However, this reduction in strength is less than 10% compared to the control concrete. The figures show that the rate of strength development (slope) of concrete with fly ash is slower in comparison with the control concrete.

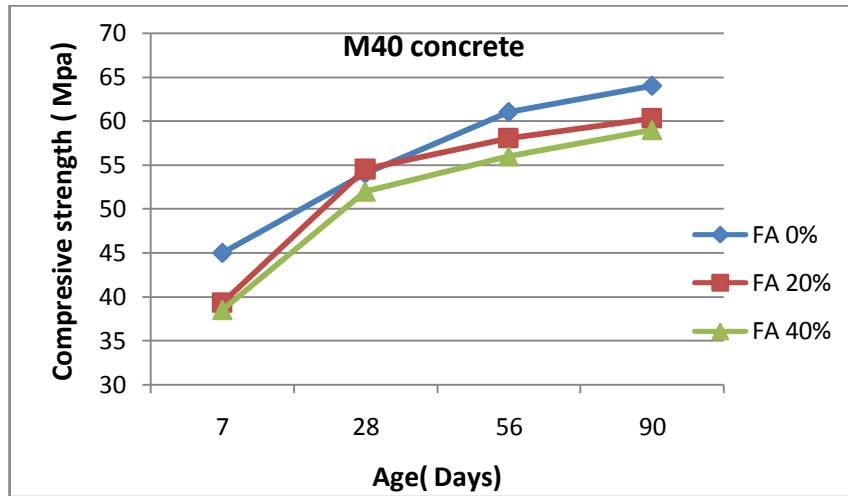


Fig 3.35 Compressive strengths of SFRC (Vf=1%) with different percentage of fly ash (M₄₀ Mix)

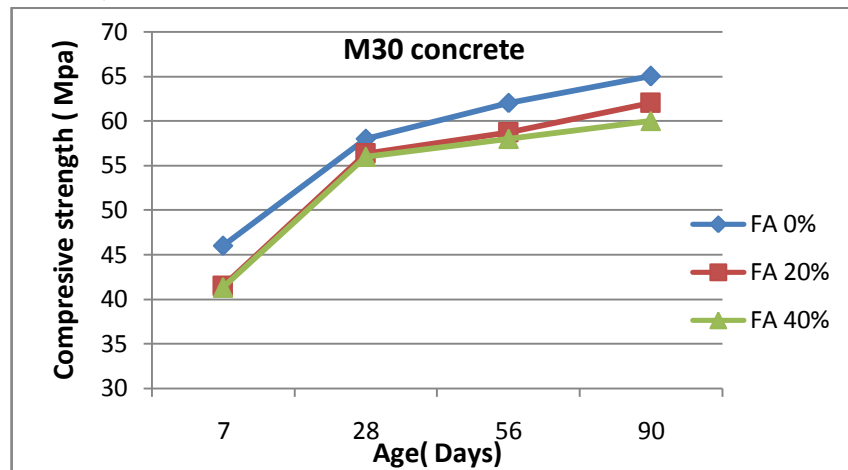


Fig 3.36 Compressive strengths of SFRC (Vf=1%) with different percentage of fly ash (M₃₀ mix)

3.9.6 Effect of insertion of steel fibers into fly ash-cement concrete on strength

Fig 3.37 to 3.40 show the effect of incorporation of steel fibers into fly ash-cement concrete on strength characteristics such as compressive, flexure and splitting tensile strengths and modulus of elasticity at the age of 28 days. The addition of steel fibers was found to enhance the strength characteristics of both 20% and 40% fly ash-cement concrete. Fly ash-cement concrete with fiber content of 1% had shown higher strength than that of 0.5% steel fiber. The increase in compressive strength was in the range of 10-15% when 1% steel fibers were used with 20% and 40% fly ash-cement concrete.

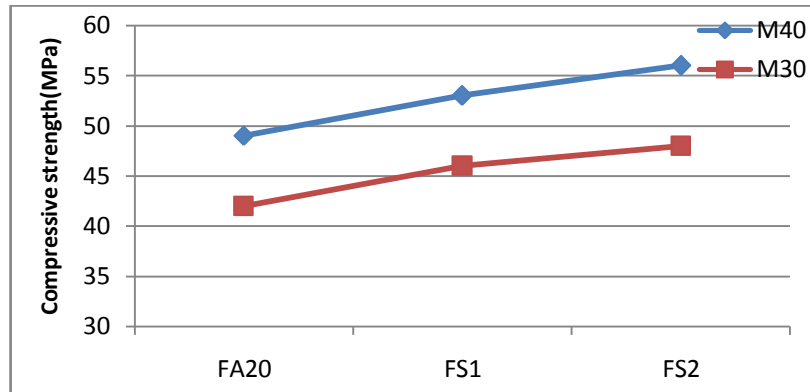


Fig 3.37 Effect of steel fibers in fly ash (20%) concrete on compressive strength (28 days)

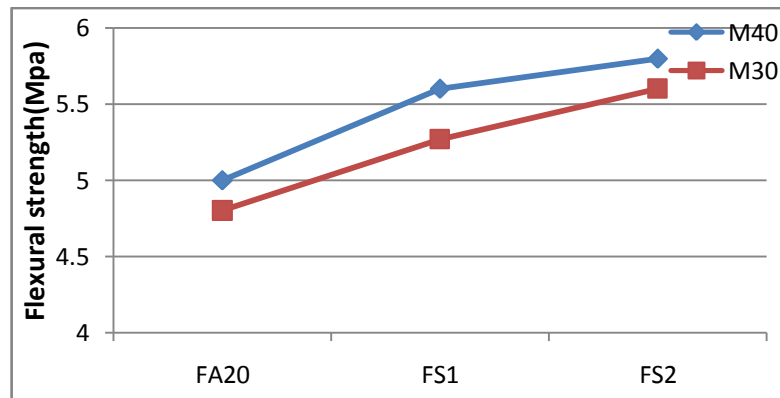


Fig 3.38 Effect of steel fibers in fly ash (20%) concrete on flexural strength (28 days)

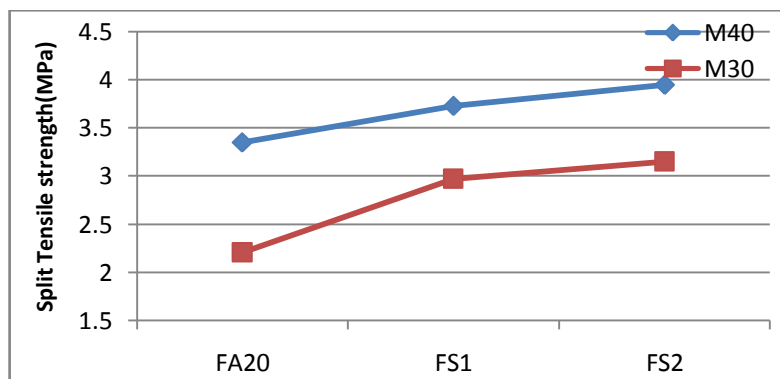


Fig 3.39 Effect of steel fibers in fly ash (20%) concrete on split tensile strength (28 days)

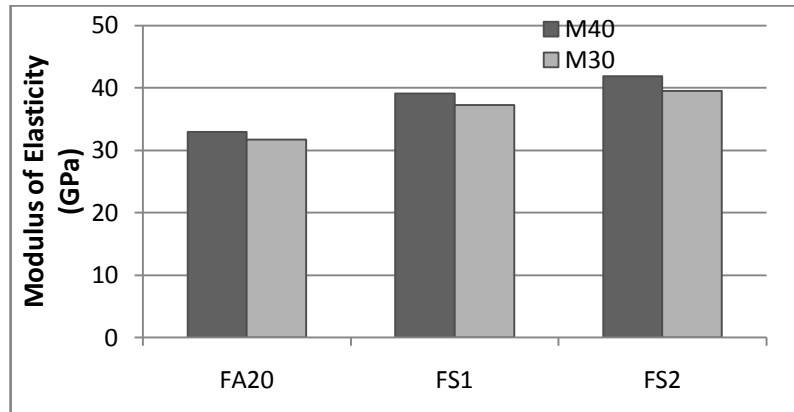


Fig 3.40 Effect of steel fibers in fly ash (20%) concrete on modulus of elasticity

From the figures it can be observed that the trends of strength enhancement for both M₃₀ and M₄₀ grade of concrete are similar when steel fibers (0.5%, 1%) were used with fly ash concrete (20%, 40%). The increase in tensile strength is in the range of 16-20% when 1% steel fibers were used with 40% fly ash- cement concrete.

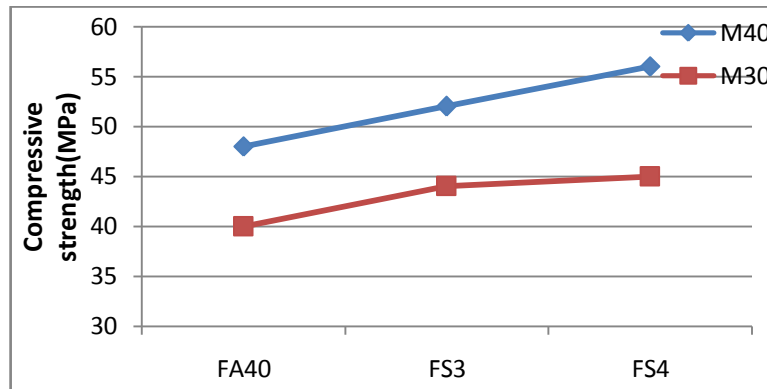


Fig 3.41 Effect of steel fibers in fly ash (40%) concrete on compressive strength (28 days)

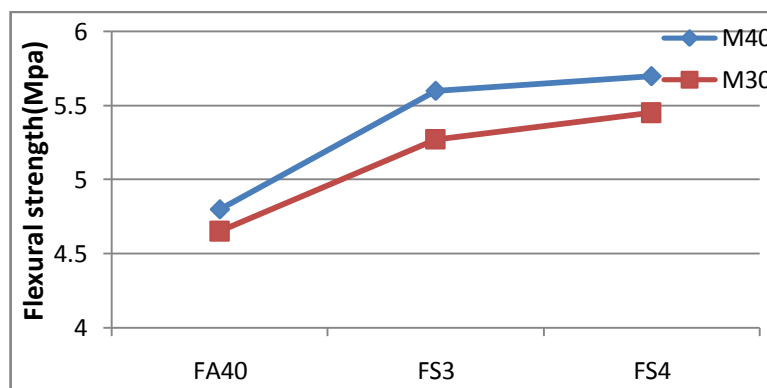


Fig 3.42 Effect of steel fibers in fly ash (40%) concrete on flexural strength (28 days)

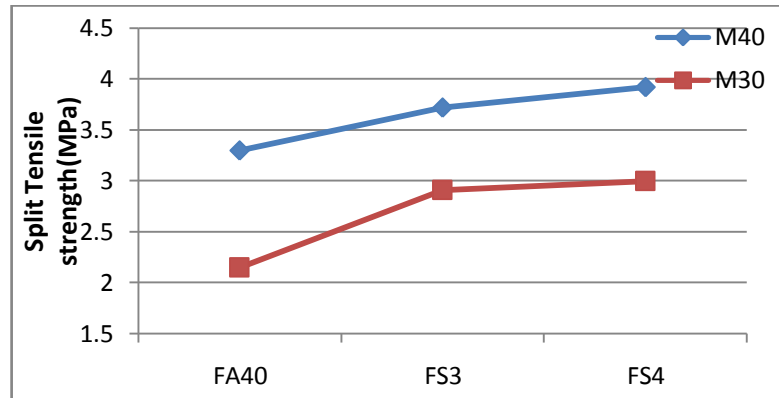


Fig 3.43 Effect of steel fibers in fly ash (40%) concrete on split tensile strength (28 days)

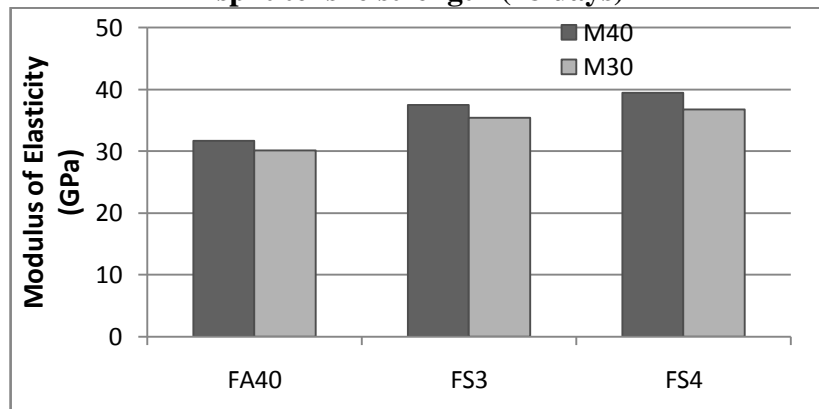


Fig 3.44 Effect of steel fibers in fly ash (40%) concrete on modulus of elasticity

3.9.7 Relationship between compressive strength and flexural strength

The general relationship between compressive strength and flexural strength for concrete is given by

$$f_r = k\sqrt{f_{ck}}$$

where k is a constant, ' f_{ck} ' characteristic strength of concrete and ' f_r ' flexural strength. Both characteristic strength and flexural strength were calculated using following relation:

f_{ck} = Mean compressive strength – 1.65* assumed standard deviation

f_r = Mean flexural strength – 1.65* assumed standard deviation

where mean compressive and flexural strengths are the experimental results.

Standard deviations (as per IS 10262(1982)

For compressive strength:

M40 concrete: 6.6 MPa ; M₃₀ Concrete : 6.0MPa

For flexural strength: M40 concrete: 0.55 MPa ; M₃₀ Concrete : 0.50MPa

The value of coefficient k obtained from calculated values of f_{ck} and f_r for different concretes used in the study are tabulated in Tables 3.16 and 3.17

Table 3.16 Relationship between compressive strength and flexural strength for M₄₀ concrete

Sl. No	Type of Mix	Average Compressive Strength (MPa)	f_{ck} (MPa)	Average Flexural Strength (MPa)	f_r (MPa)	Coefficient k
1	R	50	39.4	5.10	4.193	0.67
2	FA20	50	38.8	5.00	4.093	0.66
3	FA40	48	37.1	4.8	3.893	0.64
4	HS1	54	43.1	5.60	4.693	0.71
5	HS 2	58	47.1	5.80	4.893	0.71
6	FS1	55	43.6	5.60	4.693	0.71
7	FS2	56	45.4	5.80	4.893	0.73
8	FS3	52	41.1	5.60	4.693	0.73
9	FS4	56	45.1	5.70	4.793	0.71

Table 3.17 Relationship between compressive strength and flexural strength for M₃₀ concrete

Sl. No	Type of Mix	Average Compressive Strength (MPa)	f_{ck} (MPa)	Average Flexural Strength (MPa)	f_r (MPa)	Coefficient k
1	R	45	35.1	4.80	3.975	0.67
2	FA20	42	32.1	4.80	3.975	0.70
3	FA40	40	30.1	4.65	3.825	0.61
4	HS1	50	40.1	5.20	4.375	0.69
5	HS 2	53	43.1	5.77	4.845	0.75
6	FS1	46	36.1	5.27	4.445	0.74
7	FS2	48	38.1	5.60	4.775	0.77
8	FS3	44	34.1	5.27	4.445	0.76
9	FS4	45	36.1	5.45	4.625	0.77

From the Tables 3.16 & 3.17 it is observed that the value **k** varies from 0.71 to 0.77 for steel fiber reinforced fly ash concrete. The value of k for reference concrete is 0.67 and the value suggested by IS 456 (2000) for plain concrete is 0.7. The value of ‘k’ in general relationship between flexural strength and compressive strength is proposed by considering steel fibers and fly ash content.

$$k = k_1 * k_2 * k_3 \text{ -----(3.10)}$$

where k_1 = constant for reference concrete = 0.7 (as suggested by IS 456)

$$k_2 = \text{constant for SFRC} = 0.09(\text{SF})+1$$

SF is the steel fiber content in percentage

$$k_3 = \text{constant for fly ash concrete} = 0.6(\text{FA}/100)^2 - 0.318(\text{FA}/100) + 1$$

FA is the fly ash content in percentage

To verify the validity of proposed model for estimating the flexural strength from characteristic compressive strength, Chi square test was employed and the results are given in Table 3.18. Percentage root mean squared error (PRMSE) is also determined to justify the results.

Table 3.18 Chi-square test for prediction model of flexural strength

	Mix	fr(o) (observed) (MPa)	fr(p) (predicted) (MPa)	$[\text{fr}(\text{o}) - \text{fr}(\text{p})]^2$	$\chi^2 = \frac{[\text{fr}(\text{o}) - \text{fr}(\text{p})]^2}{[\text{fr}(\text{p})]}$
M ₄₀	R	4.193	4.206	0.040344	0.009182
	FA20	4.093	4.424	0.008951	0.002137
	FA40	3.893	4.203	0.056481	0.013674
	HS1	4.693	4.597	0.011955	0.002489
	HS 2	4.893	5.012	0.117942	0.022523
	FS1	4.693	4.639	0.002933	0.000632
	FS2	4.893	4.937	0.001978	0.000401
	FS3	4.693	4.543	0.022416	0.004934
	FS4	4.793	4.964	0.0293	0.005902
	M ₃₀	R	3.975	4.147	0.029642
FA20		3.975	3.809	0.02758	0.007241
FA40		3.825	3.720	0.010895	0.002928
HS1		4.375	4.632	0.066148	0.01428
HS 2		4.845	5.009	0.026942	0.005379
FS1		4.445	4.221	0.050155	0.011882
FS2		4.775	4.523	0.063438	0.014025
FS3		4.445	4.138	0.094043	0.022725
FS4		4.625	4.441	0.033738	0.007596

Sample size n=18

$$\chi^2_{\text{calculated}} = 0.155079$$

$$\chi^2_{\text{critical}} = 5.697 [0.995, 17]$$

Percentage root mean squared error (PRMSE) = 3.86%

From the analysis it is observed that, the $\chi^2_{\text{calculated}} = 0.155079$ which is much lesser than χ^2_{critical} from the Chi-square distribution table for $\alpha=0.995$ and degree of freedom [17] is 5.697. This clearly indicates that the developed model is a best fit to estimate flexural strength. The PRMSE value is 3.86% is also found to be very low. Fig 3.45 shows that there is a good correlation between observed and predicted values as the points are clustered near diagonal lines.

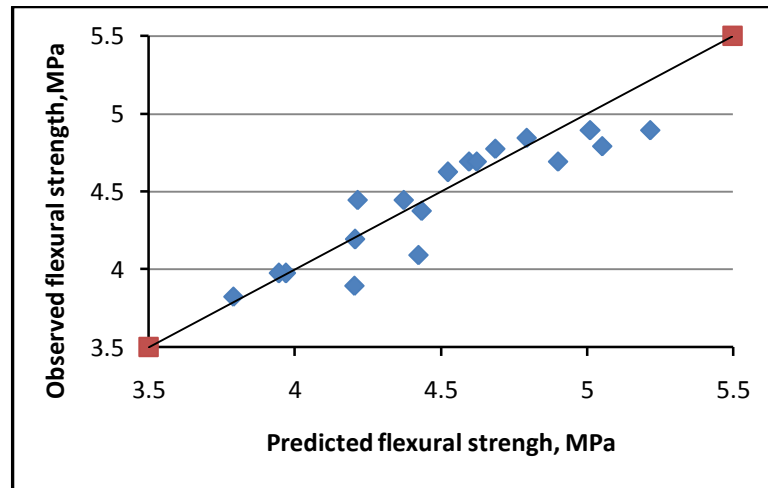


Fig 3.45 Plot of Observed flexural strength v/s predicted flexural strength

3.9.8 Relationship between compressive strength and modulus of elasticity

The general relationship between modulus of elasticity and compressive strength for concrete is represented by
$$E_c = k\sqrt{f_{ck}} \text{ -----(3.11)}$$

where E_c = Modulus of elasticity; f_{ck} = Characteristic strength of concrete

k = a constant

Modulus of elasticity ' E_c ' was obtained using following relation:

$$E_c = \text{Mean modulus of elasticity} - 1.65 \times \text{assumed standard deviation}$$

where mean modulus of elasticity was obtained from experimental results.

Assumed standard deviations, M_{40} concrete: 2500 MPa ; M_{30} Concrete : 2300MPa

Values of coefficient k for different concretes, obtained from the characteristic strength f_{ck} and modulus of elasticity E_c are tabulated in Tables 3.19 and 3.20 for M_{40} and M_{30} concretes respectively.

Table 3.19 Relationship between compressive strength and modulus of elasticity for M_{40} concrete

Sl. No	Type of Mix	Average compressive strength (MPa)	f_{ck} (MPa)	Mean modulus of elasticity (MPa)	E_c (MPa)	Coefficient k
1	R	50	39.4	32772	28977	4614
2	FA20	50	38.8	32943	29148	4681
3	FA40	48	37.1	31742	27617	4534
4	HS1	54	43.1	42647	38852	5917
5	HS 2	58	47.1	44131	40336	5877
6	FS1	55	43.6	39079	35284	5343
7	FS2	56	45.4	41883	38088	5650
8	FS3	52	41.1	37478	33683	5253
9	FS4	56	45.1	39450	35655	5309

Table 3.20 Relationship between compressive strength and modulus of elasticity for M_{30} concrete

Sl. No	Type of Mix	Average compressive strength (MPa)	f_{ck} (MPa)	Mean modulus of elasticity (MPa)	E_c (MPa)	Coefficient k
1	R	45	35.1	32089	27964	4720
2	FA20	42	32.1	31656	27531	4859
3	FA40	40	30.1	30137	26342	4801
4	HS1	50	40.1	37214	33089	5225
5	HS 2	53	43.1	40099	35974	5480
6	FS1	46	36.1	37233	33108	5510
7	FS2	48	38.1	39473	35348	5727
8	FS3	44	34.1	35336	31211	5345
9	FS4	45	36.1	36680	32555	5418

From Tables 3.19 and 3.20 it is seen that the value of **k** varies between 4534 and 5917 for fly ash and steel fiber concrete, whereas for reference concrete it is in between 4600-4700. The value suggested in IS 456(2000) is 5000.

To estimate modulus of elasticity of concrete from compression strength incorporating the effect of addition of steel fiber and fly ash, the constant ‘k’ is proposed using the equation 3.12.

$$k = k_1 * k_2 * k_3 \text{ -----(3.12)}$$

where k_1 = constant for reference concrete = 5000 (as suggested by IS)

$$k_2 = \text{constant for SFRC} = 0.154(\text{SF})+1$$

SF is the steel fiber content in percentage

$$k_3 = \text{constant for fly ash concrete} = 0.318(\text{FA}/100)^2 - 0.293(\text{FA}/100) + 1$$

FA is the fly ash content in percentage

To verify the validity of proposed model for estimating the modulus of elasticity from characteristic compressive strength, Chi square test was employed and the results are given in Table 3.21. The percentage root mean squared error (PRMSE) is also determined to justify the results.

Table 3.21 Chi-square test for prediction model of modulus of elasticity

	Mix	Ec (observed) GPa	Ec (predicted) GPa	$[Ec(o) - Ec(p)]^2$	$\chi^2 = \frac{[Ec(o) - Ec(p)]^2}{[Ec(p)]}$
M ₄₀	R	28.98	31.38	5.797	0.185
	FA20	29.14	29.72	0.323	0.011
	FA40	27.62	28.44	0.669	0.024
	HS1	38.85	35.35	12.244	0.346
	HS 2	40.34	39.60	0.543	0.014
	FS1	35.28	33.93	1.844	0.054
	FS2	38.09	37.09	0.988	0.027
	FS3	33.68	32.23	2.102	0.065
	FS4	35.66	36.18	0.275	0.008
	M ₃₀	R	27.96	29.62	2.751
FA20		27.53	27.03	0.252	0.009
FA40		26.34	25.61	0.532	0.021
HS1		33.09	34.10	1.023	0.030
HS 2		35.97	37.88	3.634	0.096
FS1		33.11	30.87	5.007	0.162
FS2		35.35	33.98	1.868	0.055
FS3		31.21	29.36	3.425	0.117
FS4		32.56	32.37	0.035	0.001
					Σ

Sample size n=18

$$\chi^2_{\text{calculated}} = 1.317$$

$$\chi^2_{\text{critical}} = 5.697 \quad [0.995, 17]$$

Percentage root mean squared error(PRMSE)= 4.726%

From the analysis it is observed that, the $\chi^2_{\text{calculated}} = 1.317$ which is much lesser than χ^2_{critical} from the Chi-square distribution table for $\alpha=0.995$ and degree of freedom [17] is 5.697. This clearly indicates that the developed model is a best fit to estimate modulus of elasticity incorporating fly ash and steel fibers. The PRMSE value is 4.726% is also found to be very low. Fig 3.46 shows that there is a good correlation between observed and predicted values as the points are clustered near diagonal lines. The modulus of elasticity of FS4 concrete is estimated as 34000MPa and 30000 MPa for M₄₀ and M₃₀ concrete respectively while designing the rigid pavements.

Fig 3.46 represents the correlation between the observed modulus of elasticity and predicted value of modulus of elasticity based on the proposed equation.

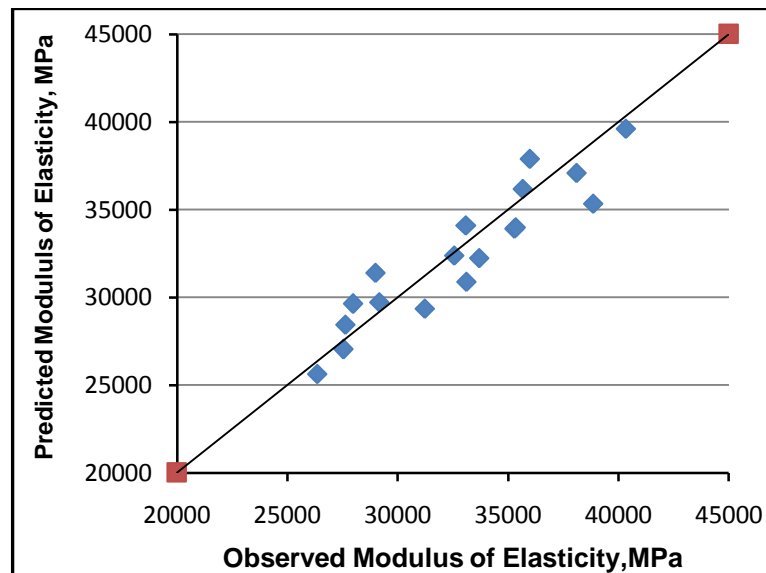


Fig 3.46 Plot of observed modulus of elasticity v/s predicted modulus of elasticity

3.10 SUMMARY

In this chapter, detailed investigations carried out to characterize the constituent materials used in this study, were discussed in detail. The mix design for M₄₀ and M₃₀ concrete was carried out based on available guidelines. The increase in volume of concrete due to addition of fly ash was adjusted with quantity of fine aggregates and increased volume due to incorporation of steel fibers was neglected. The use of graded aggregates of 31.5mm and down size in preparation of steel fiber reinforced concrete with and without fly ash was found satisfactory. The parametric studies were conducted on both fresh and hardened concretes to establish the variation in strength properties due to the inclusion of steel fiber and fly ash. The use of 40 percent fly ash in replacement of cement tends to improve workability. Also, with same amount of water it helped in gaining the lost workability due to incorporation of steel fibers. The test results show that the use of steel fiber (1%) with either Portland cement concrete or fly ash concrete improve the compressive, flexural and split tensile strength properties of the concrete. The flexural and split tensile strengths of steel fiber reinforced fly ash concrete were almost equal or slightly lesser than that of steel fiber concrete. This reveals that the partial replacement of cement by fly ash do not affect adversely the tensile behaviour of SFRC. This result is encouraging to use a waste material, fly ash, as partial replacement to cement in rigid pavements thereby reducing the cost of construction. Mathematic models for flexural strength and elastic modulus were established using one parameter, characteristic compressive strength to facilitate pavement design.

CHAPTER 4

FATIGUE STUDIES AND ANALYSIS

4.1 GENERAL

Construction material subjected to repetitive or cyclic loading have to be qualified for their fatigue behaviour. Generally, their behaviour is considered to be satisfactory at a particular stress level, if they withstand two million cycles of repetitive loading without distress or failure at that stress level. The addition of fibre in the concrete matrix improves the flexural strength, flexural fatigue strength, impact strength, shock resistance, ductility, and flexural toughness in concrete, besides delaying and arresting crack propagation. Fatigue is often described by a parameter “Fatigue life”, which essentially represents the number of cycles the material can withstand under a given pattern of repetitive loading before failure. Fatigue cracking in concrete pavements is a key failure mechanism, and is the result of repeated applications of load at stress levels less than the flexural strength of the concrete. Fatigue testing is a very time consuming and expensive process and a more number of samples have to be tested. An upper limit of 1,50,000 cycles was selected in this investigation. The test was terminated when the failure of the specimen occurred or the upper limit was reached, whichever was earlier. In the experimental investigation it was found that the specimen reached the upper limit at stress level 65%. Hence, in this study the stress levels were limited to 70%, 75%, 80% and 85%. As the uncertainty involved in this test is very high, the maximum stress level was restricted to 85%. A probabilistic analysis of fatigue test data was carried out to ascertain the fatigue life of the material. In this chapter, basic information pertaining to the fatigue study followed by the test procedure, methodology and interpretation of results were presented.

4.1.1 S-N Curve

To predict the fatigue life of a material, the relationship between stress level (ratio of maximum applied stress to the modulus of rupture) and the number of repetitions ‘N’ causing the failure was often used by most of the researchers. The relationship

established is known as Wohler equation and is shown by S-N Curve or Wohler curve (Oh, 1986). A typical Wohler diagram is presented in Fig 4.1. Certain materials (such as steel) have endurance limit which represents a stress level below which the material can sustain infinite repetition of load (curve A). Some other metals such as aluminium do not exhibit well defined endurance limit (curve B). This S-N curve enables one to predict the mean fatigue life of concrete under given stress level or amplitude of cyclic stress (Roylance 2001).

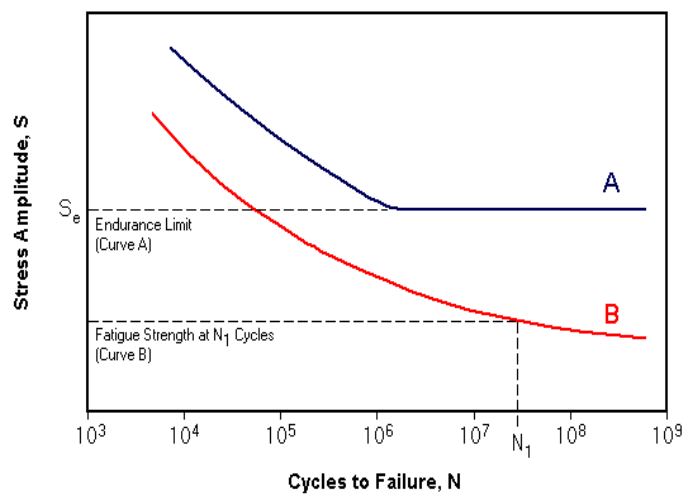


Fig 4.1 Typical Wohler diagram

(source:[http://www.ux.uis.no/Lemu.g.hirpa/KdB/ME/S-N diagram.pdf](http://www.ux.uis.no/Lemu.g.hirpa/KdB/ME/S-N%20diagram.pdf))

In general, S-N curves represent progressive structural deterioration and gradual breaking of bonds (Oh 1986) and can be represented by

$$\text{Stress level } S = \frac{\sigma_{\max}}{MR} = a - b \log(N) \quad \text{--(4.1)}$$

Where, σ_{\max} = Maximum applied stress;

MR = Modulus of rupture of beam;

N = no. of load repetition to cause failure

a and **b** are the experimental coefficients which vary with the loading condition

PCA model (Packard and Tayabji 1983), Darter's zero maintenance models (Darter and Barenberg 1977) are the examples of such fatigue models. Another form of

fatigue equation is a power function developed from concrete pavement slab in the AASHTO Road Test (Shi et al. 1993)

$$S = \frac{\sigma_{\max}}{MR} = A N^{-B} \quad \text{-- (4.2)}$$

where A and B are the regression coefficients.

Endurance Limit: Certain materials have a fatigue limit or endurance limit which represents a stress level below which the material does not fail and can be cycled infinitely. If the applied stress level is below the endurance limit of the material, the structure is said to have an infinite life.

Miner's hypothesis

Miner's hypothesis on the fatigue damage theory has been widely used in pavement design and evaluation (Rao and Roesler 2008). Miner's fatigue damage accumulation hypothesis (Miner, 1945) is an empirical relation, which assumes that damage accumulates linearly and is given as follows:

$$\text{Fatigue Damage} = \sum \frac{n_i}{N_i} \quad \text{-- (4.3)}$$

where

n_i = Number of actual load applications under conditions represented by i.

N_i = Number of allowable load applications until failure under conditions represented by i.

Miner's hypothesis allows the summation of fatigue damage from loads of varying magnitudes and under a multitude of environmental conditions. According to Miner's hypothesis, materials should fracture when the fatigue damage equals unity, although under a calibrated system with reliability, this damage sum does not necessarily have to be unity (Rao and Roesler 2008). There is widespread acceptance of Miner's hypothesis in pavement engineering for thickness design and failure analysis (Puttappa et. al 2004, IRC 58- 2002).

4.2 FATIGUE MODELS

Several fatigue curves for concrete pavement have been developed using field and laboratory data which relate the stress level to the number of loads until failure (Rao and Roesler 2008).

1) Zero-Maintenance Design Beam Fatigue Model (Darter and Barenberg 1977)

—This model was developed using concrete beams, with failure defined as complete beam fracture. Load stresses are calculated at the bottom of the beam using elastic bending beam equation.

$$\log N = 17.61 - 17.61 SR \quad \text{--(4.4)}$$

where, N = Number of stress applications to failure for the given stress ratio SR.

2) Calibrated Mechanistic Design Field Fatigue Model (Salsilli et al 1993)—

This model was developed using Corp of Engineers (COE) field aircraft data and American Association of State Highway Officials (AASHO) Road Test data, with failure defined as 50 percent slab cracking. Load and temperature curling stresses are calculated at the slab edge using the finite element program, ILLI-SLAB.

$$\log N = \left[\frac{-SR^{-5.367} \log [1-P]}{0.0032} \right]^{0.2276} \quad \text{-- (4.5)}$$

where, P = Cracking probability.

3) ERES/COE Field Fatigue Model (Darter 1988)—

This model was developed using Corp of Engineers (COE) field aircraft data, with failure defined as 50 percent slab cracking. Load stresses were calculated at the slab edge using the influence chart software, H-51, and reduced by a factor of 0.75 to account for load transfer and support conditions.

Cumulative Fatigue Damage Analysis of Concrete Pavement Using Accelerated Testing Results

$$\log N = 2.13 SR^{-1.2} \quad \text{-- (4.6)}$$

4) Foxworthy Field Fatigue Model (Foxworthy 1985)

-This model was developed using Corp of Engineers (COE) field aircraft data, with failure defined as 50 percent slab cracking. Load stresses were calculated at the slab edge using the finite element program, ILLI-SLAB.

$$\log N = 1.323(1/SR) + 0.588 \quad \text{-- (4.7)}$$

5) PCA Beam Fatigue Model (Packard and Tayabji 1983)— This model was developed using concrete beams, with failure defined as complete beam fracture. Load stresses were calculated at the bottom of the beam using the bending beam equation.

$$\text{For } SR \geq 0.55 \quad \log N = 11.737 - 12.077 SR \quad \text{-- (4.8)}$$

$$\text{for } 0.45 < SR < 0.55 \quad N = \left[\frac{4.2577}{SR - 0.4325} \right]^{3.268} \quad \text{-- (4.9)}$$

$$\text{for } SR \leq 0.45 \quad N = \text{unlimited}$$

This model has been adopted in IRC 58:2002 for design of rigid pavements based on fatigue behaviour.

6) Slab Fatigue model (Roesler and Hiller 2008) – This model was developed based on fully-supported slab fatigue tests, repeatedly loaded at the edge of the slab and represents 50 percent probability of fatigue failure:

$$N = \left[\frac{1.2968}{\sigma / \text{MOR}_{beam}} \right]^{32.57} \quad \text{-- (4.10)}$$

4.3 PROBABILISTIC ANALYSIS OF THE FATIGUE DATA

As the fatigue test data of concrete show considerable scatter and are random in nature, a probabilistic approach can be introduced for analysing the fatigue data and evaluating probability of unfavourable performance (Oh 1986). The ASTM guidelines for fatigue testing and the statistical analysis of fatigue data suggest that the fatigue life may be assumed to be normally distributed and thus a lognormal distribution is extensively used (Mohammadi and Kaushik 2005). Later, experimental studies on the basis of physically valid assumptions have shown that the distribution of fatigue life of concrete under given stress level follows the Weibull distribution and is most commonly employed in assessing reliability of composite structures (Sakin and Ay 2008). A Weibull distribution is characterized by three parameters: 1) the shape parameter (α) which describes the shape of the distribution; 2) the characteristic life or scale parameter (μ); and 3) the location parameter (n_0).

The probability density function (PDF) $f_N(n)$ and the cumulative distribution function (CDF) $F_N(n)$ may be expressed in the following forms (Oh 1986, Shi et al. 1993, Mohammadi and Kaushik, 2005)

$$f_N(n) = \frac{\alpha}{\mu - n_0} \left(\frac{n - n_0}{\mu - n_0} \right)^{\alpha - 1} \exp \left[- \left(\frac{n - n_0}{\mu - n_0} \right)^\alpha \right]; n \geq n_0 \quad -- (4.11)$$

and

$$F_N(n) = 1 - \exp \left[- \left(\frac{n - n_0}{\mu - n_0} \right)^\alpha \right]; n \geq n_0 \quad -- (4.12)$$

where n is the specific value of a random variable N ; α =shape parameter or Weibull slope at stress level S ; μ =scale parameter or characteristic life at which 63.2% of specimen fail under given stress level S ; and n_0 =location parameter or minimum life at stress level S .

The hazard function can be obtained from

$$h_N(n) = \alpha \left(\frac{n - n_0}{\mu - n_0} \right)^{\alpha - 1}; n \geq n_0 \quad -- (4.13)$$

The hazard function or failure rate function of Weibull distribution increases with time or with an increase in the number of cycles for $\alpha \geq 1$ only, which is compatible with the expected fatigue behaviour of engineering material (Singh and Kaushik 2000). When location parameter is set to zero ($n_0=0$), it is reduced to a two parameter Weibull distribution. There are several methods of estimating external parameters namely: 1) Graphical method; 2) Method of maximum likelihood; and 3) Method of moments.

4.3.1 Graphical Method

The probability that the member survives during the given interval may be expressed as: $L_T(t) = P(T > t) = 1 - F_T(t)$,

where, $L_T(t)$ = reliability function and $F_T(t)$ = probability distribution function of T .

The survivorship function may be obtained by:

$$L_N(n) = 1 - F_N(n) = \exp \left[- \left(\frac{n}{\mu} \right)^\alpha \right] \quad --(4.14)$$

Taking logarithm on both sides:

$$\ln(L_N(n)) = \left[- \left(\frac{n}{\mu} \right)^\alpha \right] \quad -- (4.15)$$

Taking logarithm on both sides again:

$$\ln[\ln(1/L_N(n))] = \ln \left[- \left(\frac{n}{\mu} \right)^\alpha \right] = \alpha \ln n - \alpha \ln \mu \quad \text{---(4.16)}$$

Equation (4.16) may be written in the following form: $Y = \alpha X - B$ which represents a linear relationship between Y and X with slope of α and intercept B , where $Y = \ln[\ln(1/L_N(n))]$; $X = \ln n$; $B = \alpha \ln \mu$.

In order to obtain a graphic form of Equation (4.16), the fatigue life data at a given stress level are arranged in ascending order of cycles to failure. The empirical survivorship function $L_N(n)$ for each fatigue life data ranked in the order of number of cycles to failure at a given stress level is calculated using the mean rank, $L_N(n) = 1 - [i/(k+1)]$, in which i denotes order number ($i = 1, 2, 3, \dots, k$) and k represents the number of fatigue data (sample size) under consideration at a particular stress level S .

A graph is then plotted between $\ln \left[\ln \left(\frac{1}{L_N(n)} \right) \right]$ and $\ln(n)$, and the data falls approximately along a straight line assuming n_0 as zero. The slope of best fit straight line drawn through the data provides an estimate of the shape parameter α . The characteristic life μ can be obtained using the equation $B = \alpha \ln \mu$, where B is a constant on the straight line obtained from the graph.

4.3.2 Method of Moments

Estimating the parameters by method of moments requires necessary sample mean and sample variance. The sample mean and variance of Weibull distribution are given by:

$E(N) = \mu \Gamma(1 + \frac{1}{\alpha})$; $E(N^2) = \mu^2 \Gamma(1 + \frac{2}{\alpha})$ in which $\Gamma(\)$ represents Gamma function.

Then sample mean $\mu_N = E(N)$ and sample variance $\sigma_N^2 = E(N^2) - (E(N))^2$

$$\text{And } V_N^2 = (\sigma_N / \mu_N)^2 = \frac{\Gamma(1 + \frac{2}{\alpha})}{\Gamma^2(1 + \frac{1}{\alpha})} - 1 \quad \text{-- (4.17)}$$

Coefficient of Variation (COV) = $V_N = (\sigma_N / \mu_N)$

The dimensionless parameter α can be approximately reduced to:

$$\alpha = V_N^{-1.08} \quad \text{-- (4.18)}$$

$$\text{and } \mu = \mu_N / \Gamma\left(1 + \frac{1}{\alpha}\right) \quad \text{-- (4.19)}$$

Equations (4.18) and (4.19) can be used to estimate the values of parameters of the Weibull distribution.

4.3.3 Least Squares Method (LSM)

This method is commonly used in engineering problems. Consider the linear relation between two variables, as in the case of Equation (4.16)

$\ln[\ln(1/L_N(n))] = \alpha \ln n - \alpha \ln \mu$ is a linear equation.

$$\text{Mean } \bar{x} = \frac{1}{n} \sum_{i=1}^n \ln \left\{ \ln \left[\frac{1}{L_N(n)} \right] \right\}; \quad L_N(n) = 1 - [i/(k+1)] \quad \text{and} \quad \bar{Y} = \frac{1}{n} \sum_{i=1}^n \ln x_i$$

$$\text{Shape parameter } \hat{\alpha} = \frac{\left\{ n \sum_{i=1}^n \ln x_i \left(\ln \left[\frac{1}{L_N(n)} \right] \right) \right\} - \left\{ \sum_{i=1}^n \left(\ln \left[\frac{1}{L_N(n)} \right] \right) \right\} \sum_{i=1}^n \ln x_i}{\left\{ n \sum_{i=1}^n (\ln x_i)^2 \right\} - \left\{ \sum_{i=1}^n (\ln x_i) \right\}^2} \quad \text{-- (4.20)}$$

$$\text{Scale parameter } \hat{\mu} = e^{\left(\bar{Y} - \frac{\bar{x}}{\hat{\alpha}} \right)} \quad \text{-- (4.21)}$$

4.3.4 Maximum Likelihood Estimator (MLE) Method

The method was introduced by Harter and Moore (1965). Let $x_1, x_2 \dots x_n$ be a random sample of size n drawn from a probability density function $f_x(x, \theta)$ where θ is an unknown parameter. The likelihood function of the sample is the joint density of n random variables and is the function of unknown parameter. Thus:

$$L = \prod_{i=1}^n f_x(x, \theta) \quad \text{-- (4.22)}$$

is the likelihood function. The maximum likelihood estimator of θ is θ^* and the value θ maximizes L .

In order to use MLE to estimate the Weibull parameters, i.e. the shape and the scale parameters, consider the PDF of Weibull distribution, then likelihood function will be:

$$L(x_1, x_2 \dots x_n; \alpha, \mu) = \prod_{i=1}^n \frac{\alpha}{\mu} \left(\frac{x_i}{\mu} \right)^{\alpha-1} e^{-\left(\frac{x_i}{\mu} \right)^\alpha} \quad \text{-- (4.23)}$$

On taking logarithm and differentiating w.r.t α and μ , and equating to zero, two eliminating equations are obtained. Elimination of μ from these equations and simplification will result in estimator $\mu^* = \alpha$. This may require an iterative procedure. Once α is determined, μ can be estimated (Mohammad 2000)

4.3.5 Availability Workbench(AWB) -Weibull Module

Availability workbench from ISOGRAPH is powerful simulation software for improving the asset performance. Using the Availability workbench one can optimize reliability and maintenance strategies, analyse system availability, perform Weibull analysis and establish the life cycle cost. Weibull analysis is a method used to analyse historical failures and produce probabilistic failure distributions based on the data. Weibull analysis module is extremely easy to use; data may be entered manually by the user, imported from elsewhere or copied and pasted from the clip board. The software automatically fits data provided to the required distribution. The results can be displayed graphically as a cumulative probability plot or conditional probability density plot, as shown in Fig 4.2 (www.availabilityworkbench.com).

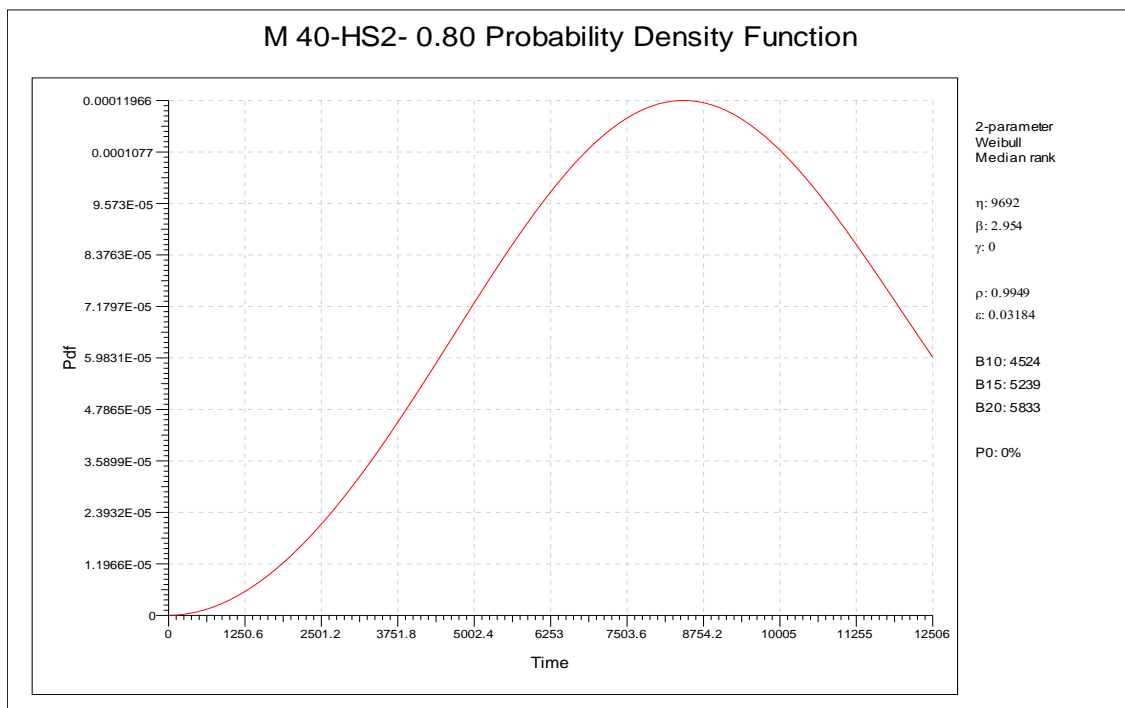


Fig 4.2 Weibull distribution - probability density function plot

4.4 DESIGN FATIGUE LIFE

The design life N_D should be selected such that only a small probability of failure will occur. Design life may be selected corresponding to the acceptable design reliability. The design reliability may be expressed as $P[N > N_D] = 1 - P_f$ where P_f is the probability of failure (Oh 1986).

$P_f = P[N < N_D] = F_N(n)$, the design life corresponding to permissible probability is obtained from:

$$N_D = \mu \left[\ln \frac{1}{1 - P_f} \right]^{\frac{1}{\alpha}} \quad \text{-- (4.24)}$$

And required mean fatigue life is then obtained from

$$N_D = \frac{E[N]}{\varphi} \quad \text{where } \varphi = \Gamma(1 + 1/\alpha)(P_f)^{-1/\alpha}$$

$$E(N) = \mu \Gamma\left(1 + \frac{1}{\alpha}\right)$$

4.5 ACCELERATED FATIGUE TESTING EQUIPMENT

The equipment used in the present study for fatigue analysis was developed in Bangalore University (Reddy and Veeraraghavan 2010) and was manufactured by M/s Spranktronics, Bangalore. Fig 4.3 shows the Accelerated Fatigue testing equipment used in this study and it has the following main components:

1. Loading Frame and loading system
2. Load sensing devices
3. Deflection recording system (LVDTs)
4. Servo Amplifier system
5. Control unit to monitor load and repetitions
6. Computer system



Fig 4.3 Accelerated Fatigue (repeated load) test set up

The loading system consists of a double acting hydraulic cylinder with suitable mounting flanges. It is associated with a power pack unit consisting of pump coupled with motor (1 HP, 3-phase, 1440 rpm), valves and filters, heat exchanger (cooling system), servo valve, pressure gauge etc. A 20 kN (2000 kg) capacity load cell Load cells (Transducers) was used to sense the applied load to the specimen during testing.

Deflection Recorder: LVDTs were used to sense the deflections with the help of suitable signal conditioners and display panels.

Frequency and Waveform of loading: The loading is generally with half sinusoidal waveform (zero -maximum load-zero). The application frequency can be between 1-5 Hz with or without rest period.

Servo Amplifier System: It is used to link the function generator and the servo valve. Control Unit is used to monitor the load and the repetitions. It is connected to the PC with an ADD ON Card to acquire or log the data.

4.6 METHODOLOGY

The repeated load test was carried out on beam specimens of size 100 x100 x 500 mm. The beams were simply supported over a span of 400 mm and loaded at third points. The tests were carried out in load control using a constant amplitude half sinusoidal waveform at a frequency of 2Hz without any rest period in an MTS Servo Hydraulic machine. The minimum load was kept to zero and the maximum load selected based on the stress level; the ratio of applied stress to average static flexural stress (modulus of rupture). As the stress level decreases the number of repetitions required for failure increases, lower stress levels (below 0.65) were kept out of the scope of study. Fig 4.4 shows the failure mechanism of beam under flexural fatigue test and Fig 4.5 shows the crack propagation during fatigue test before failure of specimen.

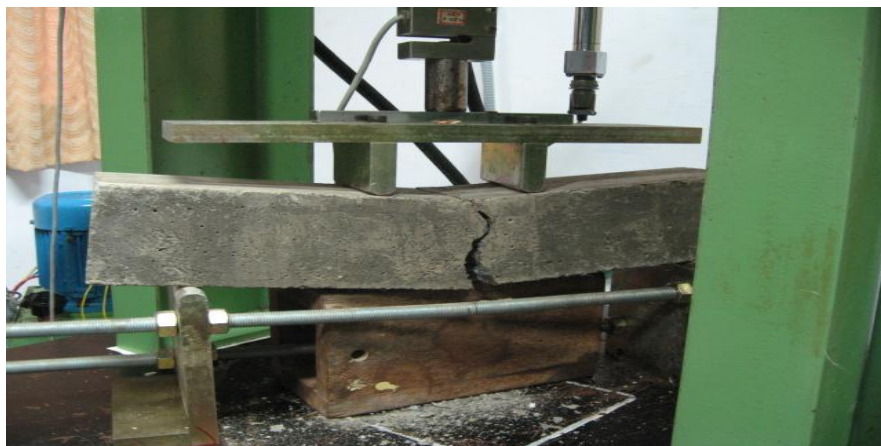


Fig 4.4 Failure mechanism of beam under flexural fatigue test



Fig 4.5 Crack propagation during flexural fatigue test

4.7 FATIGUE TEST RESULTS

Five concrete beam specimens each for both M₃₀ and M₄₀ were tested in repetitive load equipment at stress ratios (levels) 0.70, 0.75, 0.80 and 0.85 for all the designated mixes as presented in Tables 4.1 and 4.2. Outliers were identified and excluded from the analysis. The fatigue life data were arranged in ascending order. The fractured surface of steel fibre reinforced fly ash concrete beam and failed specimens during fatigue test are shown in Figs 4.6 and 4.7.

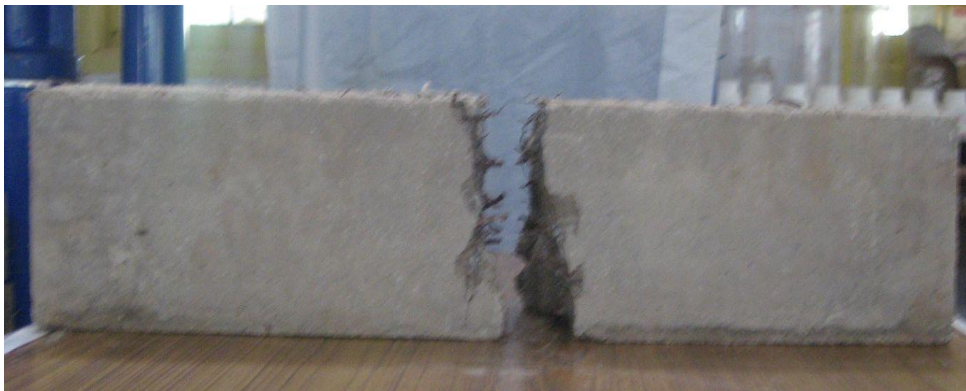


Fig 4.6 Fractured surface of Steel Fiber Reinforced Fly ash concrete beam



Fig 4.7 Failed specimens (FS3)

Table 4.1 Fatigue life data (number of cycles to failure) in ascending order for M₃₀ concrete

Designation	Order No. (i)	Stress Levels			
		0.85	0.80	0.75	0.70
R (Control concrete)	1	90	1665	11150	35343
	2	156	2240	18680	45675
	3	265	3200	28935	73444
	4	308	4260	32849	83151
	5	360	5170	35118	-
HS1 (Steel fibers 0.5%)	1	126	2356	10764	32413
	2	228	2413	11864	41373
	3	268	4135	26810	53264
	4	328	5600	49197	75756
	5	417	6337	51500	90300
HS2 (Steel fibers 1.0%)	1	158	2247	14105	28130
	2	190	3520	24500	37656
	3	235	4263	34750	48344
	4	332	4575	37900	67405
	5	424	10370	45617	86172
FS1 (Fly ash 20% + Steel fibers 0.5%)	1	135	2000	9977	44353
	2	215	4597	14776	58745
	3	294	4883	23446	74597
	4	300	7687	35292	94148
	5	320	9098	54353	-
FS2 (Fly ash 20% + Steel fibers 1.0%) M	1	150	2982	13678	30807
	2	260	4402	22373	58957
	3	265	4874	30340	96444
	4	337	5438	37957	105793
	5	412	6490	59745	-
FS3 (Fly ash 40% + Steel fibers 0.5%)	1	26*	2878	25560	65743
	2	329	5143	35204	73930
	3	615	7476	41326	85051
	4	927	10850	46700	97564
	5	1409	15435	58384	114631
FS4 (Fly ash 40% + Steel fibers 1.0%)	1	167	2345	28322	67676
	2	292	3262	32611	75787
	3	416	4977	41523	87433
	4	875	6926	52110	96209
	5	1204	8974	62730	118886

* outliers excluded from analysis

**Table 4.2 Fatigue life data(number of cycles to failure) in ascending order for
M₄₀ concrete**

Designation	Order No. (i)	Stress Levels			
		0.85	0.80	0.75	0.70
R (Control concrete)	1	72	1518	10512	35432
	2	120	2512	38035	65434
	3	150	2849	48680	84481
	4	224	8935	54355	97236
	5	235	11150	67500	112375
	6	308	-	-	-
	7	360	-	-	-
	8	665	-	-	-
HS1 (Steel fibers 0.5%)	1	100	1620	28709	52760
	2	230	2412	29880	82323
	3	268	6549	38550	89585
	4	324	10764	51112	90995
	5	756	17510	58800	97375
	6	783	-	-	104148
HS2 (Steel fibers 1.0%)	1	355	4910	7005*	25970
	2	388	7189	34209	57893
	3	531	8772	47500	73471
	4	558	9620	57375	82331
	5	743	12506	63800	99228
	6	977	-	65242	105582
FS1 (Fly ash 20% + Steel fibers 0.5%)	1	100	2334	10890	65784
	2	140	2830	28591	77696
	3	225	6676	37674	89471
	4	407	9438	64326	108298
	5	656	14290	-	115410
	6	830	-	-	-
FS2 (Fly ash 20% + Steel fibers 1.0%)	1	35*	1548	30969	68174
	2	202	3051	35732	76478
	3	389	6368	37830	87635
	4	679	8186	47500	92180
	5	984	14100	64347	112320
	6	1333	-	-	-
FS3 (Fly ash 40% + Steel fibers 0.5%)	1	83	956	20622	66800
	2	217	2083	32184	77380
	3	337	4081	45505	82917
	4	538	5350	46056	95318
	5	680	6634	59952	102450
			10000*		

FS4 (Fly ash 40% + Steel fibers 1.0%)	1	45*	2043	10438	62378
	2	142	5280	27674	84599
	3	196	5904	39020	94460
	4	518	7560	64200	111528
	5	665	9755	72434	112311
	6	1484	-	-	-

* outliers excluded from analysis

The stress level versus fatigue life data for each designated mix was presented in the form of S-N curves and can be depicted in Fig. 4.8. The best fit lines were drawn to obtain the regression equations and were given in Table 4.3. General S-N curve using all the fatigue life data irrespective of material and the grade of concrete is drawn and shown in Fig 4.9. The comparative fatigue life at different stress levels using different fatigue models are also given in Table 4.4.

Table 4.3 Regression Equations (S-N curves)

	M₄₀	M₃₀
REFERENCE	SR=-0.0218 ln(N)+0.9679, R ² =0.8866	SR=-0.024 ln(N)+0.9822, R ² =0.9179
HS1	SR=-0.0197 ln(N)+0.9515, R ² =0.85	SR=-0.025 ln(N)+0.9924, R ² =0.8977
HS2	SR=-0.027 ln(N)+1.0257, R ² =0.8762	SR=-0.0249 ln(N)+0.9926, R ² =0.884
FS1	SR=-0.0233 ln(N)+0.9866, R ² =0.874	SR=-0.024 ln(N)+0.9872, R ² =0.8959
FS2	SR=-0.0226 ln(N)+0.9812, R ² =0.8461 Log N=18.85-19.20*SR	SR=-0.024 ln(N)+0.989, R ² =0.898 Log N= 17.90 -18.09*SR
FS3	SR=-0.0232 ln(N)+0.9817, R ² =0.9042	SR=-0.0285 ln(N)+1.041, R ² =0.9005
FS4	SR=-0.022 ln(N)+0.975, R ² =0.8317 Log N=19.24-19.74*SR	SR=-0.0251 ln(N)+1.0051, R ² =0.9028 Log N= 17.39-17.30*SR
ALL	SR=-0.0239 ln(N)+0.9920 R ² =0.8741	SR=-0.0246 ln(N)+0.9939 R ² =0.8881
Together M₃₀&M₄₀	SR=-0.0241 ln(N)+0.9914, R ² =0.8821 Log N=17.866-18.02*SR	

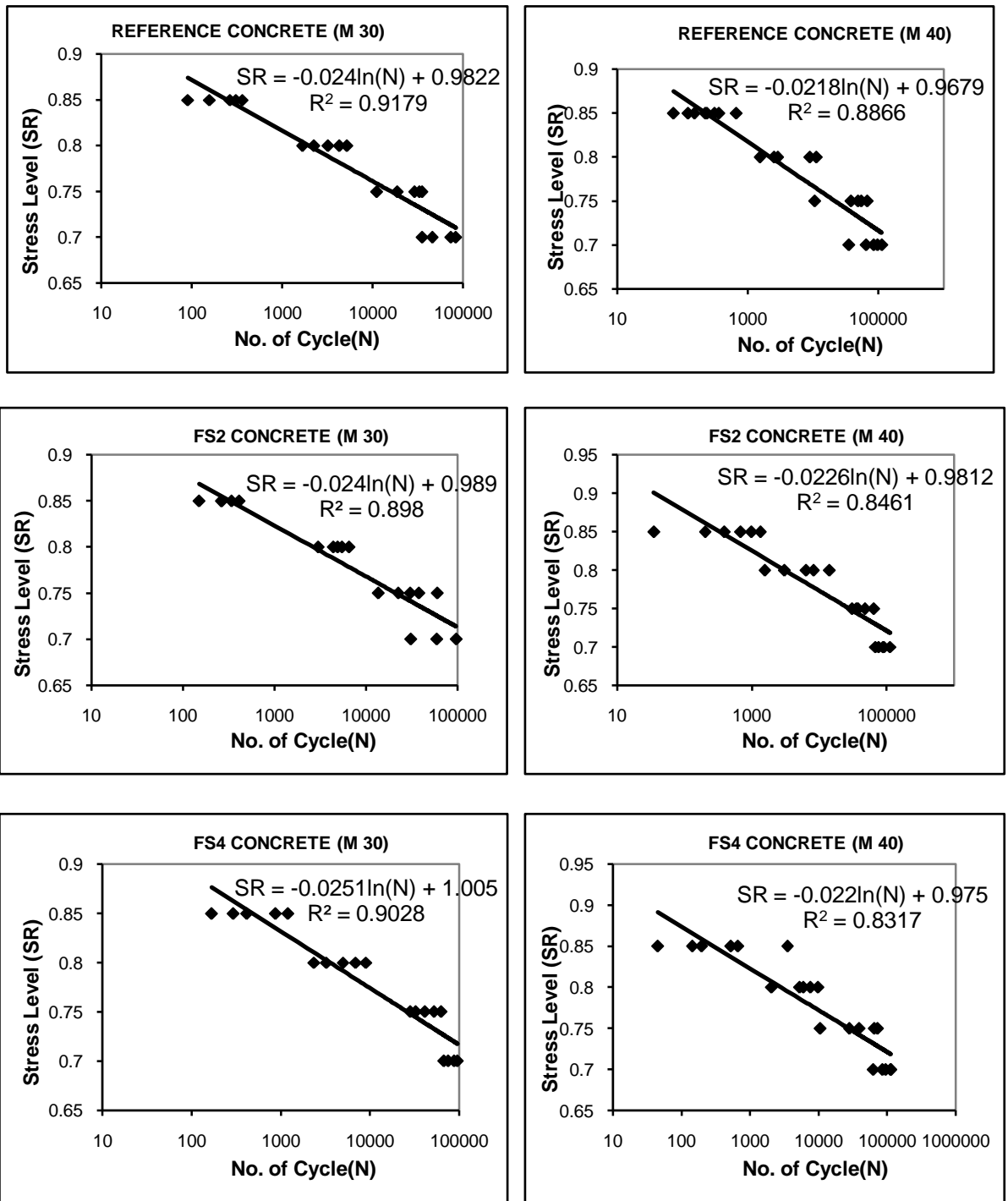


Fig 4.8 S-N Curves for REF, FS2 and FS4 mixes (M₃₀ & M₄₀)

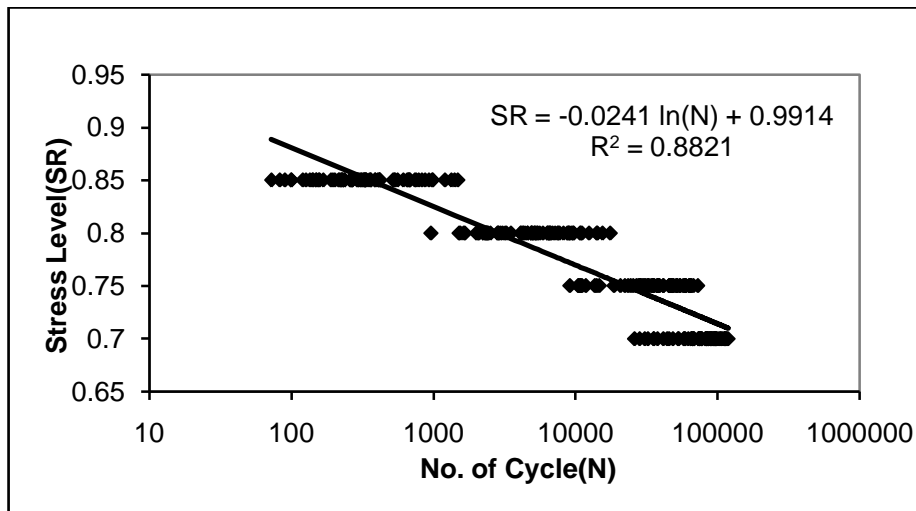


Fig 4.9 S-N curve considering all the fatigue data

The general purpose S-N equation ($SR > 0.60$) for the design of pavements can be written as:

$$\text{Log } N = 17.866 - 18.02 * SR \quad \text{--- (4.25)}$$

for $SR \leq 0.60$ N- unlimited (more than 2 million cycles)

Fig 4.10 represents the graphical representation of general purpose S-N curve.

Table 4.4 Comparison of different fatigue models

SR	No. of cycles to failure				
	Present Regression equation	Zero-Maintenance Design Beam Fatigue Model (Darter 1977)	PCA Beam Fatigue Model /IRC model (Packard and Tayabji 1983)	CMDFF P=0.5 (Salsilli et. al 1993)	ERES/ COE (Darter 1988)
0.45			unlimited		
0.50			762042	3627315	78245
0.55			124351	689717	23153
0.6	unlimited	unlimited	30960	177803	8548
0.65	1419727	1457136	7708	57667	3731
0.7	178311	191867	1919	22329	1853
0.75	22395	25264	478	9940	1019
0.8	2813	3327	119	4947	608
0.85	353	438	30	2696	388
0.9	44	58	8	1582	261
0.95	6	8	2	988	184
0.99	1	1	1	704	143

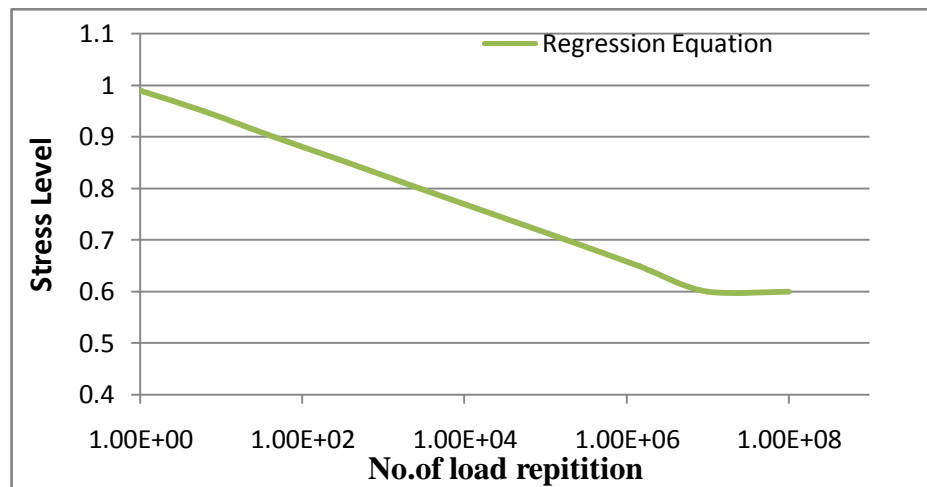


Fig 4.10 General S-N curve for Design of Rigid pavements

4.8 ANALYSIS OF THE FATIGUE DATA

As the fatigue data of different concrete mixes were shown considerable scatter, probabilistic approach was introduced for analysis. The two-parameter Weibull distribution was employed in assessing the reliability, as used by different researchers to describe fatigue data (Mohammadi and Kaushik 2005, Sakin and Ay 2008). To estimate parameters of the distribution the following methods were employed.

- a) Graphical method
- b) Method of moments
- c) Method of Least square
- d) Weibull module of Availability Workbench(AWB)

The fatigue life data of various mixes are analysed using graphical method and shown in Fig 4.11(a-d).

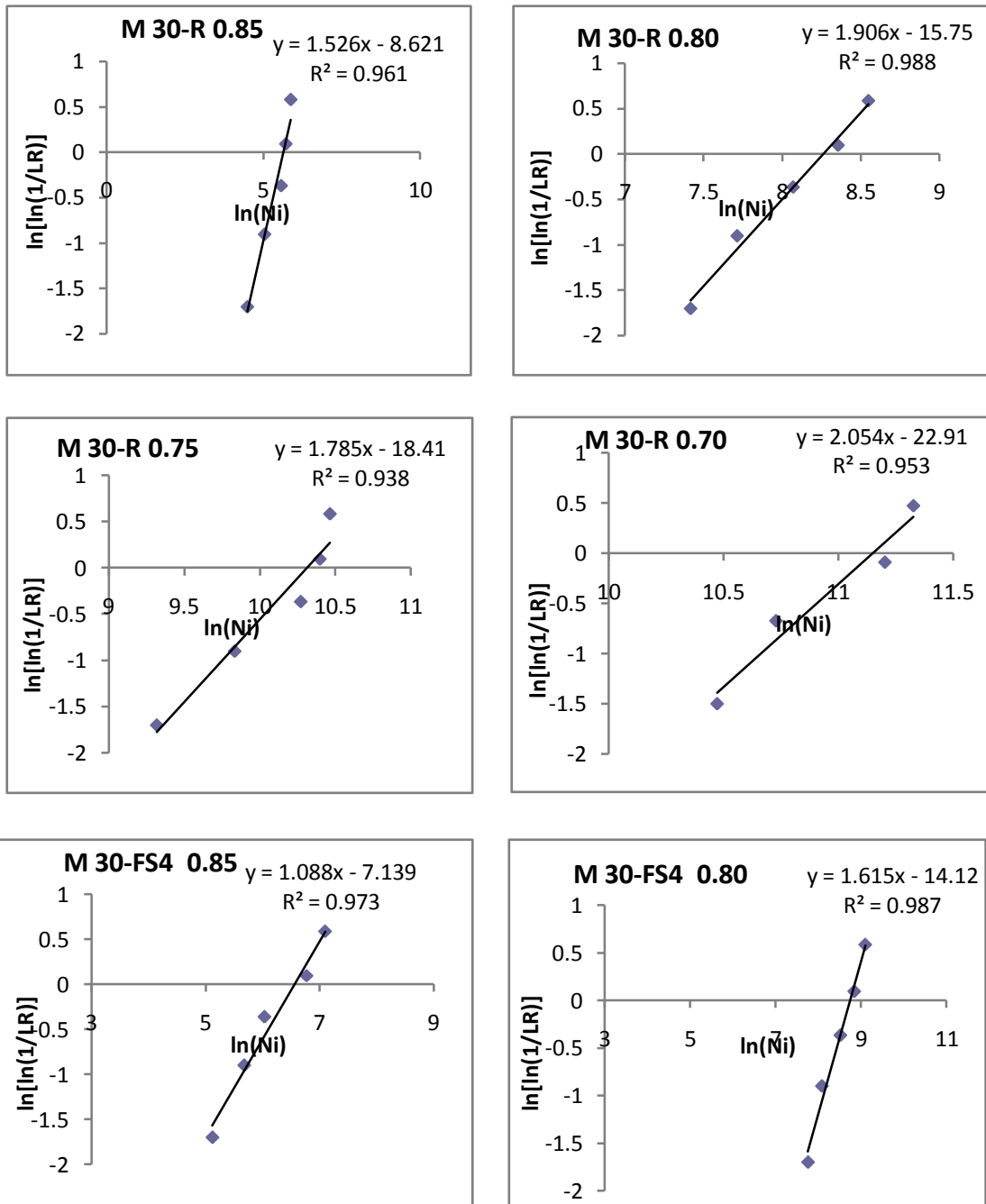
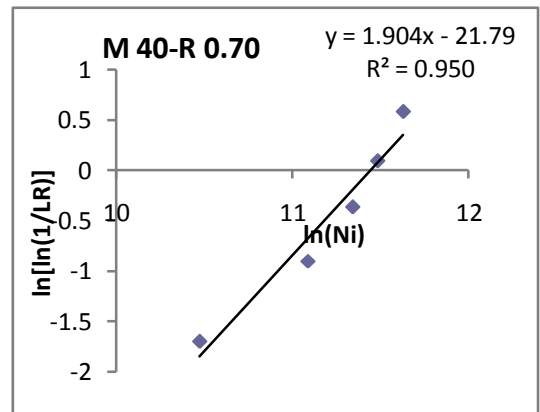
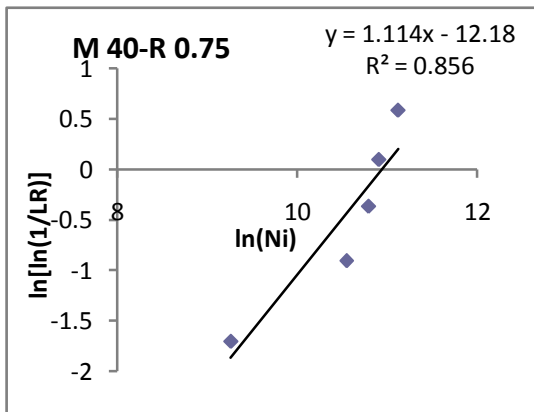
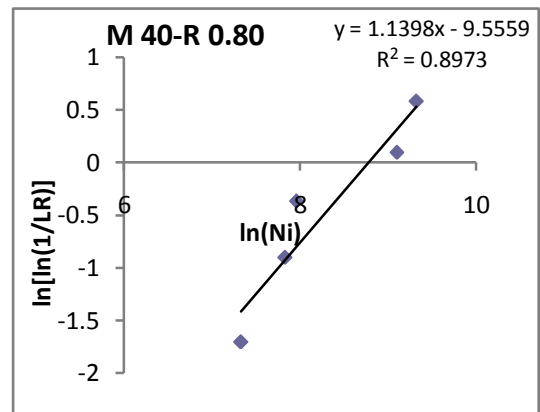
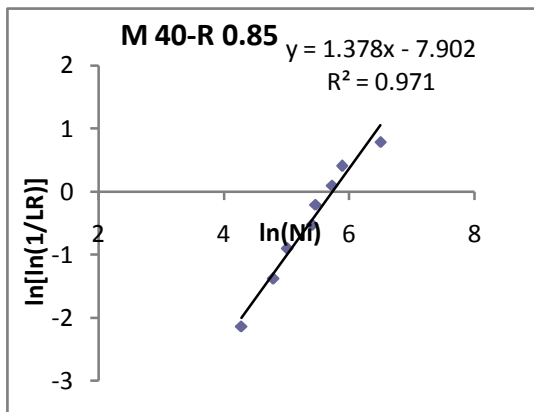
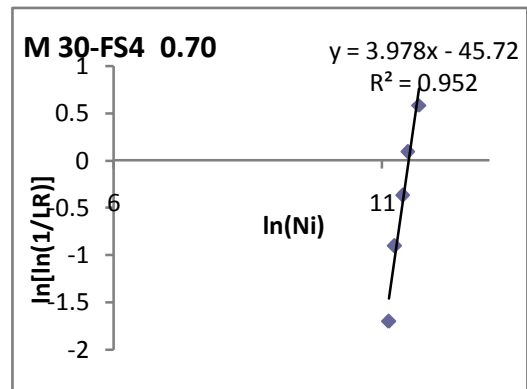
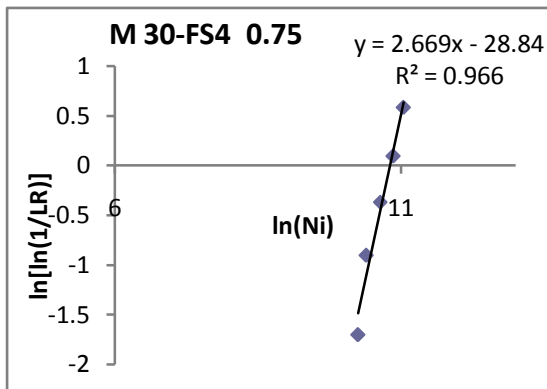
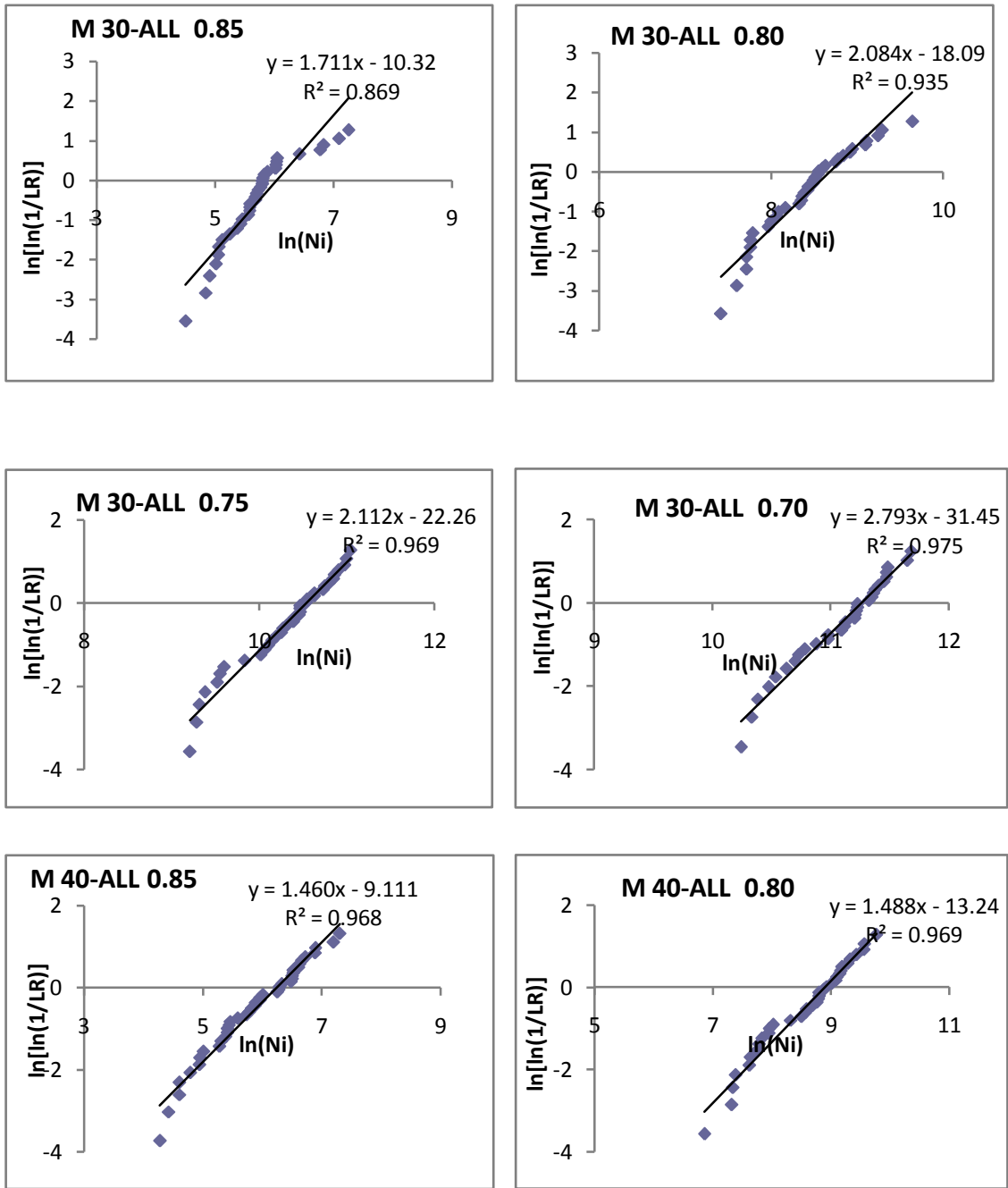


Fig 4.11-a Graphical method to evaluate Weibull parameters (M₃₀ concrete REF and FS4)



**Fig 4.11-b Graphical method to evaluate Weibull parameters
(M₃₀ concrete -FS4 and M₄₀ Concrete REF)**



**Fig 4.11-c Graphical method to evaluate Weibull parameters
(M₃₀ concrete and M₄₀ concrete All data)**

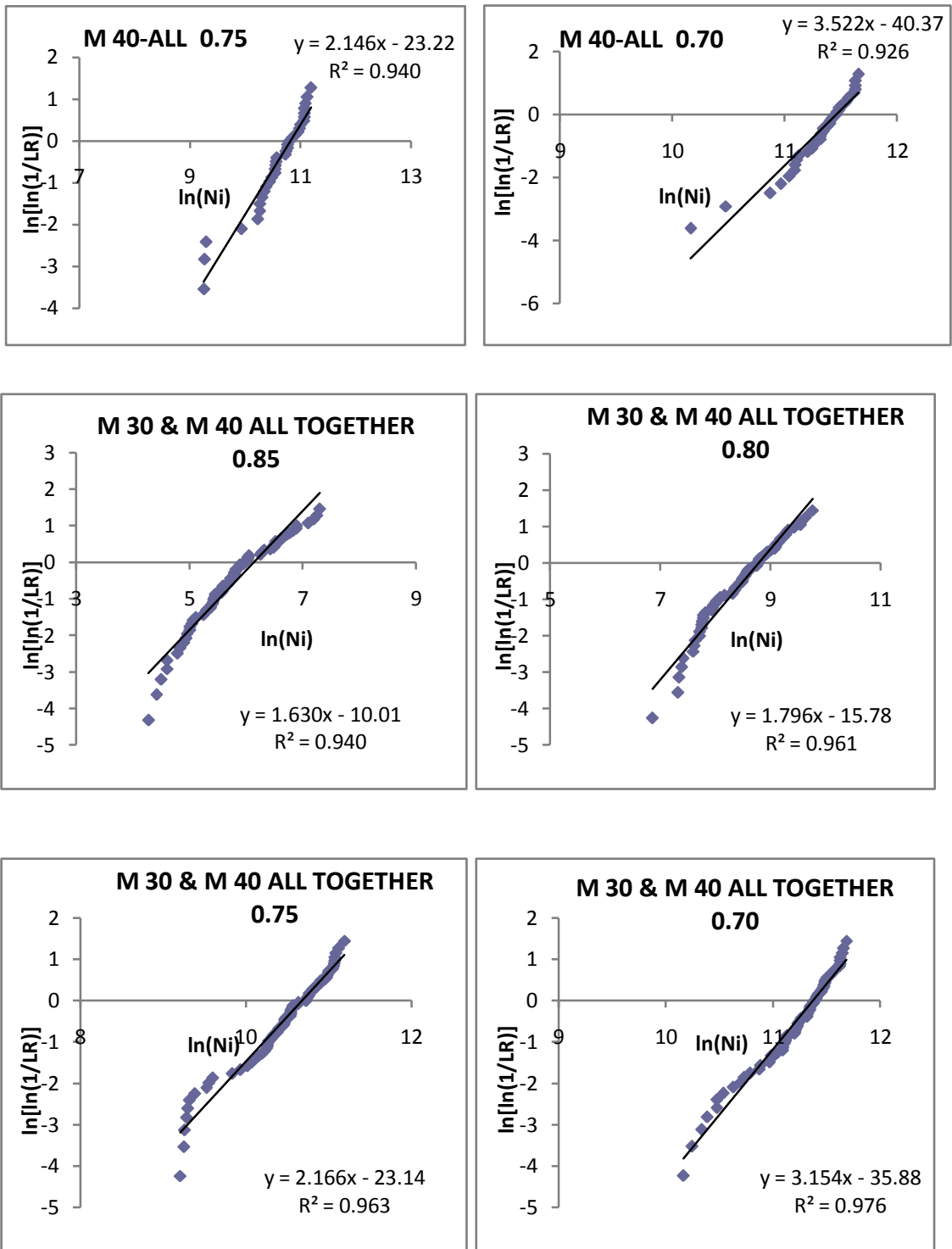


**Fig 4.11-d Graphical method to evaluate Weibull parameters
(M₃₀ and M₄₀ together)**

The results of estimation of parameters of Weibull distribution obtained from other methods for the Reference concrete (R), concrete with steel fibres and fly ash (FS) at various stress levels are presented in Appendix I.

4.8.1 Method of Selection of Weibull Parameters

The Weibull parameters obtained by various methods were compared and selected based on the minimum mean squared error (MSE) as well as accuracy needed for the analysis (Mohammad 2000).

$$\text{MSE} = \frac{\sum_{i=1}^n \{\hat{F}(x_i) - F(x_i)\}^2}{n} \quad \text{-- (4.26)}$$

Where $\hat{F}(x_i) = 1 - e^{-\left(\frac{x_i}{\mu}\right)^\alpha}$ and median rank $F(x_i) = \frac{i-0.3}{n+0.4}$

From the distribution parameters obtained using different methods, it can be concluded that all the methods yield similar values of distribution parameters at each given stress level. Table 4.5 summarizes the Weibull parameters selected based on minimum squared error.

On observation, it is clear that the method of least squares and AWB yield minimum mean squared error followed by the graphical method. Averaging of the results obtained by various methods is also yields lower squared error in many cases, but it requires lot of resources and time. The graphical method is simpler one and requires less computing time. The characteristic life or scale parameter (μ) ranges from 271 to 960 for M₃₀ concrete mixes and 301 to 839 for M₄₀ concrete mixes at the stress level of 0.85. When all the fatigue data were put together the value was 478 at that stress level. Similar observations were made for other stress levels also. No specific trend was observed with the use of steel fibre or fly ash. Hence it can be concluded that the grade of concrete or the material do not have any impact on the fatigue life, as such its own flexural strength is used in calculation of stress level. However, the use of steel fibres enhance the flexural strength of concrete thereby the stress level reduces for a given load stress, which results in increased number of load stress repetition. The value of shape parameter (α) was found to be more than 1 for all the mixes, which truly indicates the progressive degradation of material strength after every repetition.

Hence, fatigue life of steel fibre with fly ash can be suitably described by two parameter Weibull distribution.

Table 4.5 Weibull parameters selected for various mixes based on MSE

Stress level		0.85	0.80	0.75	0.70	
M 30	R	μ	277	3798	29433	69601
		α	1.79	2.21	2.17	2.05
	HS1	μ	315	4844	35630	68182
		α	2.54	2.11	1.30	2.01
	HS2	μ	305	5394	37130	61300
		α	2.5	1.72	1.87	2.30
	FS1	μ	288	6637	31749	75121
		α	2.86	1.76	1.46	3.20
	FS2	μ	324	5326	37951	91446
		α	2.71	4.14	1.82	1.73
	FS3	μ	960	9724	46250	98060
		α	1.64	1.58	3.34	4.33
	FS4	μ	681	3164	48740	97260
		α	1.27	1.89	3.09	4.64
M 40	R	μ	301	6206	54210	94108
		α	1.47	1.14	2.11	2.29
	HS1	μ	490	8846	46657	96860
		α	1.02	1.02	3.07	4.87
	HS2	μ	681	9692	59690	83498
		α	2.31	2.95	3.85	2.73
	FS1	μ	419	8321	42290	100947
		α	1.37	1.29	1.41	3.78
	FS2	μ	839	7702	48954	94384
		α	1.38	1.19	2.92	5.34
	FS3	μ	449	4519	46800	91075
		α	1.28	1.35	2.48	6.09
	FS4	μ	679	7254	50852	102331
		α	1.06	1.69	1.31	4.19
Combined M₃₀ & M₄₀		μ	478	6513	43110	86735
		α	1.43	1.79	2.24	3.28

4.9 GOODNESS OF FIT TEST FOR THE FATIGUE DATA

From the above analysis, the fatigue life of normal and steel fibre reinforced concrete with mixed fibre content and fly ash at various stress levels can be described by two parameter Weibull distribution. The Weibull parameters selected based on minimum squared mean error for various methods are significant. It would be more convincing to perform a goodness-of-fit test, in addition to show that it is a valid distribution model for the statistical description of fatigue life of plain and steel fibre concrete. The Kolmogorov-Smirnov test, recommended for Weibull distribution of the dataset, was used for this purpose (Mohammadi and Kaushik 2005). The Kolmogorov–Smirnov test can be conducted by using the following equation:

$$D = \max_{i=1}^k [|F^+(X_i) - F_N(X_i)|] \quad \text{--(4.27)}$$

Where,

$F^+(X_i) = i/k$ = observed cumulative histogram.

i = order number of the data point.

k = total number of data points in the sample under consideration at a given stress level.

$F(X_i)$ = hypothesized cumulative distribution function given by Eq (4.12).

Tables 4.6 to 4.11 show the calculated results by the Kolmogorov–Smirnov test for M_{30} and M_{40} grade concrete of Ref, FS2 and FS4 mixes.

Table 4.6 Kolmogorov–Smirnov test for Reference concrete (M_{30})

Stress Level	i	X_i	$F^+(X_i) = i/k$	$F(X_i)$	$ F^+(X_i) - F(X_i) $
0.85	1	90	0.2	0.125127	0.074873
	2	156	0.4	0.300795	0.099205
	3	265	0.6	0.602987	-0.00299
	4	308	0.8	0.701538	0.098462
	5	360	1	0.797823	0.202177*
0.80	1	1665	0.2	0.14924	0.05076
	2	2240	0.4	0.267533	0.132467
	3	3200	0.6	0.49581	0.10419
	4	4260	0.8	0.724393	0.075607
	5	5170	1	0.86151	0.13849

0.75	1	11150	0.2	0.114567	0.085433
	2	18680	0.4	0.311221	0.088779
	3	28935	0.6	0.618501	-0.0185
	4	32849	0.8	0.718904	0.081096
	5	35118	1	0.769383	0.230617
0.70	1	35343	0.25	0.220626	0.029374
	2	45675	0.5	0.344054	0.155946
	3	73444	0.75	0.672568	0.077432
	4	83151	1	0.763075	0.236925

*maximum difference from test, $D_t < D_c = 0.565$ for $n=5$ and 5% significance level from K-S table

$D_t < D_c = 0.624$ for $n=4$ and 5% significance level from K-S table

Table 4.7 Kolmogorov–Smirnov test for FS2 concrete (M_{30})

Stress Level	i	X_i	$F^+(X_i) = i/k$	$F(X_i)$	$ F^+(X_i) - F(X_i) $
0.85	1	150	0.2	0.148766	0.051234
	2	260	0.4	0.447594	-0.04759
	3	265	0.6	0.462533	0.137467
	4	337	0.8	0.666383	0.133617
	5	412	1	0.829282	0.170718
0.80	1	2982	0.2	0.086623	0.113377
	2	4402	0.4	0.365153	0.034847
	3	4874	0.6	0.499776	0.100224
	4	5438	0.8	0.663776	0.136224
	5	6490	1	0.896345	0.103655
0.75	1	11150	0.2	0.102023	0.097977
	2	18680	0.4	0.240614	0.159386
	3	28935	0.6	0.456859	0.143141
	4	32849	0.8	0.536489	0.263511
	5	35118	1	0.580342	0.419658
0.70	1	30807	0.25	0.141224	0.108776
	2	58957	0.5	0.373723	0.126277
	3	96444	0.75	0.665939	0.084061
	4	105793	1	0.723834	0.276166

*maximum difference from test, $D_t < D_c = 0.565$ for $n=5$ and 5% significance level from K-S table

$D_t < D_c = 0.624$ for $n=4$ and 5% significance level from K-S table

Table 4.8 Kolmogorov–Smirnov test for FS4 concrete(M₃₀)

Stress Level	<i>i</i>	<i>X_i</i>	$F^+(X_i) = \frac{i}{k}$	<i>F</i> (<i>X_i</i>)	$ F^+(X_i) - F(X_i) $
0.85	1	167	0.2	0.154464	0.045536
	2	292	0.4	0.289044	0.110956
	3	416	0.6	0.414185	0.185815
	4	875	0.8	0.747121	0.052879
	5	1204	1	0.872807	0.127193
0.80	1	2345	0.2	0.433175	-0.23318
	2	3262	0.4	0.653317	-0.25332
	3	4977	0.6	0.90502	-0.30502
	4	6926	0.8	0.987674	-0.18767
	5	8974	1	0.999233	0.000767
0.75	1	28232	0.2	0.168915	0.031085
	2	62611	0.4	0.885608	-0.48561
	3	41523	0.6	0.456356	0.143644
	4	52110	0.8	0.707554	0.092446
	5	62730	1	0.887058	0.112942
0.70	1	67676	0.2	0.169616	0.030384
	2	75787	0.4	0.269679	0.130321
	3	87433	0.6	0.456671	0.143329
	4	96209	0.8	0.613582	0.186418
	5	118886	1	0.921022	0.078978

*maximum difference from test, $D_t < D_c = 0.565$ for $n=5$ and 5% significance level from K–S table

Table 4.9 Kolmogorov–Smirnov test for Reference concrete (M₄₀)

Stress Level	<i>i</i>	<i>X_i</i>	$F^+(X_i) = \frac{i}{k}$	<i>F</i> (<i>X_i</i>)	$ F^+(X_i) - F(X_i) $
0.85	1	72	0.125	0.114958	0.010042
	2	120	0.25	0.227995	0.022005
	3	150	0.375	0.30178	0.07322
	4	224	0.5	0.476751	0.023249
	5	235	0.625	0.500919	0.124081
	6	308	0.75	0.644551	0.105449
	7	360	0.875	0.727736	0.147264
	8	665	1	0.959509	0.040491
0.80	1	1518	0.2	0.181954	0.018046
	2	2512	0.4	0.299968	0.100032
	3	2849	0.6	0.337454	0.262546
	4	8935	0.8	0.780215	0.019785
	5	11150	1	0.85776	0.14224

0.75	1	10512	0.2	0.030906	0.169094
	2	38035	0.4	0.377154	0.022846
	3	48680	0.6	0.549275	0.050725
	4	54355	0.8	0.634194	0.165806
	5	67500	1	0.795721	0.204279
0.70	1	35432	0.2	0.101281	0.098719
	2	65434	0.4	0.352798	0.047202
	3	84481	0.6	0.542071	0.057929
	4	97236	0.8	0.659641	0.140359
	5	112375	1	0.77713	0.22287

*maximum difference from test, $D_t < D_c = 0.565$ for $n=5$ and 5% significance level from K-S table

$D_t < D_c = 0.457$ for $n=8$ and 5% significance level from K-S table

Table 4.10 Kolmogorov–Smirnov test for FS2 concrete(M₄₀)

Stress Level	i	X_i	$F^+(X_i) = i/k$	$F(X_i)$	$ F^+(X_i) - F(X_i) $
0.85	1	202	0.2	0.130772	0.069228
	2	389	0.4	0.292636	0.107364
	3	679	0.6	0.526107	0.073893
	4	984	0.8	0.712366	0.087634
	5	1333	1	0.849593	0.150407
0.80	1	1548	0.2	0.137718	0.062282
	2	3051	0.4	0.282672	0.117328
	3	6368	0.6	0.549525	0.050475
	4	8186	0.8	0.658777	0.141223
	5	14100	1	0.871726	0.128274
0.75	1	30969	0.2	0.230965	-0.03097
	2	35732	0.4	0.328869	0.071131
	3	37830	0.6	0.375676	0.224324
	4	47500	0.8	0.599773	0.200227
	5	64347	1	0.891595	0.108405
0.70	1	68174	0.2	0.1614	0.0386
	2	76478	0.4	0.277605	0.122395
	3	87635	0.6	0.489766	0.110234
	4	92180	0.8	0.585822	0.214178
	5	112320	1	0.920509	0.079491

*maximum difference from test, $D_t < D_c = 0.565$ for $n=5$ and 5% significance level from K-S table

Table 4.11 Kolmogorov–Smirnov test for FS4 concrete(M₄₀)

Stress Level	<i>i</i>	<i>X_i</i>	$F^+(X_i) = i/k$	<i>F</i> (<i>X_i</i>)	$ F^+(X_i) - F(X_i) $
0.85	1	142	0.2	0.173363	0.026637
	2	196	0.4	0.235033	0.164967
	3	518	0.6	0.527916	0.072084
	4	665	0.8	0.623997	0.176003
	5	1484	1	0.898788	0.101212
0.80	1	2043	0.2	0.110845	0.089155
	2	5280	0.4	0.442684	-0.04268
	3	5904	0.6	0.506431	0.093569
	4	7560	0.8	0.657787	0.142213
	5	9755	1	0.807902	0.192098
0.75	1	10438	0.2	0.118067	0.081933
	2	27674	0.4	0.362794	0.037206
	3	39020	0.6	0.506801	0.093199
	4	64200	0.8	0.74259	0.05741
	5	72434	1	0.795973	0.204027
0.70	1	62378	0.2	0.118099	0.081901
	2	84599	0.4	0.362714	0.037286
	3	94460	0.6	0.51085	0.08915
	4	111528	0.8	0.761693	0.038307
	5	112311	1	0.771646	0.228354

*maximum difference from test, $D_t < D_c = 0.565$ for $n=5$ and 5% significance level from K–S table

From the above tables, considering all the cases the maximum difference is 0.419658. The critical value D_c for $n=5$ and $n= 8$ at 5% significance level is found to be 0.565 0.457 respectively from Kolmogorov–Smirnov Table. As $D_t < D_c$ ($0.4197 < 0.457$), the two parameter Weibull distribution model is acceptable at 5% significance level for all the cases.

4.10 SURVIVAL PROBABILITY AND S-N-P_f RELATION

The analysis carried out in the preceding section shows that the fatigue life data of normal concrete and SFRC with and without fly ash follows the two parameter Weibull distribution, which can be used to calculate the fatigue lives corresponding to different failure probabilities. Rearranging the general equation obtained by the graphical solution (Eq 4.16) and substituting $(1-P_f)$ for L_N the expression obtained is:

$$\ln(n) = \left[\frac{\ln\left\{\ln\left(\frac{1}{1-P_f}\right) + \alpha \ln(\mu)\right\}}{\alpha} \right] \quad \text{-- (4.28)}$$

Where P_f is the failure probability
 μ Scale parameter of Weibull distribution
 α Shape parameter of Weibull distribution

Using the values of Weibull distribution parameters α and μ as obtained earlier (given in Table 4.5) for a given fatigue life data, the above equation can be used to calculate fatigue lives of fly ash SFRC corresponding to different failure probabilities ($P_f = 0.05, 0.5, 0.95$). The fatigue lives thus obtained are listed in Tables 4.12 to 4.14. The S-N- P_f Curve incorporating various failure probabilities is depicted in Fig 4.12 and it can be used to obtain the flexural fatigue lives of fly ash-steel fibre reinforced concrete for the desired level of the failure probability.

Table 4.12 Calculated fatigue lives (N_D) corresponding to different failure probabilities

($P_f = 95\%, 50\%, 5\%$) for M_{30} concrete

Designation	Failure Probability(P_f)	Stress Level			
		0.85	0.80	0.75	0.70
R	0.95	511	6240	48800	118866
	0.50	226	3218	24859	58206
	0.05	53	991	7488	16345
FS2	0.95	515	6942	69349	172425
	0.50	278	4875	31029	73987
	0.05	93	2599	7421	16426
FS4	0.95	1616	5654	69517	123205
	0.50	510	2606	43289	89873
	0.05	66	657	18639	51278

Table 4.13 Calculated fatigue lives (N_D) corresponding to different failure probabilities ($P_f = 95\%, 50\%, 5\%$) for M_{40} concrete

Designation	Failure Probability(P_f)	Stress Level			
		0.85	0.80	0.75	0.70
R	0.95	635	16248	91182	151952
	0.50	235	4500	45566	80190
	0.05	40	458	13266	25724
FS2	0.95	1858	19365	71281	115913
	0.50	643	5660	43179	88123
	0.05	98	635	17702	54117
FS4	0.95	1912	13885	117503	132963
	0.50	481	5840	38442	93760
	0.05	41	1251	5268	50367

Table 4.14 Calculated(Design) fatigue lives (N_D) corresponding to different failure probabilities for any concrete

Designation	Failure Probability (P_f)	Stress Level			
		0.85	0.80	0.75	0.70
Combined M_{30} & M_{40}	0.95	1030	12022	70356	121191
	0.90	856	10379	62558	111847
	0.75	601	7817	49878	95817
	0.50	370	5307	36603	77565
	0.25	200	3247	24718	59324
	0.10	99	1853	15786	43675
	0.05	60	1239	11448	35069

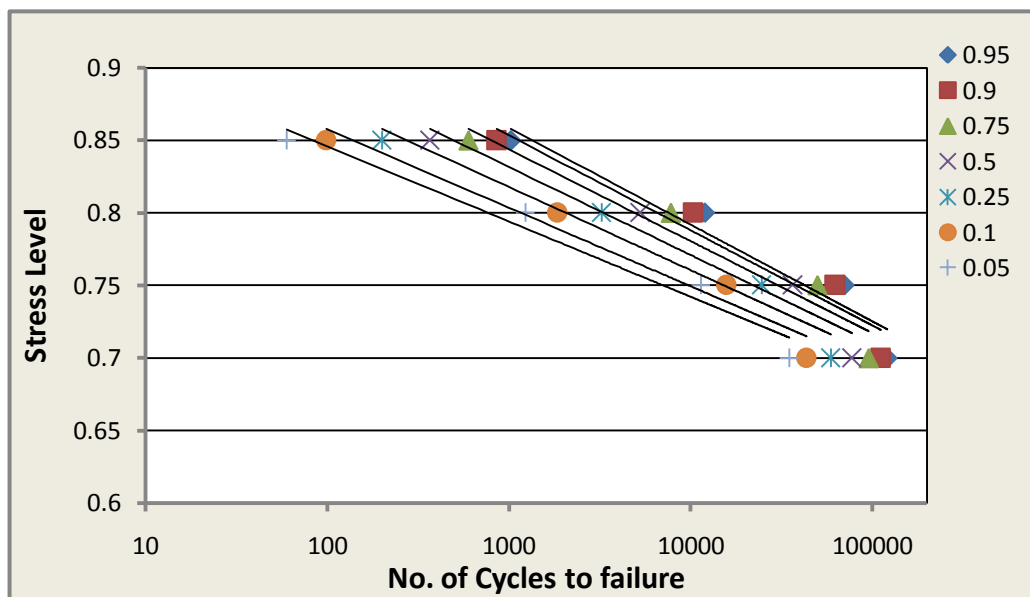


Fig 4.12 S-N- P_f Curve for combined data at various failure probabilities

4.11 DISCUSSIONS

The S-N diagrams plotted based on the experimental fatigue data showed a wide scatter as reported in many literatures. The regression analysis was carried out on experimental fatigue data for various mixes and also for the combined data to develop the relationship between stress level and the number of load cycles to cause failure. As the number of cycles to failure significantly increases with decreasing stress level, logarithmic relation is used for developing the fatigue model as a best fit curve. The fatigue models for all the mixes irrespective of strength and the material follow the similar trend with coefficient of determination 0.85 to 0.9 (Table 4.3). When all the fatigue data were used to develop general equation, it also follows similar trend with a regression coefficient of 0.88. The developed fatigue model was compared with fatigue models available in literatures (Table 4.4) and it was found that the model quite resembles the Zero-Maintenance Design Beam Fatigue Model (Darter 1977). The fatigue model adopted by IRC for designing rigid pavement (IRC58-2002) is also compared and is found that IRC (or PCA) model is very conservative in prediction of fatigue life. **Hence, new fatigue model has been proposed for design of rigid pavements.**

The Weibull distribution is most commonly employed in assessing reliability of composite structures. The investigation was carried out to find out the suitability of the distribution for fly ash-SFR Concrete. The fatigue life data of various mixes were analysed using graphical method. From Figs 4.11(a) to (d), it can be observed that the experimental data follows two-parameter Weibull distribution with a statistical coefficient of determination close to 0.95. Other methods, like method of least squares, method of moment and Weibull module of available statistical software Availability Workbench from ISOGRAPH, were used to evaluate parameters of Weibull distribution and compared. The shape parameter and scale parameter (characteristic life) obtained from different methods are quite comparable.

From the Table 4.5 it can be seen that the value of shape parameter (α) was higher than one for all the mixes. This indicates that the hazard function increases with increasing number of cycles to cause fatigue failure (Fig 4.13).

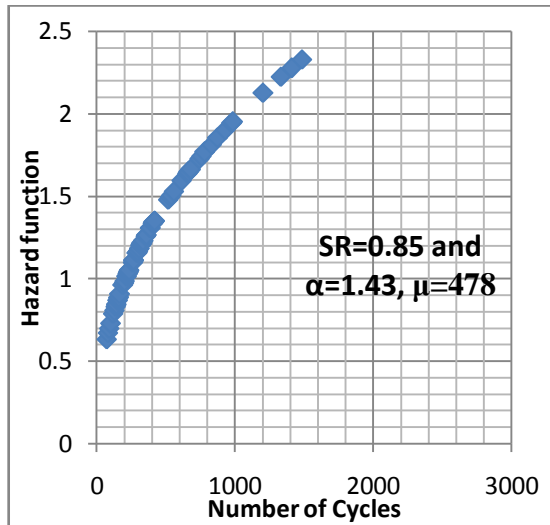


Fig 4.13 Hazard function of Weibull distribution v/s number of cycles for stress level=0.85

The analysis showed that the distribution represents the true form of gradual failure under repetitive loading. Thus the design fatigue life calculated is compatible with expected fatigue behaviour of engineering materials and is justifying that the data follows two-parameter Weibull distribution. Hence, it can be used for statistical analysis of the fatigue life.

No typical trend/relation was observed with shape parameter and fatigue stress level (Fig 4.14). However, when all the data are put together, the shape parameter tends to increase with decrease in fatigue stress level.

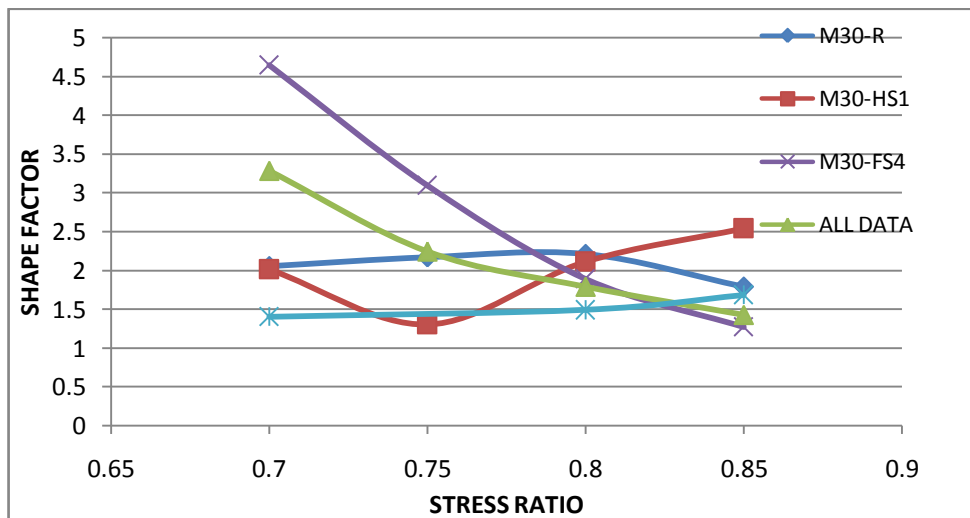


Fig 4.14 Shape parameters at various stress level

The failure probabilities have been introduced into the S-N curve to estimate the fatigue life of fly ash SFR concrete. The fatigue equation for various failure probabilities can be used to obtain flexural fatigue strength of the concrete. The design life for various probabilities (50% and 80%) were compared with those available in literature (Joshi et al. 2004) and presented in Table 4.15. It can be observed that at 50% failure probability the results were found to nearly match with previous studies. However, at higher failure probability, results were found to differ each other. This may be due to the variation in testing methodologies.

Table 4.15 Comparison of stress ratios corresponding to different fatigue lives (for different failure probabilities)

	Number of repetitions		
ACI 215	10^3	10^5	10^6
$P_f=0.50$	0.8	0.72	0.66
$P_f=0.80$	0.9	0.88	0.83
Joshi et. al 2004			
$P_f=0.50$	0.8082	0.6967	0.6409
$P_f=0.80$	0.8269	0.7390	0.6844
Present study			
$P_f=0.50$	0.83	0.70	0.64
$P_f=0.80$	0.86	0.72	0.66

4.11.1 Effect of addition of steel fibres on fatigue life of the concrete

Fig 4.15 shows the effect of addition of steel fibers on the fatigue life of plain concrete. To demonstrate the effect, the S-N curve was drawn with stress level based on the flexural strength of equivalent plain concrete. From the figure it is clearly observed that the addition of steel fibers enhances the fatigue life of the concrete. For a given stress level, concrete with 1% steel fibers (HS2) can sustain more number of load repetition. It is also indicated that an increase in fiber content can improve the fatigue capacity of the concrete. Figs 4.16 and 4.17 demonstrate the effect of addition of 20% and 40% fly ash as partial replacement of cement in SFRC respectively. From the figure it can be seen that the S-N curves follow quite similarly to the SFRC without fly ash.

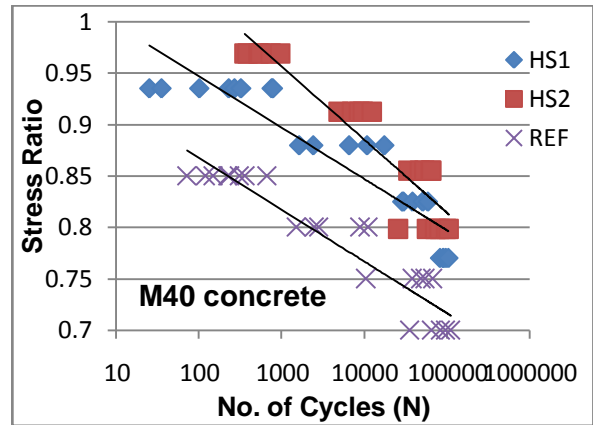
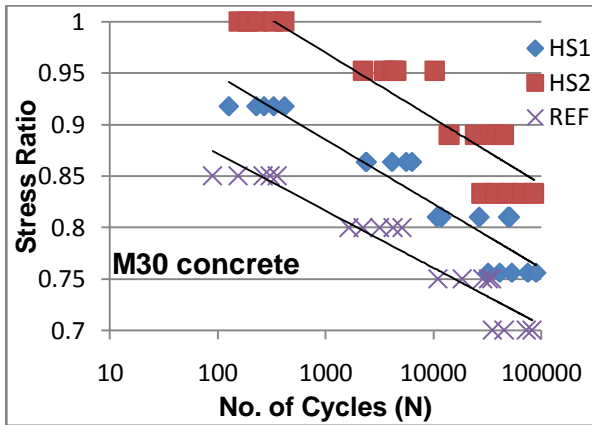


Fig 4.15 S-N curve of M₃₀ and M₄₀ concrete with and without steel fibers

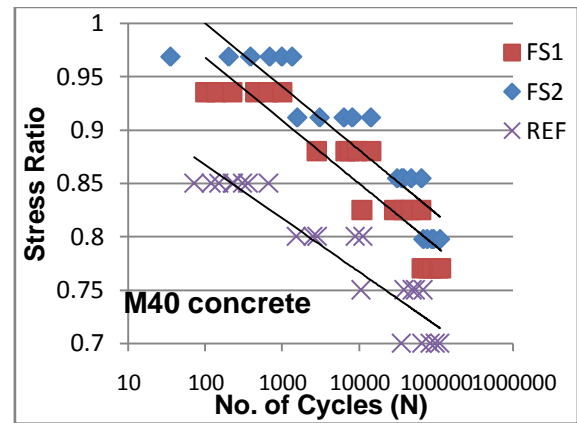
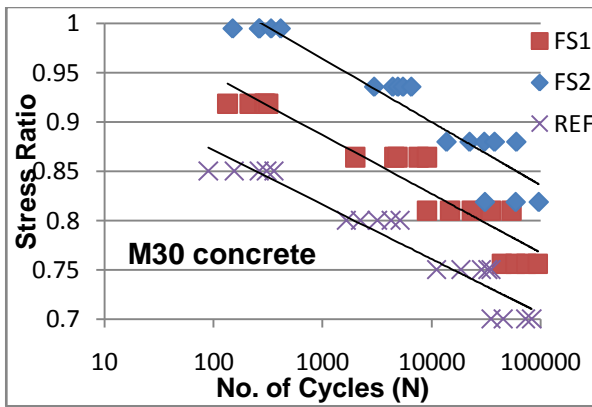


Fig 4.16 S-N curves of fly ash concrete (20%) with steel fibers

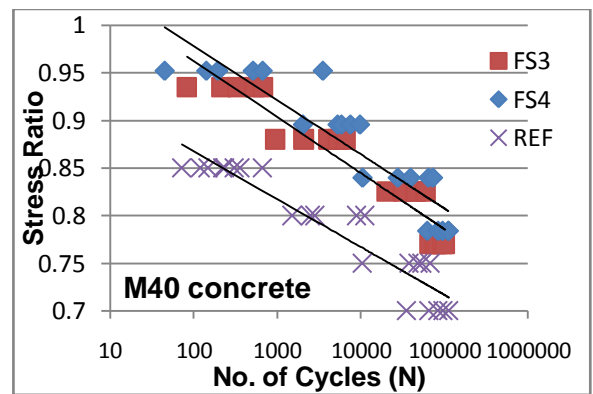
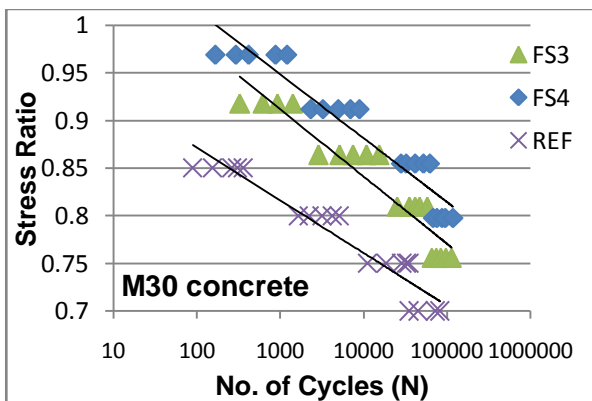


Fig 4.17 S-N curves of fly ash concrete(40%) with steel fibers

4.11.2 Effect of addition of fly ash on fatigue life of the steel fiber concrete

Fig 4.17 and 4.18 depict the S-N curves drawn for M₃₀ and M₄₀ grade steel fiber reinforced concrete with steel fibers 0.5% and 1.0% respectively. From Fig 4.17 it can be observed that S-N curves for HS1, FS1 and FS3 are almost overlapping indicating that the materials have similar fatigue life. Also, when compared with reference concrete it shows improved fatigue life. Similar trend can be observed in Fig 4.18 for HS2, FS2 and FS4. Thus, it shows that the addition of fly ash in SFRC does not alter its fatigue behaviour.

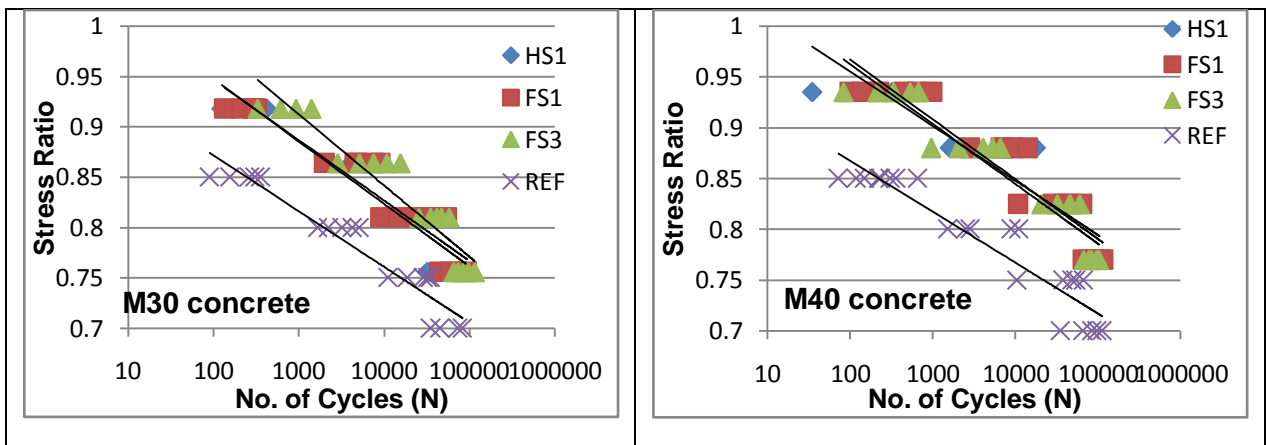


Fig 4.18 S-N curves of steel fiber concrete(0.5%) with and without fly ash

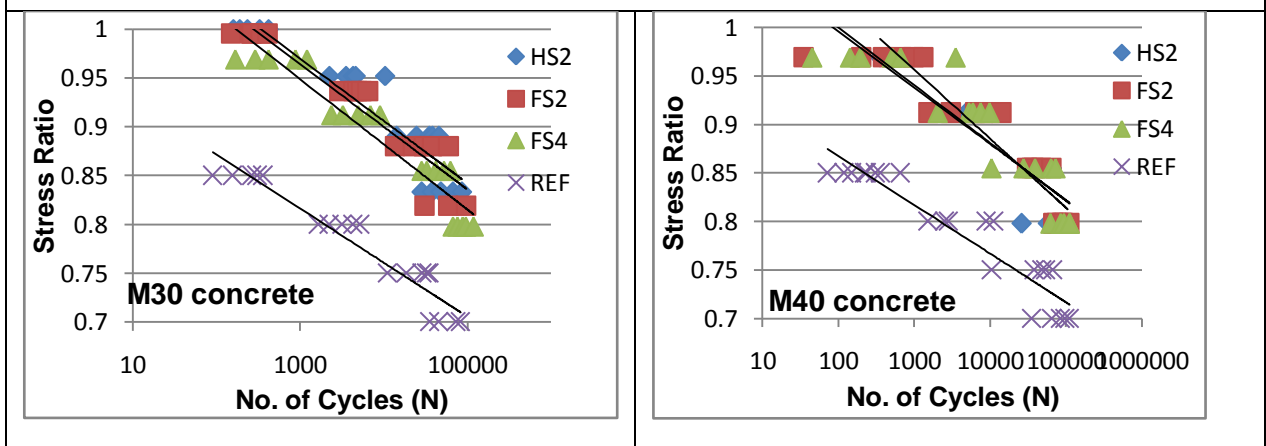


Fig 4.19 S-N curves of steel fiber concrete (1.0%) with and without fly ash

4.12 SUMMARY

The addition of steel fibres benefits the fatigue performance of concrete under flexural cyclic loading. This can be attributed to the fact that the fibres are able to bridge the micro cracks and arrest their growth, thereby prolonging the fatigue life of concrete. Further, the inclusion of fibres induces more ductile behaviour to the concrete. The experimental studies have shown that the use of fly ash along with steel fibres enhances the flexural strength and the fatigue life of plain concrete. This may be due to reactive silica particles available in fly ash utilised in secondary hydration process. A better fatigue model was developed which can be used in the design of rigid pavements.

CHAPTER 5

TEMPERATURE STUDIES ON CONCRETE SLAB

5.1 GENERAL

Induced thermal or warping stress is one of the major concerns while designing concrete pavements. Curling stress is generally affected by temperature differential between the surfaces, self-weight of slab and the support under the concrete slab. Pavement temperature profile can be quite useful in the analysis of stresses due to temperature gradient within the slab. This study establishes the actual temperature profile across the pavement thickness based on the recorded temperature data using temperature probe (RTD) at five locations, viz. top, top-middle, middle, bottom-middle and bottom. Investigations were carried out to identify the effect of fly ash utilization as partial replacement of cement (20% and 40% by weight) on the temperature differential. The effect of thickness on the temperature differential was also studied using four different thicknesses of the slab (150mm, 200mm, 250mm and 300mm). The temperature across the pavement slab at regular time intervals was recorded throughout a day and the same was plotted adopting suitable curve to establish the temperature distribution equation. Using these equations, the temperature stresses were analyzed and compared with those calculated based on available literature.

5.2 TEMPERATURE DATA ACQUISITION SYSTEM

Block diagram and photographs of temperature data acquisition system are shown in Figs 5.1 and 5.2.

The temperature data acquisition system consists of the following units:

1. RTD signal conditioning unit
2. Data acquisition system
3. Resistance Temperature Detector (RTD) sensors
4. Output Unit

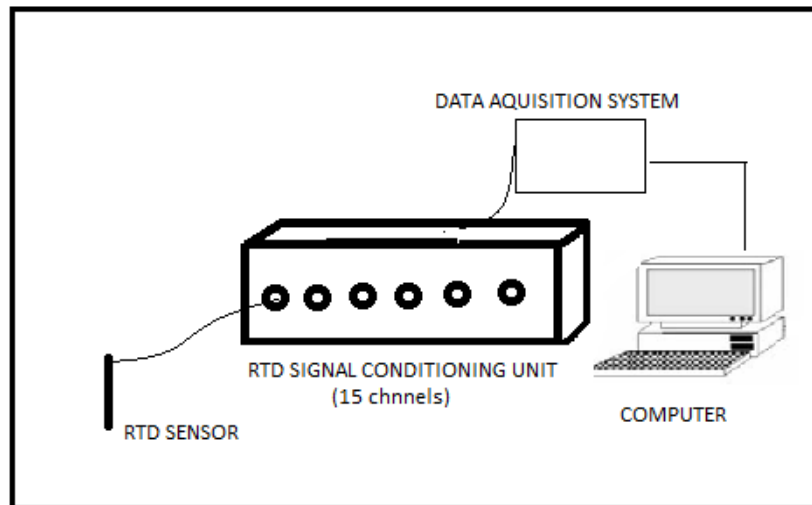


Fig 5.1 Block diagram of Temperature data acquisition unit

The resistance temperature detector (RTD) signal conditioning unit receives the voltage change signal from RTD sensors whenever there is a change in temperature. Then the signals are transferred to the data acquisition system at regular intervals where they are converted to digital form. With proper modulation and amplification of signals, the temperature is displayed in a computer connected to it. The instrument used can acquire data from 15 sources through 15 channels. The displayed temperature from 15 channels is refreshed simultaneously at regular intervals and also stored in the computer.

5.2.1 Resistance Temperature Detector (RTD)

The resistance temperature detector (RTD) shown in Fig 5.3 is a helical coil of platinum wire-bifilar wound on a glass or ceramic bobbin. This construction minimizes strain on the wire while maximizing the resistance. The bifilar winding reduces the effective enclosed area of the coil to minimize magnetic pickup and its related noise. Once the wire is wound on to the bobbin, the assembly is then sealed with a coating of molten glass. The sealing process not only assures that the RTD will maintain its integrity under extreme vibration but it also limits the expansion of the platinum metal at high temperature. Unless the coefficients of expansion of the platinum and the bobbin match perfectly, stress will be placed on the wire as the temperature changes, resulting in a strain-induced resistance change. This may result in a permanent change in the resistance of the wire.



Fig 5.2 Temperature Data Acquisition unit

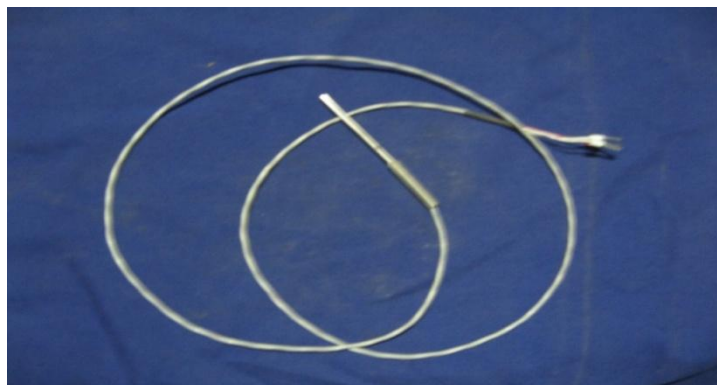


Fig 5.3 RTD sensor

5.3 PREPARATION OF SPECIMENS

1m x 1m concrete slab specimens were used in this investigation to establish the temperature profile. Four different slab thicknesses, viz. 150mm, 200mm, 250mm, and 300mm were used in each cases of reference concrete and the concrete with 20% and 40% fly ash. A total of 12 slabs were cast. Five holes (10mm dia) were drilled at the centre of the slab for the insertion of RTD sensor, up to specified depths viz. bottom(d), bottom- middle($0.75d$) , middle ($0.5d$), top-middle($0.25d$) and top, where 'd' is the thickness of slab. RTD sensors were introduced in to the drilled holes in such a way that they were in contact with the concrete. The holes were then filled with thermocoal to avoid any variation in results (Fig 5.4 and 5.5).



Fig 5.4 Location of drilled holes and RTD sensors



Fig 5.5 Test slabs with temperature sensors

The lead wires of the RTD were connected to the signal-conditioning unit of temperature data acquisition system. At a time, the temperature data from three slabs were recorded every hour for 5 minutes duration and the average was computed. Three such temperature data were recorded during summer peak season (April-May) and average of the three temperatures was taken for the analysis.

5.4 TEMPERATURE DATA

The temperature data for various slab specimens at different depths were recorded during the months of April - May 2010 and hourly average temperature is presented in Appendix II-1. The average ambient temperature at various hours of the day at Surathkal was also recorded, which are reported in Table 5.1. The hourly variations at various depths of slab are depicted in Figs 5.6 to 5.9.

Table 5.1 Hourly variation of ambient temperature on 21-05-2010

Time	9.00	10.00	11.00	12.00	13.00	14.00	15.00	16.00
Temperature (°C)	34.8	35.2	36.1	37.3	38.0	36.3	35.2	34.7
Time	17.00	18.00	19.00	20.00	21.00	22.00	23.00	24.00
Temperature (°C)	34.5	34.1	33.8	33.3	33.0	32.8	32.3	31.5
Time	1.00	2.00	3.00	4.00	5.00	6.00	7.00	8.00
Temperature (°C)	30.8	30.5	29.3	29.0	29.2	30.0	32.8	34.3

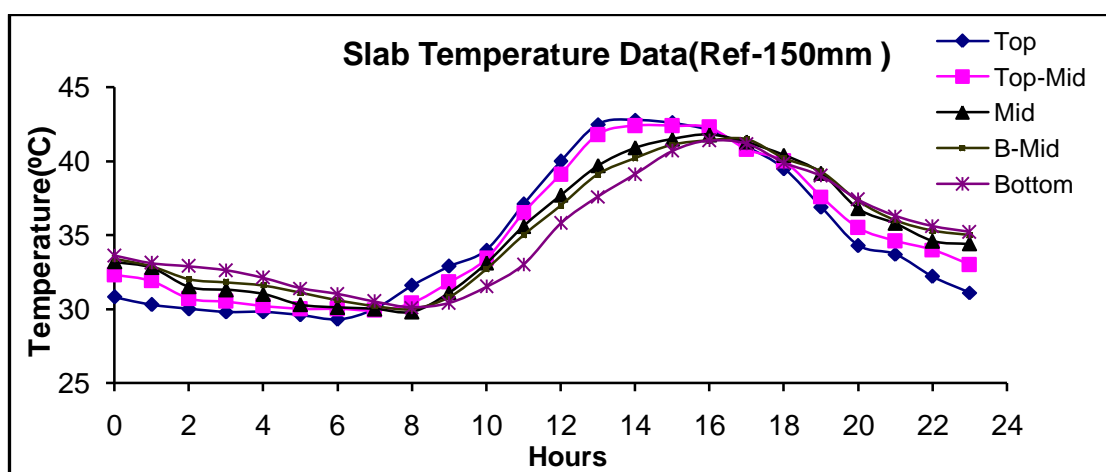


Fig 5.6a Hourly variation of temperature across the thickness-150mm (REF concrete) during April –May 2010

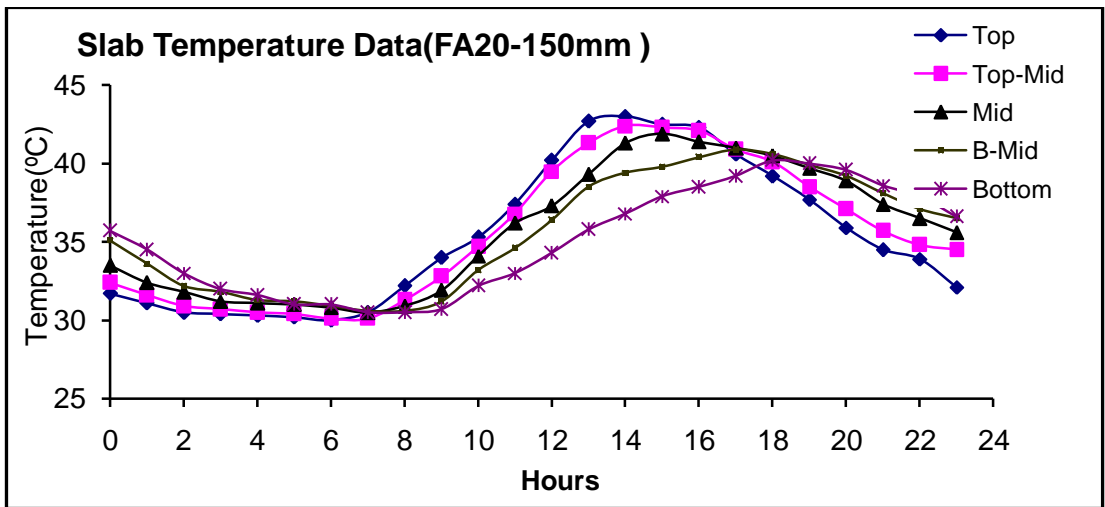


Fig 5.6b Hourly variation of temperature across the thickness-150mm (FA20 concrete) during April –May 2010

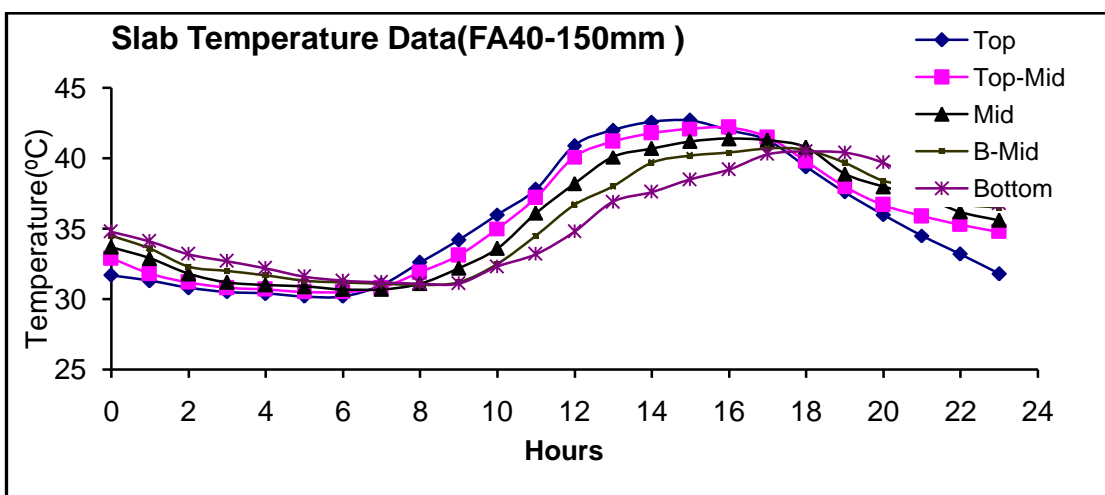


Fig 5.6c Hourly variation of temperature across the thickness-150mm (FA40 concrete) during April –May 2010

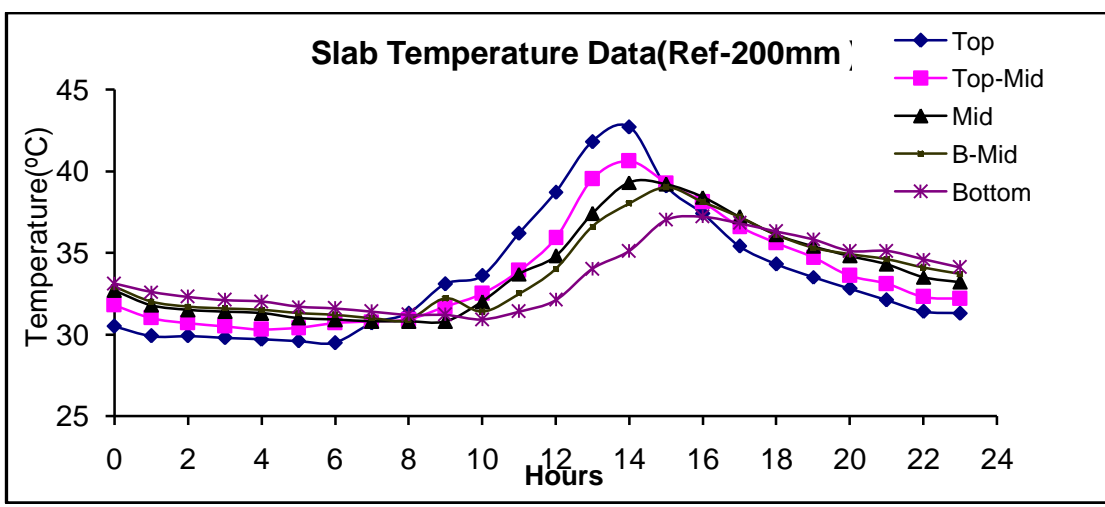


Fig 5.7a Hourly variation of temperature across the thickness-200mm (REF concrete) during April –May 2010

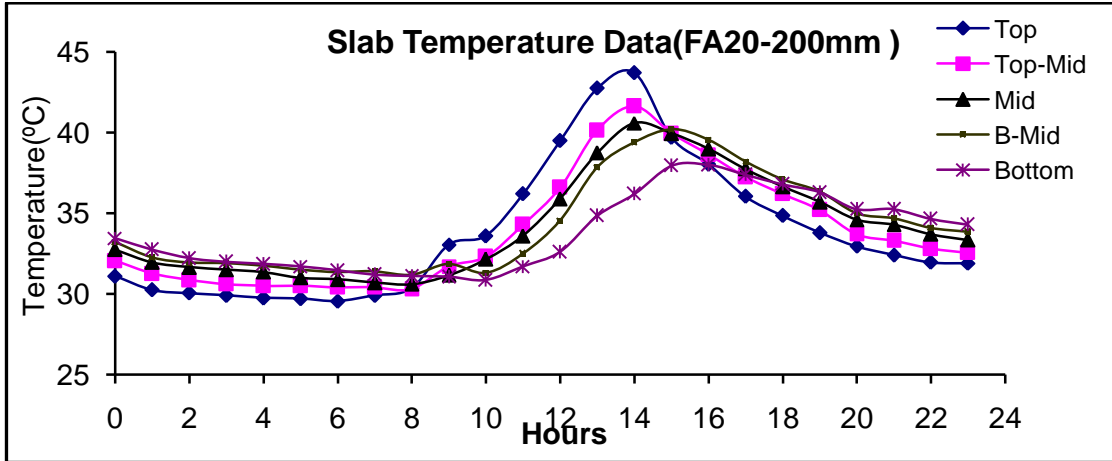


Fig 5.7b Hourly variation of temperature across the thickness-200mm (FA20 concrete) during April –May 2010

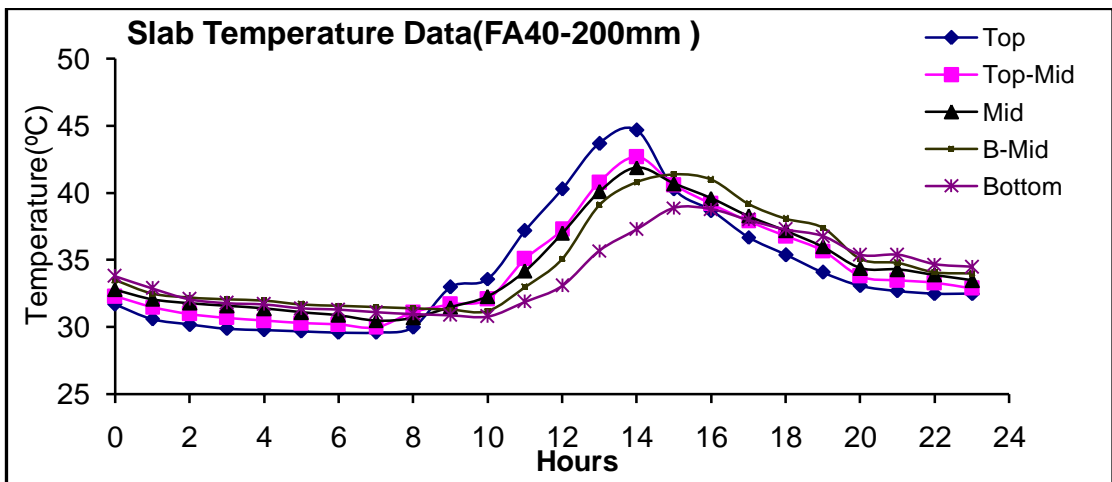


Fig 5.7c Hourly variation of temperature across the thickness-200mm (FA40 concrete)

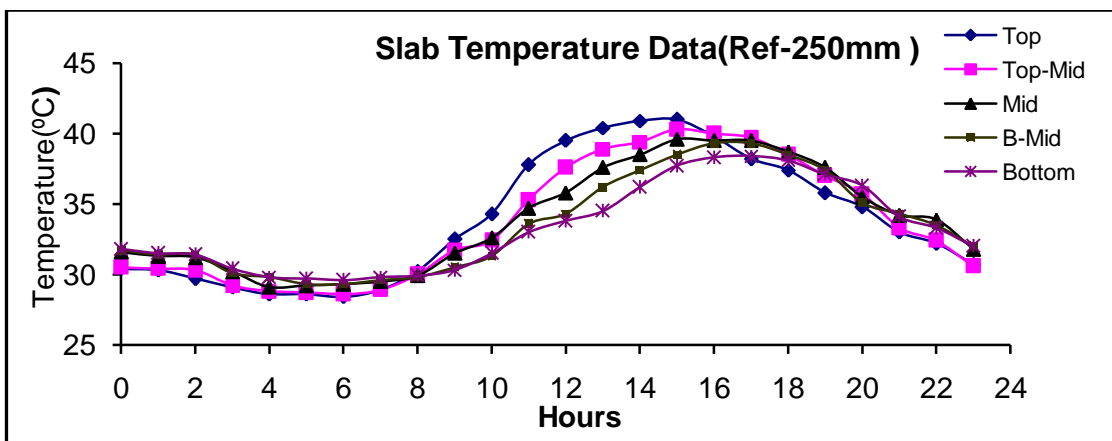


Fig 5.8a Hourly variation of temperature across the thickness-250mm (REF concrete) during April –May 2010

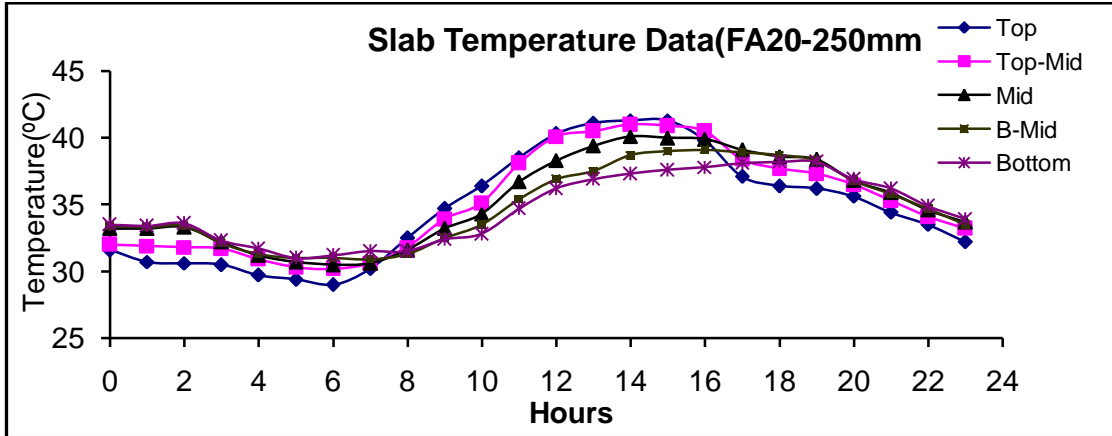


Fig 5.8b Hourly variation of temperature across the thickness-250mm (FA20 concrete) during April –May 2010

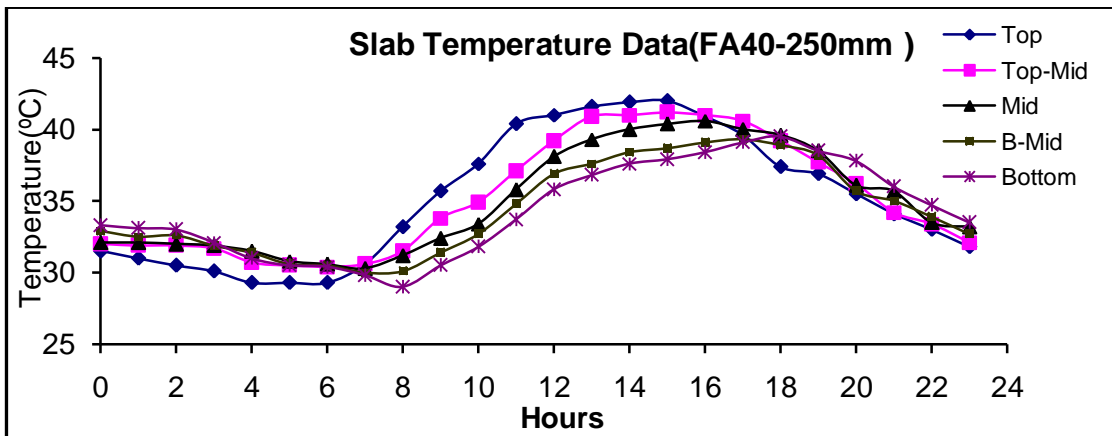


Fig 5.8c Hourly variation of temperature across the thickness-250mm (FA40 concrete) during April –May 2010

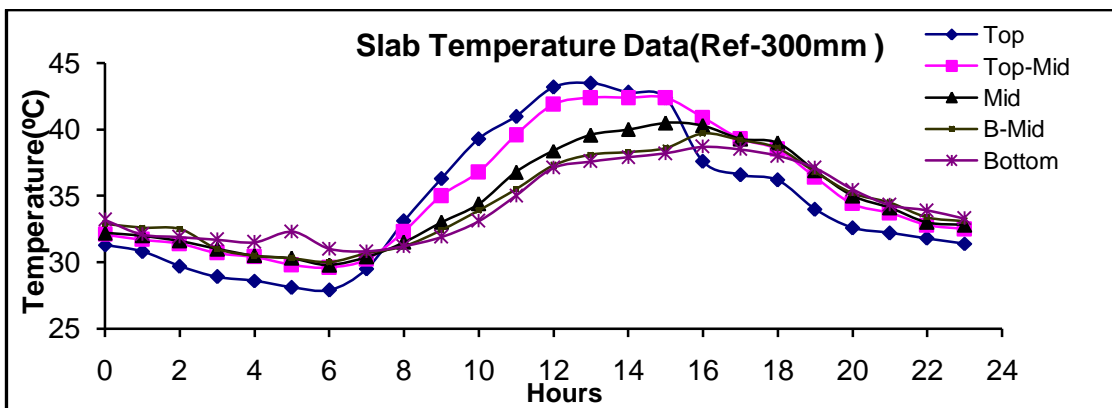


Fig 5.9a Hourly variation of temperature across the thickness-300mm (REF concrete) during April –May 2010

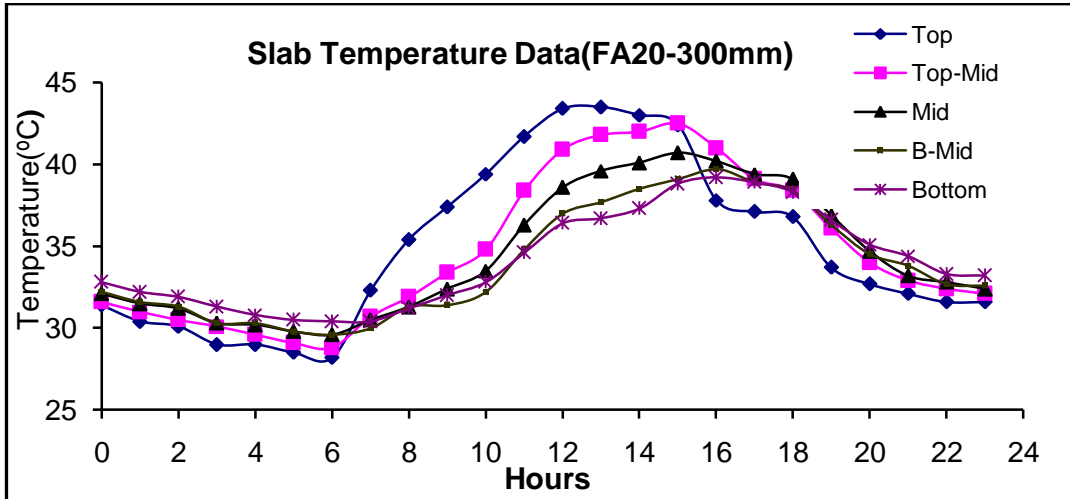


Fig 5.9b Hourly variation of temperature across the thickness-300mm (FA20 concrete) during April –May 2010

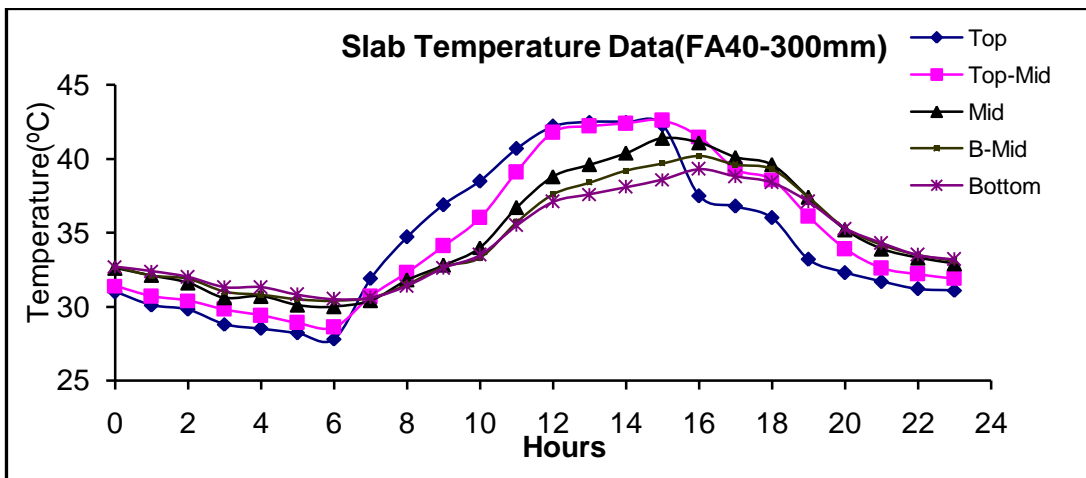


Fig 5.9c Hourly variation of temperature across the thickness-300mm (FA40 concrete) during April –May 2010

5.5 TEMPERATURE DIFFERENTIAL

The difference in temperature between the top and bottom surfaces of the slab at different duration of time of a day was calculated from the observed temperature data in the month of April-May 2010. Figs 5.10a to 5.10d show the actual hourly temperature differential for different thicknesses in all the three cases.

It can be seen that the maximum positive and negative temperature differential were observed between 12.00-14.00 hrs and 22.00-24.00 hrs for almost all the cases. The maximum positive temperature differential (top surface is hotter than bottom) recorded was 7.9°C and maximum negative temperature differential (bottom is hotter than top surface) was 4.5°C. In 24 hrs duration, zero temperature differentials indicating the uniform temperature across the section occur two times. Daily temperature variation at a point follows sinusoidal curve consisting of two peaks: one in the afternoon and other at early morning hours. Similarly the temperature differentials in a day also follow sinusoidal curve.

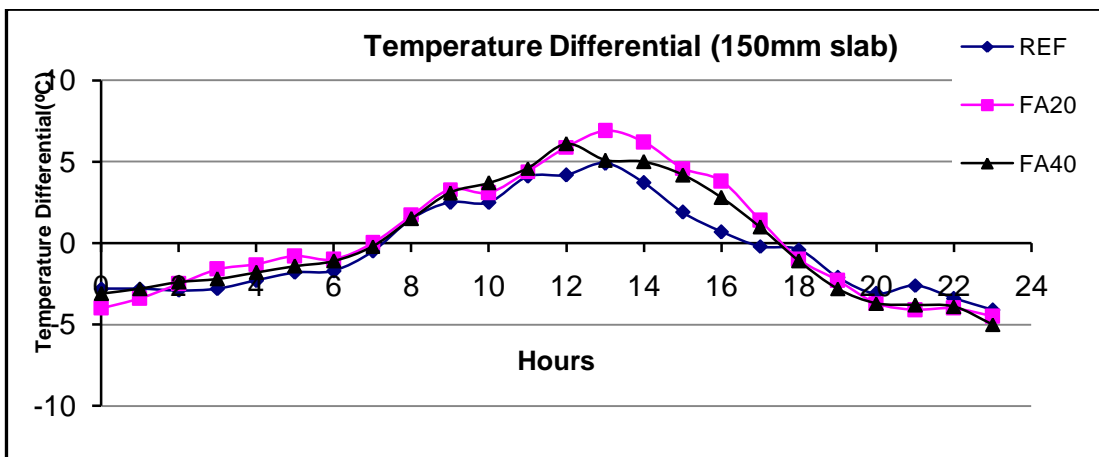


Fig 5.10a Temperature Differential between the surfaces across the thickness-150mm during April –May 2010

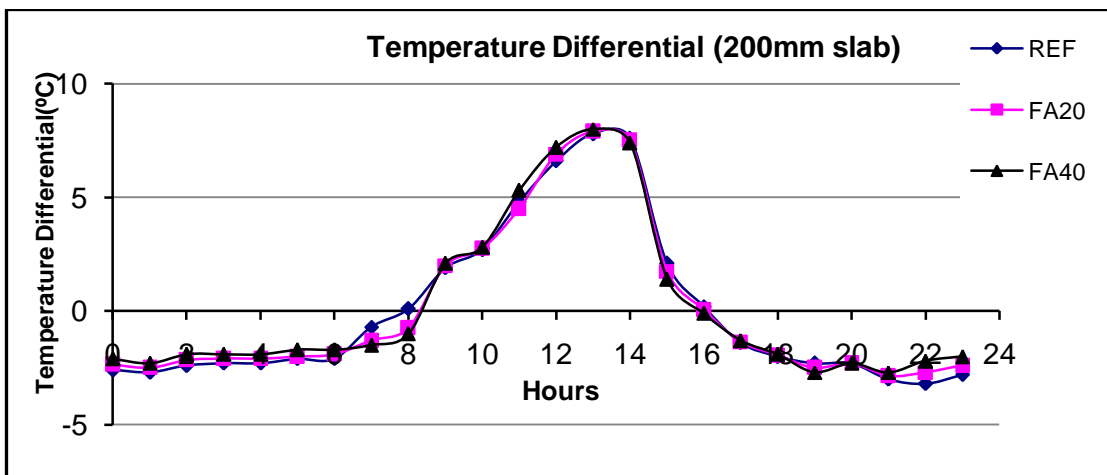


Fig 5.10b Temperature Differential between the surfaces across the thickness-200mm during April –May 2010

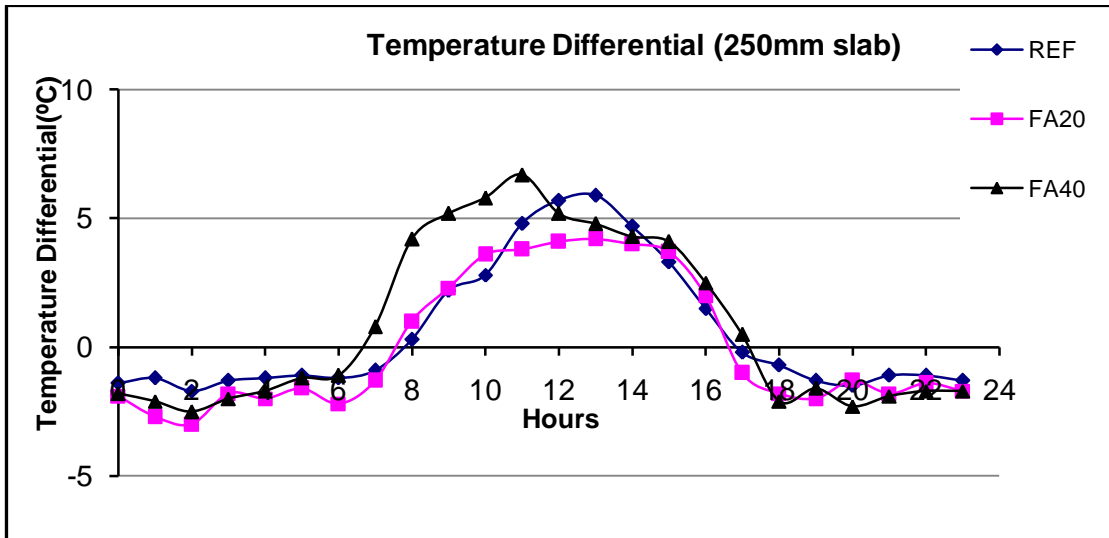


Fig 5.10c Temperature Differential between the surfaces across the thickness-250mm during April –May 2010

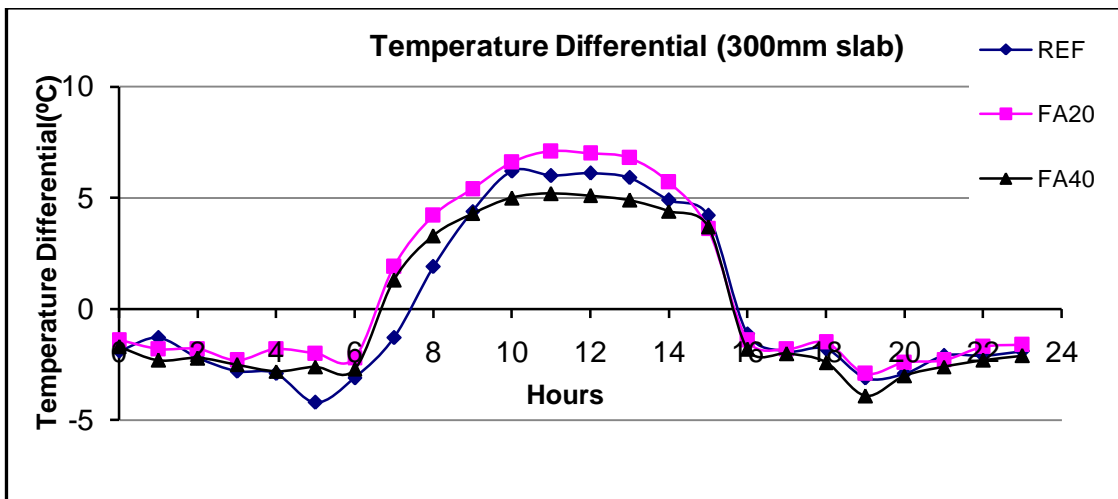


Fig 5.10d Temperature Differential between the surfaces across the thickness-300mm during April –May 2010

5.6 TEMPERATURE PROFILES

Typical temperature distribution curves for various concrete mixes across the thickness of 150mm slab specimens are presented in Figs 5.11. Temperature distribution profiles across 200mm, 250mm and 300mm thick slabs are presented in Appendix II-2. It is apparent from the figures that the temperature distributions along the thickness of the slab are nonlinear as observed by many researchers. But, in the bottom half portion (depth $h/2$ from the bottom surface), the distribution is almost linear. The nonlinearities of temperature distribution along pavement thickness for the

depth $h/2$ from the bottom surface of the slabs were not as pronounced as they were for the depth $h/2$ from the top surface.

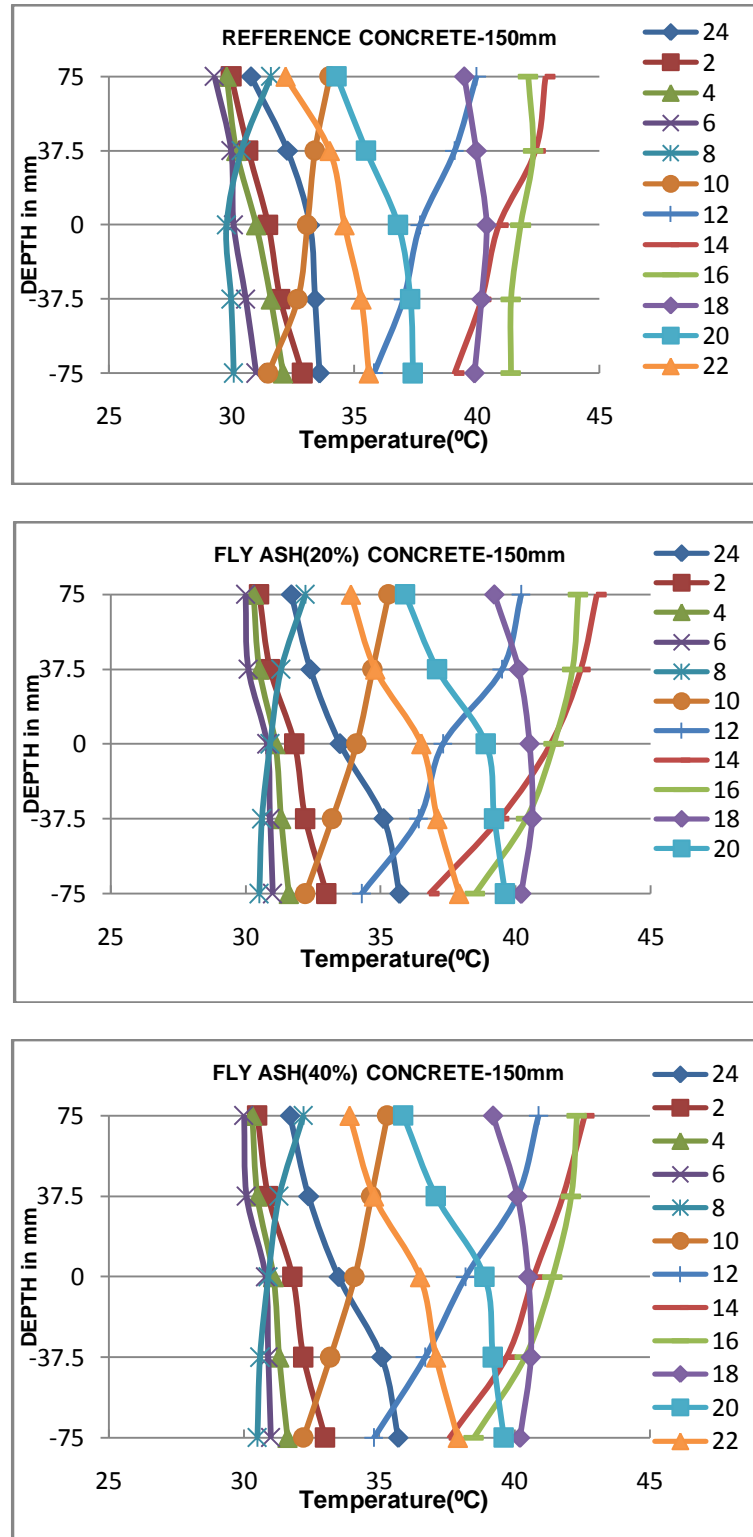


Fig 5.11 Temperature profiles across 150mm thick slab specimens (REF, FA20, FA40)

In the case of thicker slabs, the distribution for the hours of positive temperature differential (i.e., the temperature of the top surface is higher than that of the bottom), the profile is steeper than that for the hours of negative temperature differentials (i.e., the temperature of the bottom is higher than that of the top).

The difference between maximum and minimum temperature at the top surface was about 12.6 to 15.4°C and the same at bottom surface was 7 to 11.3°C. The difference between maximum and minimum temperature at the bottom surface was about 7 to 8°C for thicker slabs (250 mm and 300 mm) whereas for 150mm and 200mm thick slab it was 9.4-11.3°C. No particular trend has been observed when fly ash was used as cement replacement. However, it was observed in many cases that there is a small reduction in difference in maximum to minimum temperature. This indicates that the addition of fly ash in concrete as partial replacement does not alter the heat transfer mechanism of concrete slabs and hence, no additional thermal stress would induce in pavements due to incorporation of fly ash.

5.6.1 Temperature Distribution Equations

The nonlinearity in the temperature distribution has been proven by experimental data presented by several investigators (Richardson and Armaghani 1987; Armaghani et al. 1987; Thompson et al. 1987; Choubane and Tia 1995). Many researchers (Choubane & Tia 1995; Ioannides & Khazanovich 1998; Liu & Fwa, 2003; Hiller & Roesler, 2010) adopted quadratic equation for defining the non-linear temperature profile as a function of depth to avoid complexity involved in higher order polynomial. However, some others used third degree polynomials (Mohammad & Hansen 1996; Zhang et. al., 2003). In this research, comparison of quadratic and third degree polynomial non-linear temperature profile of recorded data was done using regression coefficient (R^2) and are presented in Appendix II-3. The best-fit curves are shown in Figs 5.12a & b and the typical equations are tabulated in Table 5.2. These equations were used to characterize the respective thermal gradient components.

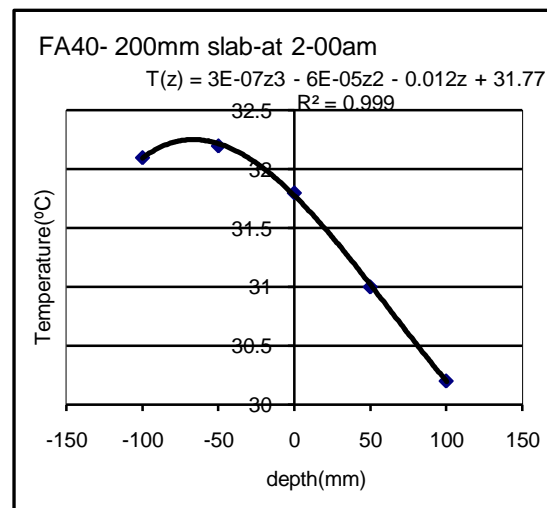
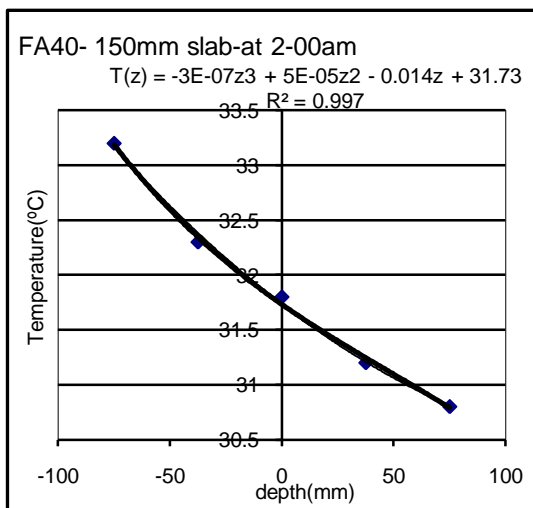
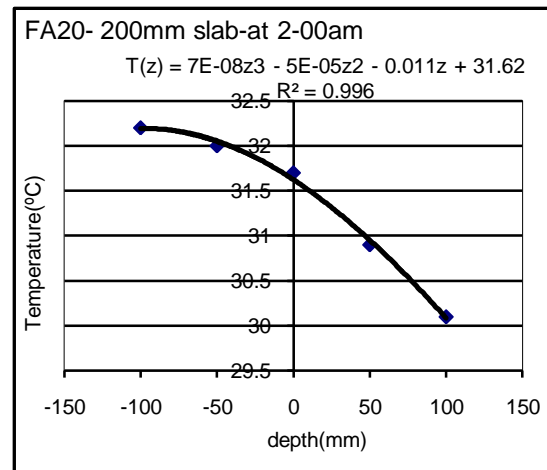
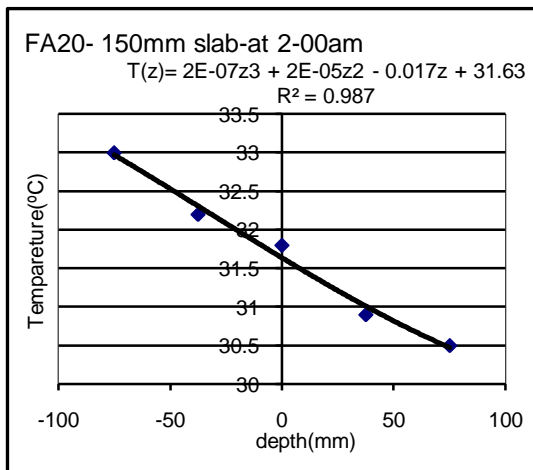
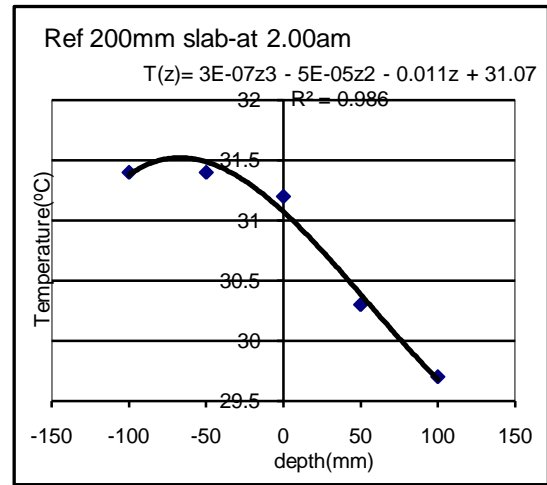
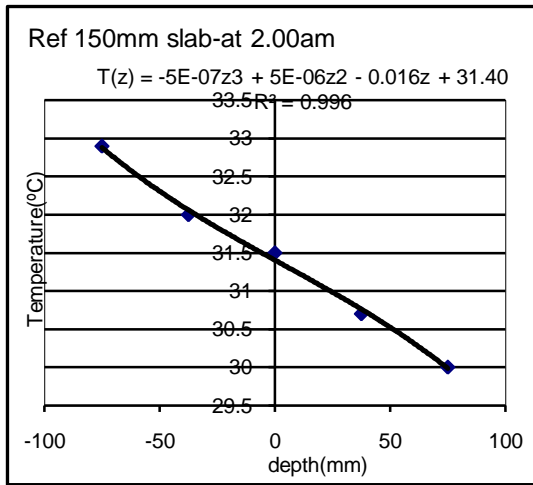


Fig 5.12a Temperature profile across thickness (150mm&200mm) at 02.00hours

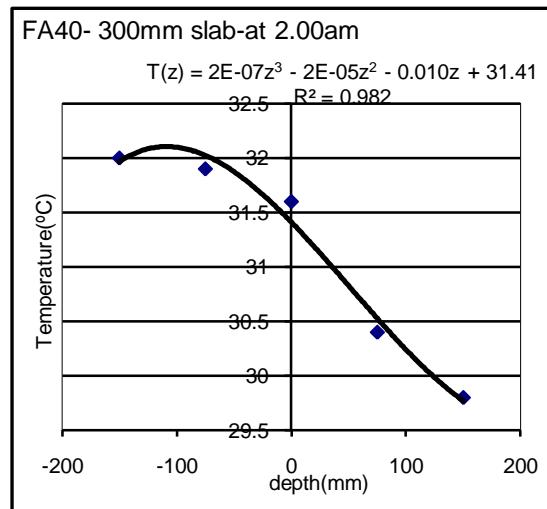
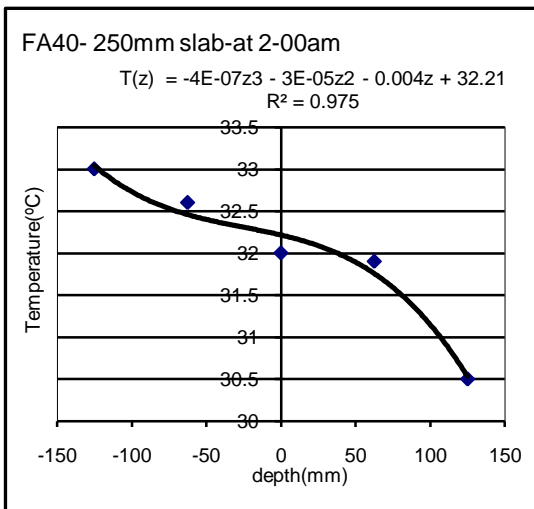
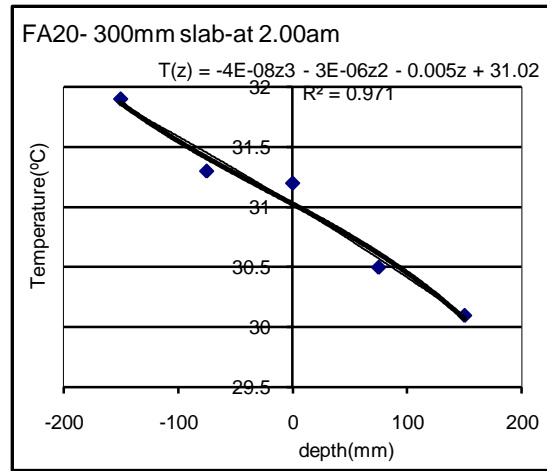
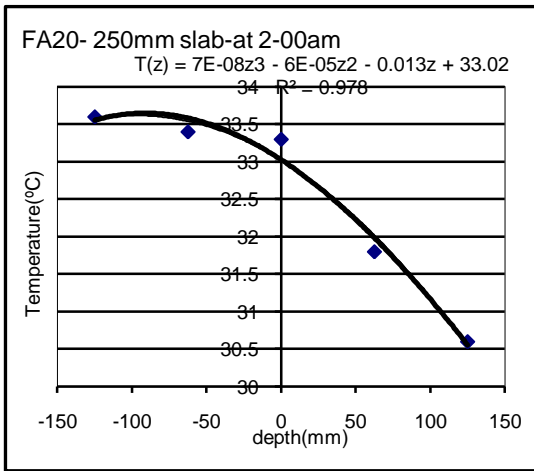
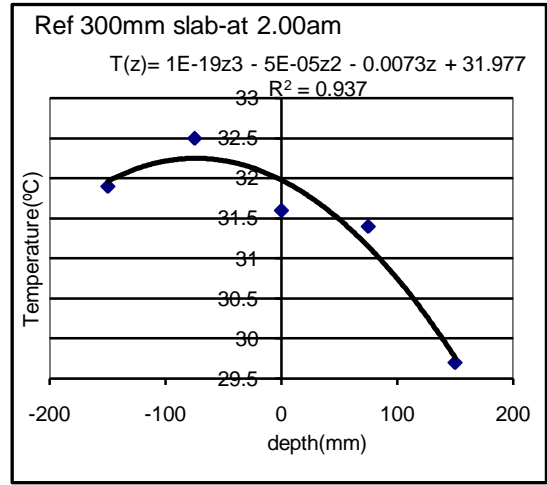
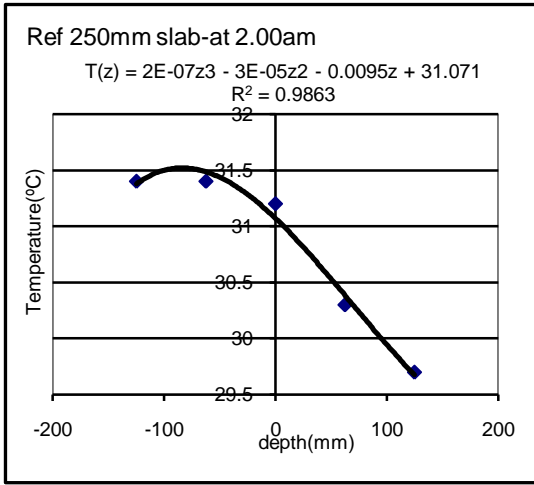


Fig 5.12b Temperature profile across thickness (250mm&300mm) at 02.00 hours

Table 5.2 Third degree polynomial equation of temperature distribution across the thickness(150mm) using regression

TIME	3rd Degree Polynomial Equation	R²
REFERENCE CONCRETE -150mm		
2-00am	$T(z) = -5E-07z^3 + 5E-06z^2 - 0.016z + 31.40$	0.996
10-00am	$T(z) = 2E-06z^3 - 7E-05z^2 + 0.006z + 33.12$	0.999
4-00pm	$T(z) = -2E-06z^3 - 2E-05z^2 + 0.014z + 41.84$	0.994
10-00pm	$T(z) = -1E-06z^3 - 1E-04z^2 - 0.016z + 34.81$	0.994
FA20 CONCRETE -150mm		
2-00am	$T(z) = 2E-07z^3 + 2E-05z^2 - 0.017z + 31.63$	0.987
10-00am	$T(z) = 2E-07z^3 - 6E-05z^2 + 0.019z + 34.05$	0.999
4-00pm	$T(z) = 6E-07z^3 - 0.0002z^2 + 0.021z + 41.46$	0.999
10-00pm	$T(z) = 9E-07z^3 - 7E-05z^2 - 0.032z + 36.22$	0.986
FA40 CONCRETE -150mm		
2-00am	$T(z) = -3E-07z^3 + 5E-05z^2 - 0.014z + 31.73$	0.997
10-00am	$T(z) = -2E-06z^3 + 1E-04z^2 + 0.036z + 33.60$	1
4-00pm	$T(z) = -1E-06z^3 - 0.0002z^2 + 0.025z + 41.46$	0.998
10-00pm	$T(z) = 1E-06z^3 - 0.0002z^2 - 0.018z + 36.27$	0.998

5.7 DEVELOPMENT OF EQUATION FOR NONLINEAR TEMPERATURE PROFILE

General form of temperature profile in 3rd degree polynomial

$$T(z) = A + Bz + Cz^2 + Dz^3 \quad \text{--(5.1)}$$

Where T(z) is the temperature in degree Celsius at distance z from the mid plane or mid depth

z is the vertical distance measured from the mid depth

z = +h/2 at the top

z = -h/2 at the bottom

A, B, C, D are the regression coefficients

This equation was used to characterize the thermal gradient components, viz. axial, linear and nonlinear. The temperature component causing axial displacement can be determined by integrating the temperature across the section and dividing this integral (area under temperature profile) by thickness of the slab (Ioannides and Khazanovich 1998).

$$T(z) = T_{axial} + T_L(z) + T_{NL}(z) \quad --(5.2)$$

$$\begin{aligned} T_{axial} &= \frac{1}{h} \int_{-\frac{h}{2}}^{\frac{h}{2}} T(z) \cdot dz = \frac{1}{h} \int_{-\frac{h}{2}}^{\frac{h}{2}} (A + Bz + Cz^2 + Dz^3) \cdot dz \\ &= A + \frac{Ch^2}{12} \end{aligned} \quad -- (5.3)$$

$$T_{Total} - T_{axial} = A + Bz + Cz^2 + Dz^3 - A + \frac{Ch^2}{12} = Bz + Cz^2 + Dz^3 - \frac{Ch^2}{12} \quad --(5.4)$$

The temperature component causing bending of the slab (linear component) is determined by taking the moment of remaining area after subtracting axial component from total area under the profile, and equating to the linear temperature component ($T_{curling}$) distribution which would produce the same moment (Zhang et al. 2003).

$$M = \frac{1}{h} \int_{-\frac{h}{2}}^{\frac{h}{2}} \left(Bz + Cz^2 + Dz^3 - \frac{Ch^2}{12} \right) z \cdot dz$$

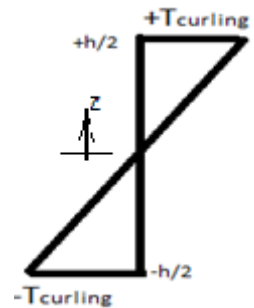
$$M = \frac{Bh^3}{12} + \frac{Dh^5}{80} \quad --(5.5)$$

Linear component of temperature distribution that varies from $+T_{curling}$ to $-T_{curling}$

$$\text{Thus Moment } M = Tc \frac{h^2}{6}$$

$$\text{Equating with (7) , } Tc = \frac{Bh}{2} + \frac{3Dh^3}{40}$$

and corresponding linear temperature component T_L at any depth z from mid depth can be written as



$$T_L(z) = Bz + \frac{3Dh^2z}{20} \quad \text{--(5.6)}$$

The stress due to linear temperature component

$$\sigma_L(z) = \frac{-E\alpha T_L(z)}{(1-\mu^2)} (Cx + \mu Cy)$$

Where C_x and C_y can be obtained from Bradbury chart based on length or width of slab and radius of relative stiffness.

From equations (5.3) (5.4) (5.5) & (5.8),

Nonlinear temperature component can be determined as $T_{NL}(z) = T(z) - T_{axial} - T_L(z)$

$$T_{NL}(z) = Cz^2 + Dz^3 - \frac{Ch^2}{12} - \frac{3Dh^2z}{20} \quad \text{--(5.7)}$$

Equation (5.7) gives generalized non linear temperature component at any depth z , which in turn gives the nonlinear stress component. It is termed as residual stress (Mohamed & Hansen 1996) or self equilibrating stress (Roesler 2010).

$$\text{At top surface } (z = +h/2) \quad T_{NL}(+h/2) = Ch^2/6 + Dh^3/20$$

$$\text{Bottom surface } (z = -h/2) \quad T_{NL}(-h/2) = Ch^2/6 - Dh^3/20$$

$$\text{Mid depth } (z=0) \quad T_{NL}(0) = -Ch^2/12$$

Residual or Self equilibrating stress

$$\sigma_{NL}(z) = \frac{-E\alpha}{1-\mu} T_{NL}(z) \quad \text{--(5.8)}$$

In the present study, Slab of 3500 mm wide, 4500 mm long was analysed for thermal stresses.

The other parameters considered were: Modulus of elasticity of concrete 31000MPa, Poisson's ratio 0.15, Modulus of subgrade reaction 0.098N/mm³ and Coefficient of thermal expansion of concrete 10x10⁻⁶/°C.

Bradbury coefficients (C_x and C_y) were considered based on L_x/l and L_y/l ratio.

Maximum temperature stress occurs at interior of the slab.

5.8 COMPARISON OF ANALYTICAL RESULTS

In the study, the third degree polynomial equations given in Appendix II-3 were used to describe temperature distributions across the slab thickness. They were characterized with four regression coefficients A, B, C, and D. Using these regression coefficients, the curling stress can be determined at various locations. Tables 5.3a to 5.3d give the comparison of two methods of evaluation of temperature stresses: linear and non linear temperature distribution across the thickness.

Table 5.3a Calculation of stress using nonlinear and linear temperature gradient assumptions for 150mm thick slab

		REF		FA20		FA40	
		2.00am	2.00pm	2.00am	2.00pm	2.00am	2.00pm
Regression Coefficients	A	31.406	41.166	31.637	41.266	31.731	40.837
	B	-0.0167	0.0309	-0.0176	0.0396	-0.0142	0.0262
	C	5E-06	-3E-05	2E-05	-2E-04	5E-05	-1E-04
	D	-5E-07	1E-06	2E-07	3E-07	-3E-07	1E-06
T _{axial} (°C)		31.42	41.11	31.67	40.89	31.82	40.65
T _L (°C)-top		-1.38	+2.57	-1.27	+3.05	-1.14	+2.22
-bottom		+1.38	-2.57	+1.27	-3.05	+1.14	-2.22
T _{NL} (°C)-top		-0.07	0.06	0.11	-0.70	0.14	-0.21
-bottom		0.10	-0.28	0.04	-0.80	0.24	-0.54
-mid		-0.01	0.06	-0.04	0.38	-0.09	0.19
σ _L (top)(MPa)		0.62	-1.16	0.57	-1.37	0.51	-1.00
σ _L (Bottom) (MPa)		-0.62	1.16	-0.57	1.37	-0.51	1.00
σ _{NL} (top) (MPa)		0.03	-0.02	-0.05	0.30	-0.06	0.09
σ _{NL} (Bottom) (MPa)		-0.04	0.12	-0.02	0.34	-0.10	0.23
σ _{NL} (mid)(MPa)		0.004	-0.02	0.02	-0.16	0.04	-0.08
Total Stress (MPa) @Top		0.65	-1.18	0.53	-1.07	0.46	-0.91
@Bottom		-0.67	1.28	-0.59	1.71	-0.62	1.23
@Mid		0.004	-0.02	0.02	-0.16	0.04	-0.08
Temp differential (°C)		-2.90	+3.7	-2.5	+6.2	-2.4	+5.0
Stress linear assumption (MPa) @top		0.65	-0.83	0.56	-1.40	0.54	-1.13
@Bottom		-0.65	0.83	-0.56	1.40	-0.54	1.13

Sign convention:

Stress: + indicates tensile stress

Temperature differential: + indicates top surface is hotter

Table 5.3b Calculation of stress using nonlinear and linear temperature gradient assumptions for 200mm thick slab

		REF		FA20		FA40	
		2.00am	2.00pm	2.00am	2.00pm	2.00am	2.00pm
Regression Coefficients	A	30.071	39.369	31.623	40.677	31.774	41.951
	B	-0.0118	0.022	-0.0112	0.0182	-0.0128	0.013
	C	-5.00E-05	-5.00E-05	-5.00E-05	-7.00E-05	-6.00E-05	-9.00E-05
	D	3.00E-07	2.00E-06	7.00E-08	2.00E-06	3.00E-07	2.00E-06
T _{axial} (°C)		29.90	39.20	31.46	40.44	31.57	41.65
T _L (°C)-top		-1.00	+3.40	-1.08	+3.02	-1.10	+2.50
-bottom		+1.00	-3.40	+1.08	-3.02	+1.10	-2.50
T _{NL} (°C)-top		-0.21	0.47	-0.31	0.33	-0.28	0.20
-bottom		-0.45	-1.13	-0.36	-1.27	-0.52	-1.40
-mid		0.17	0.17	0.17	0.23	0.20	0.30
σ _L (top)(MPa)		0.40	-1.37	0.43	-1.21	0.44	-1.00
σ _L (Bottom) (MPa)		-0.40	1.37	-0.43	1.21	-0.44	1.00
σ _{NL} (top) (MPa)		0.09	-0.20	0.13	-0.14	0.12	-0.09
σ _{NL} (Bottom) (MPa)		0.19	0.48	0.15	0.54	0.22	0.60
σ _{NL} (mid)(MPa)		-0.07	-0.07	-0.07	-0.10	-0.09	-0.13
Total Stress (MPa) @Top		0.49	-1.57	0.56	-1.36	0.56	-1.09
@Bottom		-0.21	1.85	-0.28	1.75	-0.22	1.60
@Mid		-0.07	-0.07	-0.07	-0.10	-0.09	-0.13
Temp differential (°C)		-2.4	+7.6	-2.1	+7.5	-1.9	+7.4
Stress linear assumption (MPa) @top		0.48	-1.53	0.42	-1.51	0.38	-1.49
@Bottom		-0.48	1.53	-0.42	1.51	-0.38	1.49

Sign convention:

Stress: + indicates tensile stress

Temperature differential: + indicates top surface is hotter

Table 5.3c Calculation of stress using nonlinear and linear temperature gradient assumptions for 250mm thick slab

		REF		FA20		FA40	
		2.00am	2.00pm	2.00am	2.00pm	2.00am	2.00pm
Regression Coefficients	A	31.071	38.423	33.026	40.066	32.214	39.837
	B	-0.0095	0.0151	-0.0131	0.0192	-0.0041	0.022
	C	-3.00E-05	7.00E-06	-6.00E-05	-5.00E-05	-3.00E-05	-7.00E-06
	D	2.00E-07	2.00E-07	7.00E-08	-2.00E-07	-4.00E-07	-3.00E-07
T _{axial} (°C)		30.91	38.46	32.71	39.81	32.06	39.80
T _L (°C)-top		-0.95	+2.12	-1.56	+2.17	-0.98	+2.40
-bottom		+0.95	-2.12	+1.56	-2.17	+0.98	-2.40
T _{NL} (°C)-top		-0.16	0.23	-0.57	-0.68	-0.63	-0.31
-bottom		-0.47	-0.08	-0.68	-0.36	0.00	0.16
-mid		0.16	-0.04	0.31	0.26	0.16	0.04
σ _L (top)(MPa)		0.32	-0.71	0.52	-0.72	0.33	-0.80
σ _L (Bottom) (MPa)		-0.32	0.71	-0.52	0.72	-0.33	0.80
σ _{NL} (top) (MPa)		0.07	-0.10	0.24	0.29	0.27	0.13
σ _{NL} (Bottom) (MPa)		0.20	0.04	0.29	0.16	0.00	-0.07
σ _{NL} (mid)(MPa)		-0.07	0.02	-0.13	-0.11	-0.07	-0.02
Total Stress (MPa) @Top		0.38	-0.80	0.76	-0.43	0.59	-0.67
@Bottom		-0.12	0.74	-0.23	0.88	-0.33	0.73
@Mid		-0.07	0.02	-0.13	-0.11	-0.07	-0.02
Temp differential (°C)		-1.7	+4.7	-3.0	+4.0	-2.5	+4.3
Stress linear assumption (MPa) @top		0.28	-0.78	0.50	-0.67	0.42	-0.72
@Bottom		-0.28	0.78	-0.50	0.67	-0.42	0.72

Sign convention:

Stress: + indicates tensile stress

Temperature differential: + indicates top surface is hotter

Fig 5.13 provides the pictorial representation of stresses due to linear temperature gradient assumption and non-linear temperature gradient assumption across the thickness. It can be observed that the stress calculated using linear assumption is either under-estimates or over-estimates the actual stress calculated based on the

nonlinear assumption. The difference is very small (in the range of 0.3 to 0.5MPa) to be taken into account in the design of pavements. However, use of steel fibers enhances the modulus of rupture of the concrete to balance this discrepancy.

Table 5.3d Calculation of stress using nonlinear and linear temperature gradient assumptions for 300mm thick slab

		REF		FA20		FA40	
		2.00am	2.00pm	2.00am	2.00pm	2.00am	2.00pm
Regression Coefficients	A	31.977	40.18	31.029	40.194	31.411	40.691
	B	-0.0073	0.031	-0.0051	0.0248	-0.0109	0.0236
	C	-5.00E-05	9.0E-06	-3.0E-06	-1.00E-06	-2.00E-05	-2.0E-05
	D	1.00E-19	-7.0E-07	-4.0E-08	-3.00E-07	2.00E-07	-4.0E-07
T _{axial} (°C)		31.602	40.247	31.006	40.1865	31.261	40.54
T _L (°C)-top		-1.095	+3.232	-0.846	+3.1125	-1.23	+2.73
-bottom		+1.095	-3.2325	+0.846	-3.1125	+1.23	-2.73
T _{NL} (°C)-top		-0.75	-0.81	-0.099	-0.42	-0.03	-0.84
-bottom		-0.75	1.08	0.009	0.39	-0.57	0.24
-mid		0.375	-0.0675	0.0225	0.0075	0.15	0.15
σ _L (top)(MPa)		0.29	-0.87	0.23	-0.83	0.33	-0.73
σ _L (Bottom) (MPa)		-0.29	0.87	-0.23	0.83	-0.33	0.73
σ _{NL} (top) (MPa)		0.32	0.35	0.04	0.18	0.01	0.36
σ _{NL} (Bottom) (MPa)		0.32	-0.46	0.00	-0.17	0.24	-0.10
σ _{NL} (mid)(MPa)		-0.16	0.03	-0.01	0.004	-0.06	-0.06
Total Stress (MPa) @Top		0.61	-0.52	0.27	-0.65	0.34	-0.37
@Bottom		0.03	0.41	-0.23	0.67	-0.09	0.63
@Mid		-0.16	0.03	-0.01	0.004	-0.06	-0.06
Temp differential (°C)		-2.2	+4.9	-1.8	+5.7	-2.2	+4.4
Stress linear assumption (MPa) @top		0.29	-0.66	0.24	-0.76	0.29	-0.59
@Bottom		-0.29	0.66	-0.24	0.76	-0.29	0.59

Sign convention:

Stress: + indicates tensile stress

Temperature differential: + indicates top surface is hotter

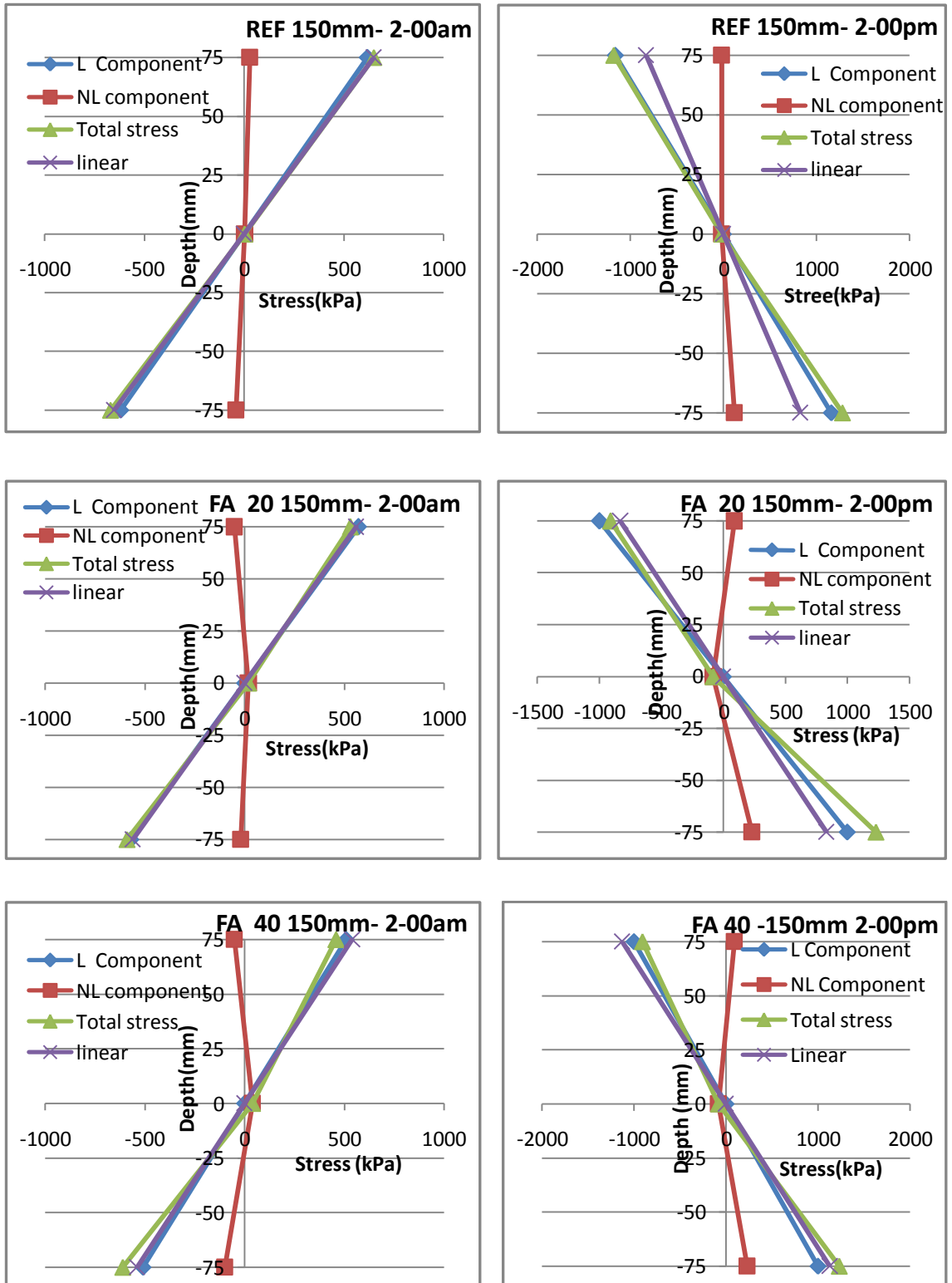


Fig 5.13 Comparison of stress due to linear and non linear temperature distribution across the thickness of slab(150mm)

A comparison of stresses calculated assuming 3rd degree polynomial distribution of temperature gradient with software EverFE was carried out for the temperature data obtained from field study. From Fig 5.14 it can be observed that the stress values are closely matched with stresses obtained from EverFE software with nonlinear (4 point) temperature distribution, indicating the two methods were in close agreement in calculating curling stresses. However, EverFE is not capturing peak compressive and tensile stresses, as seen in the Fig 5.14.

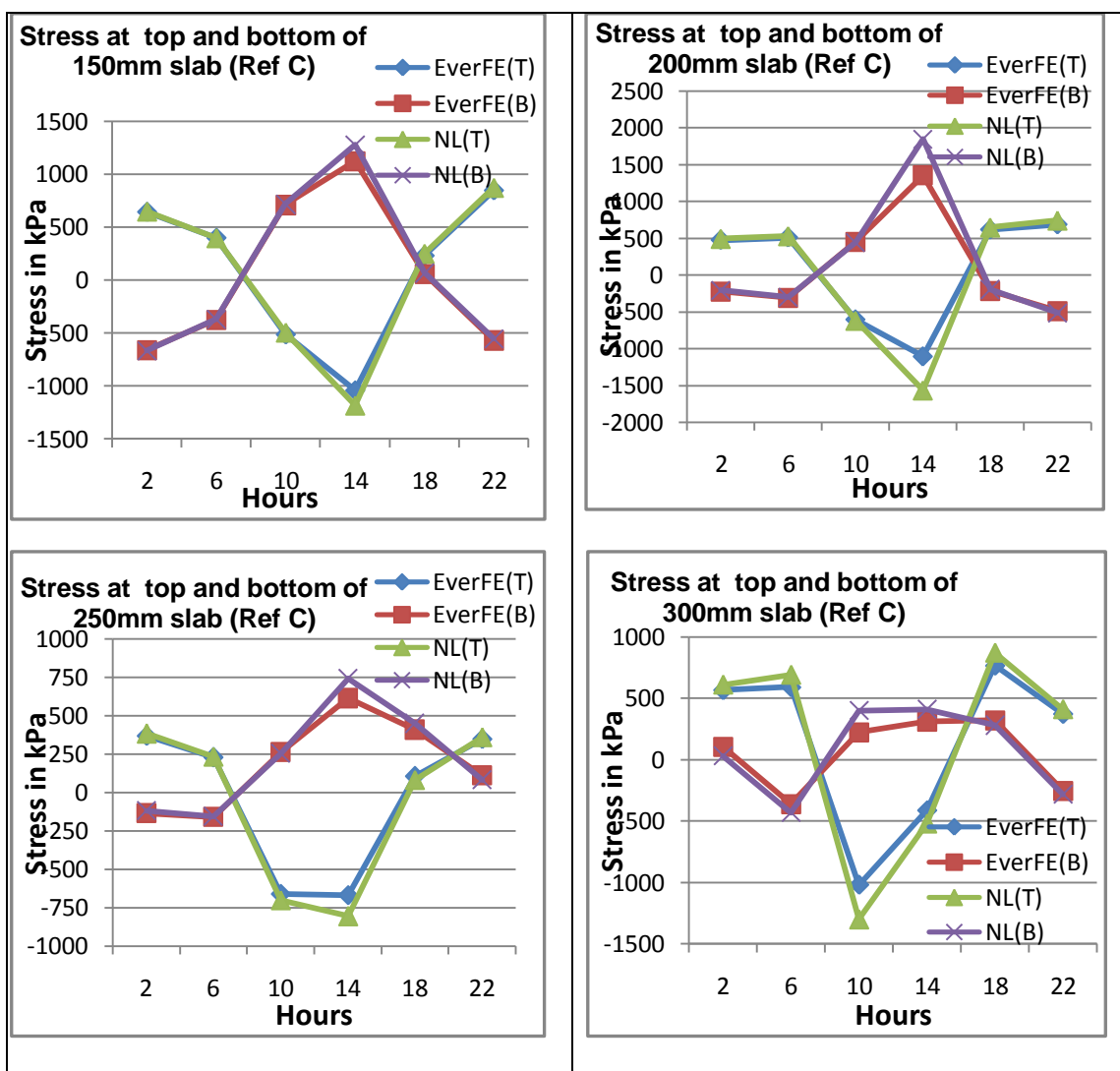


Fig 5.14 Comparison of stresses at top and bottom using nonlinear temperature distribution (3rd degree polynomial) and EverFE software

The comparison of stresses were also done with NOLA approach (Hiller et al.) and Quadratic equation (Liu et al.) and are presented in Table 5.4 and typically represented in Fig 5.15

Table 5.4 Comparison of stress due to nonlinear component by various approaches

300mm thick slab (Reference Concrete)									
Self Equilibrating Stress (kPa)									
Hour	top			bottom			Mid		
	NL(T)	NL(Q)	NL(N)	NL(T)	NL(Q)	NL(N)	NL(T)	NL(Q)	NL(N)
2	320	320	227	320	320	227	-160	-160	-114
6	416	128	99	-160	128	99	-64	-64	-56
10	-494	-448	-512	-402	-448	-512	224	224	256
14	345	-58	-99	-460	-58	-99	29	29	50
18	748	575	540	403	575	540	-288	-288	-270
22	179	64	43	-51	64	43	-32	-32	-21
250mm thick slab (Reference Concrete)									
Hour	top			bottom			Mid		
	NL(T)	NL(Q)	NL(N)	NL(T)	NL(Q)	NL(N)	NL(T)	NL(Q)	NL(N)
2	67	133	185	200	133	185	-67	-67	-92
6	17	40	85	63	40	85	-20	-20	-43
10	-289	-222	-85	-155	-222	-85	111	111	43
14	-98	-31	-14	36	-31	-14	16	16	7
18	200	266	270	333	266	270	-133	-133	-135
22	89	222	327	355	222	327	-111	-111	-163
200mm thick slab (Reference Concrete)									
Hour	top			bottom			Mid		
	NL(T)	NL(Q)	NL(N)	NL(T)	NL(Q)	NL(N)	NL(T)	NL(Q)	NL(N)
2	91	142	114	193	142	114	-71	-71	-57
6	233	114	114	-6	114	114	-57	-57	-57
10	-136	-85	-71	-34	-85	-71	43	43	36
14	-199	-142	-156	-283	-142	-156	71	71	78
18	347	227	227	108	227	227	-114	-114	-114
22	63	114	57	165	114	57	-57	-57	-28
150mm thick slab (Reference Concrete)									
Hour	top			bottom			Mid		
	NL(T)	NL(Q)	NL(N)	NL(T)	NL(Q)	NL(N)	NL(T)	NL(Q)	NL(N)
2	28	-8	14	-44	-8	14	4	4	7
6	74	16	14	-42	16	14	-8	-8	-7
10	-32	112	99	256	112	99	-54	-54	-50
14	-24	48	-14	120	48	-14	-24	-24	7
18	100	160	199	160	160	199	-80	-80	-99
22	232	180	199	88	180	199	-80	-80	-99

NL(T)-stress due to nonlinear component using Third degree polynomial for temperature distribution
 NL(Q)- stress due to nonlinear component using Quadratic equation for temperature distribution(Liu et al. 2003)

NL(N)- stress due to nonlinear component using NOLA approach(Hiller et al. 2010)

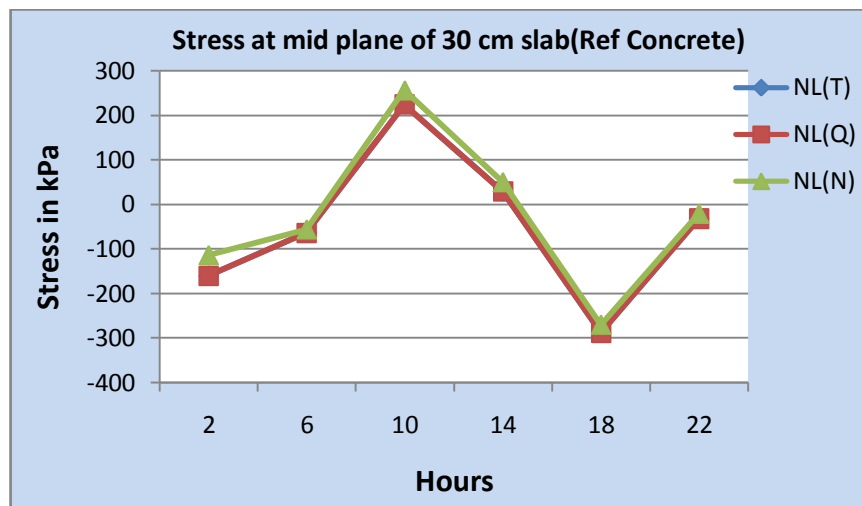
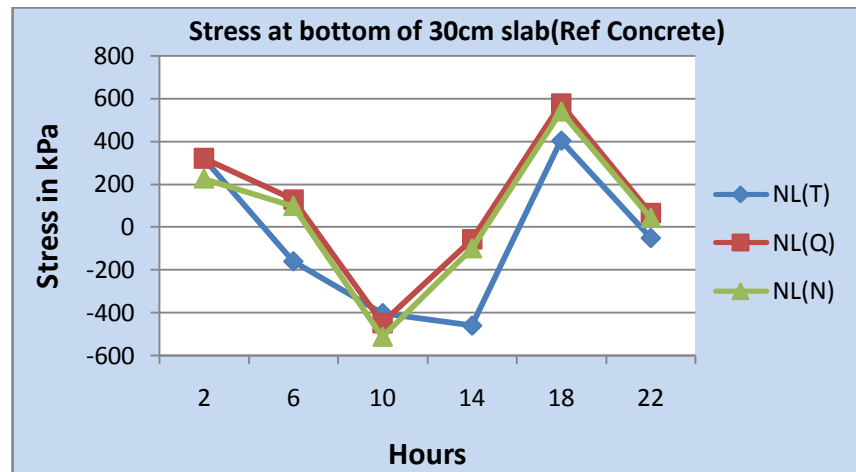
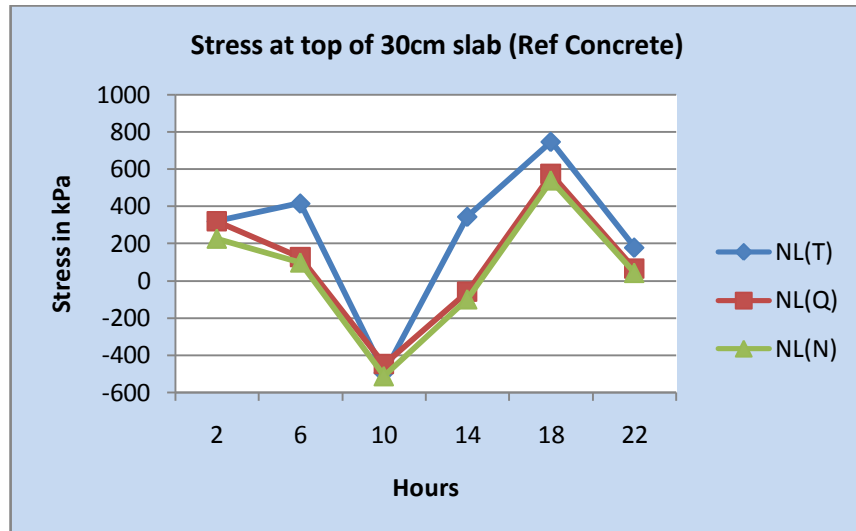


Fig 5.15 Comparison of stresses at different timings for 300mm thick slab
 NL(T)-stress due to nonlinear component using Third degree polynomial for temperature distribution
 NL(Q)- stress due to nonlinear component using Quadratic equation for temperature distribution
 NL(N)- stress due to nonlinear component using NOLA approach(Hiller et al. 2010)

5.9 DISCUSSIONS

Temperature studies were carried out on different slab specimens exposed to the ambient temperature. As the air temperature increases around the slab, the slab temperature also increases by absorbing the thermal energy. The hourly temperature data of the concrete slab at different depths follows sinusoidal variation. The top surface was found to be hotter than the bottom surface during the day time (7.00-18.00hrs) and the bottom was found to be hotter than the top surface between 18.00 - 7.00hrs. At around 6.00-7.00 hrs and 17.00-18.00 hrs the temperature across the thickness was found to be uniform. At the top surface, a maximum peak temperature of 42°-44°C was recorded between 13.00 -15.00 hrs and a minimum peak temperature of 27°-30°C at around 4.00 -6.00hrs. It was also observed that the difference between the maximum and minimum temperature at top surface is quite large compared to the bottom surface. It shows that thermal diffusivity rate in concrete is very low. From the observed temperature data it can be concluded that on the top surface, the thermal absorption characteristics of the concrete are not much altered due to the use of fly ash.

The temperature differential between the top and bottom surfaces is an important parameter in evaluating temperature stresses. The maximum positive temperature differential (7.9°C) is found to be higher than the maximum negative temperature differential (4.5°C). As per IRC 58:2002 the temperature differential to be considered for calculating temperature stress in coastal Karnataka region bounded by hills, varies from 14.6°C to 17°C for thickness 150mm to 300mm. Thus values given in code are found to be highly conservative. However, further investigations are needed to evaluate the temperature differential along with moisture content.

The temperature variation within the concrete slab is nonlinear. During the day time, as the temperature increases on the surface of concrete slab, the temperature profile becomes steeper. As the heat conduction is more at the depth of $h/2$ from the top surface, there is a further increase in steepness of temperature profile curves. During hours 0.00-5.00 the hourly temperature profiles become parallel to each other indicating constant rate of cooling. There is no change found in thermal characteristics

when fly ash is added to the concrete. Hence, for concrete pavements, the addition of fly ash can be recommended.

The third degree polynomial curve is best suited for representation of the temperature profile across the thickness, compared to the quadratic curve. However, the use of quadratic curve can also be justified with the regression equation coefficient of 0.8 to 0.99, neglecting some exceptions. The stress calculation at various hours of a day is carried out using non-linear and linear temperature profiles. It is observed that the stress calculated using non-linear profile was found to vary in the range of 10 to 30% higher than that of calculated using linear profile. This additional stress in pavement further reduces the design life of the pavements. Higher flexural strength of steel reinforced concrete than the normal concrete can overcome this deficiency.

The curling stresses were calculated using coefficients of regression equation obtained from actual temperature data and compared using software EverFE. The resulting stress as at the top and the bottom surface obtained by EverFE and the regression equation were found to be almost equal. However, the value of peak stress calculated by EverFE was slightly lesser than the value obtained by the regression equation. The stress values calculated using non-linear approach were compared with other approaches such as NOLA (Hiller et al.) and quadratic equation (Liu et al.) and it was found that the stress calculated using the first approach at the mid plane was closely matching with the other two methods, whereas at the top and bottom it was found to be different.

5.10 SUMMARY

Based on the field data of temperature across the thickness of the slab, it was found that the variation is non-linear and follows a third degree polynomial. The variation in maximum stresses calculated using linear and non-linear temperature profile are about 10 to 30%. As SFRC material is having better flexural strength than normal concrete, premature failure of pavements due to enhanced temperature stress can be avoided. As addition of fly ash does not change thermal characteristics of concrete, use of fly ash in concrete pavement is highly recommended.

CHAPTER 6

LOAD STUDY ON SFRC SLABS

6.1 GENERAL

This chapter discusses the experimental investigation of slabs on ground under wheel load with the objective of understanding the stress behaviour. The steel fiber reinforced fly ash concrete slabs of 900 mm x 900 mm, 150 mm thick were investigated in this study. Strain gauges and data acquisition system were used to measure the strains at the centre and the edge of the slab under the action of the load.

6.2 EXPERIMENTAL SET UP

In this investigation, four steel fiber reinforced fly ash concrete slabs (FS1, FS2, FS3 and FS4) along with one conventional concrete slab (R) were tested. A square slab of dimension 900mm x 900mm with thickness 150mm was tested under wheel load (analysed as patch load) at centre as well as at the edge. The slab was supported by 16 steel supports placed at 225mm centre to centre in both directions to resemble Winkler soil foundation. These steel supports are square steel hollow box of size 100mm x 60mm with thickness 3mm. A steel rod of 20mm diameter, 20mm height was kept at the centre of box to ensure the full contact and load transfer from the slab. Similar springs had been used by Sorelli et al. (2006). The average stiffness of the spring was determined by a load test on the box spring (Fig 6.1) and a graph of load verses deflection was plotted (Fig 6.2). From the plot, the stiffness (load required to produce unit deflection) was found out using regression equation. For 1mm deflection, the load estimated was 500kg (= 5kN). Thus the estimated spring stiffness was equal to 5kN/mm.



Fig 6.1 Testing arrangement for stiffness of steel box

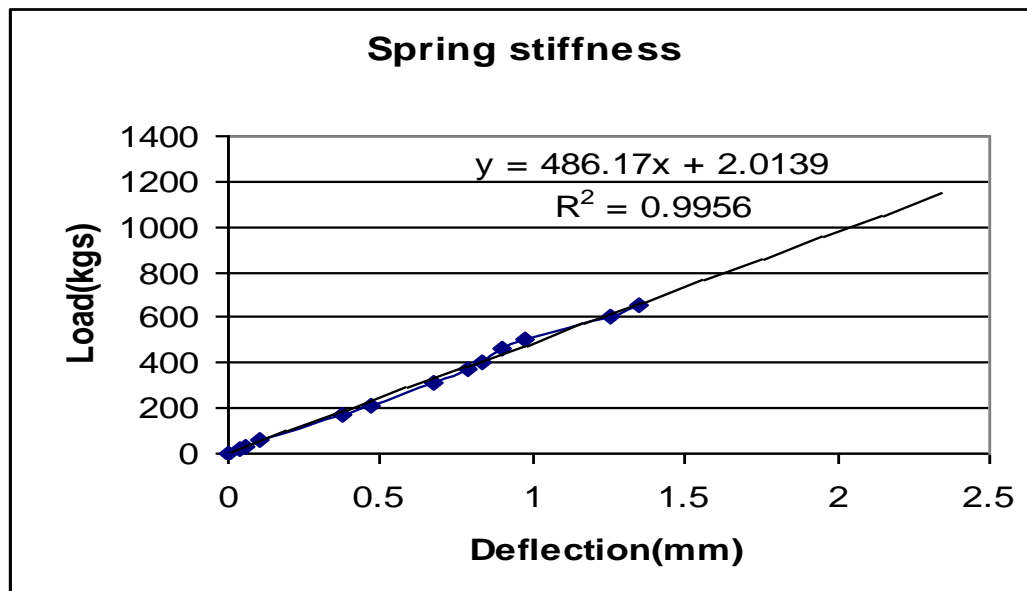
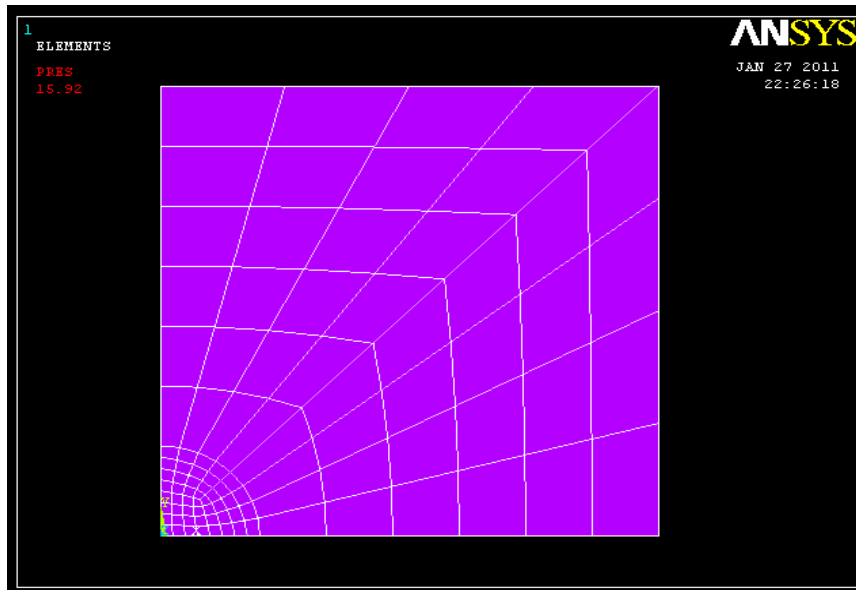


Fig 6.2 Plot of load v/s deflection of a box spring

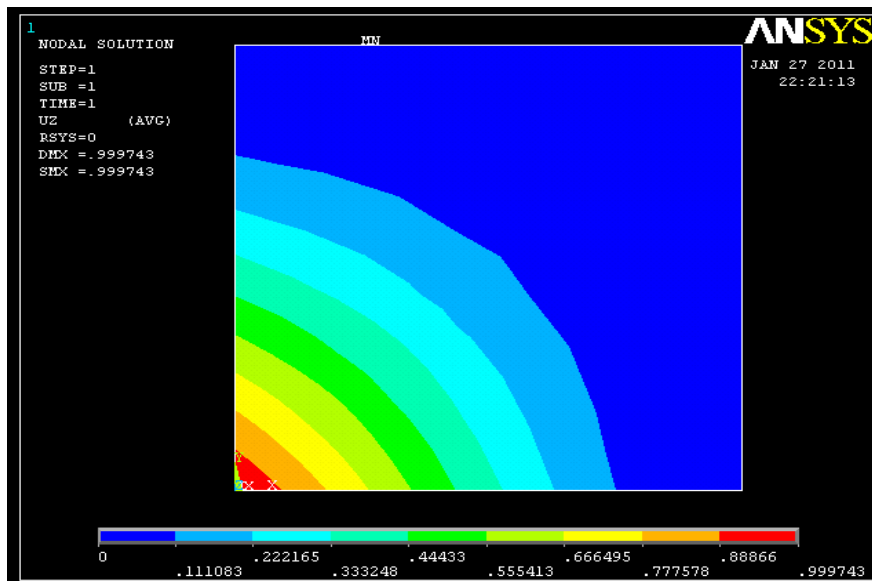
To verify the experimental results and the behaviour of the spring, the spring box was modelled (Fig 6.3) using ANSYS software. When the intensity of pressure was

15.92N/mm² over circular area of diameter 20mm, the central deflection observed was 1mm. Thus the total load required for 1mm deflection (using ANSYS) is

$$W = \pi r^2 * \text{loading pressure} = \pi * 20^2 * 15.92 = 5000 \text{ N} = 5 \text{ kN}$$



(a)



(b)

**Fig 6.3 Spring box model (ANSYS) a) meshing and loading
b) Deflection contours**

Both experimental and the analytical values of spring stiffness was 5 kN/mm and the box behaves like linear elastic spring. When such springs were placed with an effective area of support 225mm x 225mm, the modulus of subgrade reaction 'k' was equal to 0.098N/mm^3 (9.8kg/cm^3), which corresponds to the modulus of subgrade reaction of dry lean concrete (approximately 0.1N/mm^3)(IRC58-2002). Fig 6.4 shows the arrangement of the springs.



Fig 6.4 Arrangement of box springs

Uniaxial Strain gauges were used to capture the strain due to bending at the bottom of the slab, when subjected to patch loading. The instrumentation used to measure the slab strains consisted of strain conditioner/amplifier from National Instruments (Fig 6.5).



Fig 6.5 Data Acquisition Unit

The strain data acquired were recorded using data acquisition system and the connected PC with necessary available software. Four strain gauges of N2A-06-10-CBE120 type by Micro Measurements, Vishay Precision Group Inc. with resistance of $120 \pm 2 \Omega$ were used. Two strain gauges at centre (G1 & G2) and two at edge (G3 & G4) were fixed using specified adhesive in two mutually perpendicular directions, as shown in Fig 6.6. The strain gauges were connected to the acquisition system using lead wires. Two critical loading positions, viz centre and edge loadings were considered for the study (L1 & L2).

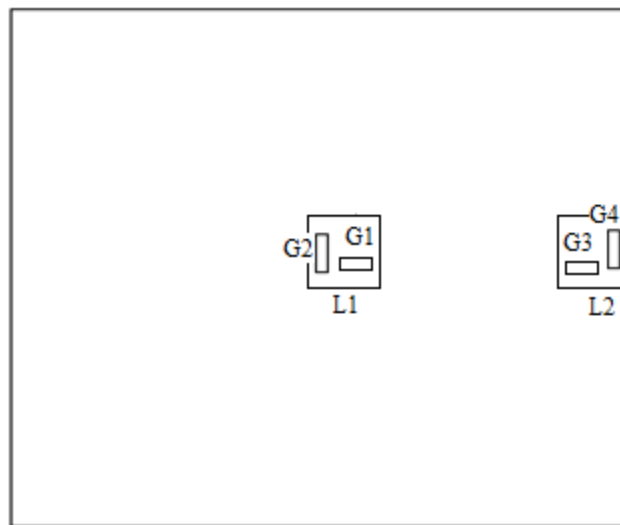


Fig 6.6 Position of strain gauges and load
G1, G2, G3, G4-straingauge position and L1, L2 loading position

Fig 6.7 shows the arrangement for placing of slab over the steel springs. The slabs were loaded to an area of 125mm x125mm by a hydraulic jack using a loading frame. During the tests, strains were recorded at pre-determined position using strain gauges. Fig 6.8 depicts the loading arrangement for central and edge loading.



Fig 6.7 Placing of slab over steel box springs



(a)



(b)

Fig 6.8 Loading arrangement a) Centre loading b) Edge loading

Strain gauges were designed to convert mechanical motion into an electronic signal. Strain gauge would change resistance only due to the deformations of the surface to which the sensor was attached. When a load is applied to the surface, the resulting change

in surface length was communicated to the resistor and the corresponding strain was measured in terms of the electrical resistance of the foil wire, which vary linearly with strain. The foil diaphragm and the adhesive bonding agent must work together in transmitting the strain, while the adhesive must also serve as an electrical insulator between the foil grid and the surface. The electric signals were converted into microstrains and stored in a computer. The proving ring of 500kN was used to observe the applied load. The load was increased monotonically with an increment of 5kN till attaining the required value; a rest period of 5 minute was given to observe the accumulated strain at that level of loading before it was loaded further. Recording of strain data is shown in Fig 6.9.



Fig 6.9 Recording of data

The maximum load on the slab was limited to 40 kN over an area of 125mmx125mm with a pressure of 2.56N/mm^2 , which is quite higher than the tyre pressure of 0.8N/mm^2 (8kg/cm^2) on the concrete pavement generally adopted for design. For most of commercial vehicles the commonly used tyre inflation pressures range from 0.7 MPa to 1.0MPa (IRC 58-2002).

6.3 RESULTS

From the obtained data, load verses strain graphs were plotted. Figs 6.10a to 6.10c show the raw data of strain at different time instants (sampling) observed by various strain gauges under the increasing load.

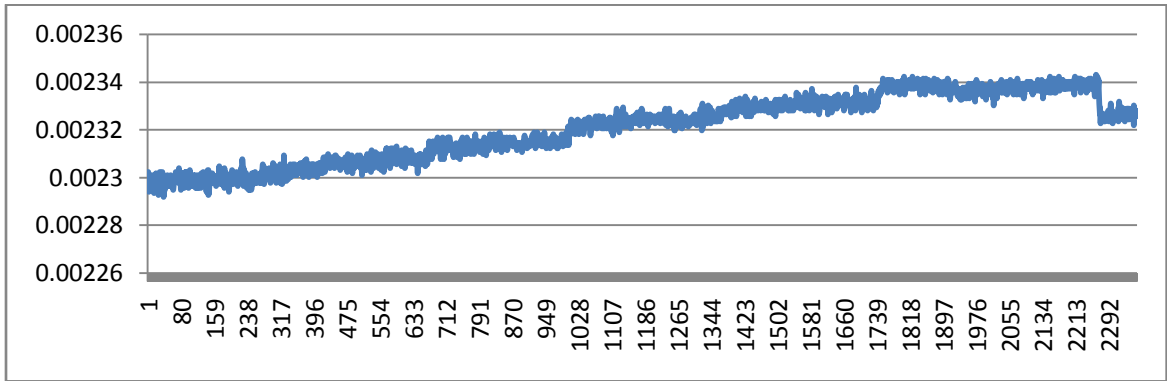


Fig 6.10a Strain at different instants of time (REF gauge 1)-Central loading

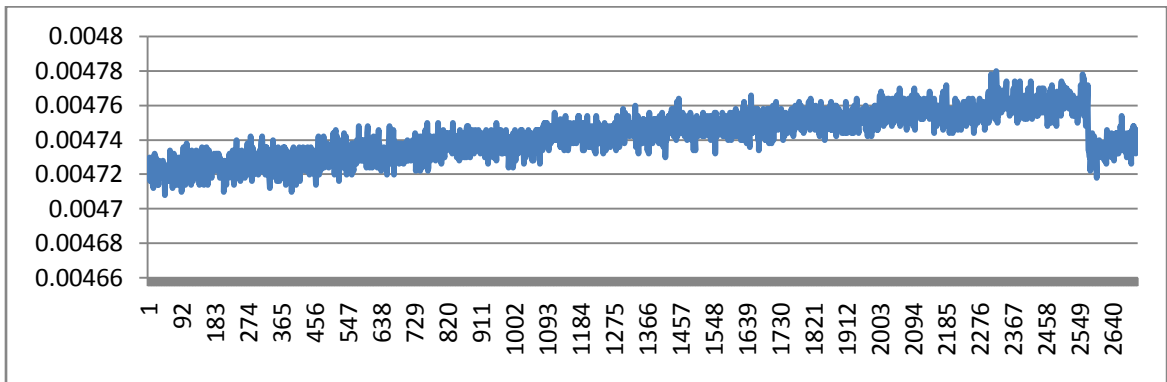


Fig 6.10b Strain at different instants of time (FS4 gauge 2)-Central loading

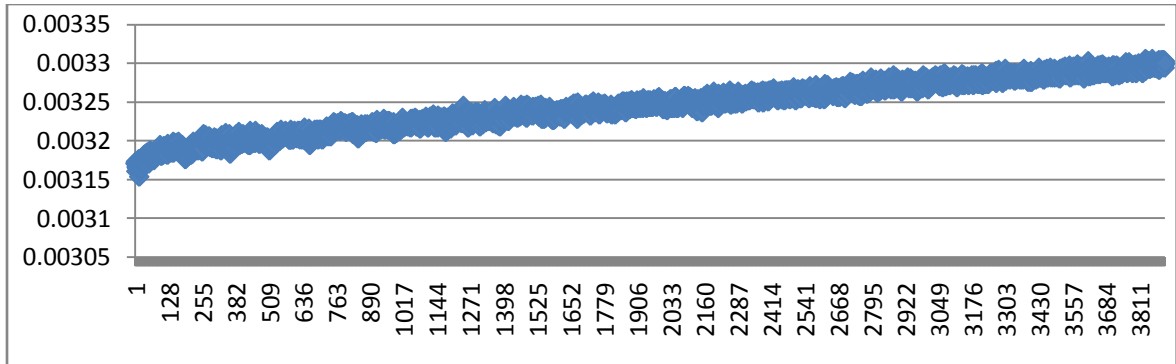


Fig 6.10c Strain at different instants of time (FS4 gauge 4)-Edge loading

Fig 6.11 depicted the load verses strain relationship under centre and edge loading for steel fiber fly ash concrete (FS4). From the graph it can be observed that the load strain curve (stress-strain) vary linearly. This indicates that the slab material is within the elastic limits even up to the tyre pressure of 2.5MPa. However, maximum tyre contact pressure experienced by 11R22.5(Radial), 10x20(Bias), 425/65R22.5(wide-base) types of tyres are 0.945MPa, 0.849MPa and 1.020MPa respectively under the wheel loads of 4.1T, 3.6T and 5.6T (Park, 2008). Hence, the elastic analysis of the slab under wheel load as per Westergaard or modified IRC equations can be used for fly ash steel fiber concrete too. The slope of load-strain equation was found to be higher in the case of FS4 concrete signifying higher modulus of elasticity.

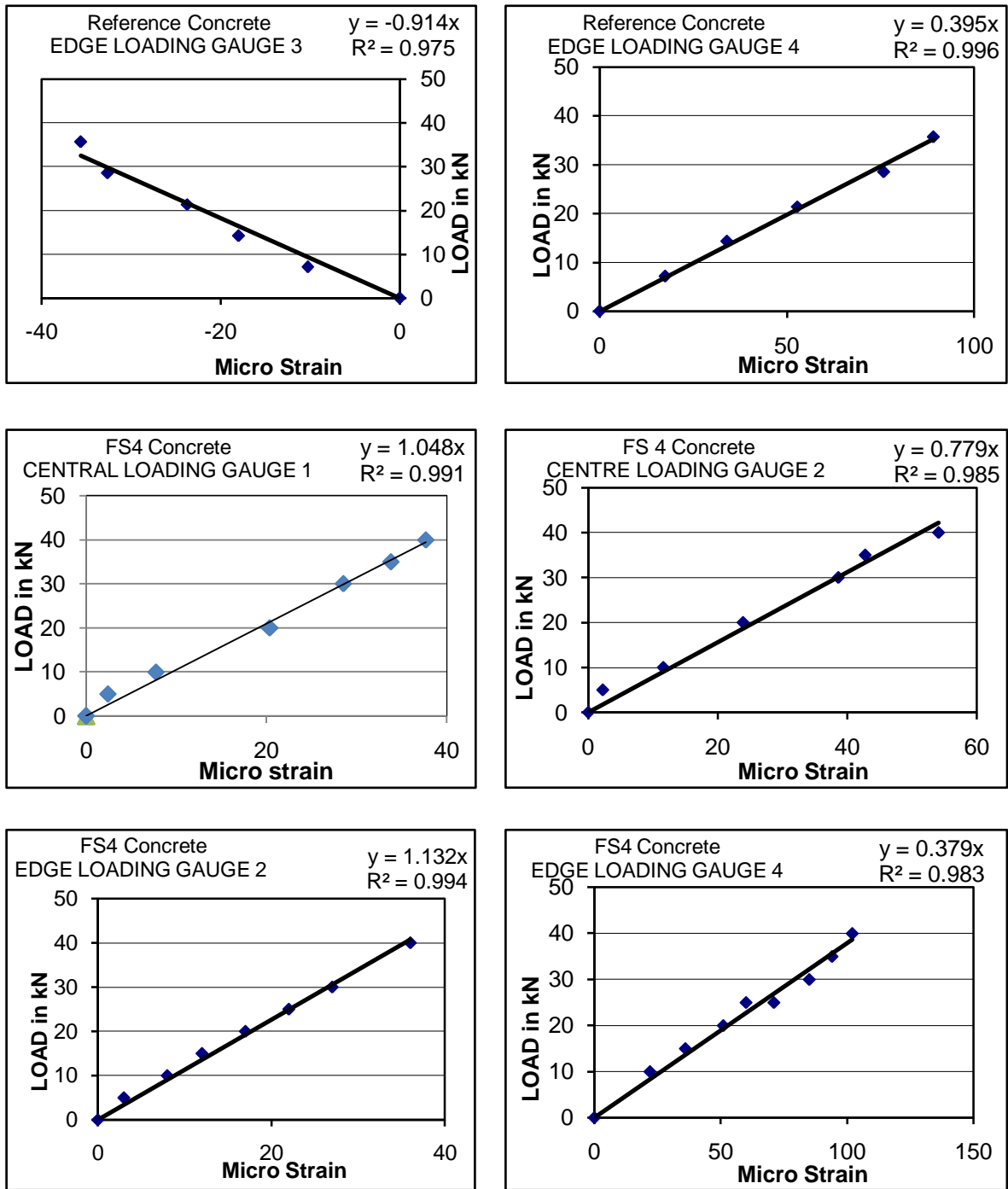


Fig 6.11 Load v/s strain relation in Fly ash SFRC (FS4) under central and edge loading

The slab and spring support was modeled using the ANSYS software. By using different modulus of elasticity and Poisson's ratio for the model, strains were calculated at centre under different loading intensities (zero to 40kN). The strain contour under central loading is demonstrated in Fig 6.12. The significant values of Poisson's ratio for concrete were taken as 0.15 and 0.2 for the study (Neville 1995). The modulus of elasticity of concrete used in the study vary between 25000 MPa to 40000 MPa covering a wide range of values for different concretes (refer 3.9.8). From the graph (Fig 6.13), the modulus of elasticity of fly ash steel fiber reinforced concrete (FS4) can be estimated as 34000N/mm². The change in Poisson's ratio from 0.15 to 0.20 has very little impact on the load –strain relationship.

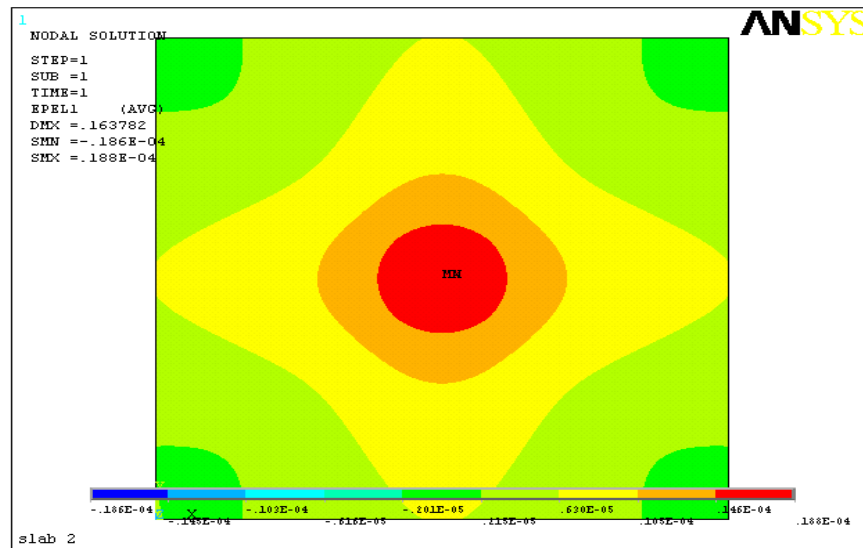


Fig 6.12 ANSYS strain contour under central loading(E= 30000, $\mu=0.15$)

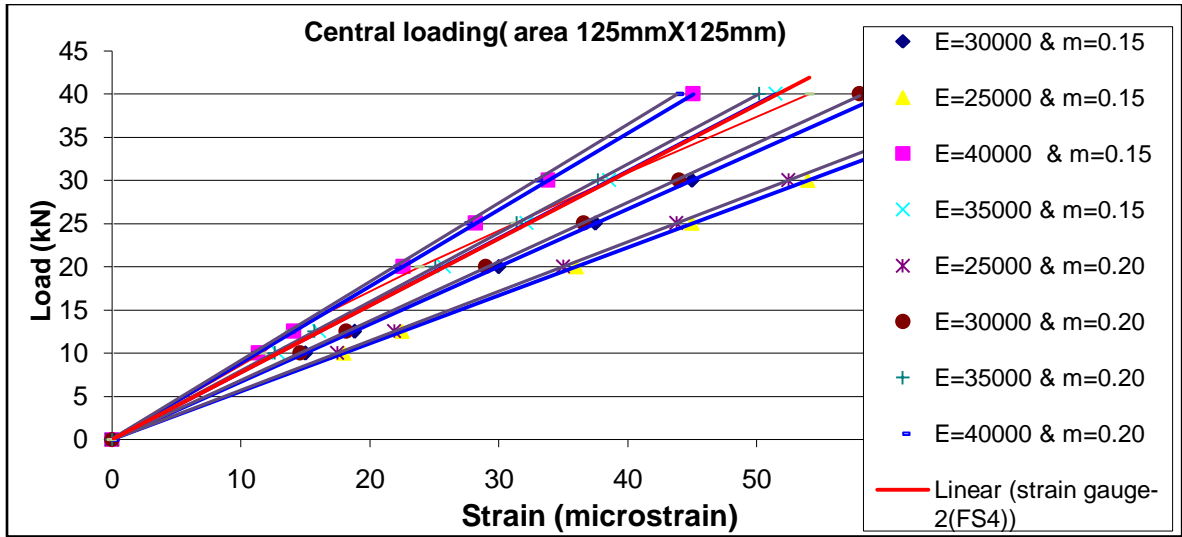


Fig 6.13 Comparison of strain gauge data with ANSYS results

The moduli of elasticity of various concretes (M_{40}) were calculated using the prediction model given in section 3.9.8 using characteristic strength of concrete $f_{ck}=40\text{MPa}$, and are reported in Table 6.1. Using these values along with Poisson's ratio of 0.15, slabs of 150mm were modeled in ANSYS Software. The strains at various gauge positions were calculated. Comparison of experimental results and the strain obtained by the ANSYS software at various gauge positions for FS4 are presented in Fig 6.14. Other graphs are presented in Appendix III. From the graphs, it is observed that experimental results were closely matching with ANSYS results.

Table 6.1 Predicted Modulus of Elasticity of Various Concretes of grade M_{40}

Type of Mix	Modulus of Elasticity (MPa)
R	31623
FS1	32495
FS2	34818
FS3	31799
FS4	34072

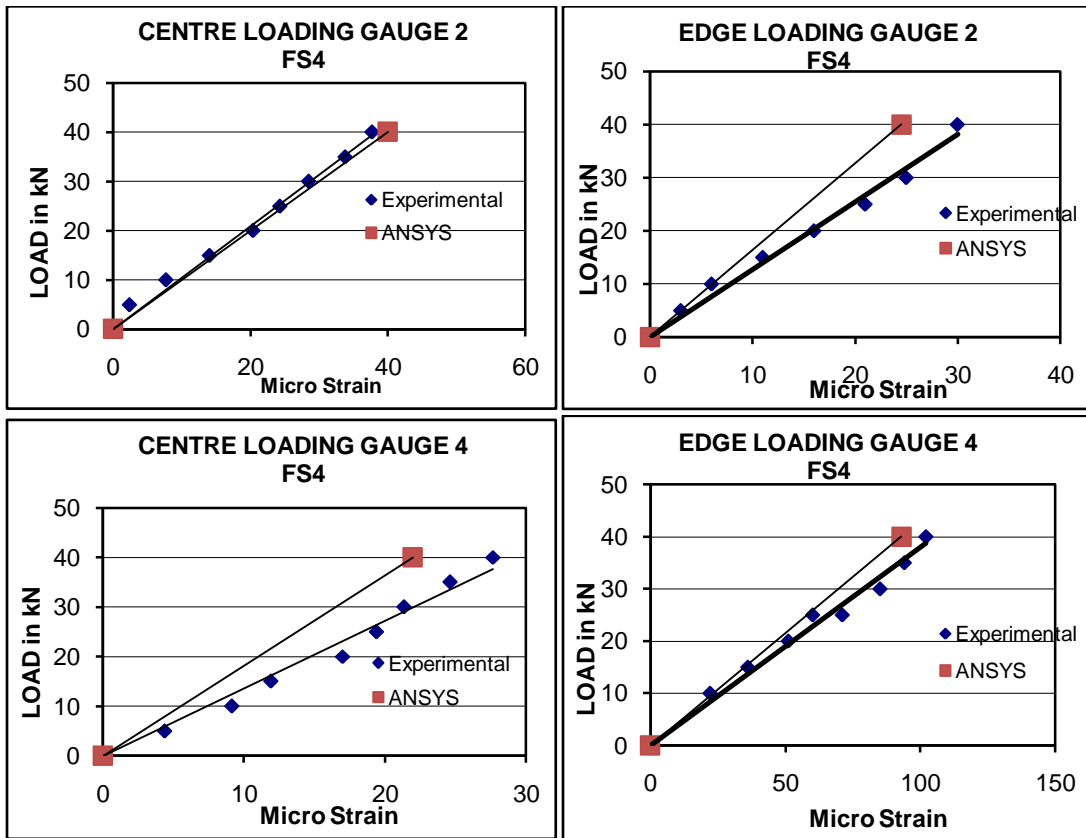


Fig 6.14 Comparison of experimental and ANSYS results

From the plots given in Fig 6.14 and in Appendix III, it can be observed that the strains recorded by strain gauge (experimental) and from the ANSYS analysis are very close to each other. Under the central loading, all the four strain gauges recorded positive strains indicating extension. This extension induces tensile stresses in the slab. In the case of edge loading, strain gauge 1 and 3 recorded negative strains. This indicates that, these positions are subjected to compressive stresses during edge loading.

6.4 STRESS ANALYSIS

The analytical study was extended by modeling the slab with actual field dimensions (4.5m x 3.5m) using steel fibre fly ash concrete (FS4). Using modulus of elasticity of the FS4 concrete predicted with ANSYS (referring Fig 6.14); the critical stress in the

pavement slab of different thickness when subjected to load due to dual wheel assembly at the middle of longer edge (Fig 6.15) was investigated using ANSYS software.

Parameters considered for the analysis

Modulus of Elasticity: 34000N/mm^2

Poisson's Ratio : 0.15

Slab dimension 4.5m long, 3.5 m wide

Tyre imprint area: (Park, 2008)

Case1: 200mm x 250mm with axle load 16.4T

Wheel load 4.1 T with tire contact pressure 0.911N/mm^2

Case 2: 225mm x 250mm with axle load 22.4T

Wheel load 5.6T with tire contact pressure 1.0 N/mm^2

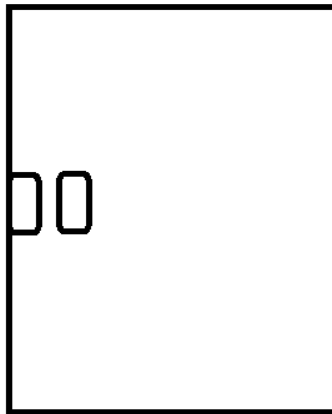


Fig 6.15 Loading position of dual wheel load assembly

Table 6.2 gives the edge stress values for fly ash SFRC (FS4) for different thicknesses of slab and varied modulus of subgrade reaction. The same is shown pictorially in Fig 6.16. From the figure, it is observed that the modulus of sub grade reaction has a very little impact over the stresses when the thickness of slab is more than 250mm.

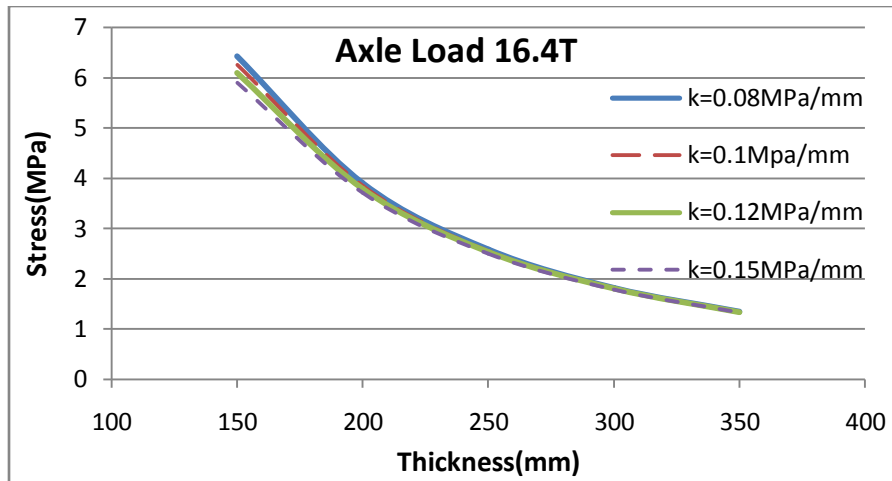


Fig 6.16 Edge load stress v/s thickness of slab obtained using ANSYS

Table 6.2 Edge load stresses in fly ash SFRC (FS4)

CASE 1: axle load 16.4T				
THICKNESS (mm)	Stress (N/mm ²)			
	k=0.08N/mm ³	k=0.10N/mm ³	k=0.12N/mm ³	k=0.15N/mm ³
150	6.434	6.259	6.103	5.897
200	3.902	3.843	3.788	3.711
250	2.579	2.553	2.535	2.504
300	1.818	1.809	1.799	1.785
350	1.347	1.342	1.337	1.331
CASE 2: axle load 22.4T				
	k=0.08N/mm ³	k=0.10N/mm ³	k=0.12N/mm ³	k=0.15N/mm ³
150	7.558	7.345	7.156	6.907
200	4.595	4.524	4.457	4.363
250	3.040	3.013	2.986	2.949
300	2.144	2.133	2.121	2.104
350	1.589	1.583	1.577	1.569

The stress values obtained by ANSYS are compared with IITRIGID software results (IRC 58: 2002) and are depicted in Fig 6.17. From the figure it is observed that both the methods yield very close results. However, IITRIGID gives slightly higher stress value in case of thicker slabs (20% to 30% more than the ANSYS results).

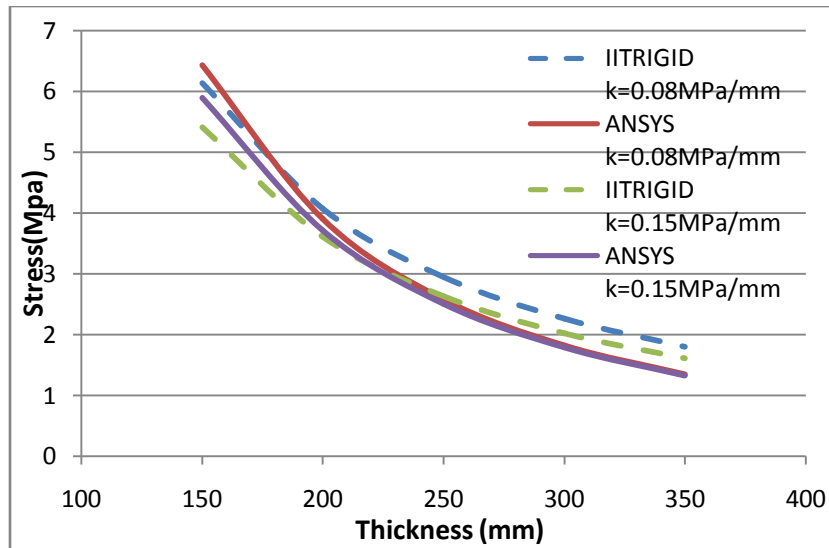


Fig 6.17 Comparison of stress in slab due to edge load

6.5 SUMMARY

The load versus strain graphs clearly signifying higher modulus of elasticity of fly ash steel fiber reinforced concrete. The load–strain relation follows linear expression representing the elastic behavior. When the slab was unloaded, the residual strain observed was of very small quantity indicating regain of its original shape. The stress calculated using IITRIGID and ANSYS were matching significantly. However, for thicker slabs, the effect of subgrade modulus (k) was insignificant in case of ANSYS whereas it mattered for IITRIGID.

CHAPTER 7

PAVEMENT DESIGN

7.1 GENERAL

Based on the experimental investigation on materials and the proposed models, typical design of pavement thickness was carried out for both high and low volume roads as per the guidelines specified in IRC 58(2002). The fatigue model proposed by IRC and fatigue equation proposed in this thesis was used to calculate the pavement thickness and the results were compared. IITRIGID was used to obtain the stresses in the pavement slab. The maximum stress due to axle load and the temperature differentials also were calculated. Thermal stresses were computed using the conventional method and the additional stresses were considered to address the nonlinear temperature distribution across the thickness. The temperature differential proposed by IRC 58 (2002) was adopted for calculations.

7.2 DESIGN STRESSES AND PARAMETERS

Table 7.1 gives the predicted flexural strength and modulus of elasticity of different materials based on the prediction models given in section 3.9.7 and 3.9.8. The characteristic strengths of High volume and Low volume roads were taken as 40 MPa and 30 MPa respectively. The 90 days flexural strength is often used in design of rigid pavements and hence, projected flexural strength for 90 days was obtained by multiplying 28 days strength with a factor of 1.2 (i.e. $1.2 \cdot f_r$).

Table 7.1 Predicted Flexural strength and Modulus of Elasticity

Sl. No	Type of Mix	High volume roads (M ₄₀)			Low volume roads (M ₃₀)		
		Pred. Value of f _r (MPa)	90 day flexural strength (MPa)=1.2 *f _r	Pred. Value of E _c (MPa)	Pred. Value of f _r (MPa)	90 day flexural strength (MPa) =1.2*f _r	Pred. Value of E _c (MPa)
1	R	4.43	5.32	31623	3.83	4.60	27386
2	FS1	4.44	5.33	32495	3.85	4.62	28142
3	FS2	4.64	5.57	34818	4.01	4.81	30154
4	FS3	4.48	5.38	31799	3.88	4.66	27539
5	FS4	4.68	5.62	34072	4.05	4.86	29508

parametrs used(IRC 58:2002):

1. Tyre pressure 0.8N/mm²
2. Modulus of subgrade reaction 0.1N/mm³
3. Poisson's ratio -0.15
4. Coefficient of thermal expansion of concrete 1.0x 10⁻⁶/°C
5. Allowance for additional stress due to nonlinear temperature profile 10%
6. Length of slab (L) for High volume road 4.50 m
Low volume road 3.75 m

Tables 7.2 and 7.3 give the axle load spectrum used in this study for high volume and low volume roads respectively.

Table 7.2 The axle load spectrum for high volume road (IRC 58-2002)

Single Axle load		Tandem Axle load	
Axle load class, tonnes	Percentage of axle loads	Axle load class, tonnes	Percentage of axle loads
19-21	0.6	34-38	0.3
17-19	1.5	30-34	0.3
15-17	4.8	26-30	0.6
13-15	10.8	22-26	1.8
11-13	22.0	18-22	1.5
9-11	23.3	14-18	0.5
Less than 9	30.0	Less than 14	2.0

Table 7.3 The axle load spectrum for Low volume road

Single axle load (tonnes)	Percentage of axle loads
13 – 15	1
11 – 13	4
09- 11	45
07 – 09	50

7.3 FATIGUE MODELS USED

The fatigue model proposed in section 4.7(Equation 4.26) was used. For comparison of design thickness, IRC fatigue model (IRC 58: 2002) was used.

Proposed Fatigue model

For $SR > 0.60$

$\text{Log } N = 17.866 - 18.02 * SR$

For $SR \leq 0.60$

$N = \text{unlimited}$

IRC Fatigue Model

For $SR \geq 0.55$

$$\text{Log } N = 11.737 - 12.077 \text{ SR}$$

For $0.45 < SR < 0.55$

$$N = \left[\frac{4.2577}{SR - 0.4325} \right]^{3.268}$$

For $SR \leq 0.45$

N = unlimited

7.4 DESIGN THICKNESS

Pavement thickness calculated using fatigue model recommended by IRC and the proposed fatigue model. The reference concrete and the steel fiber fly ash concretes were considered in this study. IITRIGID, a software was used to calculate the maximum load stress for each axle load. The fatigue life consumed (fatigue damage) during design life of the pavement under each load was calculated based on the relation between stress ratio and the number of repetitions. As per Minor's hypothesis, the accumulated damage due to each load (cumulative fatigue life consumed) was limited to unity. Table 7.4 gives the calculated thickness of pavement for different types of concrete based on proposed and IRC fatigue models. Specific design calculations are given in Appendix IV.

Table 7.4 Calculated thickness of pavement for reference and steel fiber fly ash concrete

Type of concrete	Calculated thickness of pavement in mm					
	High volume Roads			Low volume Roads		
	IRC Model	Proposed Fatigue model	% reduction in thickness	IRC Model	Proposed Fatigue model	% reduction in thickness
REF	300	250	16.7	220	200	9.09
FS1	280	240	14.3	220	200	9.09
FS2	280	230	17.9	220	190	13.6
FS3	280	240	14.3	220	200	9.09
FS4	280	230	17.9	220	190	13.6

7.5 TEMPERATURE STRESSES

The recommended temperature differential for coastal areas bound by hills as per IRC 58(2002) for different thicknesses of slab is given in Table 7.5.

Table 7.5 Temperature Differential for coastal areas(IRC 58-2002)

Thickness (mm)	200mm	250mm	300mm
Temperature Differential (°C)	15.8	16.2	17.0

Table 7.6 shows the calculated thickness of pavement for different types of concrete based on combined load and temperature stresses. Specific design calculations are given in Appendix IV.

Table 7.6 Calculated thickness based on combined wheel load and temperature

Type of concrete	Calculated thickness of pavement in mm	
	High volume Roads	Low volume Roads
REF	280	240
FS1	280	235
FS2	270	230
FS3	275	235
FS4	270	230

7.6 DISCUSSIONS

From the design thickness calculation based on fatigue consideration (Table 7.14) it can be seen that there is a reduction of about 10 to 15% in pavement thickness required for both high and low volume roads when the proposed fatigue model was used. When steel fiber reinforced fly ash concrete (FS4) was considered in place of normal concrete, a reduction of 20mm in thickness was observed. In the case of high volume roads, the

pavement thickness governed by fatigue approach when IRC model was used, whereas combined load and temperature stresses governs the design thickness in the case of proposed fatigue model. In the case of low volume roads, the thickness required based on combined load and temperature stress was higher than that required for fatigue. However, it is observed that the thickness required for steel fiber reinforced fly ash concrete is less compared to the normal concrete.

7.7 SUMMARY

The design thickness of the pavement calculated using the IRC fatigue model and the proposed fatigue model were discussed in this chapter. The required thickness for a given load spectrum is marginally reduced when the proposed model is used. The total stress due to the combined effect of edge loading and the temperature stresses were also used to finalize the thickness. In most of the cases it has been shown that the combined stress was critical than the fatigue strength in deciding the design thickness. Use of steel fiber reinforced fly ash concrete for pavement tends to reduce marginally the thickness but the fatigue life is longer.

CHAPTER 8

CONCLUSIONS

A detailed experimental study was conducted to utilize fly ash and steel fibers in concrete for eco-friendly rigid pavements. Different tests were conducted to investigate strength characteristics of various mixes. Repeated load test to predict fatigue life, temperature across the slab thickness to evaluate thermal stresses and slab load test to know the load deformation characteristics of fly ash-steel fiber slabs were also conducted. The major conclusions drawn are as follows.

Material characterization and Design of mixes

The use of graded aggregates of size 31.5mm and down in preparation of steel fiber reinforced concrete with and without fly ash was found satisfactory. Also, the use of mixed steel fibers (long and short) was found to be effective in enhancing the strength properties of concrete. Hence, **large sized aggregates can be effectively used with mixed steel fibers.**

Effect of fly ash and steel fibers on strength characteristics

The use of fly ash as partial replacement in two percentages viz. 20% and 40% in concrete with and without mixed steel fibers (0.5% and 1%) was investigated. With the increase in the fly ash content in concrete, the compressive strength tended to decrease. Compared to the reference concrete, the reduction in 28 day compressive strength of 4% and 11% for M₄₀ and M₃₀ mixes respectively was observed when 40 % fly ash was used. The reduction in flexural strength and split tensile strength for 40% fly ash concrete was about 6%. The use of 1% steel fibers in conventional concrete increased the compressive strength by 18%, flexural strength by 13% and split tensile strength by 10%. When 40% of cement was replaced by fly ash in steel fibre reinforced concrete (1% volume fraction), the strength properties of that concrete were reduced by marginal value, but recorded an increase of 10% all the strength properties in comparison with the reference concrete. The 28 day compressive strength of 20% fly ash with 1% of steel fibers was marginally higher than that of conventional concrete. Further, this improvement continued with further curing of 90 days. **The addition of fly ash and steel fibers together in conventional concrete improves the strength properties and, hence, it can be used for cost effective, eco-friendly pavements.**

Fatigue strength of Concrete

The use of steel fibers (1%) enhances the flexural fatigue performance of concrete and, hence, it can sustain more repetitions compared to conventional concrete under similar loading conditions. The fatigue performance of steel fiber reinforced fly ash concrete (FS4) was also found to be similar to that of steel fiber concrete and better than the reference concrete. **The use of 40% fly ash with 1% steel fiber can sustain more load repetitions as well as higher load stresses than the plain concrete.**

A new fatigue model based on S-N diagram, $\text{Log } N = 17.866 - 18.02 * SR$ was suggested for the pavement design, where N- number of cycle to failure and SR= stress ratio.

Effect of Temperature profile

The temperature distribution within the slab depends on the thermal characteristics of the material. As the air temperature increased around the slab, the slab temperature also increased by absorbing the thermal energy. The hourly variation of temperature at different depths followed a sinusoidal variation. The slope of temperature profile at upper half of the slab thickness was more than that at the bottom half. This shows that the thermal diffusivity in concrete is very small. **The thermal absorption characteristics were found to have unchanged by the addition of fly ash to the conventional concrete.** The temperature profile across the thickness was found to be nonlinear and a third degree polynomial curve fitted well to the recorded temperature data. Regression coefficients of third degree polynomial curve were used to calculate the thermal stresses. The resulting stress was found to be 10-30% higher than that obtained using the conventional linear temperature gradient assumption.

Load Deformation Characteristics

A Slab load test was carried out to study the behaviour of steel fiber reinforced fly ash concrete slab under a single wheel load. The load versus strain relationship under central and edge loading for reference concrete and steel fiber fly ash concrete showed a linear variation even up to the pressure of 2.5MPa, which is much beyond the conventional tyre inflation pressure of 0.8MPa. This indicated that the slab material is within the elastic limits under the normal loading. Hence, **well established Westergaad's equation or prevailing modified IRC equations also holds good for calculation of load stresses in design of steel fiber fly ash concrete pavements.** The slope of load-strain equation was found to be higher in case of steel fiber fly ash concrete with 1% steel fiber and 40% fly ash as cement replacement (FS4)

signifying higher modulus of elasticity. From the analytical study, the modulus of elasticity of fly ash steel fiber concrete was found to be close to 35000MPa. No significant effect of Poisson's ratio of concrete on load- strain characteristic was observed within the range 0.15 to 0.2 of concrete.

Developed Mathematical models

In the design of rigid pavement, the flexural strength and elastic modulus are the important parameters. Based on the experimental results of the research, the predictive models for the flexural strength and the elastic modulus were developed with characteristic compressive strength. Compressive strength was the only parameter needed, as most of the mix design procedures were based on this parameter. The new general fatigue model was suggested as a result of this research. Based on the new fatigue model and modified IRC equations for combined load and temperature stresses, the pavement design was carried out to ascertain the thickness. **The results show that the use of steel fiber fly ash concrete requires less thickness as compared to normal concrete.**

8.1 SCOPE FOR FURTHER STUDY

- Only 20% and 40% of fly ash were considered in this investigation. Further study can be continued by establishing optimum quantity of fly ash and optimum amount of steel fibers.
- Hybrid mixture of steel fibers consisting of different types of fibers with varied percentages can be used for the investigation.
- The fatigue behaviour of FA-SFRC can be studied under compound loading.
- Fatigue study along with temperature cycles can be carried out.
- Temperature study can be extended for the whole season to establish temperature profile and moisture gradient.

REFERENCES

ACI 544.1R-96 (1996) “ Report on Fiber Reinforced Concrete” American Concrete Institute, Farmington Hills.

ACI 544.2R-89(1989) “Measurement of Properties of Fiber Reinforced Concrete” American Concrete Institute, Farmington Hills.

ACI 544.3R-93(1993) “Guide for Specifying, Proportioning, Mixing, Placing, and Finishing Steel Fiber Reinforced Concrete.” ACI Mat. Journal ,V.90, No.1, 94-101.

ACI 544.4R-88 (1988) “Design Considerations for Steel Fiber Reinforced Concrete.” American Concrete Institute, Farmington Hills.

ACI Committee 318(2008) “Building Code Requirements for Structural Concrete” (ACI 318M-08), American Concrete Institute, Farmington Hills, Michigan,

Australian Standard AS3582.1(1998) “Supplementary Cementitious Materials for Use With Portland and Blended Cement – Part 1: Fly Ash”, ISBN 0 7337 1688 1, Standards Australia international.

Adkins, D. F. and Merkley, G.P. (1990) “Mathematical Model of Temperature Changes in Concrete Pavements”, Journal of Transportation Engineering, V. 116, No. 3, 349-358

Agarawal, R., Singh, A. K. and Singhal, D. (1996) “Effect of fiber reinforcing index on compressive strength and bond strength of steel fiber reinforced concrete”, Institute of Engineers(India) No.77(1), 37-40

Ahmad, I., Rahman, M. H., Seraj, S. M. and Hoque, A. M. (1998). “Performance of plain concrete runway pavement.” J. Perform. Construction .Facilities., 12(3), 145–157.

Ahmaruzzaman, M. (2010) “A review on the utilization of fly ash”, Progress in Energy and Combustion Science (36(3) June, pp327-363

Alliche, A. and Francois, D. (1992) “Damage of Concrete in Fatigue”, Journal of Engineering Mechanics, V.118, No. 11, 2176- 2190

Armaghani, J. M., Dempsey, B. J., Hill, H. and Vogel, J. (1987) “Temperature Response of Concrete Pavements.” Transportation Research Record 1121, Transportation Research Board, National Research Council, Washington D.C., 23–33.

Atis, C. D. (2003) “High volume fly ash concrete with high strength and low drying shrinkage”, *J. Mater. Civ. Eng.*, 15(12),153-156

Atis, C. D. and Karahan, O. (2009) “Properties of steel fiber reinforced fly ash concrete”, *Construction and Building Materials*” V. 23, No.1, 392-399

Barenberg, E. J. and Zollinger, D. G. (1990). “Validation of concrete pavement responses using instrumented pavements” *Transportation Research Record 1286*, Transportation Research Board, National Research Council, Washington D.C., 67–77.

Bayasi, M. Z. and Soroushian, P. (1992) “Effect of steel fiber reinforcement on fresh mix properties of concrete”.*ACI Materials Journal*, V.89 no.5, 369–374.

Bayasi, M. Z. and Kaiser, H.(2001) “Steel Fibers as Crack Arresters in Concrete”, *Indian Concrete Journal*, V.75, No.3, 215-219

Berndt, M. L.(2009) “Properties of sustainable concrete containing fly ash, slag and recycled aggregate”,*Construction and building materials*,No.23,2606-2613

Bhattacharya (2005) “Scope of Concrete Roads in India” the Keynote address at National Workshop on Sustainability of Road Infrastructure-Scope of Concrete Roads jointly organized by CMA India and ICI, Kolkata, Sept, 2005

Bilodeau, A., Sivasundaram, V., Painter, K. E. and Malhotra, V. M. (1994) “Durability of concrete incorporating high volume fly ash from sources in US”, *ACI Mat. Journal*, V.91 No.1, 3 -12

Binodkumar, Tike, G. K. and Nanda, P. K.(2007) “ Evaluation of Properties of High volume fly ash concrete for pavements”, *J. Mater. Civ. Eng.*, 19(10), 906-911

Bishoff, P. (2003) “Tension Stiffening and Cracking of Steel Fiber-Reinforced Concrete.” *J. Mater. Civ. Eng.*, 15(2), 174–182

Bouzoubaa, N., Zhang, M.H., Bilodeau,A. and Malhotra,V.M.(1998) “ Laboratory produced high-volume fly ash blended cements: physical properties and compressive strength of mortars”,*Cement and Concrete Research*,28(11), 1555-1569

Brill, D. R. and Parsons, I. D. (2001) “Three-Dimensional Finite Element Analysis in Airport Pavement Design”, *Int. Journal of Geomechanics*, V.1, No. 3, 273–290

CAC (2012), <http://www.transportation.alberta.ca/content/doctype57/Production/Pavement-Fuel.pdf>, Cement Association of Canada, last accessed Sept 2012

CMA (2007) “Fuel saving on Concrete Pavement” <http://www.cmaindia.org>, Cement Manufacturers Association India, last accessed July 2007

CPAM (2012), <http://www.concreteisbetter.com/vs.html>, Concrete Paving Association of Minnesota, last accessed Sept 2012

Chakravarthy, S.M., and Kadiyali, L.R. (1989), “Economics of Concrete Roads” Indian Concrete Journal, 63, 239-243

Chanvillard, G. and Pierre-Claude, A. (1996) “Pull out Behavior of corrugated Steel Fibers qualitative and Statistical results”, Advanced cement based Material, V4, 28-41

Choubane, B., and Tia, M. (1992). “Nonlinear temperature gradient effect on maximum warping stresses in rigid pavements”, Transportation Research Record 1370, Transportation Research Board, Washington, D. C., 11–19

Choubane, B. and Tia, M. (1995) “Analysis And Verification of Thermal gradient Effects on Concrete Pavement”, Journal of Transportation Engineering, V.121, No.1. 75-81

Darter, M. I. (1988) A Comparison Between Corps of Engineers and ERES Consultants, Inc. Rigid Pavement Design Procedures. Technical Report Prepared for the United States Air Force SAC Command. Savoy, IL.

Darter, M. I. and Barenberg, E.S. (1977) Design of Zero Maintenance Plain Jointed Concrete Pavement, Report No. FHWA-RD-77-111 Vol 1, Federal Highway Administration.

Davids, W. G. (2003) EverFE Theory Manual, University of Maine, Civil Engineering Department, Orono, Main, USA. Available from Internet: <http://www.civil.umaine.edu/EverFE/>.

Dayal, U., Sinha, R., and Kumar, V. (1999) “Fly ash Disposal and Deposition: Beyond 2000 A.D” Proceedings of the National Conference on "Fly ash Disposal and Deposition: Beyond 2000 A.D", IIT Kanpur

Desai, J. P. (2004) “Construction of HVFA Concrete Pavements in India: Four Case studies”, Indian Concrete Journal, V. 78, No.11, 58-66

FHWA (2012), <http://www.fhwa.dot.gov/infrastructure/materialsgrp/flyash.htm> last accessed Sept 2012

Faraggi, V., Jofre, C. and Kraemer, C. (1987). "Combined effect of traffic loads and thermal gradient on concrete pavement design." Transportation Research Record 1136, Transportation Research Board, National Research Council, Washington D.C., 108–118.

Ferrara, L. and Meda, A.(2006), "Relationships between fibre distribution, workability and the mechanical properties of SFRC applied to precast roof elements", Materials and Structures, 39, 411–420.

Foxworthy, P. T.(1985) Concepts for the Development of a Nondestructive Testing and Evaluation System for Rigid Airfield Pavements. Ph. D. Dissertation, University of Illinois, Urbana, IL.

Fwa, T. F., Shi. X. P. and Tan. S. A.(1996) "Use of Pasternak Foundation Model in Concrete Pavement Analysis", J. Transp. Eng, V.122, No.4, 323-328

Gao, J., Sun, W., and Morino, K.(1997), "Mechanical properties of steel fiber-reinforced, high-strength, lightweight concrete, Cement and Concrete Composites, 19(4), 307–313 [http://dx.doi.org/10.1016/S0958-9465\(97\)00023-1](http://dx.doi.org/10.1016/S0958-9465(97)00023-1),

Gebler, S.H. and Klieger (1986) "Effect of fly ash on physical properties of concrete" Fly ash, Silica fume, Slag and Natural Pozzolanas in Concrete, Vol 1, Ed. V M Malhotra ACI SP-91, 1-50(Michigan).

Gencil, O., Ozel, C., Brostow, W. and Martı́nez-Barrera, G. (2011) "Mechanical properties of self-compacting concrete reinforced with polypropylene fibres" Materials Research Innovations, 15(3) ,216-225

Ghosh, S., Battacharya, C. and Ray, S.P.(1989) "Tensile strength of Steel fiber Reinforced Concrete", Institute of Engineers (India) , 69(1), 222-227

Hiller, J.E. and Reosler, J.R.(2010), "Simplified Nonlinear Temperature Curling Analysis for Jointed Concrete Pavements", Journal of Transportation Engineering(ASCE), 136(7) 654-663

Harik, I. E., Jianping, P., Southgate, H. and Allen, D.(1994) "Temperature effect on rigid pavements". Journal of Transportation Engineering, 120(1), 127-143

Hsu, T. C. C.(1981), "Fatigue of plain concrete", ACI Mat. Journal, V. 78, No.4, 292-305

Hudson, W. R. and Flanagan, P. R.(1987). “An examination of environmental versus load effects on pavements.” Transportation Research Record 1121, Transportation Research Board, National Research Council, Washington D.C., 34–39.

Ioannides, A. M. and Khazanovich, L.(1998), “Nonlinear Temperature Effects on Multilayered Concrete Pavements”, J of Trans Engineering, V. 124, No. 2, 128-136

Janssen, D. J. and Snyder,.M.B. (2000) “Temperature-Moment Concept for Evaluating Pavement Temperature Data”, Journal of Infrastructure Systems, V. 6, No. 2, 81-83

Jerath, S. and Hanson, N. (2007) “Effect of fly ash content and aggregate gradation on the durability of concrete pavements”, J. Mat. in Civil Engg, V.19, No. 5,367-375

Jiang, L. H. and Malhotra, V. M. (2000) “Reduction of water demand of non air entrained concrete incorporating large volumes of fly ash”, Cement and Concrete Research,30(11) 1785-1789

Johnston, C. D. and Zemp, R.W.(1991) “Flexural Fatigue Performance of Steel Fiber Reinforced Concrete – Influence of Fiber Content, Aspect Ratio and Type”, ACI Material Journal , V.88, No. 4, 374-383

Joshi,Y.P., Dhang, N. and Pandey, B.B.(2004) “Probability Analysis of Fatigue of Paving Concrete” IE(I) Journal-V 85, 163-168

Kang, S. and Kim, J. (2012) “Investigation on the flexural behavior of UHPCC considering the effect of fiber orientation distribution, Construction and Building Materials, V. 28, No.1, 57-65, doi:10.1016/j.conbuildmat.2011.07.003

Khazanovich,L.(2003) Finite Element Analysis of Curling of Slabs on Pasternak Foundation, 16th ASCE Engineering Mechanics Conference, University of Washington, Seattle.

Kuo, C.M. (1998) “Effect of Temperature differential in Concrete Pavements”, Journal of Transportation Engineering, V.124 No.2, 112-116

Kuo, C.M. and Haung, C.W.(2006) “Three-Dimensional Pavement Analysis with Nonlinear Subgrade Materials”, J. Mat. in Civil Engineering, V. 18, No. 4, 537-545

Lee, M. K and Barr, B.I.G (2004) “An Overview of the fatigue behaviour of plain and fiber reinforced concrete”, Cement and Concrete Composites 26(2004) pp 299-305

Li, H., Zhang, M. and Ou, J. (2006) "Flexural Fatigue Performance of Concrete Containing Nano-particles for Pavement", International Journal of Fatigue/doi:10.1016/j.ijfatgue.2006.10.004

Liu.W., and Fwa.T.F.(2003), "Effects of Nonlinear temperature Distribution on Thermal Stresses in Concrete Pavements", Journal of Eastern Asia Society for Transportation Studies, Vol 5, October pp1023-1034.

Lok, T. S., and Pei. J. S.(1998) Flexural Behavior of Steel Fiber Reinforced Concrete. Journal of Materials in Civil Engineering, Vol. 10, No. 2, 1998, pp. 86–97

Mahboub, K., Liu, Y. and Allen, D. L. (2004) "Evaluation of Temperature Responses in Concrete Pavements", Journal of Transportation Engineering, V.130,No.3 395-401

Malek, R. I., Khalil, Z. H., Imbaby, S. S. and Roy, D.M. (2005) "The contribution of Class F fly ash to the Strength of Cementitious Mixtures", Cement and Concrete Research , 35(6) 1152-1154

Mangaraj, B. K. and Kishnamoorthy, S.(1994) "Use of Pond Ash as Part Replacement for Mortar and Concrete", Indian Concrete Journal V. 68, No.5, 279-282

Masad, E., Taha, R., and Muhunthan, B. (1996) "Finite element analysis of temperature effects on plain-jointed concrete pavements." J. Transp. Eng., 122(5), 388–398.

Mehta, P.K. (1997) "Concrete - Microstructure, Properties and Materials" Indian Concrete Institute, Chennai

Miner, M. A.(1945) Cumulative Damage in Fatigue. Transactions, American Society of Mechanical Engineer, Vol. 67, pp. A159–A164.

Mohamed, A.R. and Hansen .W. (1996) "Prediction of Stresses in Concrete Pavements Subjected to Non-linear Gradients", Cement and Concrete Composites, No. 18, 381-387

Mohammad, A. A. (2000) "Methods for Estimating the Parameters of the Weibull Distribution" <http://interstat.statjournals.net/YEAR/2000/articles/0010001.pdf>

Mohammadi, Y. and Kaushik, S. K.(2005), "Flexural Fatigue Life Distributions of Plain and Fibrous Concrete at Various Stress Levels", J. Mat. in Civil Eng. V.17, No.6 , 650-658

Mohammed, A. E., Millard, S.G., and Barnett, S.J. (2009) “Strength development of concrete containing coal fly ash under different curing temperature conditions” World of Coal ash (WOAC) Conference, Lexington, KY, USA (<http://www.flyash.info/>)

MORTH 2012a: [www.morth.nic.in/Annual Report 2011-12](http://www.morth.nic.in/Annual%20Report%202011-12) last accessed Sept 2012

MORTH 2012b: [www.morth.nic.in/writereaddata/mainlinkFile/Passenger and freight Trafficdata.pdf](http://www.morth.nic.in/writereaddata/mainlinkFile/Passenger%20and%20freight%20Trafficdata.pdf), last accessed Sept 2012

MORTH 2012c: www.morth.nic.in/writereaddata/mainlinkFile/File420.pdf, last accessed Sept 2012

Mullick, A. K. (2005a) “Use of Fly Ash in Structural Concrete Part I: Why?”, Indian Concrete Journal V. 79, No.5, 13-22

Mullick, A. K. (2005b) “Use of Fly Ash in Structural Concrete Part II: How Much?”, Indian Concrete Journal, V. 79, No.6, 10-14

Murthy, D.S.R.(2003) “Introduction to Fatigue and Fracture”- Advanced course on Fatigue and Fracture Behaviour of Components and Structures, Allied Publishers Private Limited, Chennai

Murthy, S. R. and Ramesh, K.V.(2005) “ Flexural response of RC beams of HVFA concrete”, Indian Concrete Journal, 79(5), 47-53

Naaman, E. (2003) “Engineered Steel Fiber with Optimal Properties for Reinforcement of Cement Composite” Journal of Advanced Concrete Technology, 1(3), 241-252

Naaman, A.E. and Husamuddin, N. (1991) “Bond Slip Mechanisms of Steel Fibres in Concrete”, ACI Materials Journal V. 88 No.2, March-April 1991, pp135-145

Naik, T. R.(2008) “Sustainability of Concrete” Construction Practice Periodical on Structural Design and Construction, ASCE, 98-103

Naik, T. R., Singh, S. S. and Hossain, M. M. (1995) ‘Abrasion resistance of high-strength concrete made with class C fly ash’, ACI Mater. J., 92, (6), 649–659

Naik, T. R., Singh, S. S. and Ramme, B. W.(2002) “Effect of source of fly ash on abrasion resistance concrete”, J. Mat. in Civil Eng. V. 14, No. 5, 417-426

- Nataraj, M.C., Dhang N., and Guptha, A.P. (1999) "Stress-Strain curves for steel fiber reinforced concrete under compression", *Cement Concrete Composites*, 21, 383-390
- Neito, A. J., Chicharro, J. M. and Pintado, P. (2006) "An approximated methodology for fatigue tests and fatigue monitoring of concrete specimens", *International Journal of Fatigue*, 28, 835-842
- Neocleous, K Tlemat, H. and Pilakoutas, K. (2006) "Design issues for concrete reinforced with steel fibers, including fibers recovered from used tires" *Journal of Materials in Civil Engineering*, 18 (5), pp. 677-685
- Neville, A.M (1995) "Properties of Concrete", Fourth Edition, Pearson Education Inc, p335-342, 378, 412-421,654-660
- Obla, K.H., Hill,R.L., Thas, M.D.A., Shashiprakash, S.G. and Perebatova,O.(2003) "Properties of concrete containing Ultra-fine fly ash, *ACI Mater. J* 100(5), 426-433
- Oh, B.H (1986) "Fatigue Analysis of Plain Concrete in Flexure", *Journal of Structural Engineering*, ASCE ,Vol. 112, No. 2, 273-288
- Oh, B. H. (1991a) "Cumulative damage theory of concrete for various stress levels", *ACI materials Journal*, V. 88 No.2,122-127
- Oh, B.H. (1991b) "Fatigue life Distribution of concrete under variable amplitude fatigue loadings", *ACI materials Journal*, V. 88 No.1, 41-48
- Ozyildirim, C., Woodrow, J. and Halstead (1994) "Improved Concrete Quality with Combinations of Fly Ash and Silica Fume", *ACI Materials Journal* V. 91, No.6, 587-594
- Packard, R. G. and S. D. Tayabji.(1983) *Mechanistic Design of Concrete Pavements to Control Joint Faulting and Subbase Erosion. International Seminar on Drainage and Erodability at the Concrete Slab-Subbase-Shoulder Interfaces. Paris, France*
- Park, D.W.(2008) "Prediction of Pavement Fatigue and rutting Life using Different Tire types", *KSCE Journal of Civil Engineering*,12(5), 297-303
- Pattanaik, S. C. and Sabat, A.K. (2010) "A Study of Nalco Fly Ash on Compressive Strength for Effective Use in High Volume Mass Concrete for a Sustainable Development" *International Conference on Sustainable Technologies for Concrete Constructions*" ACI, 2010

Phull, Y.R. and Rao. J.P. (2007) “Assuring Adequacy of Concrete Pavements: Some Essential Needs”, Indian Highways, No.3, 9-19

Planning Commission Report (2011a), Power and Energy http://Planningcommission.nic.in/reports/genrep/arep_seb11_12.pdf, last accessed Sept 2012

Planning Commission Report (2011b) Road Transport http://Planningcommission.nic.in/aboutus/committee/wrkgrp11/wg11_roadtpt.doc, last accessed Jan 2012

Poblete, M., Salsilli, R., Valenzuela, A., and Spratz, P.(1987) “Field Evaluation of Thermal Deformations in Undoweled PCC Pavement Slabs”. Transportation Research Record 1207, TRB, National Research Council, Washington, D.C., 217–228.

Puttappa, C.G., Muthu, K.U., and Veeraragavan A(2004), Comparative Study of Flexural Fatigue Analysis of HPC, National Sememar on Developments in Materials & Structures, NIT, Calicut

Radhakrishna, RenukaDevi, M.V. and Udayashankar, B.C.(2009) “Use of Fly Ash in Construction Industries for Sustainable Development”, Journal of Environmental Research And Development Vol. 3 No. 4, April-June, 1211-1222

Ramli, M. and Dawood, E.T. (2011) “Effect of steel fibre on the Engineering Performance of Concrete” Asian Journal of Applied Sciences, 4(1), 97-100

Ravishankar, A.U., Venkatakrishna, H.V. and Suresha,S.N. (2006)” Mix design Aspects of Steel fiber reinforced concrete(SFRC) in pavement design, Indian Highways, 34(5),43-50

Rao, S., Roesler, J. R.(2005). Characterizing effective built in curling from concrete pavement field measurements, Journal of Transportation Engineering ASCE 131(4): 320-327. doi:10.1061/(ASCE)0733-947X(2005) 131:4(320)

Rao, S., and Roesler, J. R (2008) - cumulative fatigue damage analysis of concrete pavement using accelerated pavement testing results http://www.mrr.dot.state.mn.us/research/mnroad_project/index_files/pdfs/rao_s.pdf last accessed Sept 2008

Ramadhan, H. and Wahaab, H. I.(1997) “Temperature Variation of Flexible and Rigid Pavements in Eastern Saudi Arabia” Building and Environment, V. 32, No. 4, 367-373

Ramakrishnan, V., Brandshaug, T., Coyle, W. and Schrader, E.K.(1980) “A comparative evaluation of concrete reinforced with straight fibers and fibers with deformed ends glued together into bundles”. ACI Journal, 77(3),135–143.

Reddy, P. M., Veeraraghavan,.A, (2010) “ A Low Cost Equipment for accelerated Testing of Pavement Materials”, Conference on Trends and Advances in Transportation Engineering, Association of Bangalore University Highway Engineering Alumni, Bangalore, 71-77.

Roesler, J. R., Hiller, J.E. and Littleton, P.C.(2005) “Large-Scale Airfield Concrete Slab Fatigue” Journal of concrete pavement V. 1 No.1 ,66-87

Roylance, D (2001) “Fatigue” <http://ocw.mit.edu/courses/materials-science-and-engineering/3-11-mechanics-of-materials-fall-1999/modules/fatigue.pdf>

Russi, P. (1994) “Steel Fiber Reinforced Concrete – An Example of French Research”, ACI Material journal V. 91 No.3 273-279

Sakin, R. and Ay, I. (2008), “Statistical analysis of bending fatigue life data using Weibull distribution in gala-fiber reinforced polyester composites”, Materials and Design 29,1170-1181

Shannag, M. J., Brincker,R. and Hansen,W.(1997)” Pull out Behavior of Steel Fibers from Cement based Composite”, Cement and Concrete Research, 27, 925-966

Sharma, B. M., Sitaramanjanyalu, K., and Kanchan, P. K. (1995) “Effect of vehicle axle loads on pavement performance”, Road Transport Technology-4, University of Michigan Transportation Research Institute, Ann Arbor, 263-272

Shi,X. P., Fwa,T.F. and Tan,S.A.(1993) “Warping Stresses in Concrete Pavements on Pasternak Foundation”, J. Trans. Eng., V.119, No.6, 905-913

Siddique, R.(2003) “Effect of Fine Aggregate Replacement with Class F Fly ash on the Mechanical Properties of Concrete” , Cement and concrete research , 33, 539-547

Siddique R.(2004) Properties of concrete incorporating high volumes of class f fly ash and san fibres, Cement and Concrete Research, 34(1) p. 37-42.

Singh, S.P. and Kaushik, S.K.(2000), “Flexural Fatigue Life Distributions and Failure Probability of Steel Fibrous Concrete”, ACI Material Journal , V.97,No. 6, 658-667

Singh, S.P. and Kaushik, S.K. (2001), “Flexural Fatigue Analysis of Steel Fiber Reinforced Concrete”, ACI Material Journal , V.98,No. 4, 306-312

Singh, S.P. and Kaushik, S.K. (2003), “Fatigue strength of steel fiber reinforced concrete in flexure”, *Cement and Concrete Composites* 25, 779-786

Sorelli, L. G., Meda A., and Plizzari, G. A. (2005), “Bending and Uniaxial Tensile Tests on Concrete Reinforced with Hybrid Steel Fibers”, *Journal of Material in Civil Engineering*, 17(5), pp.519-527

Soroushian, P. and Bayasi, Z. (1991) “Fiber Type Effects on the Performance of Steel Fiber Reinforced Concrete”, *ACI Materials Journal* V. 88 No.2, 129-134

Soulioti, D. V., Barkoula, N. M., Paipetis, A. and Matikas, T. E. (2011) “Effects of Fibre Geometry and Volume Fraction on the Flexural Behaviour of Steel-Fibre Reinforced Concrete”, *Strain* , V47, S1, e535–e541

Srinivasan, P., Tiwari, A.K. and Branchhor, A.(2004) “Suitability of HVFA concrete for pavements” *Indian Concrete Journal*, 78(11) 58-61

Stroeven, P.(2009) “Stereological Principles of Spatial Modeling Applied to Steel Fiber-Reinforced Concrete in Tension”, *ACI Material Journal*, V. 106 (3), 213-223

Sun, W., Gao, J. and Morino,K. (1997) “Mechanical Properties of steel fiber Reinforced high strength Light weight Concrete”, *Cement and Concrete Composites*, No.19, 307-313

Tang, T., Zollinger. D.G. and Senadheera. S.(1993). “Analysis of Concave Curling in Concrete Slabs”. *Journal of Transportation Engineering*, V.119.No. 4, 618–632.

Thomas, J. and Ramaswamy, A.,(2007), “Mechanical Properties of steel fiber Reinforced Concrete” *Journal of Materials in Civil Engineering* Vol 19. No.5, 385-392

Thompson, M.R., Denpsy, B.J., Hill, H. and Vogel, J.(1987) “Characterizing temperature effects for pavement analysis and design” *Trans Res Records*, 1121, 14-21

Topçu, İ. B., and Canbaz, M. (2007) “Effect of different fibers on the mechanical properties of concrete containing fly ash”, *Construction and Building Materials* Vol 21,issue 7, pp1486–1491

Tripathy, P.S. and Mukherjee.S.N. (1997) “Perspectives on bulk use of fly ash”, *Allied Publishers Limited* , New Delhi.

Williamson G R (1974), The Effect of Steel Fibers on the Compressive Strength of Concrete, ACI Special Publication,44, 195-208

Yazıcı, S., Inan, G. and Tabak, V. (2007) “Effect of aspect ratio and volume fraction of steel fiber on the mechanical properties of SFRC”, Construct Build Mater 21(6):1250–1253

Yijin, L., Shiqiong, Z., Jian, Y. and Yingli, G.(2003) The Effect of Fly Ash on the Fluidity of Cement Paste, Mortar, and Concrete, International Workshop on Sustainable Development and Concrete Technology, 339-345

Yoder, E.J. and Witczak, M.W. (1975), Principles of pavement design, Second edition, John Wiley and Sons, New York.

Zhang, J., Fwa, T. F., Tan, K. H. and Shi, X. P.(2003) “ Model for Nonlinear Thermal Effect on Pavement Warping Stresses” Journal of Transportation Engineering, V. 129, No. 6, 695-702

Zhang, J. and Stang, H.(1998) “Fatigue Performance in Flexure of Fiber Reinforced Concrete”, ACI Material Journal , V.95, No.1, 58-67

Zhang, J., Stang, H. and Li, V.C. (1999), “Fatigue life prediction of fiber reinforced concrete under flexural load”, International Journal of Fatigue 21, 1033-1049

IRC:44-2008 Tentative guideline for cement concrete mix design for pavements, Indian Roads Congress, New Delhi

IRC:SP:46-1997 Steel Fibre Reinforced Concrete for Pavements, Indian Roads Congress, New Delhi

IRC:SP:62-2004 Guidelines for the Design and Construction of Cement Concrete Pavements for Rural Roads, Indian Roads Congress, New Delhi

IRC:58-2002 Guidelines for the Design of Plain Jointed Rigid Pavements for Highways, Indian Roads Congress, New Delhi

IRC:68-1976 Tentative Guidelines on Cement-Fly Ash Concrete for Rigid Pavement Construction, Indian Roads Congress, New Delhi

IS 3812:2003(Part I) Pulverized Fuel ash- Specification For use as pozzolana in cement, cement mortar and concrete, Bureau of Indian Standards New Delhi

IS 3812:2003(Part II) Pulverized Fuel ash-Specification for use as admixtures in cement mortar and concrete, Bureau of Indian Standards New Delhi

IS 383-1963 Specifications for Coarse and Fine aggregates from natural sources for concrete, Bureau of Indian Standards, New Delhi

IS 456-2000 Plain and reinforced concrete- code of practice, Bureau of Indian Standards, New Delhi

IS 516-1959 Methods of tests for strength of concrete, Bureau of Indian Standards New Delhi

IS 5816-1999 Splitting tensile strength of concrete- Method of test, Bureau of Indian Standards New Delhi

IS 8112-1989- 43 Grade Ordinary Portland Cement- Specification, Bureau of Indian Standards New Delhi

IS 10262(1982) Recommended Guidelines for Concrete Mix Design, Bureau of Indian Standards New Delhi

SP:23(1982), Handbook on Concrete Mixes (Based on IS Standards), Bureau of Indian Standards New Delhi

APPENDIX I

A- I Comparison of Weibull Parameters obtained by various methods

M_{30}			Graphical	Method of moments	AWB	Method of least squares	AVERAGE
REFERENCE	0.85	μ	284	266	277	277	276
		α	1.53	2.26	1.79	1.79	1.94
		SE	0.004287	0.005293	0.003271	0.003271	0.003706
	0.80	μ	3878	3729	3799	3789	3798
		α	1.91	2.47	2.23	2.23	2.21
		SE	0.001068	0.001866	0.001178	0.001178	0.000851
	0.75	μ	30193	28504	29520	29513	29433
		α	1.79	2.69	2.10	2.10	2.17
		SE	0.006401	0.006989	0.005208	0.005208	0.005124
	0.70	μ	69601	66674	72220	66861	68089
	α	2.05	2.84	2.60	2.51	2.5	
	SE	0.003777	0.005893	0.005708	0.004081	0.0038	
HS1 (SF 0.5%)	0.85	μ	322	308	315	315	315
		α	1.93	2.70	2.27	2.27	2.54
		SE	0.00268	0.00093	0.00107	0.00107	0.000701
	0.80	μ	4911	4699	4844	4843	4824
		α	1.82	2.46	2.11	2.12	2.13
		SE	0.004579	0.0062	0.00433	0.00434	0.00438
	0.75	μ	36816	33456	35630	35610	35378
		α	1.12	1.58	1.30	1.30	1.33
		SE	0.005678	0.00885	0.00563	0.00563	0.00579
	0.70	μ	68182	65986	66960	66948	67019
	α	2.08	2.62	2.421	2.43	2.39	
	SE	0.00184	0.00348	0.00251	0.00256	0.00238	
HS2 (SF 1%)	0.85	μ	308	299	303	305	304
		α	2.19	2.69	2.545	2.50	2.48
		SE	0.001718	0.001989	0.00141	0.00122	0.0013
	0.80	μ	5950	6034	5796	5795	5394
		α	1.49	1.90	1.74	1.74	1.72
		SE	0.0137	0.0180	0.0123	0.0123	0.0073
	0.75	μ	37130	34864	36330	36319	36160
		α	1.87	2.76	2.203	2.21	2.26
		SE	0.01339	0.0310	0.0196	0.0198	0.0208
	0.70	μ	62512	60349	61300	61289	61362
	α	1.97	2.45	2.30	2.30	2.26	
	SE	0.005292	0.00627	0.00511	0.00512	0.00512	

M_{30}			Graphical	Method of moments	AWB	Method of least squares	AVERAGE
FS1 (FA 20%, SF 0.5%)	0.85	μ	294	281	289	289	288
		α	2.33	3.61	2.75	2.75	2.86
		SE	0.010256	0.00938	0.00866	0.00866	0.00845
	0.80	μ	6850	6383	6658	6656	6637
		α	1.46	2.15	1.72	1.72	1.76
		SE	0.00466	0.00425	0.00329	0.00329	0.00321
	0.75	μ	32807	30502	31750	31936	31749
		α	1.26	1.57	1.47	1.52	1.46
		SE	0.00079	0.001	0.00057	0.00084	0.000531
	0.70	μ	77545	75551	82610	75121	79584
		α	2.61	3.49	3.11	3.20	3.1
		SE	0.00713	0.00106	0.00809	0.00041	0.000815
FS2 (FA 20%, SF 1.0%)	0.85	μ	330	318	324	324	324
		α	2.28	3.18	2.68	2.68	2.71
		SE	0.004705	0.00336	0.00327	0.00327	0.00321
	0.80	μ	5457	5326	5385	5384	5388
		α	3.1	4.14	3.53	3.53	3.55
		SE	0.003126	0.0011	0.00148	0.00148	0.00144
	0.75	μ	38897	37019	37950	37939	37951
		α	1.59	1.97	1.86	1.86	1.82
		SE	0.001405	0.00083	0.00084	0.00084	0.0008
	0.70	μ	93987	91446	92940	95385	93440
		α	1.598	1.73	1.84	1.53	1.67
		SE	0.0130	0.0121	0.0139	0.0171	0.0136
FS3 (FA 40%, SF 0.5%)	0.85	μ	995	910	1002	934	960
		α	1.36	1.86	1.741	1.67	1.64
		SE	0.000798	0.000858	0.000618	0.000145	0.000112
	0.80	μ	10014	9436	9724	9721	9724
		α	1.36	1.77	1.588	1.59	1.58
		SE	0.000657	0.000781	0.000117	0.000116	0.000104
	0.75	μ	46896	46138	46250	46243	46382
		α	2.85	3.55	3.336	3.34	3.27
		SE	0.001358	0.000513	0.000447	0.000445	0.000497
	0.70	μ	96201	98060	95280	95273	96203
		α	3.97	4.33	4.631	4.64	4.39
		SE	0.001565	0.001535	0.001571	0.001585	0.001663

M_{30}			Graphical	Method of moments	AWB	Method of least squares	AVERAGE
FS4(FA 40%, SF 1.0%)	0.85	μ	647	659	683	681	668
		α	1.31	1.39	1.269	1.27	1.31
		SE	0.00289	0.00367	0.00251	0.00250	0.00279
	0.80	μ	5990	5832	6136	6134	6023
		α	1.82	2.07	1.89	1.89	1.92
		SE	0.00088	0.00198	0.00086	0.00086	0.00101
	0.75	μ	46810	49021	48740	48769	48335
		α	3.12	3.37	3.085	3.11	3.17
		SE	0.00233	0.00281	0.00168	0.00174	0.00183
	0.70	μ	98180	100096	97260	97252	98197
		α	4.96	5.29	4.641	4.65	4.89
		SE	0.00348	0.00833	0.00184	0.00185	0.00324
M_{40}			Graphical	Method of moments	AWB	Method of least squares	AVERAGE
REFERENCE	0.85	μ	309	301	303	303	304
		α	1.38	1.47	1.56	1.56	1.49
		SE	0.00240	0.00183	0.00197	0.00197	0.00197
	0.80	μ	6206	6080	6234	6231	6188
		α	1.14	1.26	1.14	1.14	1.17
		SE	0.00771	0.0098	0.00774	0.00774	0.00815
	0.75	μ	56218	49275	57330	54016	54210
		α	1.11	2.16	4.06	1.32	2.16
		SE	0.0127	0.0078	0.0128	0.010	0.0047
	0.70	μ	93468	88435	91470	103058	94108
		α	1.9	3.14	2.24	1.87	2.29
		SE	0.0419	0.003	0.00284	0.0084	0.0027
HS1(SF 0.5%)	0.85	μ	490	457	486	475	477
		α	1.14	1.48	1.36	1.32	1.33
		SE	0.0053	0.0069	0.0062	0.0056	0.0057
	0.80	μ	8436	8761	8846	8840	8721
		α	1.1	1.20	1.02	1.02	1.09
		SE	0.00246	0.00349	0.00171	0.00171	0.0022
	0.75	μ	47258	46138	46620	46612	46657
		α	2.66	3.43	3.08	3.09	3.07
		SE	0.00393	0.00565	0.00422	0.00425	0.0042
	0.70	μ	96459	102945	96860	95364	97907
		α	3.48	5.58	4.87	4.06	4.49
		SE	0.013	0.0242	0.0079	0.0102	0.0098

M_{40}			Graphical	Method of moments	AWB	Method of least squares	AVERAGE
HS2 (SF 1%)	0.85	μ	681	666	714	672	683
		α	2.31	2.73	2.65	2.65	2.59
		SE	0.00365	0.00389	0.00759	0.00388	0.00429
	0.80	μ	9845	9500	9692	9691	9682
		α	2.52	2.66	2.95	2.96	2.77
		SE	0.00211	0.00193	0.0010	0.001	0.0011
	0.75	μ	60239	59590	59470	59462	59690
		α	3.21	3.65	3.77	3.78	3.85
		SE	0.0061	0.0048	0.00453	0.00451	0.00432
	0.70	μ	89107	83498	87100	87096	86700
		α	1.7	2.73	1.97	1.97	2.09
		SE	0.0078	0.00349	0.00545	0.00545	0.00466
FS1 (FA 20%, SF 0.5%)	0.85	μ	463	419	479	432	449
		α	1.06	1.37	1.22	1.26	1.23
		SE	0.015	0.010	0.018	0.011	0.013
	0.80	μ	8596	8032	8321	8317	8317
		α	1.11	1.48	1.29	1.29	1.29
		SE	0.0026	0.0037	0.0024	0.0024	0.0024
	0.75	μ	43879	39385	44930	40645	42210
		α	1.12	1.65	1.501	1.38	1.41
		SE	0.029	0.0021	0.0022	0.0015	0.0012
	0.70	μ	100947	101533	99930	99920	100582
		α	3.78	5.74	4.41	4.42	4.59
		SE	0.00181	0.0074	0.00183	0.00185	0.00225
FS2 (FA 20%, SF 1.0%)	0.85	μ	839	801	830	839	827
		α	1.18	1.64	1.42	1.38	1.41
		SE	0.00124	0.00206	0.0057	0.00047	0.00058
	0.80	μ	8006	7300	7705	7702	7678
		α	1.02	1.39	1.19	1.19	1.20
		SE	0.00148	0.00198	0.00085	0.00085	0.00086
	0.75	μ	48954	48874	48330	48326	48621
		α	2.92	3.6	3.99	3.40	3.48
		SE	0.00673	0.00904	0.0104	0.0071	0.0079
	0.70	μ	95199	97307	98590	94384	96370
		α	4.57	4.58	5.26	5.34	4.94
		SE	0.0032	0.0051	0.0093	0.0030	0.0044

M₄₀			Graphical	Method of moments	AWB	Method of least squares	AVERAGE
FS3(FA 40%, SF 0.5%)	0.85	μ	455	412	492	438	449
		α	1.05	1.6	1.21	1.24	1.28
		SE	0.00233	0.00275	0.00224	0.001	0.0008
	0.80	μ	4700	4314	4533	4531	4519
		α	1.11	1.7	1.297	1.3	1.35
		SE	0.00338	0.0045	0.0023	0.0023	0.0022
	0.75	μ	47711	52183	46800	46789	48371
		α	2.11	2.08	2.48	2.48	2.54
		SE	0.0045	0.0081	0.0034	0.0034	0.0037
FS4(FA 40%, SF 1.0%)	0.85	μ	869	671	840	679	765
		α	1.17	1.12	1.15	1.06	1.13
		SE	0.0117	0.0030	0.0096	0.0027	0.0056
	0.80	μ	8006	6725	7255	7254	7310
		α	1.02	2.27	1.69	1.69	1.67
		SE	0.0137	0.0046	0.0043	0.0043	0.0043
	0.75	μ	48954	48225	50870	50852	49725
		α	2.92	1.74	1.31	1.31	1.82
		SE	0.0186	0.0037	0.0023	0.0023	0.0038
ALL M₃₀& M₄₀	0.85	μ	442	478	530	461	478
		α	1.68	1.35	1.02	1.68	1.43
	0.80	μ	6460	6536	6534	6523	6513
		α	1.8	1.64	1.85	1.85	1.79
	0.75	μ	42460	43301	43270	43407	43110
		α	2.05	2.43	2.24	2.23	2.24
	0.70	μ	84752	87144	88100	86945	86735
		α	3.04	3.53	3.27	3.26	3.28

APPENDIX II

II-1 Recorded Average Temperature Data during April –May 2010

Slab of thickness 150mm		Reference Concrete										
		Temperature in °C										
Hours	0	1	2	3	4	5	6	7	8	9	10	11
Top	30.8	30.3	30.0	29.8	29.8	29.6	29.3	30.0	31.6	32.9	34.0	37.1
Top-Mid	32.3	31.9	30.7	30.5	30.2	30.0	30.0	29.9	30.4	31.8	33.4	36.5
Mid	33.2	32.8	31.5	31.3	31.0	30.3	30.1	30.0	29.8	31.1	33.1	35.6
B-Mid	33.4	32.9	32.0	31.8	31.6	31.1	30.6	30.2	30.0	30.8	32.7	35.0
Bottom	33.6	33.1	32.9	32.6	32.1	31.4	31	30.5	30.1	30.4	31.5	33.0
Hours	12	13	14	15	16	17	18	19	20	21	22	23
Top	40.0	42.5	42.8	42.6	42.1	41.0	39.5	36.9	34.3	33.7	32.2	31.1
Top-Mid	39.1	41.8	42.4	42.4	42.3	40.8	40.0	37.6	35.5	34.6	34.0	33.0
Mid	37.7	39.7	40.9	41.5	41.8	41.3	40.4	39.2	36.8	35.8	34.6	34.4
B-Mid	37.0	39.1	40.2	41.1	41.4	41.5	40.2	39.3	37.3	36.0	35.3	35.0
Bottom	35.8	37.6	39.1	40.7	41.4	41.2	39.9	39.0	37.4	36.3	35.6	35.2
FA20 Concrete												
Hours	0	1	2	3	4	5	6	7	8	9	10	11
Top	31.7	31.1	30.5	30.4	30.3	30.2	30.0	30.5	32.2	34.0	35.3	37.4
Top-Mid	32.4	31.6	30.9	30.7	30.5	30.4	30.1	30.1	31.3	32.8	34.7	36.8
Mid	33.5	32.4	31.8	31.2	31.1	31.0	30.8	30.5	30.9	31.9	34.1	36.2
B-Mid	35.1	33.6	32.2	31.8	31.3	31.2	30.9	30.6	30.6	31.2	33.2	34.6
Bottom	35.7	34.5	33.0	32.0	31.6	31.0	31.0	30.5	30.5	30.7	32.2	33.0
Hours	12	13	14	15	16	17	18	19	20	21	22	23
Top	40.2	42.7	43	42.5	42.3	40.6	39.2	37.7	35.9	34.5	33.9	32.1
Top-Mid	39.5	41.3	42.4	42.3	42.1	40.9	40.1	38.5	37.1	35.7	34.8	34.5
Mid	37.3	39.3	41.3	41.9	41.4	41.0	40.5	39.7	38.9	37.4	36.5	35.6
B-Mid	36.4	38.5	39.4	39.8	40.4	40.9	40.6	39.9	39.2	38.1	37.1	36.5
Bottom	34.3	35.8	36.8	37.9	38.5	39.2	40.2	40.0	39.6	38.6	37.9	36.6
FA40 Concrete												
Hours	0	1	2	3	4	5	6	7	8	9	10	11
Top	31.7	31.3	30.8	30.5	30.4	30.2	30.2	31	32.6	34.2	36.0	37.8
Top-Mid	32.9	31.8	31.2	30.8	30.7	30.5	30.5	30.8	31.9	33.1	35.0	37.2
Mid	33.7	32.9	31.8	31.2	31.0	30.9	30.7	30.7	31.1	32.2	33.6	36.1
B-Mid	34.5	33.6	32.3	32.0	31.7	31.3	31.2	31.1	31.0	31.2	32.5	34.5
Bottom	34.8	34.1	33.2	32.7	32.2	31.6	31.3	31.2	31.1	31.1	32.3	33.2
Hours	12	13	14	15	16	17	18	19	20	21	22	23
Top	40.9	42.0	42.6	42.7	42.0	41.3	39.4	37.6	36	34.5	33.2	31.8
Top-Mid	40.1	41.2	41.8	42.1	42.2	41.5	39.8	38.0	36.7	35.9	35.3	34.8
Mid	38.2	40.1	40.7	41.2	41.4	41.3	40.8	38.9	38.0	37.3	36.2	35.6
B-Mid	36.7	38.0	39.7	40.2	40.4	40.7	40.6	39.7	38.4	37.9	36.8	36.5
Bottom	34.8	36.9	37.6	38.5	39.2	40.3	40.5	40.4	39.7	38.3	37.1	36.8

Slab of thickness 200mm

Reference Concrete												
	Temperature in °C											
Hours	0	1	2	3	4	5	6	7	8	9	10	11
Top	30.5	29.9	29.9	29.8	29.7	29.6	29.5	30.7	31.3	33.1	33.6	36.2
Top-Mid	31.8	31.0	30.7	30.5	30.3	30.4	30.7	30.8	30.9	31.7	32.5	33.9
Mid	32.7	31.8	31.5	31.4	31.3	31.0	30.9	30.8	30.8	30.8	32.0	33.7
B-Mid	32.9	32.0	31.7	31.6	31.5	31.3	31.2	31.0	30.9	32.2	31.4	32.5
Bottom	33.1	32.6	32.3	32.1	32.0	31.7	31.6	31.4	31.2	31.2	30.9	31.4
Hours	12	13	14	15	16	17	18	19	20	21	22	23
Top	38.7	41.8	42.7	39.1	37.4	35.4	34.3	33.5	32.8	32.1	31.4	31.3
Top-Mid	35.9	39.5	40.6	39.3	38.1	36.6	35.6	34.7	33.6	33.1	32.3	32.2
Mid	34.8	37.4	39.3	39.2	38.4	37.2	36.1	35.4	34.8	34.3	33.5	33.2
B-Mid	34.0	36.6	38.0	39.0	38.1	37.2	36.1	35.3	34.9	34.6	34.1	33.7
Bottom	32.1	34.0	35.1	37.0	37.2	36.8	36.3	35.8	35.1	35.1	34.6	34.1
FA20 Concrete												
Hours	0	1	2	3	4	5	6	7	8	9	10	11
Top	31.1	30.3	30.1	29.9	29.8	29.7	29.6	29.9	30.4	33.1	33.6	36.2
Top-Mid	32.1	31.3	30.9	30.6	30.5	30.5	30.4	30.4	30.3	31.7	32.3	34.3
Mid	32.8	32.0	31.7	31.5	31.4	31.0	30.9	30.7	30.6	31.2	32.2	33.6
B-Mid	33.2	32.3	32.0	31.9	31.8	31.5	31.4	31.4	31.2	31.9	31.3	32.5
Bottom	33.5	32.8	32.2	32.0	31.9	31.7	31.5	31.2	31.1	31.1	30.9	31.7
Hours	12	13	14	15	16	17	18	19	20	21	22	23
Top	39.5	42.8	43.7	39.7	38.1	36.1	34.9	33.8	33.0	32.4	32.0	31.9
Top-Mid	36.6	40.2	41.7	40.0	38.7	37.3	36.2	35.2	33.7	33.3	32.8	32.6
Mid	35.9	38.8	40.6	40.0	39.0	37.8	36.7	35.7	34.6	34.3	33.7	33.4
B-Mid	34.6	37.9	39.4	40.2	39.6	38.2	37.1	36.4	35.0	34.7	34.1	33.9
Bottom	32.6	34.9	36.2	38.0	38.0	37.4	36.8	36.3	35.3	35.3	34.7	34.3
FA40 Concrete												
Hours	0	1	2	3	4	5	6	7	8	9	10	11
Top	31.7	30.6	30.2	29.9	29.8	29.7	29.6	29.6	30.0	33.0	33.6	37.2
Top-Mid	32.3	31.5	31.0	30.7	30.5	30.3	30.2	30.0	31.1	31.7	32.1	35.1
Mid	32.8	32.1	31.8	31.6	31.4	31.1	30.9	30.5	30.7	31.5	32.3	34.2
B-Mid	33.5	32.5	32.2	32.1	32.0	31.7	31.6	31.5	31.4	31.3	31.2	33.0
Bottom	33.8	32.9	32.1	31.8	31.7	31.4	31.3	31.1	31	30.9	30.8	31.9
Hours	12	13	14	15	16	17	18	19	20	21	22	23
Top	40.3	43.7	44.7	40.3	38.7	36.7	35.4	34.1	33.1	32.7	32.5	32.5
Top-Mid	37.3	40.8	42.7	40.6	39.2	37.9	36.8	35.7	33.8	33.5	33.3	32.9
Mid	37.0	40.1	41.9	40.7	39.6	38.3	37.2	36.0	34.4	34.3	33.9	33.5
B-Mid	35.1	39.1	40.8	41.4	41	39.2	38.1	37.4	35.1	34.8	34.1	34.0
Bottom	33.1	35.7	37.3	38.9	38.8	38	37.3	36.8	35.4	35.4	34.7	34.5

Slab of thickness 250mm

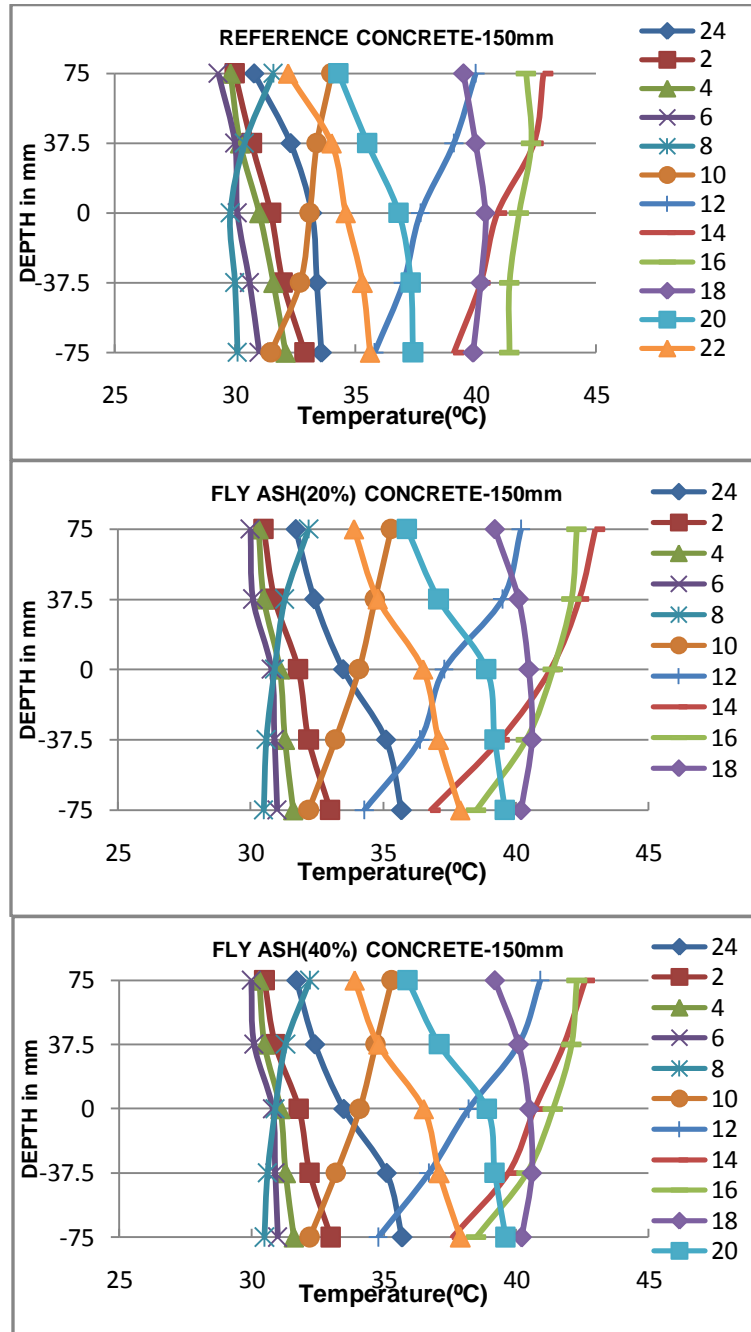
Reference Concrete												
	Temperature in °C											
Hours	0	1	2	3	4	5	6	7	8	9	10	11
Top	30.4	30.3	29.7	29.1	28.6	28.6	28.4	28.9	30.2	32.5	34.3	37.8
Top-Mid	30.5	30.4	30.3	29.2	28.8	28.7	28.6	28.9	30.0	31.7	32.4	35.3
Mid	31.6	31.3	31.2	30.2	29.1	29.2	29.3	29.5	29.9	31.5	32.6	34.7
B-Mid	31.7	31.4	31.4	30.1	29.8	29.3	29.3	29.6	29.8	30.5	31.3	33.6
Bottom	31.8	31.5	31.4	30.4	29.8	29.7	29.6	29.8	29.9	30.3	31.5	33.0
Hours	12	13	14	15	16	17	18	19	20	21	22	23
Top	39.5	40.4	40.9	41.0	39.8	38.2	37.4	35.8	34.8	33.0	32.2	30.7
Top-Mid	37.6	38.9	39.4	40.3	40.0	39.7	38.5	37.0	35.7	33.3	32.4	30.6
Mid	35.8	37.6	38.5	39.6	39.5	39.5	38.7	37.6	35.5	34.2	33.9	31.8
B-Mid	34.3	36.2	37.4	38.5	39.3	39.3	38.5	37.4	35.1	34.3	33.5	32.0
Bottom	33.8	34.5	36.2	37.7	38.3	38.4	38.1	37.1	36.3	34.1	33.3	32.0
FA20 Concrete												
Hours	0	1	2	3	4	5	6	7	8	9	10	11
Top	31.6	30.7	30.6	30.5	29.7	29.4	29.0	30.2	32.5	34.7	36.4	38.5
Top-Mid	32.0	31.9	31.8	31.7	30.9	30.3	30.2	30.6	31.8	33.9	35.1	38.1
Mid	33.2	33.2	33.3	32.2	31.2	30.7	30.5	30.6	31.6	33.2	34.3	36.7
B-Mid	33.4	33.3	33.4	32.1	31.3	31.0	31.0	30.9	31.3	32.5	33.5	35.4
Bottom	33.5	33.4	33.6	32.3	31.7	31.0	31.2	31.5	31.5	32.4	32.8	34.7
Hours	12	13	14	15	16	17	18	19	20	21	22	23
Top	40.3	41.1	41.3	41.3	39.8	37.1	36.4	36.2	35.6	34.4	33.5	32.2
Top-Mid	40.1	40.5	41.0	40.9	40.5	38.4	37.7	37.3	36.5	35.3	34.1	33.2
Mid	38.3	39.4	40.1	40.0	39.9	39.1	38.6	38.4	36.8	35.9	34.6	33.7
B-Mid	36.9	37.5	38.7	39.0	39.1	38.9	38.7	38.3	36.8	35.8	34.7	33.5
Bottom	36.2	36.9	37.3	37.6	37.8	38.1	38.2	38.2	36.9	36.2	34.9	33.9
FA40 Concrete												
Hours	0	1	2	3	4	5	6	7	8	9	10	11
Top	31.5	31.0	30.5	30.1	29.3	29.3	29.3	30.6	33.2	35.7	37.6	40.4
Top-Mid	32.0	31.9	31.9	31.7	30.7	30.5	30.4	30.6	31.5	33.8	34.9	37.1
Mid	32.1	32.1	32.0	31.9	31.5	30.8	30.6	30.3	31.2	32.4	33.4	35.8
B-Mid	32.9	32.5	32.6	31.9	31.4	30.6	30.5	30.0	30.1	31.4	32.7	34.8
Bottom	33.3	33.1	33.0	32.1	31.0	30.5	30.4	29.8	29.0	30.5	31.8	33.7
Hours	12	13	14	15	16	17	18	19	20	21	22	23
Top	41.0	41.6	41.9	42.0	40.9	39.6	37.4	36.9	35.5	34.1	33.0	31.8
Top-Mid	39.2	40.9	41.0	41.2	41.0	40.6	39.2	37.7	36.2	34.2	33.4	32.1
Mid	38.1	39.3	40.0	40.4	40.6	40.0	39.6	38.5	36.1	35.7	33.5	33.2
B-Mid	36.9	37.6	38.4	38.7	39.1	39.3	38.9	38.2	35.7	35.0	33.9	32.7
Bottom	35.8	36.8	37.6	37.9	38.4	39.1	39.5	38.5	37.8	36.0	34.7	33.5

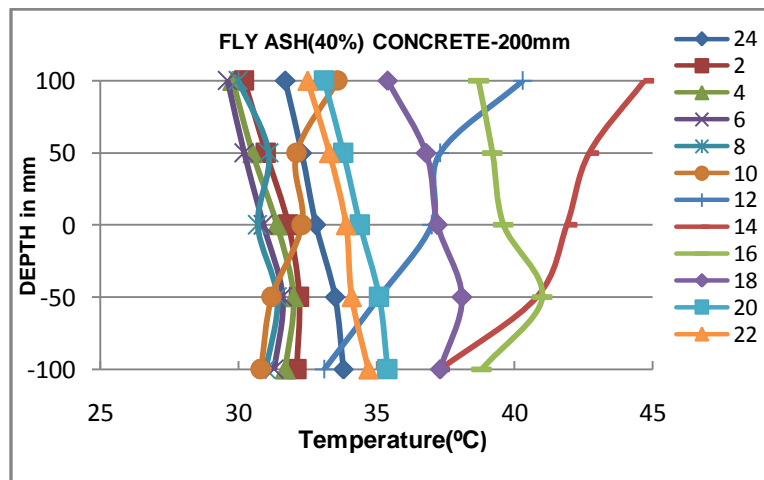
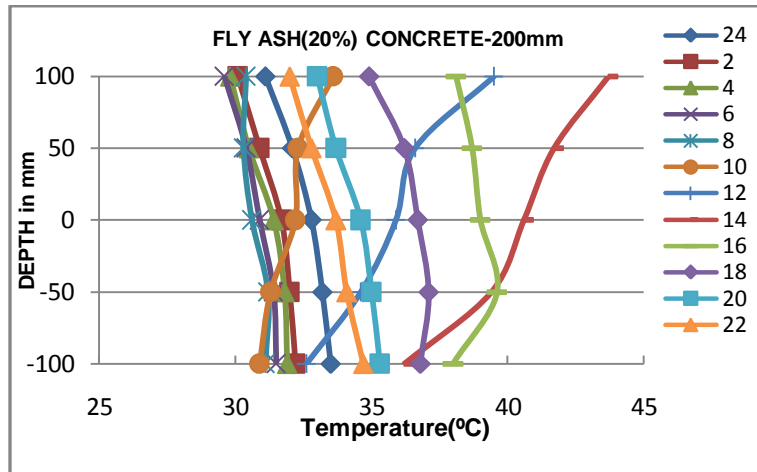
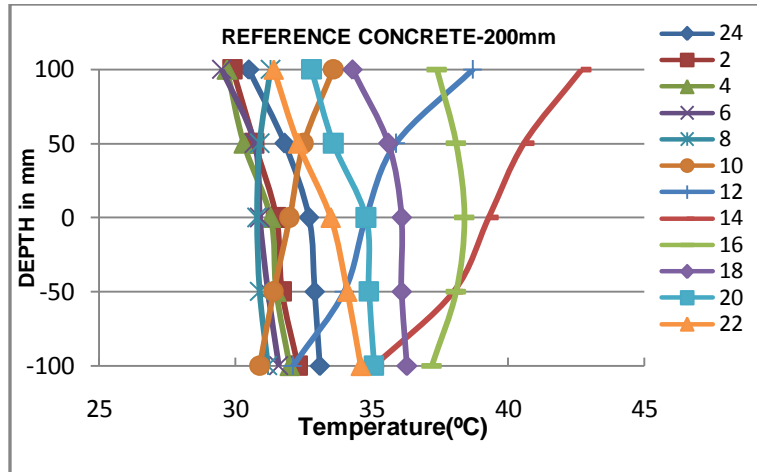
Slab of thickness 300mm

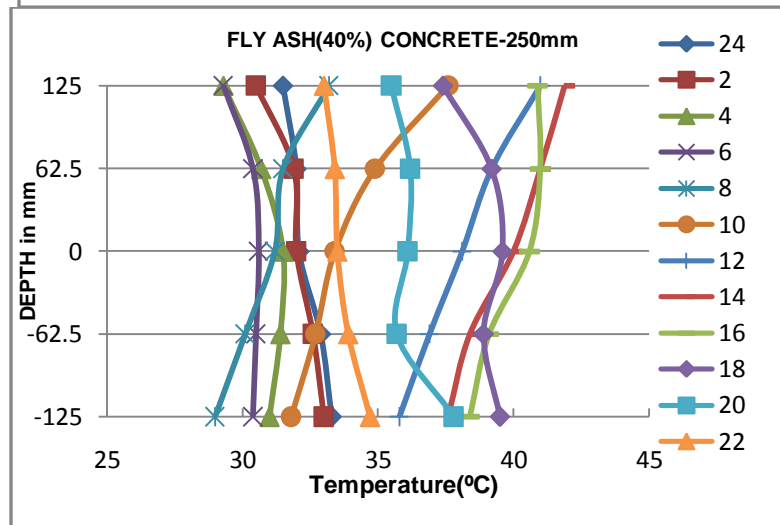
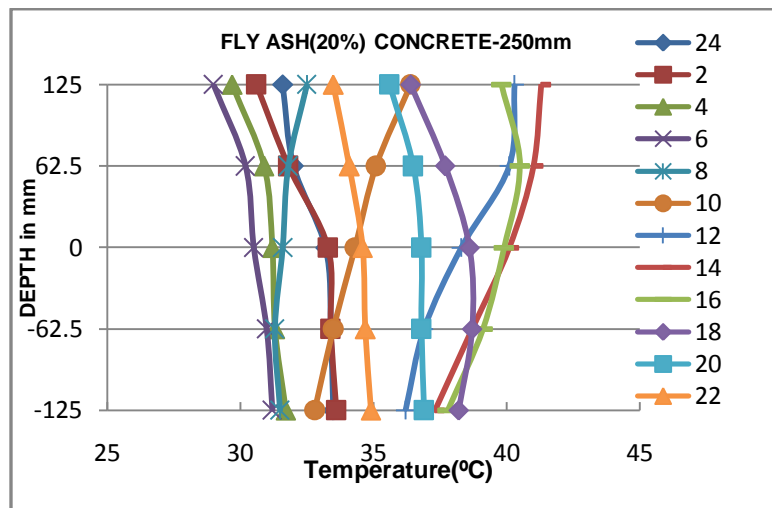
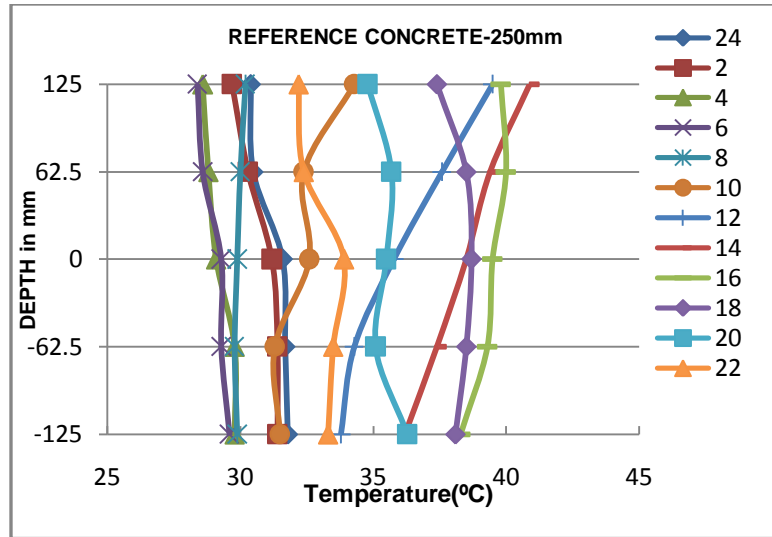
Reference Concrete												
	Temperature in °C											
Hours	0	1	2	3	4	5	6	7	8	9	10	11
Top	31.3	30.8	29.7	28.9	28.6	28.1	27.9	29.5	33.1	36.3	39.3	41.0
Top-Mid	32.1	31.7	31.4	30.7	30.4	29.8	29.6	30.2	32.3	35.0	36.8	39.6
Mid	32.2	32.0	31.6	31.0	30.5	30.3	29.8	30.4	31.5	33.0	34.4	36.8
B-Mid	32.9	32.6	32.5	31.0	30.5	30.3	30.0	30.7	31.2	32.4	33.9	35.5
Bottom	33.2	32.1	31.9	31.7	31.5	32.3	31.0	30.8	31.2	31.9	33.1	35.0
Hours	12	13	14	15	16	17	18	19	20	21	22	23
Top	43.2	43.5	42.8	42.4	37.6	36.6	36.2	34.0	32.6	32.2	31.8	31.4
Top-Mid	41.9	42.4	42.4	42.4	40.9	39.3	38.5	36.4	34.4	33.7	32.8	32.5
Mid	38.4	39.6	40	40.5	40.3	39.3	39.0	36.9	35.0	34.1	33.0	32.8
B-Mid	37.3	38.1	38.3	38.6	39.7	39.2	38.6	36.8	35.2	34.5	33.4	33.1
Bottom	37.1	37.6	37.9	38.2	38.7	38.5	38.0	37.1	35.5	34.3	33.9	33.3
FA20 Concrete												
Hours	0	1	2	3	4	5	6	7	8	9	10	11
Top	31.4	30.4	30.1	29.0	29.0	28.5	28.2	32.3	35.4	37.4	39.4	41.7
Top-Mid	31.6	31.0	30.5	30.1	29.6	29.1	28.8	30.7	31.9	33.4	34.8	38.4
Mid	32.1	31.5	31.2	30.3	30.2	29.8	29.6	30.5	31.3	32.4	33.5	36.3
B-Mid	32.2	31.6	31.3	30.3	30.3	29.8	29.6	30.0	31.3	31.4	32.2	34.8
Bottom	32.8	32.2	31.9	31.3	30.8	30.5	30.4	30.4	31.2	32.0	32.8	34.6
Hours	12	13	14	15	16	17	18	19	20	21	22	23
Top	43.4	43.5	43.0	42.4	37.8	37.1	36.8	33.7	32.7	32.1	31.6	31.6
Top-Mid	40.9	41.8	42.0	42.5	41.0	39.1	38.4	36.1	34.0	32.9	32.4	32.1
Mid	38.6	39.6	40.1	40.7	40.2	39.4	39.1	36.9	34.7	33.2	32.8	32.4
B-Mid	37.0	37.7	38.5	39.1	39.7	38.9	38.4	36.3	34.5	33.8	32.7	32.6
Bottom	36.4	36.7	37.3	38.8	39.2	38.9	38.3	36.6	35.1	34.4	33.3	33.2
FA40 Concrete												
Hours	0	1	2	3	4	5	6	7	8	9	10	11
Top	31.0	30.1	29.8	28.8	28.5	28.2	27.8	31.9	34.7	36.9	38.5	40.7
Top-Mid	31.4	30.7	30.4	29.8	29.4	28.9	28.6	30.7	32.3	34.1	36.0	39.1
Mid	32.6	32.1	31.6	30.6	30.7	30.1	30.0	30.4	31.8	32.8	34.0	36.7
B-Mid	32.7	32.1	31.9	31.0	30.8	30.5	30.4	30.6	31.5	32.7	33.3	35.7
Bottom	32.7	32.4	32.0	31.3	31.3	30.8	30.5	30.6	31.4	32.6	33.5	35.5
Hours	12	13	14	15	16	17	18	19	20	21	22	23
Top	42.2	42.5	42.5	42.3	37.5	36.8	36.0	33.2	32.3	31.7	31.2	31.1
Top-Mid	41.8	42.2	42.4	42.6	41.5	39.3	38.6	36.1	33.9	32.6	32.2	31.9
Mid	38.8	39.6	40.4	41.4	41.1	40.1	39.6	37.4	35.2	33.9	33.3	32.9
B-Mid	37.6	38.4	39.2	39.7	40.2	39.6	39.3	37.4	35.3	34.2	33.5	33.1
Bottom	37.1	37.6	38.1	38.6	39.3	38.8	38.4	37.1	35.3	34.3	33.5	33.2

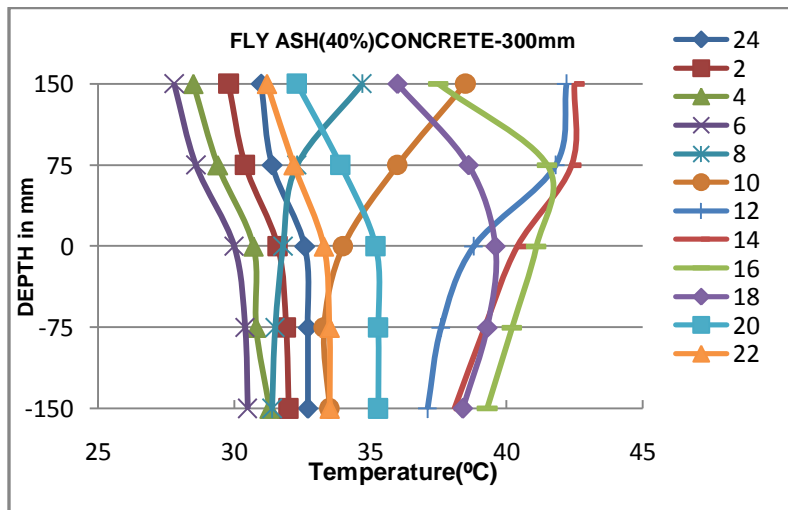
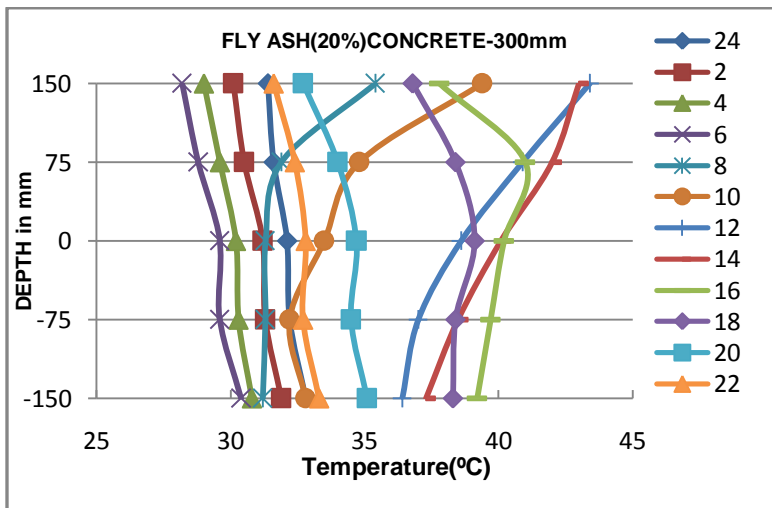
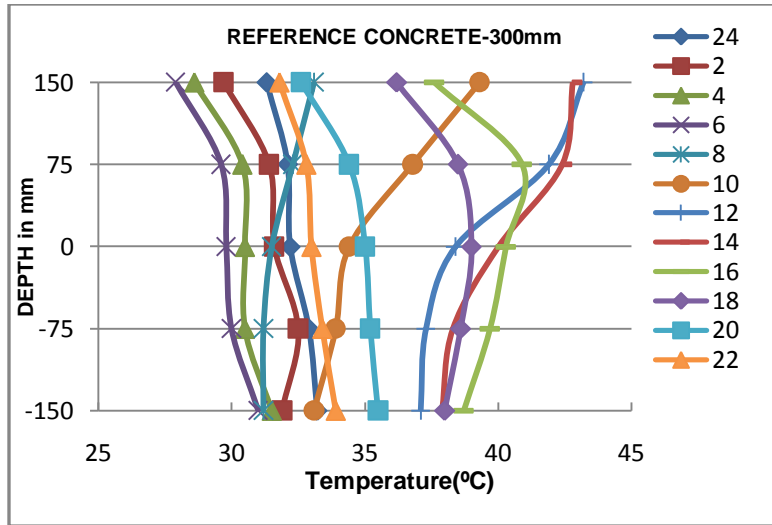
II-2 Temperature profile across the thickness of slab

Temperature profile across the thickness (150mm, 200mm, 250mm and 300mm) for REF concrete, FA 20 and FA40 are presented.









II-3 Comparison of third degree polynomial and quadratic equation of temperature distribution across the thickness using regression

TIME	3rd Degree Polynomial Equation	R ²	Quadratic Equation	R ²
REFERENCE CONCRETE -150mm				
2-00am	$T(z) = -5E-07z^3 + 5E-06z^2 - 0.016z + 31.40$	0.996	$T(z) = 5E-06z^2 - 0.018z + 31.40$	0.994
10-00am	$T(z) = 2E-06z^3 - 7E-05z^2 + 0.006z + 33.12$	0.999	$T(z) = -7E-05z^2 + 0.015z + 33.12$	0.965
4-00pm	$T(z) = -2E-06z^3 - 2E-05z^2 + 0.014 + 41.84$	0.994	$T(z) = -2E-05z^2 + 0.006z + 41.84$	0.811
10-00pm	$T(z) = -1E-06z^3 - 1E-04z^2 - 0.016z + 34.81$	0.994	$T(z) = -2E-04z^2 - 0.021z + 34.75$	0.984
FA20 CONCRETE -150mm				
2-00am	$T(z) = 2E-07z^3 + 2E-05z^2 - 0.017z + 31.63$	0.987	$T(z) = 2E-05z^2 - 0.016z + 31.63$	0.986
10-00am	$T(z) = 2E-07z^3 - 6E-05z^2 + 0.019z + 34.05$	0.999	$T(z) = -6E-05z^2 + 0.020z + 34.05$	0.999
4-00pm	$T(z) = 6E-07z^3 - 0.0002z^2 + 0.021z + 41.46$	0.999	$T(z) = -2E-4z^2 + 0.024z + 41.46$	0.997
10-00pm	$T(z) = 9E-07z^3 - 7E-05z^2 - 0.032z + 36.22$	0.986	$T(z) = -7E-05z^2 - 0.027z + 36.22$	0.983
FA40 CONCRETE -150mm				
2-00am	$T(z) = -3E-07z^3 + 5E-05z^2 - 0.014z + 31.73$	0.997	$T(z) = 5E-05z^2 - 0.015z + 31.73$	0.996
10-00am	$T(z) = -2E-06z^3 + 1E-04z^2 + 0.036z + 33.60$	1	$T(z) = 1E-04z^2 + 0.026z + 33.60$	0.983
4-00pm	$T(z) = -1E-06z^3 - 0.0002z^2 + 0.025z + 41.46$	0.998	$T(z) = -2E-4z^2 + 0.019z + 41.46$	0.988
10-00pm	$T(z) = 1E-06z^3 - 0.0002z^2 - 0.018z + 36.27$	0.998	$T(z) = -2E-4z^2 - 0.024xz + 36.27$	0.990

Table continued..

REFERENCE CONCRETE -200mm				
2-00am	$T(z) = 3E-07z^3 - 5E-05z^2 - 0.011z + 31.07$	0.986	$T(z) = -5E-05z^2 - 0.009z + 31.07$	0.975
10-00am	$T(z) = 7E-07z^3 + 3E-05z^2 + 0.007z + 31.87$	0.924	$T(z) = 3E-05z^2 + 0.013z + 31.87$	0.903
4-00pm	$T(z) = 1E-07z^3 - 1E-4z^2 - 0.0004z + 38.38$	0.999	$T(z) = -1E-4z^2 + 0.0008z + 38.38$	0.996
10-00pm	$T(z) = 3E-07z^3 - 4E-05z^2 - 0.018z + 33.38$	0.995	$T(z) = -4E-05z^2 - 0.016z + 33.38$	0.993
FA20 CONCRETE -200mm				
2-00am	$T(z) = 7E-08z^3 - 5E-05z^2 - 0.011z + 31.62$	0.996	$T(z) = -5E-05z^2 - 0.010z + 31.62$	0.995
10-00am	$T(z) = 5E-07z^3 + 3E-05z^2 + 0.008z + 31.91$	0.964	$T(z) = 3E-05z^2 + 0.012z + 31.91$	0.953
4-00pm	$T(z) = 1E-06z^3 - 1E-4z^2 - 0.0122z + 39.26$	0.922	$T(z) = -1E-4z^2 - 0.0014z + 39.26$	0.715
10-00pm	$T(z) = -7E-08z^3 - 3E-05z^2 - 0.012z + 33.58$	0.994	$T(z) = -3E-05z^2 - 0.013z + 33.58$	0.994
FA40 CONCRETE -200mm				
2-00am	$T(z) = 3E-07z^3 - 6E-05z^2 - 0.012z + 31.77$	0.999	$T(z) = -6E-05z^2 - 0.01z + 31.77$	0.990
10-00am	$T(z) = 7E-07z^3 + 3E-05z^2 + 0.007z + 31.87$	0.924	$T(z) = 3E-05z^2 + 0.013z + 31.87$	0.903
4-00pm	$T(z) = 2E-06z^3 - 1E-4z^2 - 0.023z + 40.08$	0.866	$T(z) = -1E-4z^2 - 0.0040z + 40.08$	0.514
10-00pm	$T(z) = -4E-07z^3 - 2E-05z^2 - 0.007z + 33.81$	0.994	$T(z) = -2E-05z^2 - 0.010z + 33.81$	0.982

Table continued...

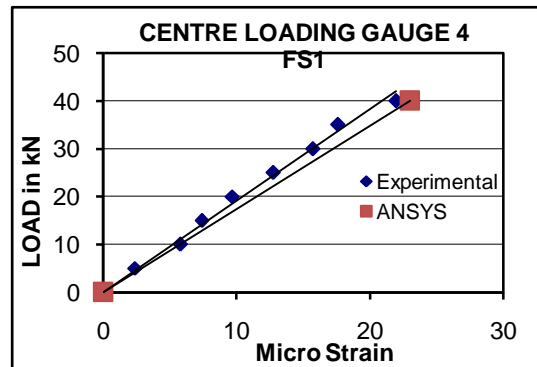
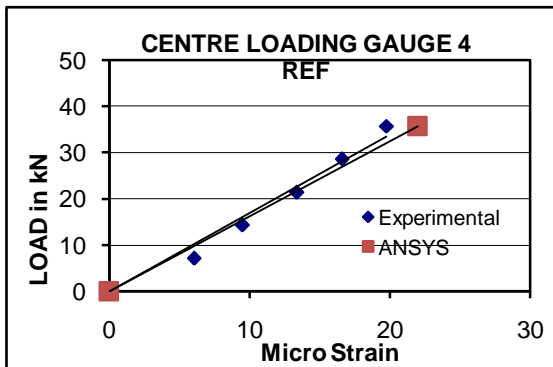
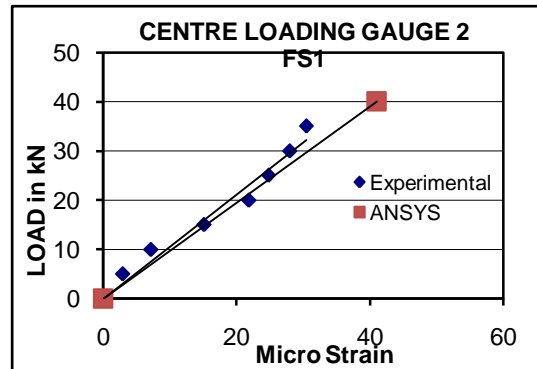
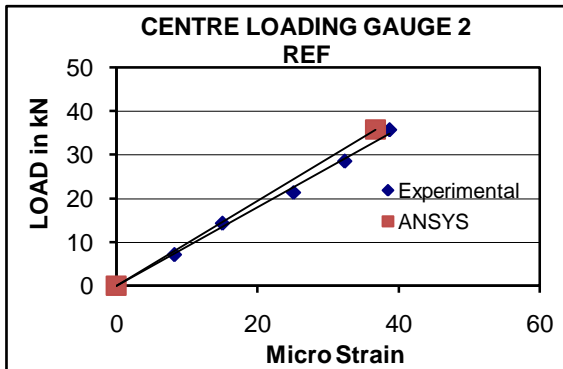
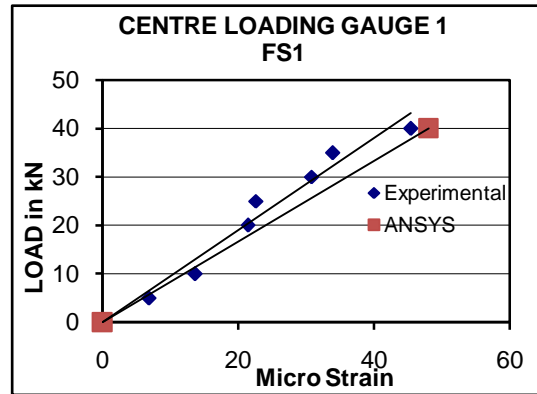
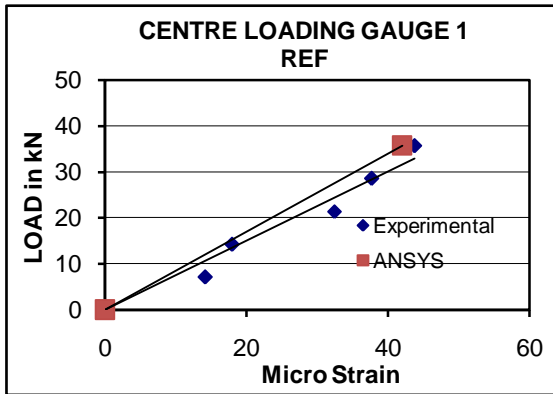
REFERENCE CONCRETE -250mm				
2-00am	$T(z) = 2E-07z^3 - 3E-05z^2 - 0.0095z + 31.071$	0.986	$T(z) = -3E-05z^2 - 0.007z + 31.07$	0.975
10-00am	$T(z) = 2E-07z^3 + 5E-05z^2 + 0.008z + 32.034$	0.890	$T(z) = 5E-05z^2 + 0.010z + 32.03$	0.883
4-00pm	$T(z) = 3E-08z^3 - 4E-05z^2 + 0.0055z + 39.68$	0.96	$T(z) = -4E-05z^2 + 0.005z + 39.68$	0.963
10-00pm	$T(z) = 4E-07z^3 - 5E-05z^2 - 0.0103z + 33.45$	0.812	$T(z) = -5E-05z^2 - 0.005z + 33.45$	0.755
FA20 CONCRETE -250mm				
2-00am	$T(z) = 7E-08z^3 - 6E-05z^2 - 0.013z + 33.02$	0.978	$T(z) = 6E-05z^2 - 0.012z + 33.02$	0.977
10-00am	$T(z) = 1E-07z^3 + 2E-05z^2 + 0.012z + 34.24$	0.999	$T(z) = 6E-05z^2 - 0.012z + 33.02$	0.977
4-00pm	$T(z) = -3E-07z^3 - 8E-05z^2 + 0.012z + 40.02$	0.993	$T(z) = -8E-05z^2 + 0.008z + 40.02$	0.978
10-00pm	$T(z) = -7E-08z^3 - 2E-05z^2 - 0.004z + 34.53$	0.992	$T(z) = -2E-05z^2 - 0.005z + 34.53$	0.989
FA40 CONCRETE -250mm				
2-00am	$T(z) = -4E-07z^3 - 3E-05z^2 - 0.004z + 32.21$	0.975	$T(z) = -3E-05z^2 - 0.009z + 32.21$	0.941
10-00am	$T(z) = 2E-07z^3 + 2E-05z^2 + 0.017z + 38.01$	0.999	$T(z) = 2E-05z^2 + 0.020z + 38.01$	0.996
4-00pm	$T(z) = -4E-07z^3 - 5E-05z^2 + 0.016z + 40.38$	0.983	$T(z) = 5E-05z^2 + 0.011z + 40.38$	0.953
10-00pm	$T(z) = -2E-07z^3 + 2E-05z^2 - 0.003z + 33.54$	0.997	$T(z) = -2E-05z^2 - 0.006z + 33.54$	0.968

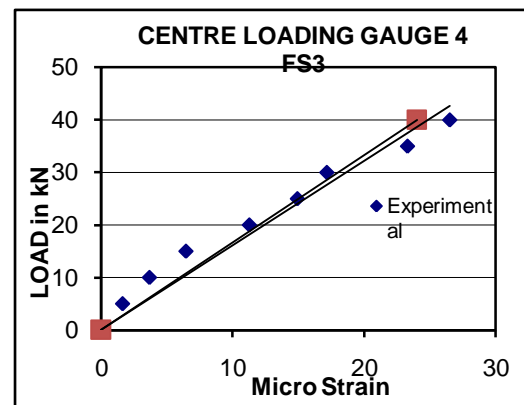
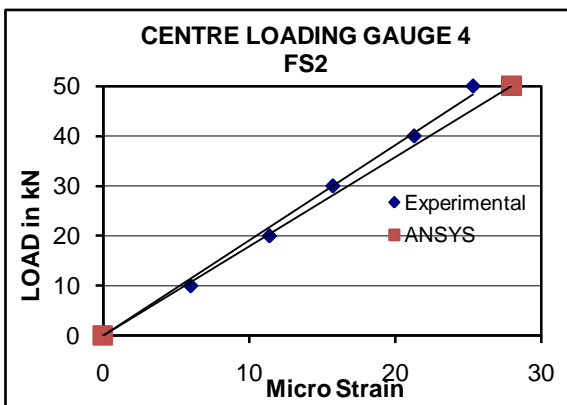
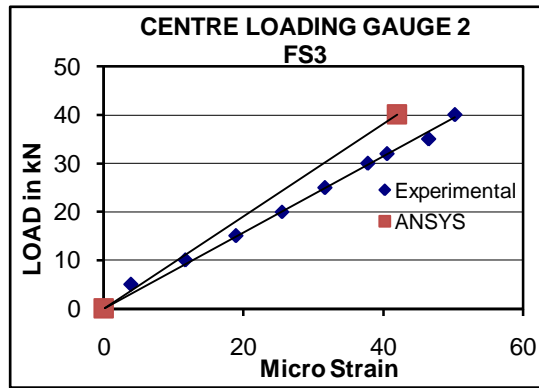
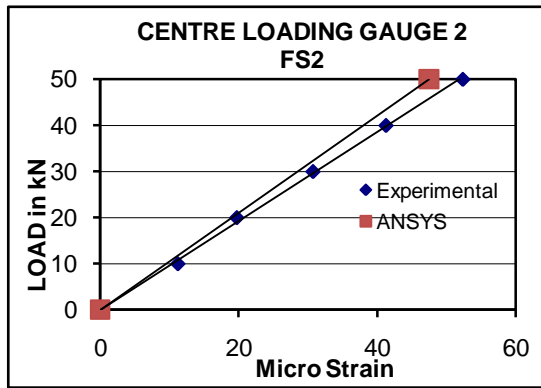
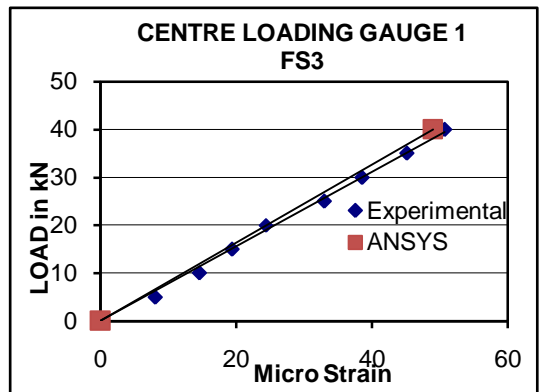
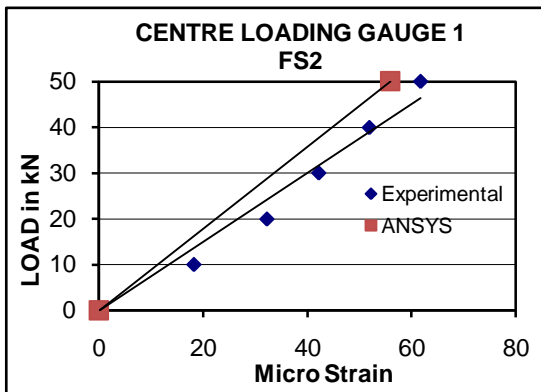
Table continued...

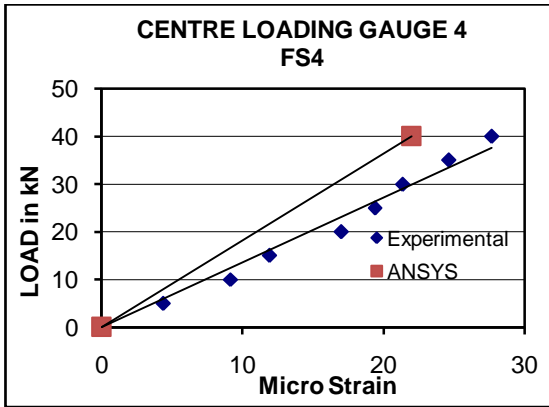
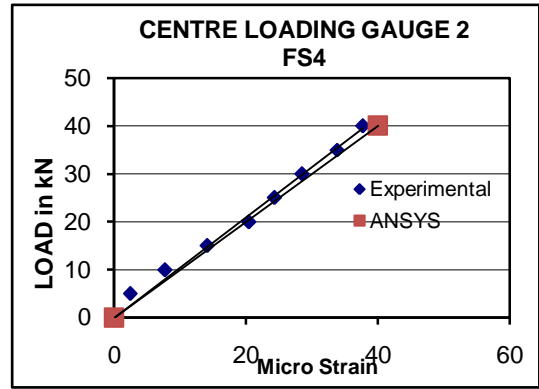
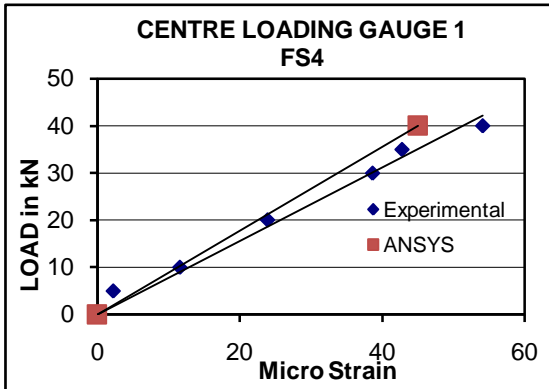
REFERENCE CONCRETE -300mm				
2-00am	$T(z) = 1E-19z^3 - 5E-05z^2 - 0.0073z + 31.977$	0.937	$T(z) = -5E-05z^2 - 0.007z + 31.97$	0.937
10-00am	$T(z) = 8E-08z^3 + 7E-05z^2 + 0.0189z + 34.74$	0.991	$T(z) = 7E-05z^2 + 0.020z + 34.74$	0.990
4-00pm	$T(z) = -7E-07z^3 - 1E-4z^2 + 0.0119z + 40.67$	0.962	$T(z) = -1E-4z^2 - 0.001z + 40.67$	0.783
10-00pm	$T(z) = -2E-07z^3 - 1E-05z^2 - 0.003z + 33.094$	0.993	$T(z) = -1E-05z^2 - 0.006z + 33.09$	0.959
FA20 CONCRETE -300mm				
2-00am	$T(z) = -4E-08z^3 - 3E-06z^2 - 0.005z + 31.02$	0.971	$T(z) = -3E-06z^2 - 0.005z + 31.02$	0.969
10-00am	$T(z) = 3E-07z^3 + 0.0001z^2 + 0.015z + 33.05$	0.988	$T(z) = 1E-4z^2 + 0.021z + 33.05$	0.982
4-00pm	$T(z) = -8E-07z^3 - 9E-05z^2 + 0.013z + 40.59$	0.947	$T(z) = -9E-05z^2 - 0.002z + 40.6$	0.667
10-00pm	$T(z) = -2E-07z^3 - 1E-05z^2 - 8E-4z + 32.68$	0.984	$T(z) = 1E-05z^2 - 0.004z + 32.68$	0.907
FA40 CONCRETE -300mm				
2-00am	$T(z) = -2E-07z^3 - 2E-05z^2 - 0.010z + 31.41$	0.982	$T(z) = -2E-05z^2 - 0.007z + 31.41$	0.965
10-00am	$T(z) = -8E-08z^3 + 9E-05z^2 + 0.018z + 34.10$	0.998	$T(z) = 9E-05z^2 + 0.016z + 34.10$	0.998
4-00pm	$T(z) = -9E-07z^3 - 1E-4z^2 + 0.013z + 41.39$	0.983	$T(z) = -1E-4z^2 - 0.003z + 41.39$	0.794
10-00pm	$T(z) = 6E-08z^3 - 4E-05z^2 - 0.009z + 33.15$	0.99	$T(z) = -4E-05z^2 - 0.007z + 33.15$	0.987

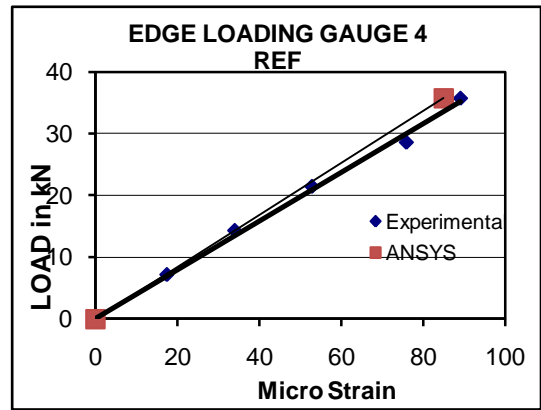
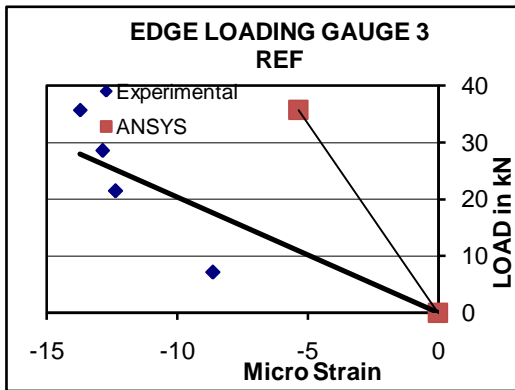
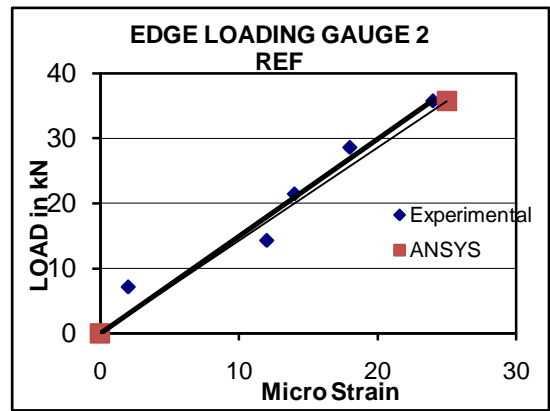
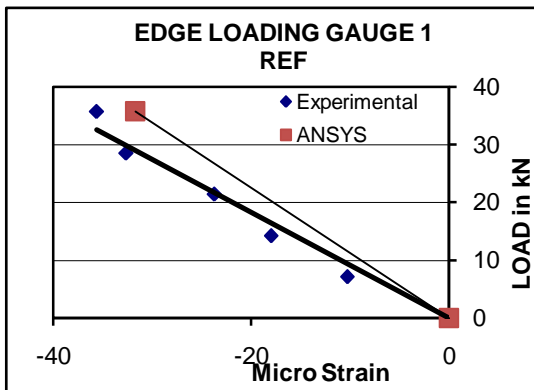
APPENDIX III

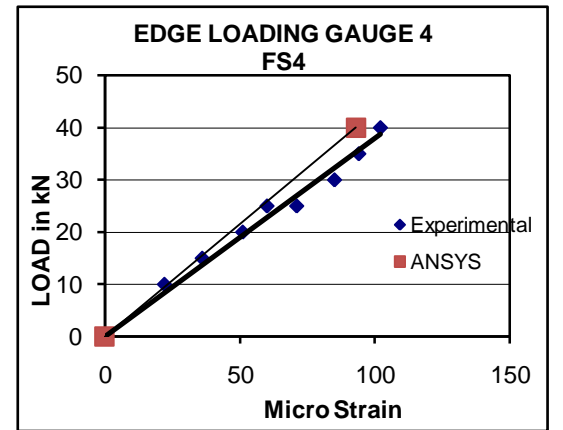
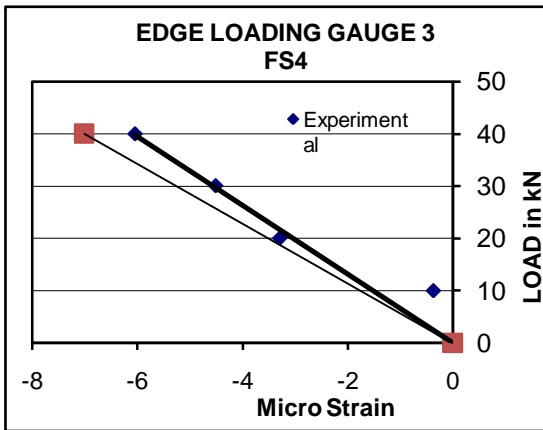
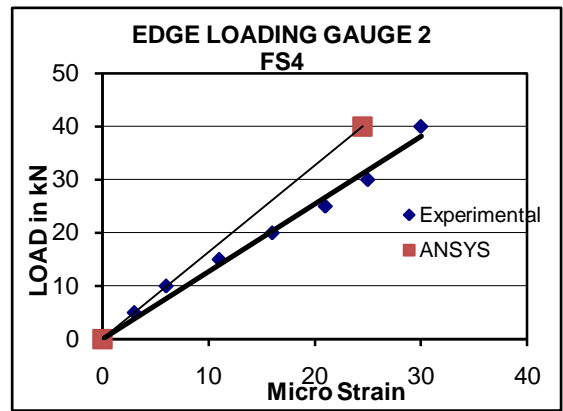
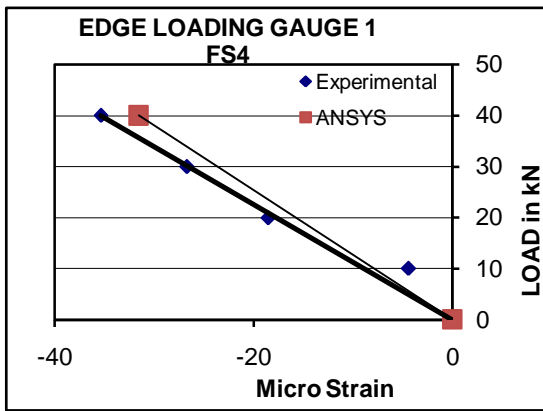
III-1 Comparison of Experimental and Analytical(ANSYS) results

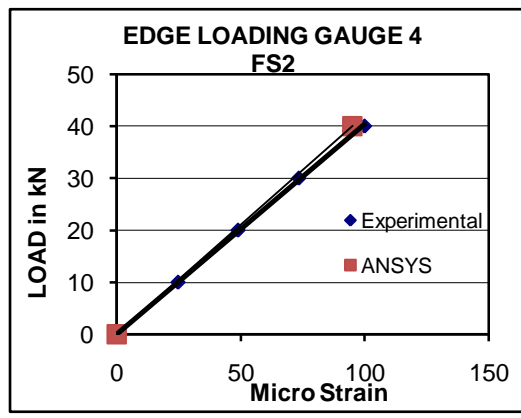
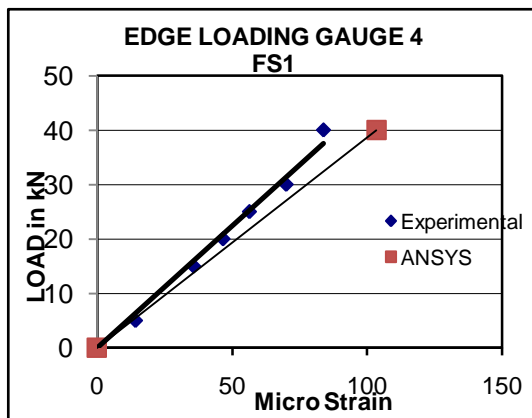
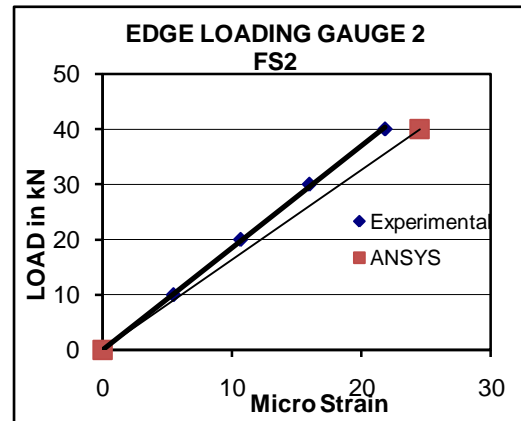
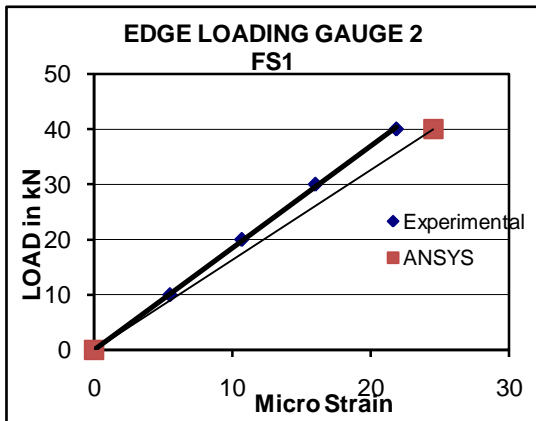
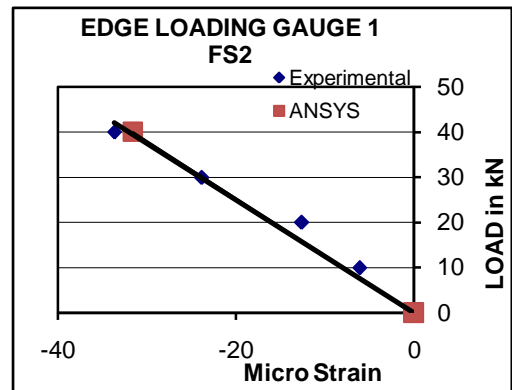
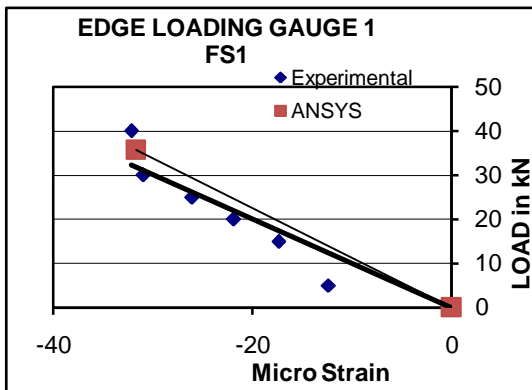












APPENDIX IV

IV-1 Pavement Design Examples-Fatigue approach

A) High volume roads

Present Traffic = **3000 CVPD**

Design life = 20 years,

Vehicle Growth Rate $r = 7.5\%$

Tyre pressure 0.8N/mm^2

$$\begin{aligned} \text{Cumulative repetition in 20 years} &= 3000 \times 365 \times \left[\frac{(1.075)^{20} - 1}{0.075} \right] \\ &= 47418626 \end{aligned}$$

$$\begin{aligned} \text{Design traffic} &= 25 \% \text{ of the total repetitions of commercial vehicles} \\ &= 11854657 \end{aligned}$$

i) Reference Concrete

Thickness = 250 mm

Flexural Strength = 5.32 MPa

Axle load (AL) (tonnes)	ALx1.2	Stress MPa	Stress Ratio	Expected Repetitions	Allowable Repetitions (IRC)	Fatigue	Allowable Repetitions (present regression Model)	Fatigue
Single axle								
20	24	3.67	0.69	71127	2534	high	270520	0.26
18	21.6	3.36	0.63	177820	13443	high	3.26×10^6	0.05
16	19.2	3.04	0.57	569023	71303	high	unlimited	
14	16.8	2.71	0.51	128030	4.85×10^5		unlimited	
Tandem axle								
36	43.2	2.67	0.50	35560	7.62×10^5		unlimited	
32	38.4	2.43	0.46	35560	1.40×10^7		unlimited	
Total						exceeds		0.31

Thickness =290 mm

Flexural Strength = 5.32MPa

Axle load (AL) (tonnes)	ALx1.2	Stress MPa	Stress Ratio	Expected Repetitions	Allowable Repetitions (IRC)	Fatigue	Allowable Repetitions (present regression Model)	Fatigue
Single axle								
20	24	2.95	0.55	71127	124351	0.57		
18	21.6	2.70	0.51	177820	485184	0.37		
16	19.2	2.44	0.46	569023	1.43x10 ⁷	0.04		
14	16.8	2.17	0.41	128030	unlimited			
Tandem axle								
36	43.2	2.23	0.42	35560	unlimited			
32	38.4	2.02	0.38	35560	unlimited			
Total						0.98		

Thickness of pavement for reference concrete

Using IRC Fatigue model : 290 mm

Using Proposed Fatigue model : 250 mm

ii) Fly Ash Steel fiber reinforced concrete(FS4)

Thickness =230 mm

Flexural Strength = 5.62MPa

Axle load (AL) (tonnes)	ALx1.2	Stress MPa	Stress Ratio	Expected Repetitions	Allowable Repetitions (IRC)	Fatigue	Allowable Repetitions (present regression Model)	Fatigue
Single axle								
20	24	3.95	0.70	71127	1919	high	178649	0.40
18	21.6	3.61	0.64	177820	10179	high	1.42x10 ⁶	0.13
16	19.2	3.28	0.58	569023	53993	high	unlimited	
14	16.8	2.92	0.52	128030	3.36x10 ⁵		unlimited	
Tandem axle								
36	43.2	2.86	0.52	35560	3.36x10 ⁵		unlimited	
32	38.4	2.60	0.47	35560	5.20x10 ⁶		unlimited	
Total						exceeds		0.53

Thickness =280 mm

Flexural Strength = 5.62MPa

Axle load (AL) (tones)	ALx1.2	Stress (N/mm ²)	Stress Ratio	Expected Repetitions	Allowable Repetitions (IRC)	Fatigue	Allowable Repetitions (present regression Model)	Fatigue
Single axle								
20	24	3.00	0.54	71127	166533	0.43		
18	21.6	2.74	0.49	177820	1.29x10 ⁶	0.14		
16	19.2	2.48	0.44	569023	unlimited			
14	16.8	2.21	0.39	128030	unlimited			
Tandem axle								
36	43.2	2.28	0.41	35560	unlimited			
32	38.4	2.07	0.37	35560	unlimited			
Total						0.57		

Thickness of pavement for Fly Ash Steel fiber reinforced concrete

Using IRC Fatigue model : 280 mm

Using Proposed Fatigue model : 230 mm

B) Low Volume Roads

Present Traffic = **150 CVPD** Design life=20 Years

Vehicle Growth Rate r = 6%

$$\text{Cumulative repetitions in 20 Years} = 150 \times 365 \times \left[\frac{(1.06)^{20} - 1}{0.06} \right]$$

$$= 20,14,011$$

Design Traffic = 25 per cent of the total repetitions of commercial vehicles

$$= 5,03,503$$

i) Reference Concrete (R)

Thickness = 200 mm

Flexural strength = 4.6 N/mm²

Axle load (AL) (tones)	ALx1.2	Stress (N/mm ²)	Stress Ratio	Expected Repetitions	Allowable Repetitions (IRC)	Fatigue	Allowable Repetitions (present regression Model)	Fatigue	
14	16.8	3.43	0.75	5035	478	exceeds	22439	0.19	
12	14.4	3.02	0.66	20140	5837		0.94x10 ⁶	0.02	
10	12.0	2.60	0.56	226576	94163		unlimited	-	
8	9.60	2.16	0.47	251752	5.20x10 ⁶		unlimited	-	
Total									0.21

Thickness =220 mm

Flexural Strength = 4.6 N/mm²

Axle load (AL) (tones)	ALx1.2	Stress (N/mm ²)	Stress Ratio	Expected Repetitions	Allowable Repetitions (IRC)	Fatigue		
14	16.8	3.048	0.64	5035	11800	0.427		
12	14.4	2.679	0.56	20140	94100	0.21		
10	12.0	2.298	0.48	226576	2.4x10 ⁶	0.095		
8	9.60	1.904	0.39	251752	unlimited	-		
Total						0.732		

Thickness of pavement for reference concrete

Using IRC Fatigue model : 220 mm

Using Proposed Fatigue model : 200 mm

ii) Fly Ash Steel fiber reinforced concrete (FS4)

Thickness = 190 mm

Flexural strength = 5.00N/mm²

Axle load (AL) (tones)	ALx1.2	Stress (N/mm ²)	Stress Ratio	Expected Repetitions	Allowable Repetitions (IRC)	Fatigue	Allowable Repetitions (present regression Model)	Fatigue
14	16.8	3.755	0.75	5035	477	10.56	22439	0.22
12	14.4	3.309	0.66	20140	5830	3.45	9.39 x10 ⁵	0.02
10	12.0	2.846	0.57	226576	7.12x10 ⁴	3.18	unlimited	-
8	9.60	2.365	0.47	251752	5.2x10 ⁶	0.05	unlimited	-
Total						17.24		0.24

Thickness =210 mm

Flexural Strength = 5.0 N/mm²

Axle load (AL) (tones)	ALx1.2	Stress (N/mm ²)	Stress Ratio	Expected Repetitions	Allowable Repetitions (IRC)	Fatigue		
14	16.8	3.253	0.65	5035	7700	0.65		
12	14.4	2.865	0.57	20140	71200	0.28		
10	12.0	2.460	0.49	226576	1.287x10 ⁶	0.176		
8	9.60	2.039	0.41	251752	unlimited	-		
Total						1.106		

Thickness =220 mm

Flexural Strength = 5.0 N/mm²

Axle load (AL) (tones)	ALx1.2	Stress (N/mm ²)	Stress Ratio	Expected Repetitions	Allowable Repetitions (IRC)	Fatigue		
14	16.8	3.048	0.61	5035	23400	0.22		
12	14.4	2.679	0.54	20140	166000	0.12		
10	12.0	2.298	0.46	226576	1.43x10 ⁷	0.02		
8	9.60	1.904	0.38	251752	unlimited	-		
Total						0.36		

Thickness of pavement for Fly Ash Steel fiber reinforced concrete

Using IRC Fatigue model : 220 mm

Using Proposed Fatigue model : 190 mm

IV-2 Pavement Design Examples-Combined load and temperature stress

A) High Volume Roads

i) Reference concrete

Thickness of slab(mm)	250	260	270	280	290	300
Temp. differential °C	16.2	16.4	16.6	16.7	16.8	17
Radius of relative stiffness(mm)	806	830	856	877	900	923
L/l	5.59	5.42	5.27	5.13	4.99	4.87
Bradbury's Coefficient C	0.84	0.81	0.775	0.745	0.72	0.684
Temperature stress (N/mm ²)	2.18	2.10	2.03	1.97	1.91	1.83
Modified temp stress (N/mm ²)	2.4	2.3	2.23	2.17	2.10	2.01
Maximum load stress-Ref (N/mm ²)	3.46	3.28	3.11	2.95	2.81	2.68
Total stress(N/mm ²)	5.86	5.58	5.34	5.12	4.91	4.69
Allowable modulus of rupture fr (N/mm ²)	5.32	5.32	5.32	5.32	5.32	5.32

ii) Fly ash Steel fiber concrete (FS4)

Thickness of slab(mm)	250	260	270	280	290
Temp. differential °C	16.2	16.4	16.6	16.7	16.8
Radius of relative stiffness(mm)	820	845	869	893	917
L/l	5.49	5.33	5.18	5.04	4.91
Bradbury's Coefficient C	0.82	0.79	0.76	0.73	0.69
Temperature stress (N/mm ²)	2.30	2.22	2.14	2.07	1.97
Modified temp stress (N/mm ²)	2.53	2.44	2.35	2.28	2.17
Maximum load stress-FS (N/mm ²)	3.51	3.32	3.15	2.98	2.84
Total stress(N/mm ²)	6.04	5.76	5.50	5.26	5.01
Allowable modulus of rupture fr (N/mm ²)	5.62	5.62	5.62	5.62	5.62

B) Low Volume Roads:

i) Reference concrete

Thickness of slab(mm)	210	220	230	240
Temp. differential °C	15.9	16	16	16.1
Radius of relative stiffness(mm)	682	706	730	754
L/l	5.5	5.31	5.14	4.97
Bradbury's Coefficient C	0.82	0.78	0.75	0.71
Temperature stress (N/mm ²)	1.79	1.71	1.65	1.57
Modified temp stress (N/mm ²)	1.97	1.88	1.82	1.73
Maximum load stress- (N/mm ²)	3.20	3.00	2.81	2.65
Total stress(N/mm ²)	5.17	4.88	4.63	4.38
Allowable modulus of rupture f_r (N/mm ²)	4.60	4.60	4.60	4.60

ii) Fly ash Steel fiber concrete (FS4)

Thickness of slab(mm)	210	220	230	240
Temp. differential °C	15.9	16	16	16.1
Radius of relative stiffness(mm)	695	720	744	768
L/l	5.4	5.21	5.04	4.88
Bradbury's Coefficient C	0.8	0.76	0.73	0.69
Temperature stress (N/mm ²)	1.88	1.79	1.72	1.64
Modified temp stress (N/mm ²)	2.07	1.97	1.89	1.80
Maximum load stress- (N/mm ²)	3.25	3.04	2.85	2.68
Total stress(N/mm ²)	5.32	5.01	4.74	4.48
Allowable modulus of rupture f_r (N/mm ²)	4.86	4.86	4.86	4.86

LIST OF PUBLICATIONS

Refereed Journals (National/International)

1. **Chandrashekhhar, A.**, RaviShankar, A.U. and Girish, M. G. (2010) “Fatigue behaviour of steel Fiber Reinforced Concrete (SFRC) with Fly ash”, Highway Research Journal (IRC), Vol.3, No.2, 9-22
2. **Chandrashekhhar, A.**, RaviShankar, A.U. and Abhishek Patil (2010), “Potential utilization of Fly ash in SFRC Pavement”, Civil Engineering and Construction Review, January, 110-117

International Conferences

1. **Chandrashekhhar, A.** and RaviShankar, A.U.(2008) “Fatigue strength studies on Hybrid Steel Fiber Reinforced Concrete for Rigid Pavements”, Proceedings of seventh RILEM International Symposium on Fiber Reinforced Concrete: Design and Application(Pro 60), IITM, Chennai, 1099-1107
2. **Chandrashekhhar, A.** and RaviShankar, A.U.(2009) “Experimental studies on utilization of waste materials for pavement quality concrete” Proceedings of International conference on Structural and Geotechnical Engineering, ASCGE-2009) BITS-Pilani, 34
3. Girish, M.G., **Chandrashekhhar, A.** and RaviShankar, A.U.(2010), “Fatigue analysis of Steel fiber reinforced concrete”, Proceedings of International conference on Developments in Roads Technology (DRT-2010), NIT Roorkeela, 461-468

BIO DATA



1	Name	CHANDRASHEKHAR.A
2	Date of Birth	01-01-1967
3	Qualification	BE in Civil Engineering M Tech (Structural Engineering)
4	Experience	16 years of Teaching experience 1991-1999 SNS Polytechnic, Sunkadakatte, Mangalore 1999-onwards KVG C E, Sullia
5	Permanent Address	Chandrashekhar.A S/o Anantha Nalluraya SADHANA, Adisubramanya Road SUBRAMANYA, 574238 DK , Karnataka, India 08257-281294, 233296, Mob: 9448725581 Email: acs.nitk@gmail.com

6 Academic Details:

Examination Passed	Year of Passing	University	Class
BE(Civil Engineering)	1988	Gulbarga University	First Class
M. Info. Tech	2003	SMU-open university	First Class with Distinction
M Tech (Structural Engineering)	2005	NITK	First Class with Distinction

7. Subjects studied during MTech(SE)

- | | |
|---|---------------------------------------|
| 1. Theory of Elasticity & Plasticity | 6. Shells and folded Plates |
| 2. Theory of Plates | 7. Adv. Design of concrete Structures |
| 3. Matrix Method of Structural analysis | 8. Adv. Design of steel structures |
| 4. Structural Optimisation | 9. Finite element method |
| 5. Structural Dynamics | 10. Earthquake Engineering |

8. Subjects studied during PhD course work

1. Pavement design
2. Pavement materials
3. Soil mechanics for Highway engineers
4. Urban Transport planning
5. Statistical methods

9. Subjects Taught in UG Level

Structural Analysis	Design of RC structures
Design of Steel structures	Concrete Technology
Pavement Design	Strength of Materials

10. Professional Body Membership

1. Life member of Indian Society for Technical Education (ISTE)
2. Life member of Indian Association for Structural Rehabilitation (IASTR)
3. Member of Indian Roads Congress (IRC)

11. Publications

National/ International journals	-05
National/ International Conferences	-05